

Experimental and Computational Studies on Oil Injected Twin-Screw Compressor

A Thesis Submitted for Award of the Degree of

Doctor of Philosophy

Nagam Seshaiah

Under the Guidance of
Prof. Sunil Kumar Sarangi



Mechanical Engineering Department
National Institute of Technology
Rourkela

Chapter I

INTRODUCTION

Gas compressors are mechanical devices used for raising the pressure of gas or vapour either by lowering its volume (as in the case of positive displacement machines) or by imparting to it a high kinetic energy which is converted into pressure in a diffuser (as in the case of centrifugal machines). The classification and use of compressors are described in the next section.

The selection of compressors for different applications is a crucial issue in the process industry. It is usually the most expensive piece of equipment and has dominant influence on cycle efficiency. The common types of compressors used in industry are reciprocating, twin screw, single screw, centrifugal, scroll and rotary vane. Compressor manufacturers are used to having a large market potential. Probably all types of compressors can be improved over what is available in the market today; but the potential return must justify the expense of research and development to achieve the improvement.

The twin screw compressor is popular and constitutes a substantial percentage of all positive displacement compressors now sold and currently in operation. Their rapid acceptance over the past thirty years is due to their relatively high rotational speeds compared to other types of positive displacement machines which make them compact, their ability to maintain high efficiencies over a wide range of operating pressures and flow rates and their long service life and high reliability.

1.1 Classification of Compressors

Compressors are broadly divided into positive displacement and dynamic type. The detailed classification of compressors is shown in Figure 1.1. The dynamic principle is utilized in the multi blade dynamic compressors. These are further sub

divided into centrifugal and axial flow types. In axial compressors, the velocity of fluid can be supersonic which is converted to a pressure head by diffusers. Positive displacement compressors are further subdivided into piston compressors in which the gas volume changes due to the action of one or more reciprocating pistons moving axially in the cylinder and Membrane compressors in which the volume variations are affected by deflection of an elastic partition. In the positive displacement rotary compressors, the compression is produced as the result of reduction of volume inside the rotating elements such as helical screws.

Compressor Specifications:

Most of the compressors are specified with the following parameters:

- Mass Flow Capacity.
- Inlet / Suction Pressure.
- Discharge / Operating Pressure.
- Inlet Temperature.
- Speed.
- Type and Volume of Gas Handled.

Dynamic compressors

Dynamic compressors are sub divided into radial flow (centrifugal) and axial flow compressors.

(a) Centrifugal Compressor

It consists of a vaned rotating disk or impeller which is used to force the gas up to the rim whereby the speed of the gas is increased. The turning of the impeller causes compression of the gas. The compressor also incorporates a diffuser as the converting element from velocity to pressure head. Centrifugal compressors are usually stationary compressors. They are used for heavy duty applications in industry. They are most suitable to applications where the pressure requirement is moderate. They are widely used in large snow-making works especially in ski resorts and also in gas turbine engines. They are also used as turbochargers and superchargers in internal combustion engines. The large air separation industry also

uses centrifugal compressors. The advantages of the centrifugal compressor are its ruggedness and relatively low cost of manufacturing. The disadvantages are its large frontal area and its relatively poor pressure ratio when compared with other types of compressors.

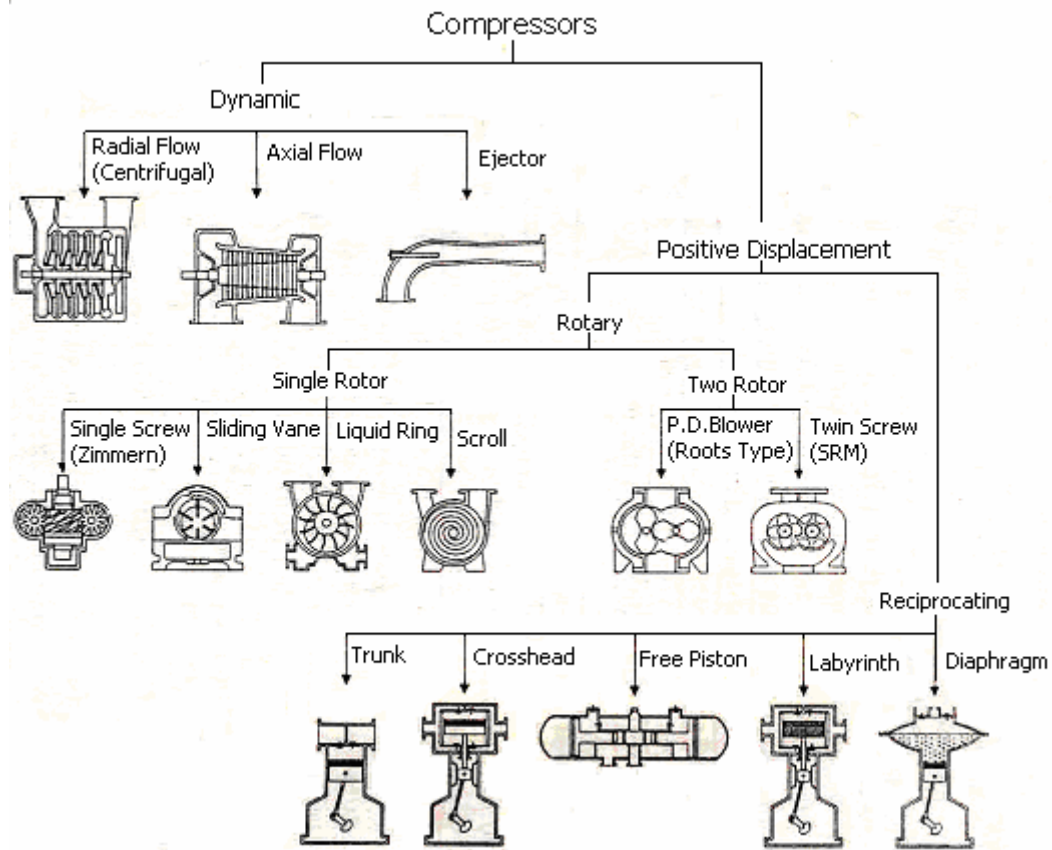


Figure: 1.1: Classification of compressors [1].

(b) Diagonal or Mixed-Flow Compressor

A mixed flow is similar in construction to that of the centrifugal compressor. It differs in that the axial and radial components are available outside the rotor. It incorporates a diffuser for turning the diagonal flow into the axial direction.

(c) Axial Flow Compressor

The axial flow compressor consists of rows of alternate rotating (rotor) and fixed (stator) blades. A row of rotors followed by a row of stators is known as a

stage and there may be many stages attached to a single shaft. Gas is drawn usually by the spinning of the numerous fans on the shaft. A series of divergent and convergent ducts form the stator. Axial flow compressors are mostly available as multi staged type. They are used in applications that require very high flow such as large gas turbine engines.

Positive Displacement Compressors

In positive displacement compressors, the compression is realized by displacement of a solid boundary and preventing the fluid by this solid boundary from flowing back in the direction of pressure gradient. These are further classified into reciprocating and rotary types.

(a) Reciprocating compressor

As the piston moves for the downward stroke, discharge valves are forced shut. The gas is then sucked into the cylinder by the suction pressure. During upward stroke the suction valves are forced shut and the gas is moved into the discharge valve. The spring loaded valves are self operated by the pressure in the cylinder.

Advantages

- High efficiency, particularly when new and after overhauls.
- Possibility of very high discharge pressures.

Disadvantages

- Requires high maintenance.
- Fixed speed.
- Creates noisy atmosphere.
- Damping requirement to arrest vibration.
- More moving parts.
- Efficiency drops off between overhauls.
- High cost.

Applications

There are no rigid rules for the application of reciprocating compressors. The power ranges between 5 and 30 HP are used for automotive work especially for intermittent duties. Compressors of greater power such as 1000 HP are meant for large process applications.

(b) Rotary Compressors

The compression is produced as a result of the positive action of rotating elements such as helical screws, scrolls or vanes. Rotary positive displacement compressors are classified into single rotor and two rotor compressors. Single rotor compressors are further classified into single screw, sliding vane/rotary vane, liquid ring, and scroll compressors. Similarly, the two rotor compressors are divided into roots blower and twin screw compressors.

(I) Single Rotor Compressor

The single rotor compressors are further classified as below.

(i) Single-screw compressor

This type of compressor uses a single main screw rotor meshing with two gate rotors with matching teeth. The main screw is driven by the prime mover, typically an electric motor. The gate rotors may be made of metal or a composite material. The screw-like grooves gather gas/vapours from the intake port, trap them in the pockets between the grooves and compressor housing, and force them to the discharge port along the meshing path. This action raises the trapped gas pressure to the discharge pressure. Single screw compressors usually employ hermetic or semi-hermetic designs for higher efficiency, minimum leakage and ease of service.

(ii) Rotary Vane Compressor

It consists of a single rotor accommodated in a cylindrical housing. As the rotor rotates, the vanes of the rotor are thrown off against the housing wall. The bearings and vanes are lubricated with oil. The segments created by the vanes change in shape and volume during a cycle. This results in the compression of the

trapped gas. Ports are used for intake and exhaust of the gas at the minimum and maximum pressure positions.

Advantages

- ❖ Simplicity in design.
- ❖ Slow rotational speed results in low wearing of parts.
- ❖ Moving parts are only the rotor and the vanes.
- ❖ The rotor can be directly driven.
- ❖ Gas discharge rate is not pulsed.
- ❖ No additional foundation required.
- ❖ Vibration free operation.
- ❖ Valveless operation.
- ❖ Requires little maintenance.

Disadvantages

- Close contact between the compression gas and lubricating oil.
- Lubrication oil necessitates disposal.
- Low pressure capability

Applications

- Landfill gas gathering and boosting.
- Digester mixing.
- Fuel gas boosting.
- Flare gas recovery.
- Wellhead gas compression.

(iii) Liquid ring compressor

In a liquid ring compressor the rotor is positioned centrally in an oval-shaped housing. Upon rotation, which proceeds without metal to metal contact, a ring of liquid is formed that moves with the rotor and follows the shape of the housing. At the two points of the closest proximity between the rotor and the housing, the liquid completely fills the chambers of the rotor. As rotation proceeds, it follows the contour of the body and recedes again, leaving spaces to be filled by the incoming gas. These spaces are connected via the cone porting to the inlet of the compressor.

As a result of the suction action thus created, gas is pulled into the compressor. As the rotation progresses, the liquid is forced back into the chambers, compressing the gas. This gas is forced out of the discharge port and then leaves the compressor via the outlet flange.

The compressor is fed continuously with liquid which serves to seal the clearances between inlet and discharge ports and removes the heat of compression. This liquid leaves the compressor together with the compressed gas and is separated from the gas in a discharge separator.

Advantages

- ♦ Virtually no gas temperature rise
- ♦ Low wear
- ♦ Reduced maintenance costs
- ♦ Reduced operation downtime
- ♦ Investment cost savings
- ♦ High operation safety
- ♦ Low noise
- ♦ Environment operation

Applications

- For compressing explosive gases
- When gases tend to polymerise or otherwise react under rising compression temperatures
- When oil free compression is required
- For vapour recovery applications
- For applications requiring tolerance to liquid carry over
- When gas scrubbing is desired
- For corrosive services

(iv) Scroll compressor

The scroll compressor consists of two scroll members each with a spiral shaped wrap and corresponding end plate. The working mechanism of scroll compressor is shown in Figure 1.2. The two scroll members are placed at the top of the compressor housing. The top scroll member is fixed to the compressor housing

while the lower member is free to orbit about the centre of the fixed scroll. The moving scroll is driven by a motor and is attached to the motor shaft. As the moving scroll orbits about the fixed scroll, the wraps of the two scroll members form lines of contact. These lines of contact form crescent shaped symmetric pockets. The gas enters the first pair of symmetric pockets at the outer periphery of the scroll set and continues to travel towards the centre. As the gas moves towards the centre, the volume of the pockets decreases thus compressing the trapped gas.

Once the gas reaches the centre of the scroll set, the tip of the moving scroll begins to uncover the discharge port located in the centre of the endplate of the fixed scroll member. Once the discharge port becomes uncovered, the discharge process begins. Because of the scroll's geometry, no discharge valve is needed; instead the tip of the moving scroll wrap uncovers the discharge port. Scroll compressors are used refrigeration and air conditioning systems as well as supercharger in automotive operations. Pulsed output is obtained which discourages its usage in industry.

(v) Roots Blower

It is a positive displacement compressor with two lobed impellers, each resembling the figure of "8". The two rotors are mechanically linked via gears such that they rotate in opposite directions. The figure of "8" shape allows the impellers to be close to but never in contact with each other and the compressor walls at every position of their rotation. The close tolerances of the components allow the impellers to move without a lubricant if required.

Roots blowers are typically used in applications where a large volume of gas must be moved across a relatively small pressure differential. This includes low vacuum applications, with the roots blower acting alone, or use as part of a high vacuum system in combination with other compressors. Roots blowers are also used as superchargers.

(II) Twin Screw Compressor

It is a positive displacement machine that uses a pair of intermeshing rotors housed in a suitable casing instead of piston to produce compression. In the double screw compressor, each rotor comprises of a set of helical lobes affixed to a shaft.

One rotor is called the male rotor and the other rotor is the female rotor. The number of lobes on the male rotor, and the number of flutes on the female, will vary from one compressor manufacturer to another. However, the female rotor will always have numerically more valleys (flutes) than the male rotor lobes for better efficiency. Either an electric motor or an engine drives the male rotor.

Twin-screw compressors are basically classified into oil free and oil injection types. Single stage oil free machines are used for low-pressure devices and oil-injected compressors are used for moderate pressure machines. Multistage designs are used for the compressors working with higher pressure ratio. Oil injection provides cooling, lubrication and sealing, thus permitting higher pressure ratio.

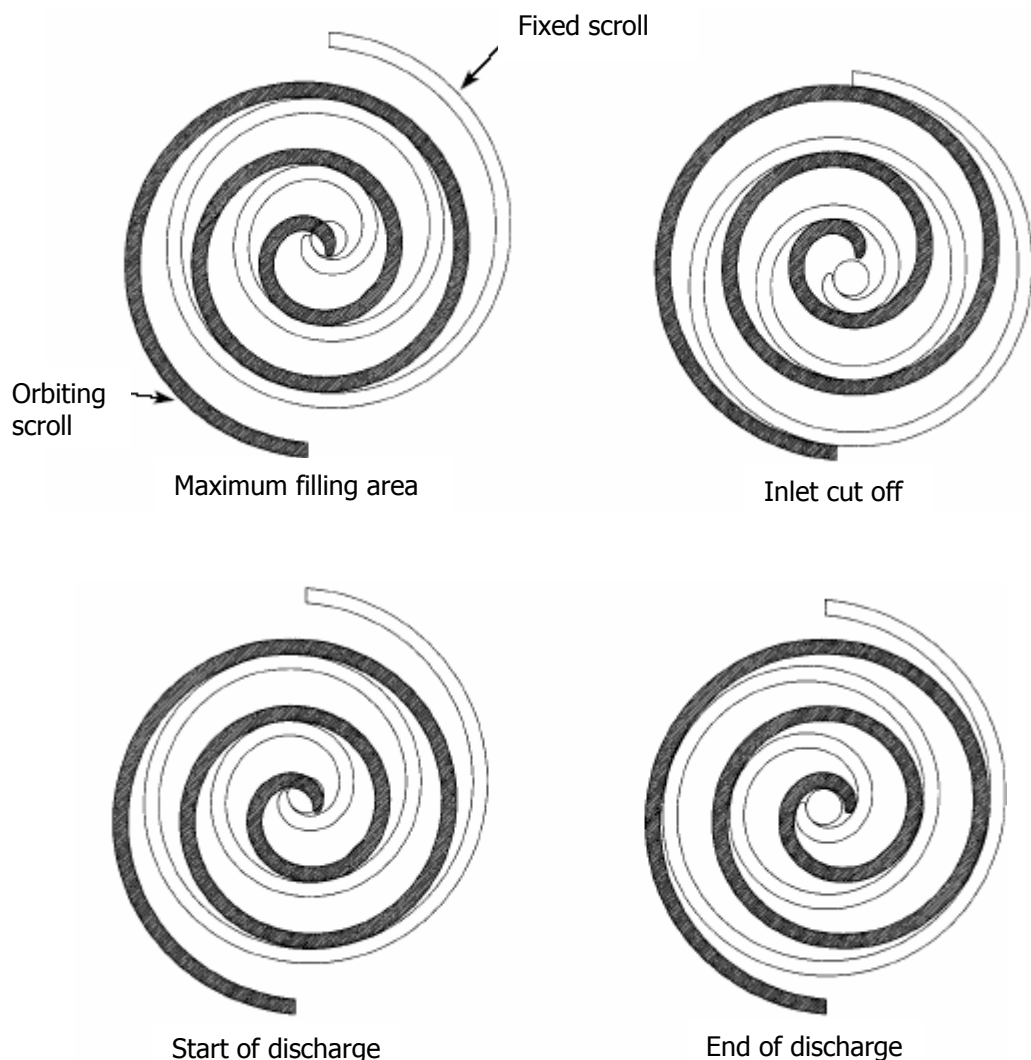


Figure 1.2: Operating principle of an orbiting scroll compressor (moving scroll is orbiting clockwise)

(i) *Oil free compressor*

Oil free operation implies that the gas compression space is entirely free from oil contamination. These compressors are suitable for compression of a wide variety of gases requiring relatively low pressure ratios at fairly constant volume flow rates. These are particularly suitable for handling contaminated, particle-laden, polymerizing, or explosive gases.

(ii) *Oil Injected compressor*

In an oil injected twin-screw compressor, the lubricating oil is deliberately injected into the gas stream to absorb the heat of compression. This enables much higher pressure ratio in a single stage without intercooling and provides significant protection against corrosive gases. Also, it permits the use of stepless capacity control by slide valve. No timing gears are required and the male rotor usually drives the female rotor through an oil film between the intermeshing profiles.

Twin-screw oil injected machines are used today for different applications both as compressor and expander. They operate on a variety of working fluids. The working fluid may be gas, dry vapour, or multi phase mixture with phase change taking place within the machine. Presently, screw compressors hold an important position in the industrial refrigeration and compression field. It occupies a position alongside reciprocating and centrifugal types as a standard choice for refrigeration compressors.

The asymmetric rotor profile of oil-injected type screw compressors reduces the leakage path cross section resulting in increased efficiency. The helical screw compressor is the only rotary unit that operates at tip speeds in excess of 0.12 Mach [2]. These machines develop pressure 7.3 times more than that of a centrifugal compressor operating at the same tip speed [3]. While the performance characteristics and flexibilities of this type machine approach that of the piston compressor, it has compression efficiency comparable to that of a centrifugal machine. Its maintenance cost also compares favourably with that of the centrifugal machines, which is less than one third of the cost of maintaining piston compressors. A schematic view of a pair of twin-screw rotors is shown in Figure 1.3.

The commercial range of oil injected screw compressors available today covers outer diameter of the male rotor between 75 and 620 mm. They produce

between 10 m³/hr and 10,000 m³/hr of gas flow rate for refrigeration and air conditioning applications and up to 60,000 m³/hr for general purpose applications. Pressure ratios of 3.5 for dry compressors and up to 15 for oil injected twin-screw compressors are available in the market. The average pressure difference is up to 15 bar but maximum pressure difference some times exceeds 40 bar [1]. Typically, the volumetric efficiency of oil injected compressor exceeds 90%.

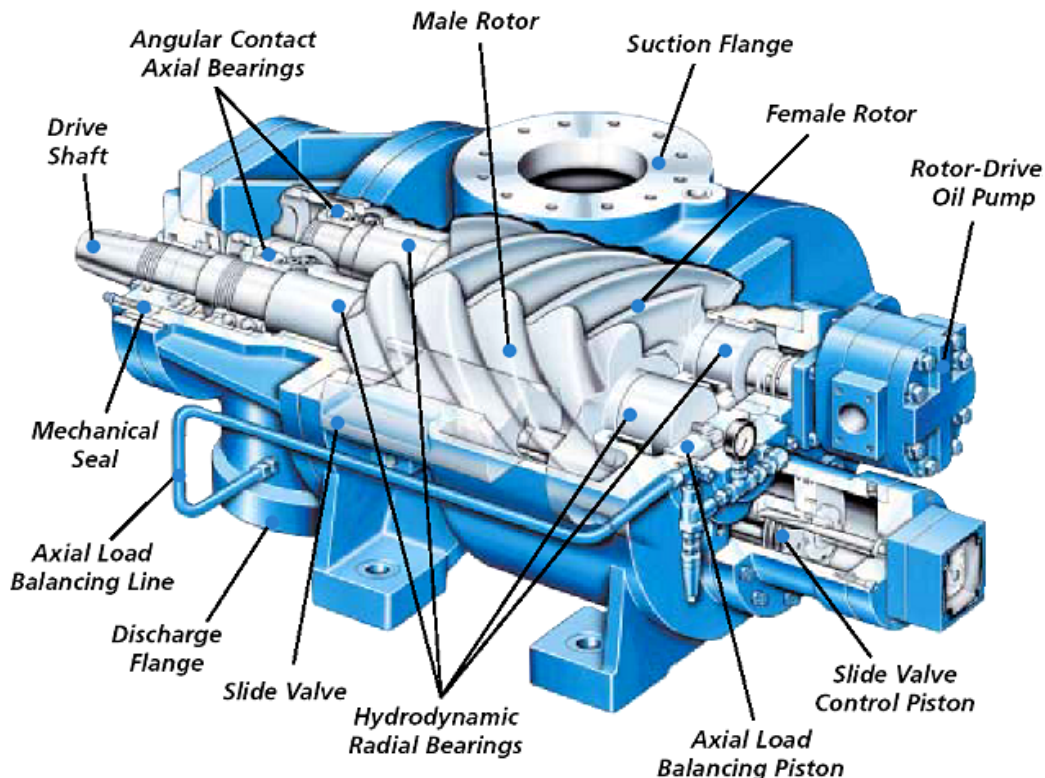


Figure 1.3: Isometric cutaway drawing of Twin-Screw compressor [4]

1.2 *Twin-Screw Compressor Applications and Advantages*

Oil injected twin-screw compressor offers several advantages over comparable machines:

- (i) Simple maintenance, low maintenance cost and Low weight.
- (ii) High reliability and long compressor life, full use of drive horsepower.
- (iii) Low operating expense, medium purchase price.
- (iv) High compression ratio (up to 16 per stage).
- (v) Operation at low suction pressure up to 66 cm Hg vacuum.

- (vi) Reduced package cost due to compactness.
- (vii) Absence of reciprocating components and low internal forces, allowing the compressor to run at higher tip speeds, resulting in more compact unit.
- (viii) The continuous flow of cooling lubricant permits high single stage compression ratio.
- (ix) High speeds and compression ratios help to maximize the available power efficiency.
- (x) Less sensitive to liquid slugging.
- (xi) Suitable for wide variety of gases.
- (xii) High ride quality and controllability.
- (xiii) High speed operation over a wide range of operating pressures and flow rates with high efficiencies.

Drawbacks

- (i) High volume of lubricant injected into a conventional screw compressor reduces power efficiency due to the oil compression phenomenon and increased stirring loss due to the presence of oil.
- (ii) Power consumption during unloading operation is normally higher than that of reciprocating type.
- (iii) Issues such as rotor deflection, casing strength, intrinsic leakage and technological deficiencies.

Applications

The rotary dual screw compressor package is ideal for numerous gas compression applications including fuel gas boosting, general construction and road building purposes and operating pneumatic tools. It has become a better choice in textile, electronic and automotive sectors, iron and steel, food and beverage, tobacco sector and petroleum refining and petrochemicals, vapour recovery, land fill and digester gas compression and propane/butane refrigeration compression. It can be applied for compression of corrosive and/or dirty process gas, poly-alpha-olefins, poly-glycols, synthesized hydrocarbons and liquefaction of gases.

A rotary compressor package can also be used to upgrade existing reciprocating compressor installations. By boosting low suction pressure, capacity may be increased at minimum cost with continued use of existing reciprocating

equipment. If an application requires large volume flow rate at low suction pressure, but discharge pressures greater than what the screw machine can provide, a combination of screw and reciprocating units with a common driver can be a better solution.

Materials

Oil injected screw compressors are built with different materials for its components.

(i) Casing

Gray cast iron is generally used to manufacture casing for air and inert gases. Cast S.G iron is used for compression of hydrocarbon and other hazardous gases, where site conditions/specifications permit a less expensive material than steel. Cast carbon steel is necessary for clean hydrocarbon and other hazardous gases and even sour and/or wet gases.

(ii) Rotors

The rotors are normally made of ferrous materials. Aluminium and plastics are feasible in certain applications. Forged carbon steel is used for air and most gas applications. In many cases, S.G (nodular) iron is also acceptable. Forged high alloy steel is preferred (typically 12-13% Cr, 4-5% Ni) for corrosive, sour and wet gases.

1.3 Geometry of Screw Compressor

The rotors of a twin-screw compressor are a form of helical gears with parallel axes and a uniform lead. The rotors make line contact and the meshing criterion in the transverse plane perpendicular to their axes is the same as that of spur gears. Two intermeshing rotors are housed in a suitable casing to achieve compression. Different views of compressor rotors and casing are shown in Figure 1.4 for better understanding of the geometry.

The rotors intermesh in the dual bores of a one-piece cylinder. The space between any two successive lobes of each rotor and its surrounding casing forms a separate working chamber of fixed cross sectional area. The length of working chamber varies as rotation proceeds due to displacement of the line contact between

the two rotors. The volume is maximum when the entire length between the lobes is unobstructed by the meshing contact between the rotors and has a minimum value of zero when there is full meshing contact with the second rotor at the discharge end. The two meshing rotors effectively form a pair of helical gear wheels with their lobes acting as teeth. The casing provides gas inlet passages, oil injection points, and compression zone and discharge ports. Rolling element bearings located near the ends of the rotor body support the screws.

Majority of screw compressors are still manufactured with four lobes in the main (male) rotor and six lobes in the gate (female) rotor with the same outer diameter. This configuration is a compromise having favourable features for both dry and oil injected compressor applications and is used for air and refrigeration or process gas compression. However, other configurations like 5/6 and 5/7, and more recently 4/5 and 3/5, are becoming increasingly popular. A configuration with five lobes in the main rotor is suitable for higher pressure ratios, especially when combined with larger helix angles. The 4/5 arrangement has emerged as the best combination for oil injected applications with moderate pressure ratios. The 3/5 configuration is favoured in dry applications, because it offers a high gear ratio between the gate and the main rotors, which may be taken advantage of to reduce the required drive shaft speed.

However, the efficient operation of screw compressors is mainly dependent on proper rotor design. Most commonly used rotor profiles are shown in Figure 1.5. An additional and important requirement for successful design of all types of compressors is an ability to predict accurately the effects of the change in any design parameter on performance. The main requirement of these types of compressors is to improve the rotor profile so that the flow area through the compressor is maximized while the internal leakage areas are minimized. Also, the internal friction due to relative motion between the contacting rotor surfaces should be made as small as possible.

Compressor designs have evolved gradually over half a century and the present trend is to realise smallest possible machines still meeting the required performance. This means, the rotor tip speeds are to be as high as possible with the limits imposed by efficiency requirements. Rolling element bearings are to be used to permit the smaller clearances than journal bearings. Similarly the ports are to be

made as large as possible to minimize suction and discharge gas speeds, and consequent pressure losses.

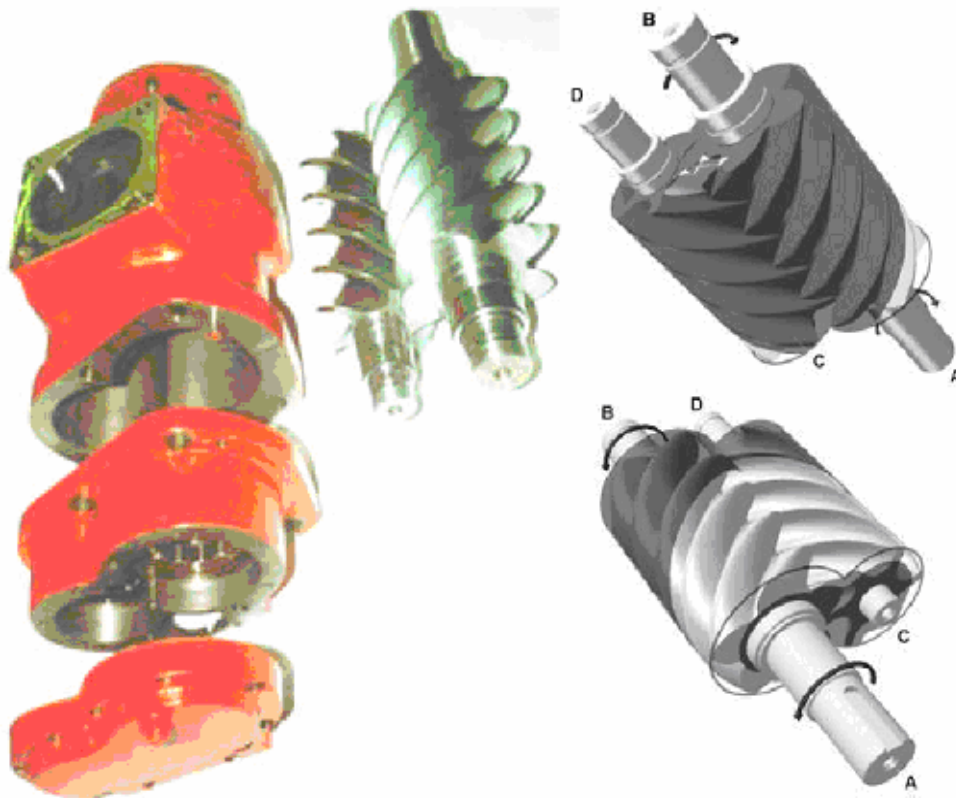


Figure 1.4: Different views of meshing screw rotors and casing [5]

An efficient screw compressor needs a rotor profile which has a large flow cross-section area, short sealing line and small blowhole area. The larger the cross sectional area, the higher is the flow rate for the same rotor size and rotor speed. Short sealing lines and smaller blowhole area reduce leakages. Higher flow rates and smaller leakage rates increase compressor volumetric efficiency. This, in turn, increases the adiabatic efficiency because less power is wasted to compress internally recirculated leakage gas.

Precision manufacture permits rotor clearances to be reduced, but the likelihood of direct rotor contact is increased despite oil flooding. Hard rotor contact leads to the deformation of the female rotor due to increased contact forces, and ultimately leads to rotor seizure. Hence, the screw profile should be designed in such a manner that the risk of seizure is minimized. The clearance between the rotor and

the housing, especially at the high-pressure end, must be properly selected. This in turn requires either expensive bearings with smaller clearances or cheaper bearings with their clearances reduced to an acceptable value by preloading.

Oil injected screw compressor which operates with high pressure difference is heavily loaded by axial and radial forces, which are transferred to the housing by the bearings. Rolling element bearings are normally chosen for small and medium screw compressors and these must be carefully selected to obtain a satisfactory design. Usually two bearings are employed on the discharge end of the rotor shafts in order to absorb the radial and axial loads separately. The contact force between the rotors is determined by the torque transferred between them and is significant when the rotors make direct contact. It is relatively small when the compressor drive is through the main rotor. If the drive is through the gate rotor, the contact forces will be substantially larger and as far as possible, this arrangement should be avoided.

The oil used for sealing the gaps is also used for bearing lubrication. Generally the oil supply to the bearings is separate to minimize frictional losses. Oil is injected into the compressor chamber at the place where thermodynamic calculations show the gas and oil inlet temperatures to coincide. The position is defined on the rotor helix for locating the injection hole located so that the oil enters tangentially in line with the female rotor tip to recover the maximum possible oil kinetic energy.

To minimize the flow losses in the suction and discharge ports, the suction port is positioned in the housing in a manner that lets the gas enter with the fewest possible bends and the gas approach velocity is kept low by making the flow area as large as possible. The discharge port size is determined by estimating the built-in-volume ratio required for optimum thermodynamic performance. The discharge port position is so adjusted as to reduce the exit gas velocity to minimum to obtain the lowest internal and discharge flow losses. The casing should be carefully dimensioned to minimize its weight containing reinforcing bars across the suction port to improve rigidity at higher pressures.

1.4 Design parameters

The performance of a screw compressor depends on a large number of design parameters. Knowledge of the effect of these parameters can help a designer

select the best performing machine for a given application. It can be improved considerably by proper selection of some of the important design parameters which influence the performance.

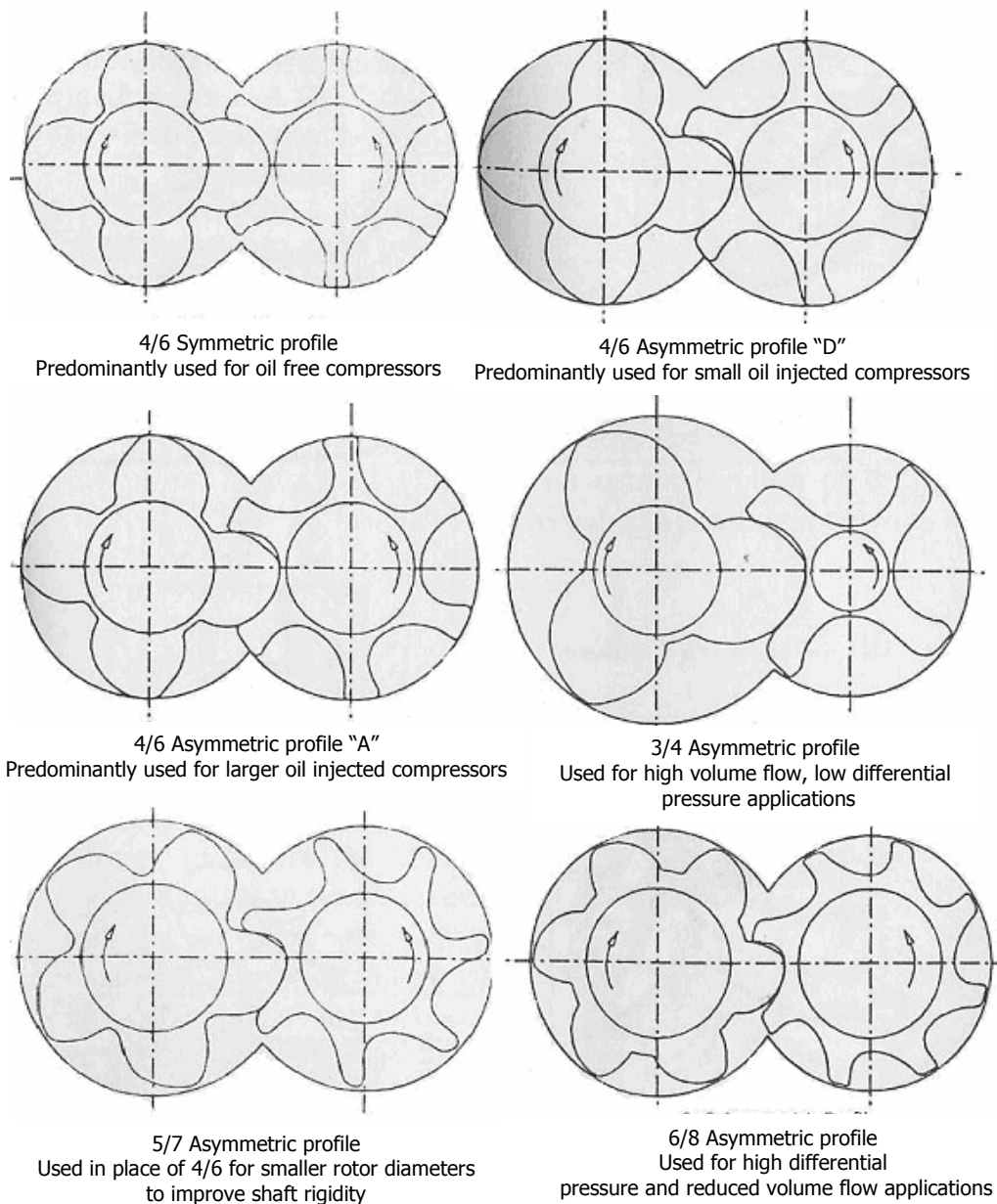


Figure 1.5: Illustration of the most commonly used rotor profiles [1]

Cycle of operation

The compression process in a screw compressor is similar to that of a reciprocating compressor, but it does not suffer re-expansion at the end of

compression cycle from clearance volume. Its p-v diagram is, therefore, very simple and it is similar to the reciprocating compressor without clearance volume as shown in Figure 1.6.

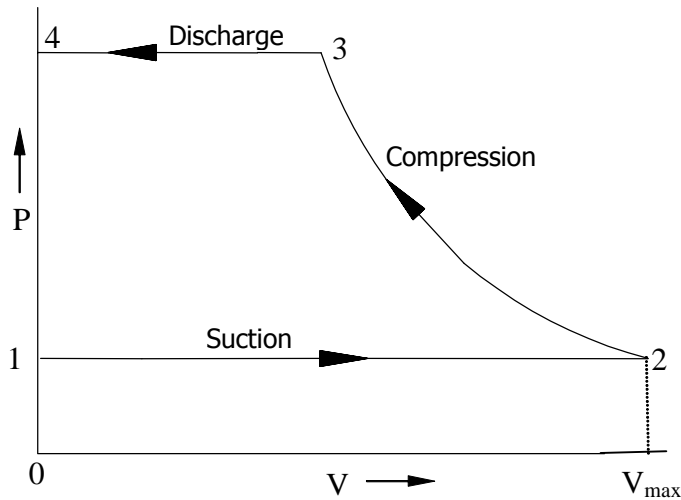


Figure 1.6: p-v diagram for reciprocating and screw compressor.

The process 1-2 is the suction process which takes place for one revolution of male rotor. The inducted gas volume of one pair of grooves is the sum of the volumes of male and female rotor grooves. Unlike that in a reciprocating compressor, the suction process in the screw compressor is simultaneously carried out with compression and discharge processes. While a part of a groove is in the suction stage, the rest of the groove undergoes compression. The phenomenon is depicted in Figure 1.7 on a p versus θ_m plot for better understanding, θ_m being the angular rotation of the male rotor. The figure shows that the compression and discharge processes occur simultaneously, the suction process for one revolution of the male rotor starting from the entrapment point '1' and ending in '2'. The compression process occurs between points '2' and '3'. The point '3' is the beginning of discharge process where the pair of compression cavities of the male and female rotors uncovers the discharge port. The point '3' determines the built-in volume ratio on the V-axis and built-in pressure ratio on the P-axis of p-v diagram.

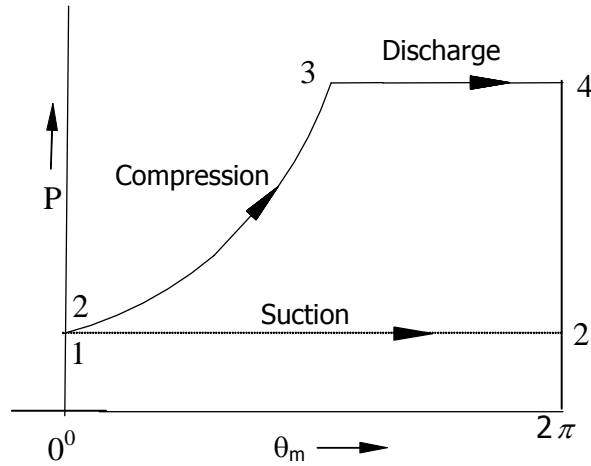


Figure 1.7: P- θ_m diagram for twin-screw compressor.

Built-in volume ratio and internal pressure ratio

Unlike reciprocating compressors, the screw compressor does not have valves. The location of the discharge port determines the maximum discharge pressure level that can be achieved in the screw threads before the compressed gas is pushed into the discharge pipe. Being a positive displacement machine, the pressure rise across the compressor is determined by the built-in volume ratio. This volume index (v_i) determines the internal pressure ratio of the compressor. For gas compressors, an approximation of the internal pressure ratio (π_i) is obtained from the relationship $\pi_i = (v_i)^k$ [6]. Only the suction pressure and the internal volume or built-in volume ratio determine the internal pressure level in the trapped pocket before the gas enters the discharge port.

Compressors that have only axial ports will have fixed volume ratios. The built-in volume ratio can be changed by changing the size or location of the discharge port. Another way to change the volume ratio is with the help of a slide valve. For these compressors, the volume ratio can be varied according to requirements while the compressor is in operation, to get better part-load efficiency. A smaller discharge port also increases the volume ratio by holding the gas inside the flute space longer than larger that held by a discharge port. The longer the gas is held inside the flute space before it is allowed to communicate with the discharge line, more rotation, more volume reduction and more pressure ratio occur.

For best efficiency, the volume ratio should be so set that the internal compression ratio matches the system compression ratio. If the internal compression ratio does not match the system compression ratio, the result is either over compression or under compression. If the internal volume ratio of the compressor is too high for a given set of operating conditions the discharge gas remains trapped longer, leading to pressure rise above the discharge pressure. This is called over compression and is represented in the p-v diagram in Figure 1.8. In this case, the gas is compressed to a value above the discharge pressure and when the discharge port opens, the high pressure gas in the screw flutes expands out of the compressor into the discharge line. This takes more energy than that required if the compression had been stopped sooner when the internal pressure was equal to the system discharge pressure.

If the internal volume ratio is too low for a given set of operating conditions, the gas pressure in the trapped volume remains below the desired discharge pressure. In this case, the discharge port opens before the set internal pressure of the compressor pocket reaches the system discharge pressure. The high pressure gas from the discharge line flows back into the flute space, equalizing the flute pressure that must be compressed again. This has been shown in Figure 1.9. Extra work is required to compress the same gas twice. Generally over-compression is less efficient than the under-compression. In over-compression, extra work is done on the entire flow stream, while in under-compression, extra work is done only on the gas that backflows into the flute space from the discharge line.

Maximum inlet (suction) pressure

Due to the availability of high volume ratio, the internal pressure ratio (π_i) in a screw compressor can be high. If the maximum allowable design discharge pressure is $P_{d(max)}$, the maximum permitted inlet/suction pressure $P_{s(max)}$ may be estimated by the relation given by Stocker [7].

$$P_{s(max)} = \frac{P_{d(max)}}{(V_i)^k} \quad (1.1)$$

The index k being the ratio of specific heats of gas

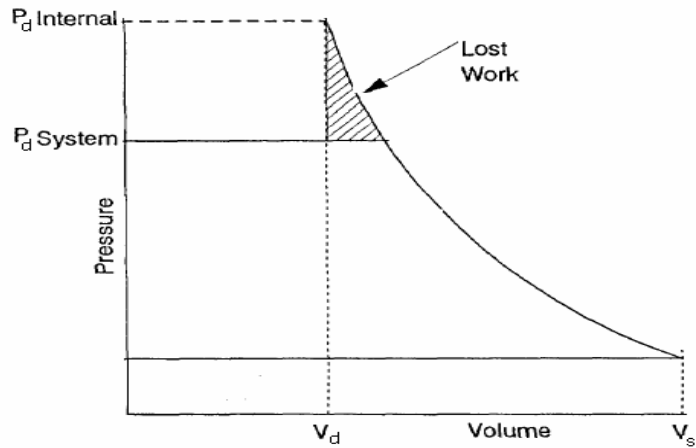


Figure 1.8: Example of over compression [8]

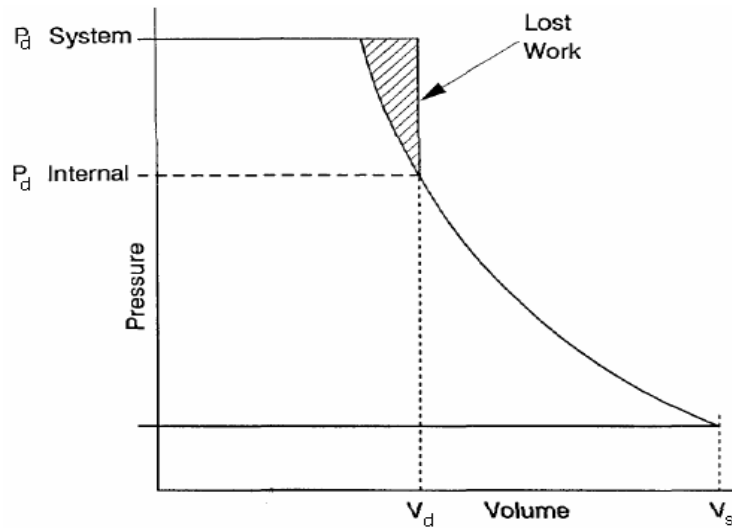


Figure 1.9: Example of under compression [8]

Oil injection considerations

For optimum efficiency, internal clearances within the screw compressor must be kept as small as possible. However due to the presence of large quantity of oil during compression process, there is less chance of contact between the rotors and casing. As the oil serves as a sealant, the rotor radial clearance to diameter ratio can be selected suitably for the oil gas mixture. It has been seen that the presence of more oil in the compression chamber, covering all the metal surfaces, acts as a

significant barrier to corrosion by the gas to be compressed. This feature has permitted the compressor to be used with gases containing sulphides and chlorides.

Another important feature of oil injected compressors is that the oil acts as a noise damper. This provides major advantages over the oil free type compressor. It is quite common in oil injection machines that the oil is supplied through a single connection and from there it is fed to the various points of use. As the injected oil acts as a coolant, the main rotor can be allowed to rotate at higher tip speeds.

Rotor circumferential velocity (tip speed)

The efficiency loss due to oil shear resulting in foaming and churning is a major design concern in oil injected compressors. As a result, these compressors are operated at lower speeds than oil free compressors. For optimum efficiency, circumferential velocity of oil screw compressors should preferably be in the range of 30-35m/s for larger compressors and 20-30m/s for smaller ones.

Number of lobes and compressor size

Based on research and experience, it has been proved that the smaller number of lobes increases the rotor volume and thus the air end size for a given displacement. Also, there is a distinct difference between female and male rotor lobes, $n_f - n_m = 2$ and $n_f - n_m = 1$ profiles. The former require considerably larger rotors for a given displacement. This happens, because in one revolution of the male rotor, two of the female cavities are idle and not taking part in the suction or compression process for the same displacement.

Number of lobes and rotor stiffness

Rotor stiffness is an important parameter since it may limit the maximum operating pressure. As the stiffness is a strong function of the groove depth on rotors, the profiles with $n_f - n_m = 2$, the female rotors are almost equal in size to the male rotors and thus inherently much stiffer.

Number of lobes and discharge port velocity

The discharge port velocity generally decreases with increase of number of lobes. This means that the discharge port losses are higher for profiles with less

number of lobes. Also, at higher tip speeds, where discharge port losses become significant, the profiles with a lower number of lobes will have poor performance.

Lobe combination

Profiles with lobe difference of '1' have marginally better performance than those with differences of '2' at all tip speeds. Based on experimentation and analysis [9] it has been proved that the 5/6 profiles have all the attributes of a good lobe combination in terms of performance, strength, and size. The performance of 3/4 combination profile at high tip speed can be improved considerably by early opening of the discharge port. Thus each design should be optimized according to the individual application.

Wrap angle

The decrease in male wrap angle has two effects: the discharge port size increases and the overlap constant decreases. When the wrap angle becomes large, the blowhole expands and the discharge port contracts. Therefore, the internal leakage mass which will re-circulate in the grooves increases and the flow resistance across the discharge port becomes higher. It is evident that the indicated torque increases as the wrap angle becomes smaller, corresponding to the increase in leakage losses. The volumetric efficiency does not vary much as the wrap angle changes. However, the adiabatic efficiency decreases as the wrap angle decreases.

L/D ratio

The relative merits of equal and unequal rotor diameters are mostly a function of manufacturing considerations than the design. Only profiles with lobe combinations differing by '2' can be practically made to have equal rotor diameters. This forces the manufacturer to select larger female addendum, which generally results in a large blowhole. A small L/D ratio means larger diameter rotors for a given displacement and larger leakage areas. At higher tip speeds, the leakage areas begin to have less influence and performance for all L/D ratios tend to cluster together. L/D ratios of 1.65 and 1.8 have shown the best overall performance.

Opening the discharge port early

One method of improving the performance is to open the discharge port early, i.e. to reduce the built in pressure ratio. This has the effect of increasing the discharge port size at the cost of some back flow compression. However, at higher tip speeds, gas inertia tends to overcome this back flow effect and significant improvement in performance can be achieved. The optimum built in pressure ratio and the other parameters such as discharge port opening angle is function of profile shape, number of lobes, wrap angle, and L/D ratio. Thus, it is necessary to determine the optimum opening angle according to profile shape and operating conditions.

Symmetric and asymmetric profiles

There have been extensive rotor profile developments in recent past. Symmetric rotor profiles are predominantly used for oil free screw compressors. The symmetrical circular arc profile in general has large blowhole area. It is always desirable that the rotor profile has smallest blowhole area. Oil injected screw compressor rotors have universally asymmetric rotor profile designs. These types of profiles have shorter sealing lines and smaller blowhole areas.

1.5 Performance Parameters

Efficient operation of screw compressor is mainly dependent on proper rotor design as discussed above. An important requirement for the successful design of a compressor is the ability to accurately predict the effect of design parameters on performance. Optimum rotor profile, oil injection rate and temperature may significantly differ when compressing different gases or vapours and when working in oil free or oil injected mode of operation.

It is difficult to calculate performance figures from first principles, as the oil is mixed with the gas being compressed. All currently available selection methods are based on empirical data derived from extensive testing on closed loop test rigs. The operation of any compressor requires an input of mechanical work. Most of this mechanical work is eventually converted to heat, principally the heat of compression and also mechanical and aerodynamic friction resulting from the operation.

The power and volumetric efficiencies of a compressor depend on inlet temperature of gas and coolant used. The volumetric efficiency mainly depends on internal leakage and inlet conditions of oil and gas. Although there are no pistons, valves or clearance volume to affect the filling ratio, the leakage losses along the rotors are important. The gas that leaks back to the suction side not only occupies space but also is at higher temperature. It is obvious that the clearances between the rotors and between the rotors and the barrel are important in minimizing the leakage. An increase in clearance of 0.01mm results in decrease of 1% in volumetric efficiency. The dimension of the oil stream also plays an important role on power performance.

The male rotor diameter and its rotational speed determine the tip speed. There is an optimum tip speed to achieve maximum efficiency for each built-in volume ratio. When the rotor speed is increased keeping the diameter constant, the displaced gas volume per unit time increases and the losses per unit gas volume become relatively smaller. As the losses due to friction and turbulence of the gas increase, the adiabatic efficiency decreases.

The relation between rotor length and diameter has influence on efficiency. Particularly at higher pressure ratios, the discharge port cross section becomes very small and shorter rotor gives less discharge losses. The shape of rotor cross section has considerable influence on the filling ratio. In fixed built-in volume ratio compressors, the compression process always ends at the same point irrespective of the line pressure. This happens when the inter lobe space comes into open contact with the discharge port.

1.6 Objectives of the Investigation

The present work aims at arriving at a better understanding of the suction, compression and discharge processes in a twin-screw compressor, particularly the thermofluid phenomena taking place inside the air end during these processes. For understanding the thermofluid processes taking place inside the screw compressor, it is necessary to build a numerical model and to validate it through experiments. Based on this understanding, it is proposed to explore the possibility of using commercially available low cost air compressors for compression of gases such as argon and helium used in cryogenic process plants.

For the development of a numerical model, the governing differential equations have been derived from control volume analysis for oil and gas separately. The leakage of gas and oil has been critically analyzed based on the analogy of flow through nozzle. Nozzle coefficients are adopted by matching experimental volumetric efficiency with that from a numerical model. The heat transfer coefficient between gas and oil is calculated from experimental observations on the variation of volumetric efficiency with suction temperature. The derivation of governing equations and the realistic implementation of leakage and heat transfer coefficient formulas are some of the important features of the numerical model.

Experimental studies have been carried out on two commercially available compressors using air, nitrogen, argon and helium as working gases. The effect of volumetric and adiabatic efficiencies on air compressor to compress other gases are evaluated and compared with the numerical model. The effect on efficiencies of the variation of suction pressure, suction temperature, oil inlet temperature, oil injection rate and pressure ratio are presented and the explanations are duly recorded.

To generate machine independent experimental data, two similar compressors with different capacities have been chosen. No experiment is complete without the estimation of the uncertainty in experimental error. An error analysis procedure has been adopted to estimate the uncertainty in the experimental data.

1.7 Organization of the Thesis

The thesis has been arranged into seven chapters. Chapter 1 (this chapter) deals with a general classification of compressors and introduction to the twin screw compressor in more detail and enumerates the objective of the present investigation. In chapter 2, a brief review of relevant literature covering theoretical and experimental studies has been presented. Chapter 3 covers the basic principles of operation, the suction and compression processes involved and the approach to mathematical analysis.

Numerical solution of the governing equations of the oil injected twin screw compressor is presented in chapter 4. The numerical model involves the variation of thermodynamic properties of gas and injected oil during compression and discharge process and also the estimation of power and volumetric efficiencies. The effects of interlobe clearance, blowhole area, quantity of injected oil and its temperature, wrap

angle etc are included in the simulation study. A description of the experimental apparatus and an uncertainty analysis are presented out in chapter 5. Experimental studies on commercially available 37 kW and 5.5 kW oil injected twin-screw air compressors are presented in chapter 6. Chapter 7, the final chapter, is confined to some concluding remarks and for outlining the scope of future work.

Chapter II

LITERATURE REVIEW

Around 1928 gear theories applicable to gas compression were developed by Nahuse of Tohoku University, Japan, and by the Russian engineer Novikov. These theories, however, were not used practically in compressor technology at that time. The first practical compressor was invented by Lysholm in 1934 and was mainly developed by SRM (Svenska Rotor Maskiner AB) of Sweden. Lysholm's compressor, which had a 3/3 profile combination, was produced in 1934. By 1937, a 4/6 Profile combination machine had been developed, and in 1938, such a compressor was manufactured in collaboration with Lysholm by James Howden & company of Glasgow, Scotland. Since the late 1950's, it has received practical applications for industrial use. The Scottish engineer Duncan Laing at James Howden & company tested the first operating screw machine in 1955.

In the 1960's, the twin-screw compressor came into existence, providing high capacity with reduced size and cost, together with an option to operate with high compression ratios allowing single stage systems for gas compression and low temperature refrigeration requirements. More recently, there has been a lot of research activity at the City University of London (at www.city.ac.uk) on methods to improve rotor design as well as volumetric and adiabatic efficiencies. Despite the rapid growth in screw compressor usage, public knowledge of the scientific basis of their design is still limited. In this chapter, relevant published literature is reviewed on the subject, focussing on design and performance.

Mathematical modelling, experimental validation, design of critical components, complete screw machine design, product development, training in machine design, advanced computerized design tools, machine process modelling, 2-D and 3-D computational fluid dynamics, modern experimental techniques,

computerized data acquisition, rotor and compressor optimization are the essential stages needed for appropriate screw compressor development [10-12]. Screw compressor rotors of various profiles can be conventionally manufactured today with small clearances at an economic cost and the internal leakages have been reduced to a small fraction of their earlier designs

Screw machines have been used today for different applications both as compressors and as expanders [11]. They operate on a variety of working fluids. The working fluid may be gas, dry vapour, or multi phase mixture with phase change taking place within the machine. These machines may operate oil flooded or with other fluids injected during compression process. In the field of air and gas compression, screw machines are continuously replacing reciprocating and vane compressors and a dramatic increase in its applications in the field of refrigeration compressors are expected in the next few years.

Comparative investigations between rotary and reciprocating compressors have been presented by Kaiser [13] and by Villadsen [14]. In their experimental investigations, various reciprocating and rotary compressors of comparable capacities have been analyzed on the basis of their thermodynamic and mechanical losses. The authors have explained the differences and have concluded that that both types of positive displacement compressors have their own merits, and that they complement each other to the extent that they may often be combined in one plant to obtain the most energy efficient installation under variable operating conditions. Different operational modes of twin-screw compressors have been explained by Sjöholm [15], who concluded that screw compressors could be adapted to every specific need without losing its favourable characteristics as a heavy-duty machine with high performance.

2.1 Compressor Design

Screw compressor designs have gradually evolved through history and the trend has been to realise as small machine as possible to meet the required performance. This means that rotor tip speeds are as high as possible with the limits imposed by efficiency requirements. Wherever possible, rolling element bearings should be used to permit the small clearances necessary instead of journal bearings. Similarly the ports are to be made as large as possible to minimize suction and

discharge gas speeds and consequent pressure losses. The oil injection port position on the compressor casing is to set at the point where thermodynamic calculations show the gas and oil inlet temperatures to coincide.

To minimize flow losses in the suction and discharge ports, the suction port should be positioned in the housing so as to let the gas enter with the fewest possible bends and the gas approach velocity kept low by making the flow area as large as possible. The discharge port size is first determined by estimating the built in volume ratio required for optimum thermodynamic performance. The casing should be carefully dimensioned to minimize its weight, containing reinforcing bars across the suction port to improve its rigidity at higher pressures. Bennewitz [16] suggests a comprehensive method for design, manufacture and quality control using computer assisted manufacturing.

Geometrical Parameters

Screw compressor rotor geometry plays a crucial role in its design and performance. For a given application, there are a number of design possibilities. But, normally only a few designs can adequately fulfil the basic requirements of reliability, high performance and low cost. The rotor profile not only affects the performance and torque distribution between the rotors, but also the axial and radial loads. The important geometrical parameters of a compressor and their influence on performance have been studied by Tang, Sjöholm and Singh [17-19].

Zhang and Hamilton [20] studied the effect of main geometric characteristics such as compression volume curve, sealing line length, flute area, wrap angle and blowhole area. Mathematical models of these parameters were formulated to develop the manufacturing software. Tang and Fleming [17] studied the effect of relative blowhole area and relative contact line length on performance and suggested some methods for geometrical parameter optimization.

Singh and Bowman [9] examined the effect of some of the geometrical parameters like number of lobes, wrap angle, L/D ratio and opening of discharge port early for a particular profile shape. The authors focussed more attention on fundamental aspects of the design process. Number of designs was created and their dimensions were normalized to male rotor diameter of the 5/6 profile to get identical displacement per unit revolution in all types of rotors. The authors applied

generalized mathematical modelling to calculate the geometrical characteristics and presented the results. It has been observed from the results that the contact or interlobe sealing line length increases strongly with the number of lobes, which has an adverse effect on performance at low male rotor tip speeds and high pressure ratio.

A parametric study on twin screw refrigeration compressor performance has been carried out numerically by You *et al* [21] for optimum rotor geometry with four commonly used lobe combinations and five different lengths to diameter ratios and wrap angles. The four lobe combinations considered in the study are 4/5, 4/6, 5/6, 5/7; the length to diameter ratio ranges from 1.0 to 2.2, and the male wrap angle ranges are from 250° to 300° . Apart from performance parameters, factors like rotor deflection, bearing load and its life and inter rotor contact forces are also included. The influence of geometrical parameters has been discussed and suggestions on choosing optimum parameter combinations presented. Female rotor deflection has been calculated since it is several times higher than that of the male rotor. It has been found that the 4/5 combination is an excellent choice since it has the smallest size and lowest weight, while the 5/6 design has the lowest input torque. The results, however, show that these two combinations have relatively larger deflections than the 4/6 and 5/7 combinations.

The authors have concluded that 4/6 and 5/7 profile combinations are the better choices for high pressure applications. Also, the 5/6 combination showed relatively higher isentropic indicated efficiency for L/D ratios up to 1.7. The 5/7 combination showed that the performance of this combination is very close to that of the 5/6 combination for L/D ratio above 1.7, and that their deflections are much smaller as shown in Figure 2.1. It has been concluded that the 5/6 combination is more appropriate for L/D ratio above 1.7, particularly for high pressure ratio applications.

Rotor Profile Generation

Any design process can be made more reliable with mathematical modelling and numerical simulation. With the advancement of computational facilities, prototyping has been reduced to a minimum. The design of screw compressor is interactive and the measured performance of the compressor has to be compared

with that specified in advance. Usually this is achieved by testing a prototype system and modifying the design until it yields satisfactory results.

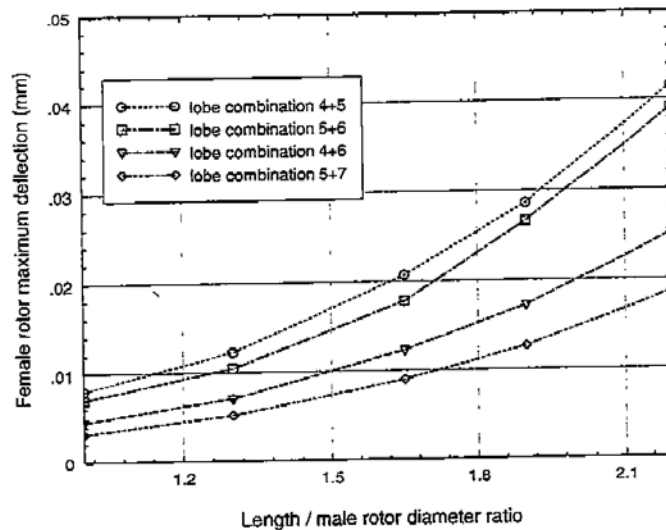


Figure 2.1: Variation of female rotor deflection with L/D_m ratio [21]

An efficient screw compressor needs a rotor profile which has a large flow cross-section area, short sealing line length and a small blowhole area, to achieve higher flow rate for the same rotor size and speed. Short sealing lines and small blowhole reduce leakage. Higher flow and smaller leakage rates will increase volumetric efficiency. This, in turn, increases the adiabatic efficiency, because less power is wasted in the compression of leaked gas, which is re-circulated internally. As precise manufacturing permits the rotor clearances to be reduced despite oil flooding, the likelihood of direct rotor contact increase on reduced clearance. Hard rotor contact leads to deformation of the female rotor due to increased contact forces and ultimately rotor seizure. Hence, the profile should be designed so that the risk of rotor seizure is eliminated.

Relatively few publications are available on screw compressor design since their large scale manufacture began only in the early nineteen seventies as a result of the introduction of the 'A' Profile by the Swedish company SRM. Arbon [1] dedicated his book exclusively to twin shaft compressors and their applications with limited details. Xing published a comprehensive book on this topic but it is written in Chinese language and is generally not available outside China. Only recently, Stosic

et al [12] have published a book emphasizing mathematical modelling and performance.

The common practice for generation of rotor profiles is to create a primary profile on one of the screw rotors and to generate a corresponding secondary profile on the other rotor using appropriate conjugate action criterion. Any curve can be used as a primary one, but traditionally the circle is the most commonly used one. The disadvantage of the classical profile generation methods is that they require significant effort when selecting original curves and the effect of modifications in design cannot easily be predicted. Zaytsev and Ferreira [22] proposed a profile generation method based on line meshing. The method is analytically derived based on the system of contact line, rotor coordinate transfer relations coupled with meshing conditions. The method is such that, as soon as the solution of the meshing condition is obtained, both rotor profiles are automatically generated.

Stosic and Hanjalic [23-26] presented a general algorithm for generation of screw rotor profile and related machine geometry. The method is convenient for the design of screw rotors as well as for improvement of existing rotors. A rack based procedure, capable of generating modern screw rotor profiles has also been included. The main advantage of the algorithm lies in its simplicity, and its capacity to enable ordinary mechanical engineers to create a variety of profiles, a privilege which was previously shared only by a limited number of exclusive specialists. The conjunctive condition has been solved numerically, thereby introducing a variety of primary arc curves. The approach has simplified the design procedure since only primary arcs need to be given, the secondary arcs being automatically generated.

Singh and Onuschak [27] developed a rapid, flexible and comprehensive computer assisted technique to analyze twin-screw rotor profile generation methods. The strength of this method lies in the reduction in time taken by the whole process from profile generation to performance prediction. This powerful profile generation tool can be used in many ways. It has been instrumental in inventing and analyzing entirely new profiles and modifying existing profiles to match particular applications, optimizing geometrical parameters of machines and understanding the importance of different leakage areas and power loss. It has also been used for generating input data such as contact line length and blowhole area for performance prediction programmes. The flow chart of program sequence used for profile generation is shown in Figure 2.2. The model has been used several times successfully for all kinds

of applications including analysis and evaluation. The profile types investigated had a wide range of shapes, number of male/female lobes (3/4 to 6/8 and in between), wrap angles (150 to 350°), L/D_m ratios (0.8 to 2) and built in pressure ratios (4 to 10).

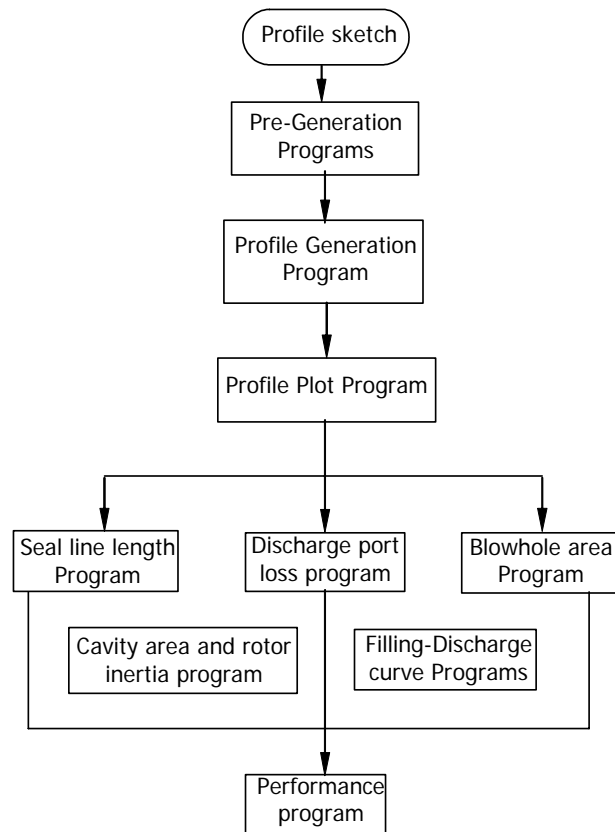


Figure 2.2: Flow chart of computer program to generate screw profile [27]

New designs of rotor profiles have been introduced [28] considering modern design concepts such as larger opening of the suction port and early exposure of the discharge port together with improved bearing systems and seal specifications to maximize work efficiency. Prototype compressors have been tested by the authors and compared with the best compressors currently available in the market. The maximum measured specific power input at a delivery pressure of 8 bar was 5.6 kW/(m³/min), which was less than the published value for any other equivalent compressor manufactured at that time.

McCreath *et al* [29] have published a paper that describes the development of two highly efficient oil free screw compressors designed for dry air delivery. Their

design is based on the use of rack generated 3/5 rotor profiles. The optimum rotor size and speed, together with the shape and position of the suction and discharge ports, were determined by mathematical modelling. The model took full account of the limitations imposed by selection of bearings and seals required to maximize endurance and reliability. Xing *et al* [30] developed a software package to design twin-screw compressors. The package was used to calculate the rotor profile, geometrical characteristics, thermodynamic performance, and forces on rotor teeth, rotor shape and cutter shape. A user friendly interface and some powerful post processing programs were also included in the package. The same package has been used for improving the performance of an existing machine.

Rotors of helical screw compressors present a challenging manufacturing problem. This is due to complex profiles and the fine tolerances necessary for machining the minimal running clearances required for efficient operation. The rotors may vary in length to diameter ratio, male to female diameter ratio, male to female lobe ratio, diameter, profile, and host of other parameters. Mould *et al* [31] presented a method which proceeded directly from an analytical description of the profile to a computer generated cutter template using a numerically controlled contouring grinder having an accuracy and repeatability in the region of 1 μm . They present a method for describing the tool paths in CNC machining starting with the mathematical theory of the design of milling cutters.

Zhou [32] developed a computer aided design method for profile generation, meshed line and contact line plotting, generation of pressure distribution diagram, blowhole area calculation, and milling cutter profile calculation and plotting. Xing *et al* [33] introduced a new theoretical approach and practical application of a CAD system to machining of twin-screw compressor rotors. It comprises of procedures for calculation of geometrical parameters of rotors, simulation of the compressor working process and optimization of the design parameters. The design process has been used to determine the manufacturing and operating parameters for several air and refrigeration compressors.

Computerized design, profile generation and simulation of meshing of rotors have been done by Faydor and Feng [34]. They have covered the conjugation of surfaces, investigation of influence of misalignment on the backlash between the surfaces, synthesis of rotor surfaces with two lines of contact and avoidance of singularities. Fluid leakage across the contact line between two conjugate helical

surfaces is the major concern in terms of machine efficiency. To characterize the geometrical shape of the leakage path and to find the contact line, an average comprehensive radius of curvature (ACRC) analysis has been proposed by Xiao *et al* [35,36]. A numerical approach is accordingly developed which is suitable for microcomputer implementation and used as a part of the CAD and performance analysis package for screw compressors.

Design Optimization

Continuous increase in demand for efficient screw compressors requires that the designs are tailor-made to address to varying duty, capacity and manufacturing capability. A suitable procedure for optimization of screw compressor shape, dimension and operating parameters needs to be developed which will lead to the most appropriate design for a given compressor duty. An optimization technique has been developed [37] and applied to the design of refrigeration twin-screw compressors. The authors also measured the operating parameters as well as rotor and compressor parameters such as wrap angle, L/D ratios and slide valve specifications. You *et al* [38] gave special attention to the male rotor crest range angle and female rotor addendum, since these parameters have a greater influence than all other rotor tip parameters on optimum lobe tip design. Xing *et al* [39] carried out research on the design of a new generation of refrigeration compressors. The rotor profile and other design parameters were optimized with the help of the software package SCCAD.

Stosic *et al* [25, 28, 40, 41] carried out the design of a family of efficient oil flooded twin screw air compressors using a software package which included almost every aspect of rotor profiling and compressor thermodynamic and geometric modelling with the capacity to transmit calculated output directly into a CAD drawing system. They have also designed a family of highly efficient screw rotors based on rack-generated profiles as shown in Figure 2.3, which can be used to replace standard asymmetric profiles. Optimization of a single stage compressor for oil-free and oil-flooded air compression and refrigeration applications has been developed by the authors as shown in Figure 2.4. These profiles are compared in Table 2.1. The results of multivariable optimization, the calculated compressor profiles and design parameters must, however, be considered with extreme caution. This is because,

multivariable optimization usually finds only local minima, which may not necessarily being the best optimization result globally. Therefore, extensive calculations have been carried out by Stosic *et al* [41] before a final decision on the compressor design has been made.

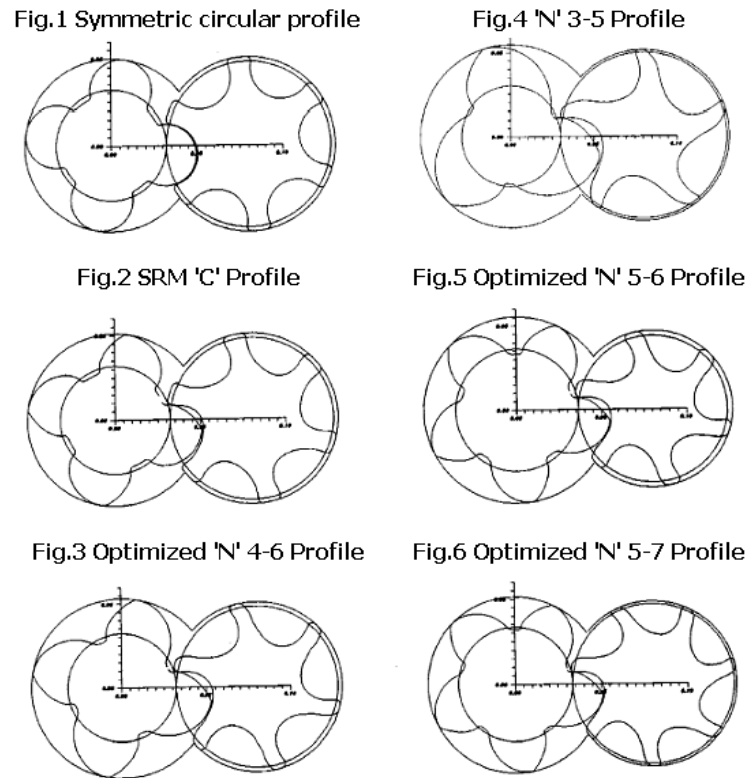


Figure 2.3: Optimized Screw Rotor Profile Designs [25]

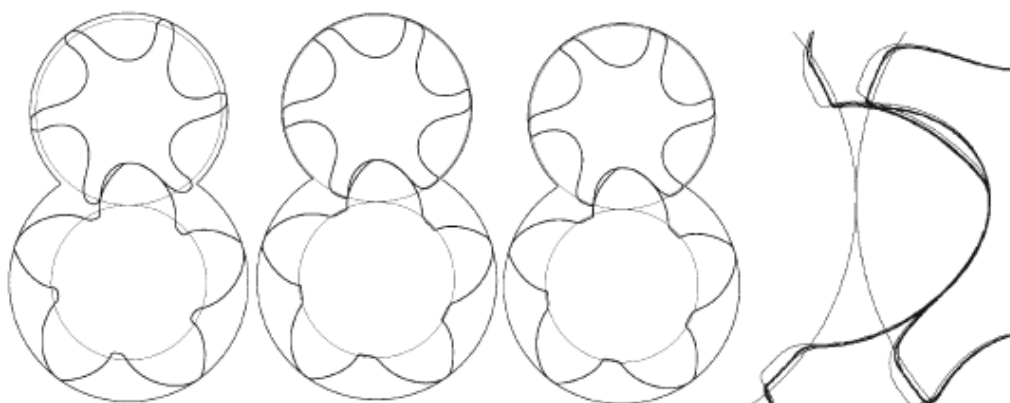


Figure 2.4: Rotor profiles optimized for oil-free and oil-flooded air and refrigeration compressor duty [41]

Table 2.1: Results of optimization calculations for dry and oil flooded air compressors and oil flooded refrigeration compressors [41]

Parameters	Dry air	Oil-flooded air	Refrigeration
r_0 [mm]	2.62	0.74	0.83
r_1 [mm]	19.9	17.8	19.3
r_2 [mm]	6.9	5.3	4.5
r_3 [mm]	11.2	5.5	5.2
Built-in volume ratio	1.83	4.1	3.7
Rotor speed [rpm]	7560	3690	3570
Oil flow [lit/min]	-	12	8
Injection position [°]	-	65	61
Oil temperature [°C]	-	33	32

Rotor Forces

Screw compressor rotors are normally subjected to severe pressure loads. The rotors, as well as their bearings must satisfy the rigidity and elasticity requirements to ensure reliable compressor operation. Bearings that support the rotors are basically considered to be ideal, under simply-supported boundary conditions. Some studies on rotor dynamics have shown that the behaviour of the rotor bearing system is, to some extent, controlled by the bearings that support the rotor. Therefore, it is important to study the dynamic performance of the rotor bearing system of screw compressors to ensure safe and long term operation. The rotor journal bearing system of a screw compressor has been numerically analyzed by Stosic and Hattori [42-44]. The analytical procedure to estimate the reliability and to optimize the bearing design has been described.

(i) Contact forces

Zhou *et al* [45] presented an improved method to determine axial and radial forces applied to the helical rotors of a refrigeration compressor. The axial force consists of two parts: the force applied to the end surfaces and the force applied to the helical profile surfaces. The radial force also consists of two parts: the force applied to the non contact segments and the force applied to the contact segments.

The authors have used the results for bearing design and rigidity calculation. The computation and plotting procedure includes the generation of profile, pressure distribution curves, rotors' meshing curves and the rotors' contact curves. The axial and radial forces of a prototype compressor have been calculated and compared with experimental results. The improved method of rotor force calculation derived by Zhou *et al* has the features of speed, flexibility, accuracy and visual display of results. This computer assisted technique has been used for different rotor profiles and for different refrigerants at different ratings. Experimental studies of compressor noise and vibration in addition to distribution of static forces have been presented by Fujiwara *et al* [46].

Adams and Soedel [47] have presented a classical model for computing rotor contact forces. Compression loads have been incorporated with contact forces to determine the bearing loads. The newly developed model allows only one rotational degree of freedom for each rotor. Backlash type clearance has been considered between the contact points in the rotor meshing zone. In addition, a method has been worked out for computing the motion due to transitions between the states. The equations have been solved using Runge-Kutta integration algorithm with time as the independent variable and the rotor angular positions and velocities as the dependent variables. The simulation has been implemented with a typical set of compressor parameters and the resulting bearing forces have been computed. The test results indicated that the compression loads, as compared to the contact forces, dominate the resulting bearing forces.

(ii) Bearing Forces

A recent study [47] has shown that compression loads dominate the bearing forces in comparison with contact forces between the rotors. The simplest way to compute the compression loads is to utilize some of the assumptions [45] to simplify the complex geometry of the rotor profile. Since the compression loads depend mainly on the rotor profile and pressures at the suction and discharge ends, this simplification affects the magnitude of the computed compression loads.

You *et al* [48] presented a suite of programs, which provides a generalized method for calculating bearing loads of a screw compressor. The method is based on analysis of geometric characteristics and incorporates a performance prediction program which can handle different rotor profiles, port designs, working media and

operating conditions. All the factors which influence the bearing loads have been taken into account including rotor contact, axial forces due to gas leakage across rotor end faces and description of gas pressure forces on helical screw surfaces. Typical results of bearing loads are presented in Figures 2.5 and 2.6 as a function of male rotor rotation angle. Studies on the rotor dynamics have shown that the behaviour of a rotor bearing system is, to some extent, controlled by the bearings that support the rotor.

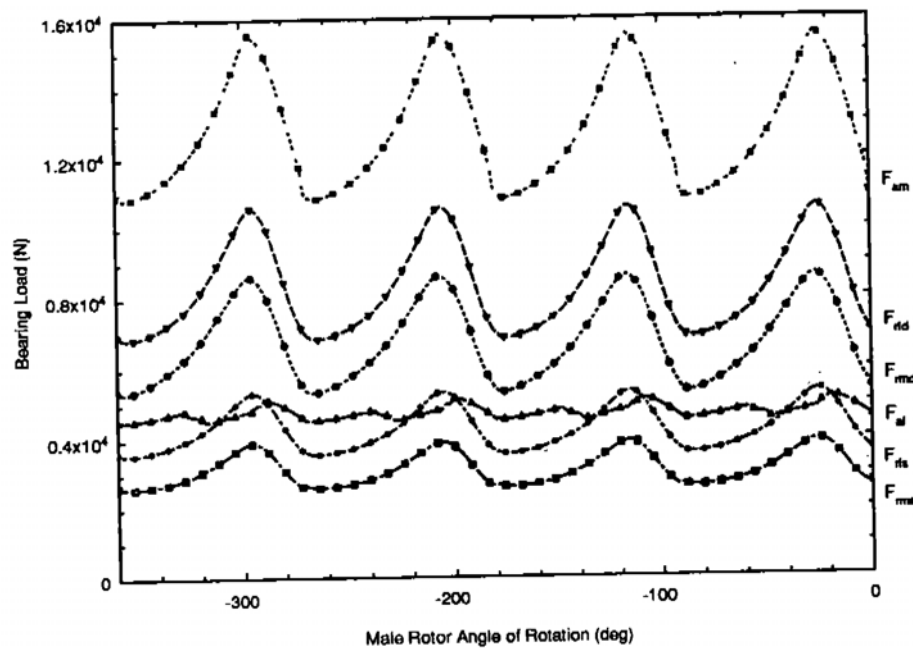


Figure 2.5: Variation of bearing loads with male rotor rotation [48]

Oscillating bearing loads occur even in the absence of rotor chatter due to several effects. Adams *et al* [49-51] have presented a numerical method for computing compression loads by integrating the pressure forces on rotor surface. In addition, a dynamic model of a rigid compressor supported by two cylindrical roller bearings and a four point contact ball bearing is developed from basic principles to analyse noise and vibration. Compression induced rotor bearing loads change with that in operating conditions. The authors have developed a generalised procedure for compression load calculation based on the geometry of the rotor profile and pressures at the suction and discharge ends by mapping the 3D rotor surface into a 2D region.

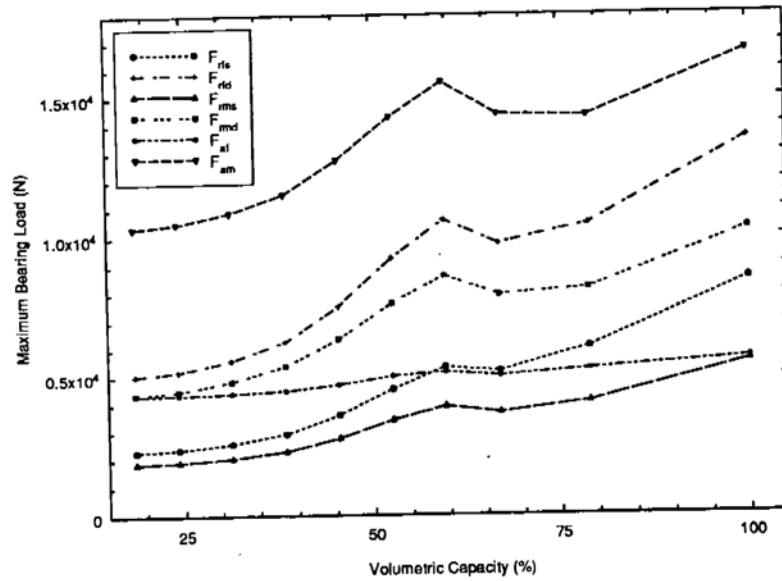


Figure 2.6: Variation of maximum bearing loads with volumetric capacity [48]

2.2 Performance

Being a positive displacement machine, a screw compressor has performance characteristics similar to those of a reciprocating compressor. The entire volume of gas is discharged after compression because there are no clearance pockets. The interlobe space of the screw compressor corresponds to the swept volume of the reciprocating compressor. Compressor designers often predict performance of machines of different sizes but of similar type or belonging to the same family. The machines essentially have the same operating conditions (suction, compression and discharge processes). However, they may differ in volume displacement. Obviously, testing to evaluate performance of various compressors of a given family is a time consuming and expensive process. Generally, performance analysis programs are employed to predict and optimize the performance prior to embarking on costly test programs.

Analysis of compressor behaviour under part load operation has been facilitated by recent advances in mathematical modelling and computer simulation. By this means, the earlier approach of process analysis and optimization by intuitive changes, verified by tedious trial and error testing, has been eliminated. As a result, the design of screw compressor flow control systems has substantially evolved

over the past few years and is likely to lead to further improvements in system performance in near future.

In most refrigeration systems the compression load varies significantly during operation. For optimum performance of the systems, compressors are to be operated efficiently over a wide range of loads for long periods. Capacity control is one of the most important aspects of compressor operation under these conditions. Stosic *et al* [52] modelled the methods of shaft speed variation, suction throttling and variation of suction volume using slide valve mechanism. Capacity control analysis has been carried out on screw compressors with 5/6 and 5/7 "N" rotor profiles for air and refrigeration compressors.

Compressor capacity control strategies minimize energy consumption. There are several methods of controlling capacity. A pulse width modulation capacity control mode has been analyzed and a cascade of capacity control for one and a group of compressors have been suggested by Alyokhin *et al* [53]. This type of capacity control method, using mathematical model and electronic control system, has resulted in considerable energy saving in refrigeration plants. The behaviour of the compressor at different operating conditions has also been studied by Alyokhin, Sjöholm and Sauls [53-55] using various capacity control methods.

Performance Prediction

Numerical modelling is an effective way of reducing experimental cost in research and development. Performance modelling and simulation of rotary compressors has been developed by several authors [56-67] to predict detailed behaviour with sufficient accuracy to investigate the dependence of performance parameters on design factors. A computer program for oil free screw compressors has been developed by Barblik *et al* [57] which provides a quick, simple, and accurate environment for modelling and analyzing their performance. The mathematical model developed provides a single database for performance, optimization of design parameters and statistical analysis which have been used for the development of the compressor.

Performance analysis of compressors has been discussed in detail by Fujiwara *et al* [64-66]. The flow and heat transfer coefficients required for computer simulation have been obtained experimentally and used in the numerical simulation.

The flow coefficients required are calculated from the efficiency versus clearance curves. Singh and Patel [67] have published a generalized computer program to predict the performance of screw compressors. It includes all leakages, viscous shear losses, oil cooling, and inlet and discharge losses. A mathematical model considering the effect of real gas properties has been presented by Xiao and Sangfors [68, 69] which predicts the effect of factors such as gas leakage, heat exchange between gas and oil and flow resistance at discharge port on the performance of the compressor.

Peng *et al* [70] have presented a paper on the basic geometry and engagement characteristics of rotor profile. Two types of new profiles have been generated, all the characteristic parameters of rotor profiles are derived and construction parameters are optimized. Oil compression phenomenon occurs at two portions of conventional compressors and degrades their isothermal efficiency. A new screw rotor profile and a new lubricant have been developed by Kishi *et al* [71] to avoid the oil compression phenomenon.

In the past, compressor performance parameters were computed from operating data by varying the rotation speed and pressure ratio to match each rotor's outer diameter and built in pressure ratio. However as it was not practical to measure the pressure rise phenomena inside the rotor grooves, this method was not useful to study tooth profile or improvements in the discharge and suction ports. Kivotada [72] analyzed compressor performance based on indicator diagram and determined the conditions inside the grooves. A small pressure sensor was built into the tooth root on the discharge side of the female rotor. The pressure change in the groove was measured from the midpoint of the suction process to the completion of the discharge. Indicated diagrams were collected for a single stage cycle and the indicated horsepower was calculated and the performance analyzed.

Responding to demands of practical application, Zhang *et al* [73] carried out a series of performance tests on a twin-screw compressor with 3.5 m³ /min free air delivery at discharge conditions under various operating parameters. They investigated several screw compressor basic parameters with air as working gas and presented many new ideas on screw compressor design.

Thermal Analysis

The compression process in a screw compressor is usually described by a range of algebraic relations obtained by the integration of the generalised continuity, momentum, and energy equations. The optimum design is sensitive to the correct selection of design and operating parameters which govern the thermodynamic and flow processes within the machine. Oil and other fluids may be injected and wet vapours may be compressed. Under these circumstances the compression process is better described by means of an open system covering fluid admission, discharge and leakage processes. The mathematical model gives an equation for the instantaneous operating volume that change with rotation angle or time, together with the differential equations for conservation of mass and energy.

Mathematical modelling and computer simulation of compressor operation have now reached such a stage that much of the traditional trial and error experimental approach to design, still widely used in the compressor industry, is no longer necessary. There have been many approaches to thermodynamic modelling of screw compressors. One of them is modelling of the compression process within a rotor pair. Compression process modelling can be carried out under a variety of rotor geometries, discharge port options, rotor and housing clearances and oil or liquid refrigerant injection. Clearance options include variations in rotor to housing clearance which is a function of position within the housing, variations in rotor-to-rotor clearance along the length of the rotor, rotor to slide valve clearances and rotor discharge end clearances. Porting options include separate radial and axial discharge ports with geometries computed from specified volume ratio and automatic adjustment of radial port geometry for slide valve unloading systems.

Modelling and simulation of rotary compressor was adopted by Mark *et al* [56] to investigate the performance sensitivity of design parameters with sufficient accuracy. Sauls [74] developed a comprehensive thermodynamic modelling system for refrigeration compressors. He suggested a combination of analytical and experimental methods leading to a complete thermodynamic model with emphasis on methods for inspection of experimental and assembly analysis to determine actual clearances in a specific test compressor.

The surfaces enclosing the compression cavity are the housing bore, the end plates and the helical surfaces of the rotors. The process of heat exchange between

the gas and the cavity surfaces is complex, not only because the surface area changes as a function of rotation angle but also because the locations change during the process. A mathematical model for describing the thermal interaction between the gas under compression and the rotors is presented by Ignatiev *et al* [75]. Simultaneous influence of the geometrical and the physical characters of the screws, the working process, the thermophysical properties of the fluid, the influence of different operating parameters and the analysis of rotor thermal distortion have been included in the model.

A complete mathematical model with computer programs has been presented by Alday and Hood [58]. Their model provides a quick, simple and accurate environment for modelling and analyzing the thermodynamic performance of a screw machine. The program provides a single database for performance optimization and statistical analysis that can be used for the development of new compressors. Wu *et al* [76] have proposed a new mathematical model for generating indicator diagrams of refrigeration twin screw compressors. The effect of internal leakage, oil injection, gas-oil heat transfer, refrigerant property and partial loading are taken into account both simultaneously and separately. The model has been verified by experimental recording of p-v indicator diagram. Haugland [77] developed a pressure indication system to monitor pressure at different locations in the compressor cavity that helped in verifying the simulation model.

Stosic *et al* [78-80] describe a numerical model of thermodynamic and fluid flow processes, which is valid for both the compressor and the expander mode of operation. It includes the use of the equations of conservation of mass and energy applied to an instantaneous trapped volume within the machine with allowances for fluid leakage, oil or other fluid injection, heat transfer and real fluid properties.

Oil Injection and Heat Transfer

Compressor performance is influenced both by the refrigerant and by the type of lubricant used. Thermodynamic efficiency of the compression process depends greatly on the oil to gas heat transfer. The oil-injected type screw compressor uses a relatively large mass of injected oil to lubricate the rotor motion, seal the gaps and reduce the temperature rise during compression. Heat transfer between oil and gas primarily occurs by convection. The heat transfer coefficient is a

function of injection parameters. To enhance it, the characteristic size of the oil droplet should be as small as possible. For this purpose, oil should be atomized into small droplets by generating an oil spray. The residence time of the droplets in the compressor cavities depends on the compressor rotational speed and is generally measured in milliseconds. The time the jet surface is exposed to the temperature difference is even smaller in oil jet injection type compressor. Therefore, it is essential to have a clear understanding of the oil injection process, particularly the oil mist injection system.

Singh and Phillips [81] developed a mathematical model to calculate the heat transfer rate between oil and gas assuming that the oil is injected in the form of non-intersecting spherical droplets. They calculated the droplet trajectories from the point of injection to the point where the droplet hits the moving boundaries of the rotors. The authors used the model to calculate the effect of heat transfer on performance and suggested some guidelines to enhance the heat transfer between oil and gas.

Stosic *et al* [82-84] published some results of mathematical modelling and experimental investigation on oil injection and its influence on thermodynamic process in twin screw compressors. The model was subsequently applied to analyze the effect of oil droplet size, position of oil injection port on the casing, oil jet speed and angle, oil inlet temperature, oil to gas mass ratio, oil viscosity and the time of oil retention in the working volume. The compressor performance was evaluated from the measurement of bulk parameters such as delivery rate, power consumption, power utilization efficiency, specific power as well as the instantaneous values of pressure and temperature at several locations over the working volume from which the indicator diagram was worked out. After comprehensive analysis of the influence of various parameters, the authors devised a new system with a more efficient nozzle.

Over the past twenty years, there are a good number of publications have appeared on theoretical modelling of screw compressors mainly focussing on the simulation of thermodynamic processes within the working chamber. Although some experimental investigations have been carried out for verifying the mathematical models, papers totally based on experimental studies leading to better understanding of the oil injection process and its effect on performance seem to be rather low in number. Peng *et al* [85] investigated the oil injection phenomenon to get a better understanding of compressor performance experimentally. The p-v diagrams of a

prototype compressor at various operating conditions were recorded and analyzed. Using a laser measuring system, the authors visualised atomised spray of injected oil and studied the effect of oil-injection parameters. Observation of oil distribution within the working chamber of a model compressor gave valuable information. It was observed that many oil droplets were flying in the working chamber. It was also observed that a thin film of oil always existed on the rotor surfaces, and that there was voluminous oil foam in the working chamber.

Hammerl *et al* [86] examined several variants of the oil injection technique where the oil was injected by nozzles into the suction port of the compressor. They concluded that a finer atomization of the oil jet, leading to increase in the surface area of oil droplets will enhance the heat transfer rate between the oil and the gas. Sangfors [87] studied the effect of oil injection parameters on compressor performance. His model included liquid evaporation, subsonic or sonic two phase leakage, heat transfer among liquid, gas and metal, flashing of dissolved gas and frictional losses due to viscous liquid between moving parts.

Sjoholm and Glenn [88, 89] analyzed the performance of screw compressors operating with a family of complex ester lubricants and with HCFC-22 and HFC-134a as working fluids. Performance of the compressors was measured with R-22 and polyalphaolefins (PAO) and R-22/complex ester lubricant combinations. The authors observed that the complex ester lubricant is the most suitable lubricant for compressors operating with R-22 and unloaded, limited cooled oil or liquid refrigerant injection. They also observed that the complex ester lubricant is superior to PAO lubricant at low pressure ratios.

The influence of degree of oil flooding, liquid refrigerant injection, vapour charge from the economizer, characteristics of refrigerants and degree of partial loading were simultaneously studied by Tang and Fleming [90]. The development of water injected operation of helical screw compressors [91,92] for delivery of lubricant-free air at gauge pressures up to 9 bar in single stage was successfully demonstrated and satisfactory solutions to anticipated problems of lubrication, oil-air isolation, construction material selection and solids deposition within the compression zone were found out. Ducruet *et al* [93] applied two different cooling modes and conducted efficiency tests on refrigeration screw compressors

The operating pressure ratio in a stage without oil injection is limited by the deformation of rotors caused by temperature rise. Rotor cooling reduces this

deformation. Stosic *et al* [43] have suggested a novel procedure to estimate and control the heat transfer in screw rotors by the injection of minute quantities of a volatile fluid. David and Anthony [94] employed three different cooling techniques: liquid refrigerant injection, thermosyphon and oil injection, on refrigerant screw compressor and proved that the oil injection system is slightly better than the other two. A test rig was built [95] to assess the performance of different types of atomizers for oil atomization. Experiments on the test rig showed that lowering the oil droplet diameter results in a considerable increase in heat transfer between gas and oil. It has been concluded that lower injected oil temperature gives better results and changing (increasing) oil flow rate gives only small gains.

Flow and Leakage

To minimize the flow losses in the suction port, the suction port should be positioned on the housing to let the gas enter with the fewest possible bends and the gas approach velocity should be kept low by making the flow area as large as possible. The discharge port size is determined by estimating the built in volume ratio required for optimum thermodynamic performance. Most of the theoretical work done on gas leakage in compressors is based on quasi one dimensional steady state models.

The shape and position of the suction and discharge ports influence the dynamic losses. The position of oil injection port and the quantity of oil injected into the working chamber affect both the outlet temperature and the power consumption. Dynamic flow loss in the suction chamber is a significant factor in reducing screw compressor efficiency but can only be roughly estimated during compressor design step due to the simplified methods of analysis used to account for these effects.

Today, computational fluid mechanics based analysis is used to estimate velocity, pressure, temperature and concentration fields within a compressor far more accurately than was done earlier. Stosic *et al* [96] applied this technique to design a suction port with minimized flow losses. The function of the discharge port on a screw compressor is to provide an exit of the gas and oil from the flutes of the rotors. The volume of flutes occupied by the gas at the beginning of discharge relative to the total volume of the cavities gives the volume ratio of the compressor. An error in calculation of these volumes will lead to error in calculation of volumetric

and adiabatic efficiencies. Sjöholm and Muralidhar have published a paper [97] on measurements on the axial discharge port and its geometric tolerance and have suggested a method to minimize discharge port losses.

Even in the absence of valves, flow through the suction and discharge ports of a screw compressor are oscillatory in nature which affects the compressor performance. Koai and Soedel [98, 99] analyzed the volume and port area curves based on rotor profiles and other geometric data. The gas conditions and flow rates through the ports were determined from thermodynamic analysis of flow phenomena through discharge and suction ports including under and over pressure conditions over a complete cycle.

Leakages are generally considered to be one of the major sources of efficiency loss in screw machines. Rotor clearances are mainly responsible for leakage. Clearances must be minimized to obtain high volumetric and power efficiencies. The gas that leaks back to the suction side not only occupies space but is also at higher temperature. It is obvious that manufacturing tolerances on rotors and the barrel are very important. An increase in tolerance by 0.01mm results in an increase of 1% in volumetric losses [100]. The dimension of the oil stream also plays an important role.

The actual profile of the compressor rotors and their engaged clearance have a great effect on volumetric efficiency and noise. Dynamic measurements on compressor rotor pair in connection with the working process and analysis of rotor profile including engaging clearance has been described in detail by Xiong [101]. Prins and Ferreira [102,103] have tested four types of quasi-static models for gas leakage which are different in mathematical formulation and solution strategy. Unfortunately, none of the models predicts the mass flow rate with sufficient accuracy and reliability, mainly due to poor modelling of viscous effects. Hangiqi and Guangxi [104] developed a computer model considering the effect of discharge port position on compressor performance at various working conditions.

For practical computation of the effects of leakage during the compression process, it is convenient to distinguish between two types of leakages according to their direction in the working chamber: gain and loss leakages. The gain leakages flow into a compression cavity from the discharge plenum and from the neighbouring working chambers which are at higher pressures. The loss leakages leave the

chambers towards the suction plenum and to the neighbouring chambers having lower pressures.

The leakage of gas and oil mixture takes place through interlobe clearance, blow holes and gaps between the plate and the rotors at the discharge end. At the lobe tip, the clearance fills with oil due to the action of centrifugal forces, and only oil leakage takes place which can be calculated by using the equation of incompressible viscous flow through a narrow gap [64]. The amount of oil leakage depends on the gap between the rotor tip and the housing, and the sealing line length. The sealing line length depends on the rotor turning angle. As the rotor starts rotating, the sealing line length decreases. It has the maximum value at the beginning of compression and is zero when the discharge process is completed.

Presence of leakage triangles (blow holes) is an inevitable consequence of the rotor profile geometry. During compression, two blowholes called leading blowhole and lagging blowhole are formed. Both are of same cross sectional area. Leakage of oil-gas mixture into the working chambers is from the leading blowhole and out of the working chamber is through lagging blowhole. Singh and Bowman [105] have presented analytical and experimental methods to calculate blowhole area and have suggested methods to verify the theoretical values. Measured values were consistent with the computed values within the measured accuracy of $\pm 4\%$. The contact line between conjugate helical surfaces is a sealing line separating the high pressure compression chamber from the suction chamber. The fluid leakage across the contact line of conjugate helical surfaces is the major concern in terms of machine efficiency. An average comprehensive radius of curvature (ACRC) analysis was proposed by Xiao and Liu [36] to characterize the geometrical shape of leakage path. A numerical approach was developed for the analysis. It is suitable for microcomputer implementation and is used as a part of the CAD system and performance analysis package.

Leakages are calculated basing on the assumption that gas and oil are uniformly mixed and thermally isolated from the surroundings [68]. The oil-gas mixture leakage rate is calculated using a standard formula for compressible fluids flowing through a convergent nozzle. The flow and blockage coefficients identify the effects of refrigerant viscosity and the sealing function of the lubricating oil used. The properties of gas and oil mixture coming out from the leakage paths and through the discharge port need to be known a priori. But in the absence of accurate

thermodynamic data, they are usually determined by comparison of theoretical models and experimental data. By comparison with laboratory tests, Sangfors [69] suggested the following assumptions for different types of leakage paths: (i) the gas/oil mixture is homogeneous in all leakage paths and (ii) the gas/oil mixture ratio is same in all leakage paths except at the lobe tip clearance, and is equal to the mixture ratio in the discharge port. The leakage rates were calculated basing on the above assumptions. Due to the presence of oil, exact determination of specific heat ratio is rather difficult. Fujiwara and Osada [64] defined an apparent ratio of specific heats and a modified gas constant and used them in their simulation models.

The average leakage area is determined by multiplying the sealing line length with an average gap (clearance) for each type of leakage [65]. The average gap/clearance is determined from actual clearance measurements on the compressor. The discharge or flow coefficients are empirically selected for each leakage to account for the presence of oil. The flow of oil gas mixture through the leakage paths is in two-phase. Exact determination of physical properties of oil-gas mixture is difficult. Based on extensive test data the oil-gas mixture properties have been determined by Sangfors [69].

It is observed that leakage of gas is significantly reduced with oil injection. Increasing the oil injection rate and the rotational speed of the shaft reduce gas leakage. Xiong and Xiao [106] published a simple and effective mathematical description for obtaining the actual engaging profile surface of rotors. They calculated the actual engaging clearances between mating rotors according to basic principles.

Vimmer[107] suggested the essential steps for numerical simulation of compressible inviscid flow in a sealing gap starting from the description of a mathematical model to its final numerical solution. For solution of the system, the cell centred finite volume formulation of the explicit two-step MacCormac scheme with Jameson's artificial dissipation was used. Zaytsev and Ferreira [108] presented a one dimensional leakage flow model for two phase ammonia-water twin-screw compressor. The model accounted for viscous and acceleration forces based on three conservation equations and the equation of state for homogeneous $\text{NH}_3/\text{H}_2\text{O}$ mixture. The governing equations were solved using a finite difference method. Results of the solution were used for calculation of shear stress and friction between the rotors and the housing. Comparison of the proposed leakage flow model with the results of the

isentropic converging nozzle model showed that the latter predicts up to two times higher leakage mass flow rate.

Leakage losses are directly proportional to the effective leakage areas. A method to determine the aggregate leakage through each path individually over a complete compression cycle is required to compute the gas leakage loss. Fleming and Tang [109] constructed a mathematical model for thermofluid processes suitable for leakage calculation. Analytical techniques were proposed for different rotational speeds and experimental methods were suggested for optimized compressor design.

The design of the rotor-casing assembly is primarily controlled by the consideration of internal leakage. Optimised rotor geometry and proper choice of clearances reduce leakage losses. To study the influence of rotor clearances on compressor efficiency, computational fluid dynamics (CFD) analysis has been carried out using FLUENT package [110]. The analysis has been done for static rotors at different positions. The results obtained have shown that the size of the clearances and the geometry of rotor lobes have significant effect on gas leakage and distribution of leakage over the three main leakage paths.

Leakage experiments on a running twin-screw compressor were carried out by Prins *et al* [111]. In their experiment, the indicated diagram was measured for different sizes of rotors and sealing line gap. Lee *at al* [112] have numerically analysed leakage performance of a screw compressor, assuming turbulent flow through a plain seal with oil injection. The effects of parameters such as rotation speed, injection speed, clearance ratio, injection angle and axial injection location on flow pattern and leakage performance have been investigated. The authors concluded that with oil injection, the total leakage of compressed gas can be reduced to acceptable levels.

Chapter III

MATHEMATICAL ANALYSIS

The mathematical modelling of screw compressor is important to understand the basic processes determining its performance. The screw compressor belongs to a family of rotary positive displacement machines whose process diagram is different from that of the conventional turbocompressor. In this chapter an attempt has been made to develop a mathematical model for the suction and compression-discharge steps. The model has been derived from the First Law of Thermodynamics applied to a control volume, ideal gas laws and other relevant relations. This model predicts the variation of temperature and pressure of gas with volume change during compression process. The variation of oil temperature has also been derived. In a reciprocating compressor, the clearance volume is the dominant factor apart from pressure ratio that determines the volumetric efficiency. Analogues to this, the leakage of gas and oil are the primary factors for the determination of volumetric efficiency of screw compressors. In the control volume analysis, the leakage mass of oil and gas in and out of the working chamber constitute the input and output streams.

3.1 The Working Principles

The twin-screw compressor has two of rotors with parallel axes, enclosed in a casing. Each rotor has a number of lobes, which are cut in helical form and mesh into each other in the casing. The casing and the grooves on the two rotors make the working chamber which corresponds to the cylinder and piston of a reciprocating compressor. The twin-screw compressor process consists of three steps, namely suction, compression and discharge as shown in Figure.3.1.

In the suction process, fresh charge is drawn into the cavities of male and female rotors through the inlet port. When the volume of the space reaches its maximum and any further rotation would result in remeshing, the rotors turn past the edges of the inlet port so that the gas in the space is trapped. The compression process starts with the entrapment of the gas and remeshing of rotors progressively reduces the volume of the space or working chamber. The trapped gas is compressed and moves towards the discharge end of the rotors. At an appropriate point (based on designed discharge pressure) the rotors pass the edge of the outlet/discharge port at the opposite end of the rotors.

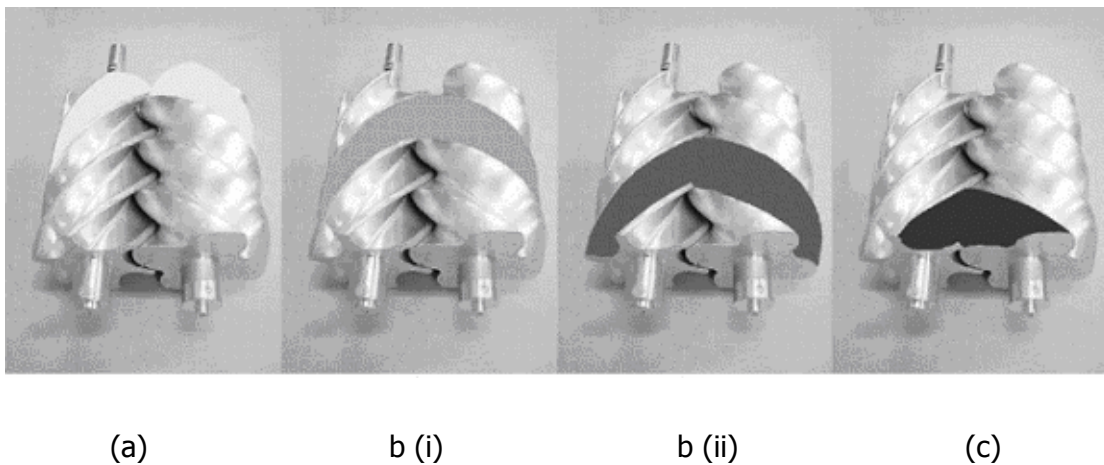


Figure 3.1: Working mechanism of twin screw compressor [113] (a) End of suction process (b) Compression process [(i) entrapment & (ii) reduction in volume] (c) Discharge process

A Typical view of a set of 5/6 screw rotors have been shown in Figure 3.2 without casing for clarity. The meshed and unmeshed volumes of a pair of cavities from the start of compression to the completion of discharge steps are shown in Figure 3.3. The shaded pair of rotor cavities is meshed for compression followed by the unmeshed cavities. The process is shown in steps, as the reduction in volume of a pair of cavities approaches the axial discharge port. Obviously, all other chambers undergo similar process simultaneously with difference of phase with the chamber shown.

When compression is taking place between the seal line and the discharge end, intake is taking place in the volume represented by dots appearing at the back of the sealing line. It is seen that as the rotors revolve, the sealing line moves towards the discharge side of the compressor.

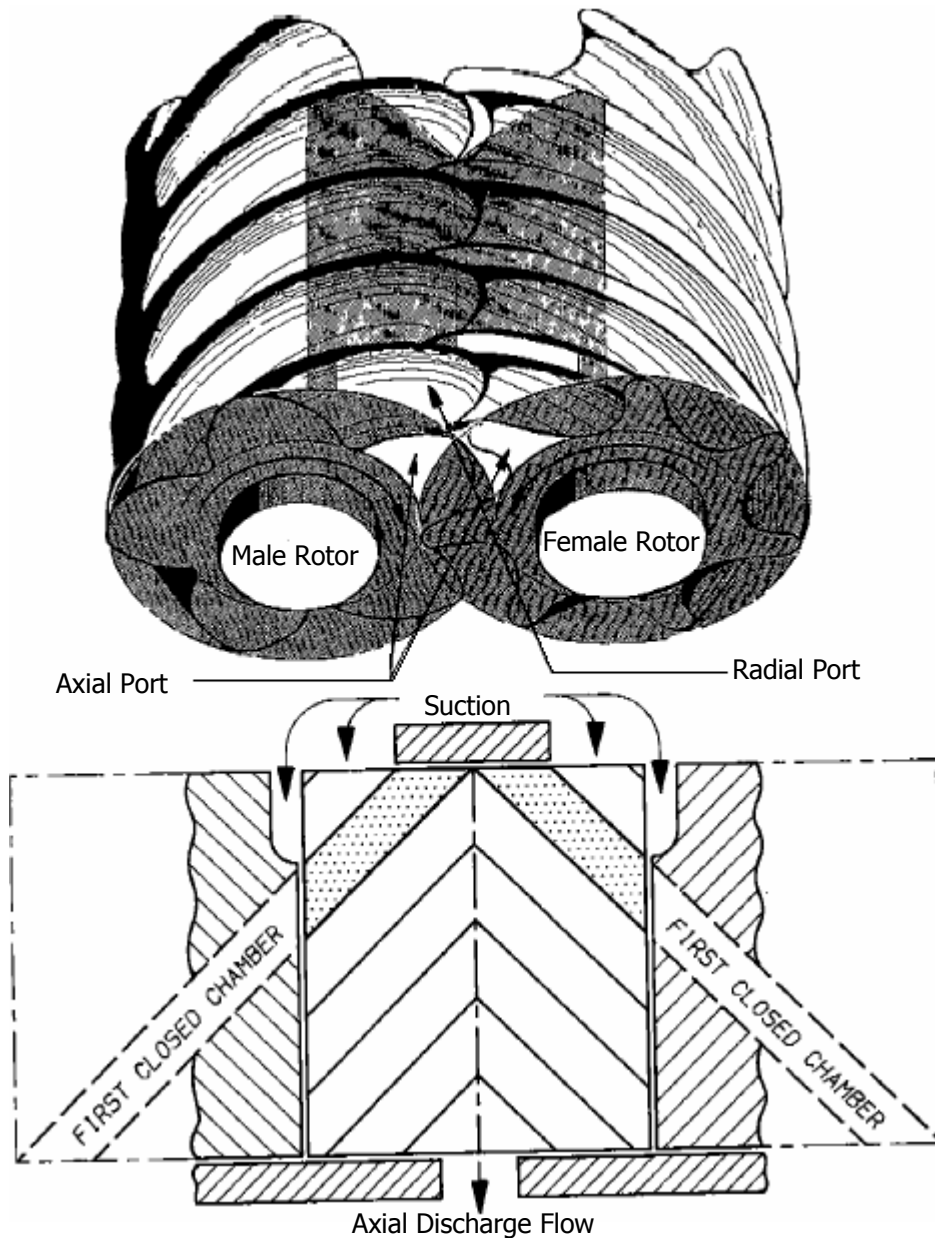


Figure 3.2: Typical view at compression side of twin-screw rotors with first closed chambers unwrapped [114]

Calculation of thermodynamic cycle Time:

The major processes in the operating cycle of a screw compressor are suction, compression and discharge. Generally the cycle time of oil injected twin-screw compressor is represented in terms male rotor rotation angle. The suction and discharge processes overlap in time, even for the same flute. While one part of a flute is under suction, the rest of it is subjected to compression or discharge.

Generally the dimensions of the rotors are so chosen that the suction process goes on for almost a full rotation, while the compression-discharge process is some what shorter.

The rotary compressor under consideration has a 5/6 combination: 5 lobes on the male rotor and 6 on the female. The total time taken for suction process of any one pair of male and female rotor cavities is almost one revolution of male rotor. Therefore, the suction process time in terms of male rotor rotation angle is close to 360° . The compression process depends on the male rotor wrap angle. This angle gives the angle of contact between male and female rotors during compression and determines the axial movement of compression process. A smaller wrap angle gives higher speed of compression, where as for larger male wrap angle, the speed of compression is lower for same volume delivery. For 5/6 rotor lobe combination, the optimum wrap angle ϕ is estimated to be approximately 300° of male rotor rotation [9]. Hence the time required for compression is determined from the angular rotation of male rotor. During discharge process, two adjacent compression processes overlap over certain rotational angle of male rotor. This means that two adjacent compression processes are simultaneously opened to discharge port for certain rotational angle of male rotor. For a wrap angle of 300° , the total discharge processes takes place approximately 60° of male rotor rotation. Thus, for the present combination, the total angular rotation of male rotor is one revolution to complete one thermodynamic cycle. During this time, suction, compression and discharge takes place simultaneously. The operation cycle is shown in Figures 1.6 and 1.7 in chapter I.

Thus, if the male rotor rotates at N_m revolutions per second, the cycle time is:

$$\Gamma = \frac{1}{N_m} \quad (3.1)$$

For the sake of analysis of suction, compression and discharge processes, the total time can be expressed by the relation [67]:

$$\Gamma = \frac{1}{N_m} \left(1 + \frac{\phi}{360} + \frac{1}{n_m} \right) \text{ sec} \quad (3.2)$$

where ϕ is male wrap angle and n_m is number of lobes on the male rotor.

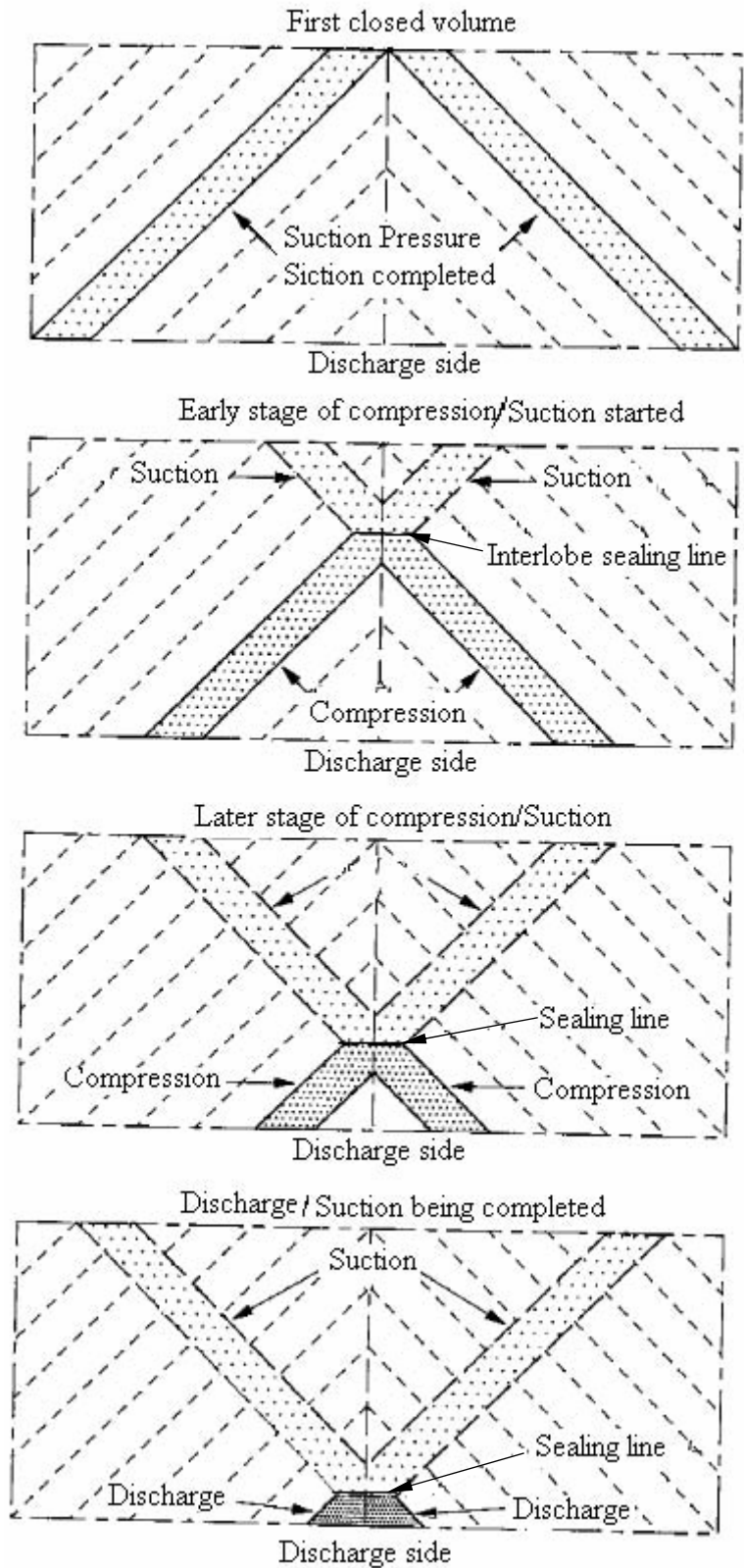


Figure 3.3: Progression of one unwrapped and meshed volume chamber during rotation (compression process) [114]

3.2 *Leakages*

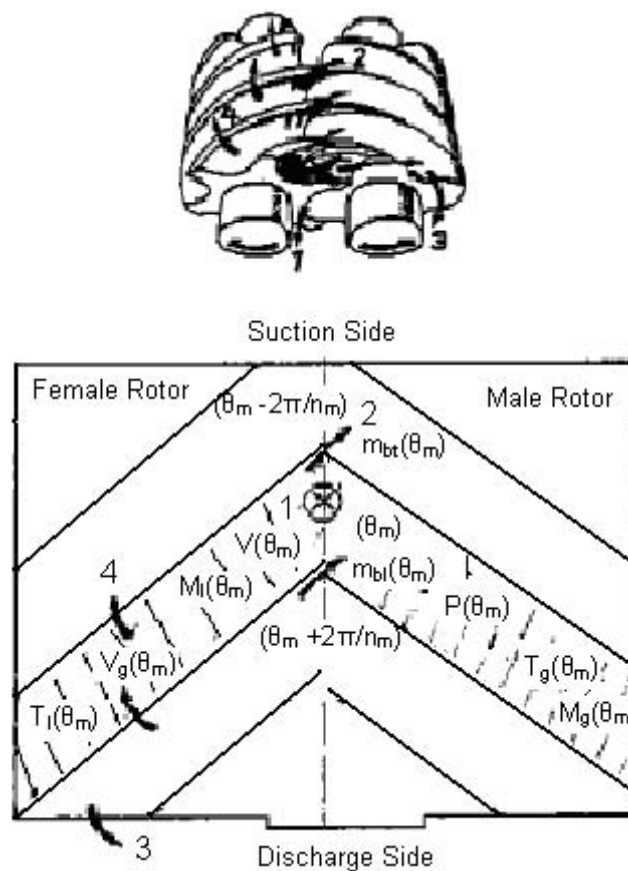
In an oil injected twin screw compressor, oil is circulated to take out the heat of compression and also to provide sealing effect between lobes, and between the rotors and the casing. Along the axial direction between the discharge and the suction sides, the pressure difference induces leakage of both gas and oil. This leakage amounts to a substantial part of the total flow rate and plays an important role in determining the performance of the compressor. At high-pressure ratio and low speed, the leakage paths constitute the major cause for reduction in efficiency.

For practical computation of the effects of leakage during compression process, it is convenient to distinguish between two types of leakages based on the direction with respect to the working chamber: gain or loss leakage. Gain leakage is taken as positive and loss leakage is taken as negative. The gain leakages come from the discharge plenum and from the neighbouring working chambers or compression cavities which are at higher pressure. Loss leakage means the gas and oil leaving the working chamber or compression cavities towards the suction plenum and to the neighbouring chambers at a lower pressure. Different leakage paths are identified and located in the compressor during compression process.

Figure 3.4 depicts different types of leakage flow passages into and out of the working chamber. The leakage flow path can be simulated as a convergent nozzle. The leakage rate depends on leakage area, flow coefficient, pressure and temperature difference between the working chamber and its adjacent chambers. The flow coefficients can be estimated by simulation to match with the experimental result, where as the leakage area can be measured for a given pair of rotors. To find the leakage flow rates, the state of the grooves adjacent to the working chamber need to be known with respect to male rotor angle. For the state of the working chamber at θ_m angle of rotation of male rotor, the preceding and succeeding chambers are at a state of $(\theta_m + 2\pi/n_m)$ and $(\theta_m - 2\pi/n_m)$ respectively, n_m being the number of lobes on the male rotor. In association with the Figure 3.4, the state of the parameters is shown with the help of a block diagram in Figure 3.5. Four major sources of internal leakages exist [115] in a screw compressor. These sources are explained below.

Leakage through interlobe clearance

The interlobe clearance promotes the leakage of gas and oil between adjacent flutes. Some design clearance is provided between the lobes to avoid wear loss. The gas and oil leakage through this clearance goes directly to the suction chamber. The leakage quantity depends on the clearance area, temperature, flow coefficient and the pressure difference between the working chamber and the suction chamber.



1-Interlobe leakage, 2-Leakage through trailing blowhole, 3-Leakage through discharge end clearance, 4-Leakage through rotor tip housing, θ_m -male rotor rotation angle

Figure 3.4: Overview of the different types of leakages through gaps in a twin-screw compressor [115]

Leakage through blowhole

Another unavoidable leakage is that through the blowhole. Presence of leakage triangles (blowholes) in twin-screw compressor is a consequence of the rotor

profile geometries. Blowhole area is defined as the smallest triangular area bounded by the housing and the two rotors in a plane normal to the primary leakage flow path between two adjacent working chambers. During compression process two blowholes are formed, which are called leading blowhole and lagging blowhole. Both blowholes are of same area. The leading blowhole is formed between the working chamber and adjacent chamber at angle of $\theta_m+2\pi/n_m$, and the lagging blowhole is formed between the working chamber and its adjacent chamber at an angle $\theta_m-2\pi/n_m$. Leakage of gas and oil mass into the working chamber takes place through leading blowhole and leakage out of the working chamber is through the lagging blowhole.

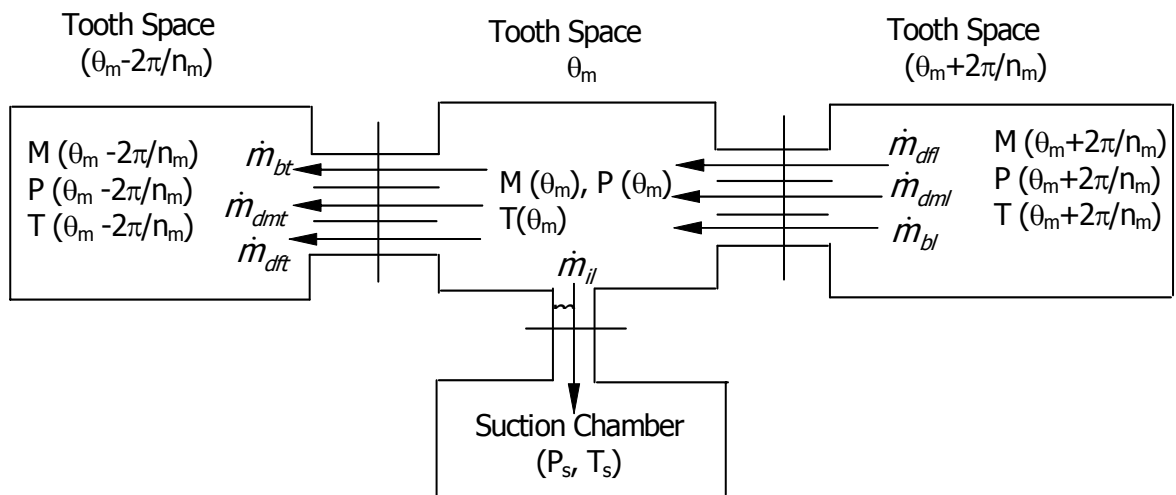


Figure 3.5: Flow model through clearance gap of a twin-screw compressor

Leakage through discharge end clearance

Another important mass leakage is through the clearance between the rotor end and the discharge end plate. Leakage of oil and gas mixture from leading cavities of male and female rotors goes to the working chamber under study through the clearance between male rotor and discharge end plate and also between the female rotor and the discharge end plate. Similarly, the leakage mass of oil and gas mixture from the working chamber goes to succeeding chamber of male and female rotor cavities.

Leakage through the rotor tip-housing clearance

The leakage mass around the rotor tip depends on the gap between the rotor tip and the housing along the sealing line length. The sealing line length, in turn depends on the rotor turning angle. As the rotors start rotating, the sealing line length decreases due to the decrease in volume of the compression chamber. It is highest at the beginning of compression and is zero at the end of the discharge process. Due to centrifugal action, the clearance at rotor tip is filled with the oil alone due to its higher density compared to the working fluid. Hence, unlike the other leakage paths, only oil leaks through this clearance passage. The oil mass leakage into the working chamber from preceding and succeeding chambers has been taken as positive and negative respectively. This type of leakage takes place from both male and female rotor tip-housing clearances to respective lagging cavities.

Figure 3.6 shows meshing of twin-screw rotors with mass leakages and leakage paths in X and Y planes. The rotors rotate in a tight casing which has not been shown in the figure for clarity. The working space comprises of a pair of grooves of male and female rotors (called working chamber) as shown by the shaded area. The gas to be compressed occupies the space in the grooves. Figure 3.7 shows the projected surface of a male rotor groove on the y-z plane. When the meshed rotors rotate, the contour of the projected surface also moves parallel to the rotor axis without change in the shape. The sealing line contour is extrapolated beyond the rotor by dotted lines to visualize the sealing lines more clearly. When the rotors rotate, a leading section of sealing line appears and as rotation continues the line moves parallel to z-axis and decreases in dimension till it eventually disappears as shown in Figure 3.8. The sealing line length varies as the rotors rotate.

Leakage Calculation

The gas and oil mass vary continuously due to leakage during compression-discharge process. The rate of change of gas and oil mass can be written as:

$$\frac{dM_g}{dt} = \dot{m}_{gi} - \dot{m}_{go} \quad (3.3)$$

and

$$\frac{dM_l}{dt} = \dot{m}_{li} - \dot{m}_{lo} \quad (3.4)$$

where M_g , and M_l are the mass of gas and oil trapped in the flutes under consideration, \dot{m}_g and \dot{m}_l being the leakage flow rates of gas and oil respectively.

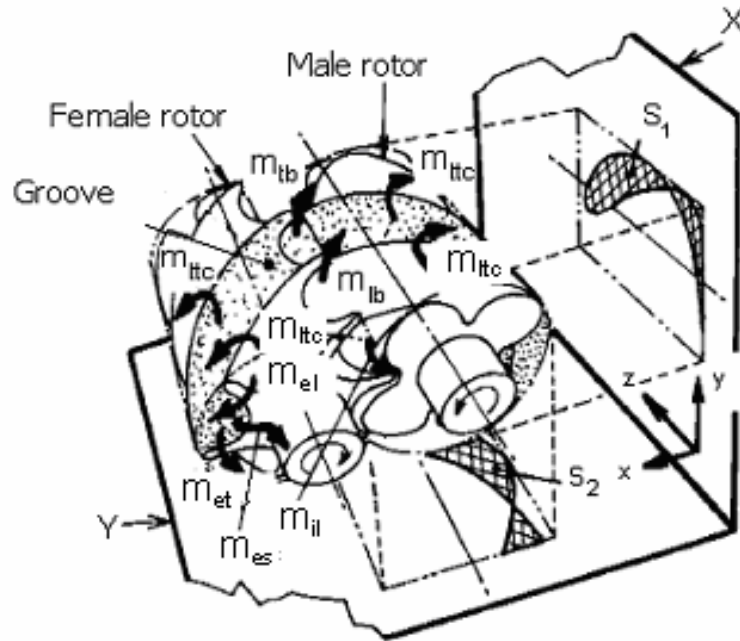


Figure 3.6: Different leakages during compression process [65]

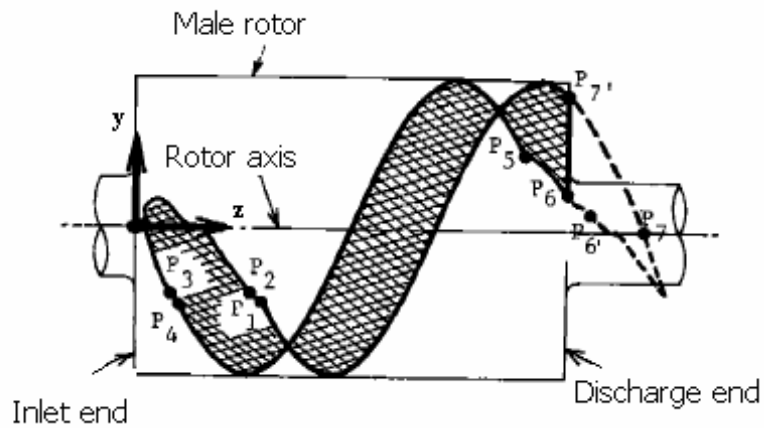


Figure 3.7: Projected area of male rotor groove on the y-z plane [65]

The gas and oil mixture leakage may be expressed in terms of local variables at any time in the working chamber and are assumed to follow the process of a convergent nozzle. Except at the lobe-tip clearance, the leakage gas and oil are

assumed to be mixed uniformly. If the pressure drop of a flowing fluid through the nozzle is considerable, the energy equation for adiabatic compressible fluid flow can be expressed as [116]:

$$\frac{\beta}{(\beta-1)} \frac{P_1}{\rho_1 g} + \frac{V_{e1}^2}{2g} + z_1 = \frac{\beta}{(\beta-1)} \frac{P_2}{\rho_2 g} + \frac{V_{e2}^2}{2g} + z_2 \quad (3.5)$$

It is assumed that the upstream and down stream leakage paths are at the same elevation (i.e. $z_1=z_2$) and the inlet velocity of the oil-gas mixture is assumed to be small compared with the outlet velocity. With these assumptions, the above equation reduces to:

$$\frac{\beta}{(\beta-1)} \frac{P_1}{\rho_1} = \frac{\beta}{(\beta-1)} \frac{P_2}{\rho_2} + \frac{V_{e2}^2}{2} \quad (3.6)$$

The conservation of mass of mixture at inlet '1' and outlet '2' leads to the equation:

$$\rho_1 A_1 V_{e1} = \rho_2 A_2 V_{e2} \quad (3.7)$$

From equations (3.6) and (3.7), after simplification, the leakage mass flow rate of gas and oil mixture is calculated to be:

$$\dot{m} = (\dot{m}_g + \dot{m}_l) = \frac{CA_c P_1}{\sqrt{T_1}} \sqrt{\frac{\beta \left(\frac{2}{(\beta-1)} \right)^{\frac{\beta+1}{\beta-1}}}{R_m}} \quad \text{for } 0 \leq r \leq \left(\frac{2}{(\beta+1)} \right)^{\frac{\beta}{\beta-1}} \quad (3.8a)$$

(for subsonic flow)

and

$$\dot{m} = (\dot{m}_g + \dot{m}_l) = \frac{CA_c P_1}{\sqrt{T_1}} \sqrt{\frac{2\beta \left(r^{\frac{2}{\beta}} - r^{\frac{\beta+1}{\beta}} \right)}{(\beta-1)R_m}} \quad \text{for } r > \left(\frac{2}{(\beta+1)} \right)^{\frac{\beta}{\beta-1}} \quad (3.8b)$$

(for supersonic flow)

where β is the ratio of specific heats, and r is the ratio of downstream (P_2) to upstream (P_1) pressure ($r = \frac{P_2}{P_1}$) and C is the flow coefficient of the nozzle. It may be noted that the pressure ratio is always less than unity. Hence, the equation (3.8b) for supersonic flow is never used although both the equations are given for mathematical completeness.

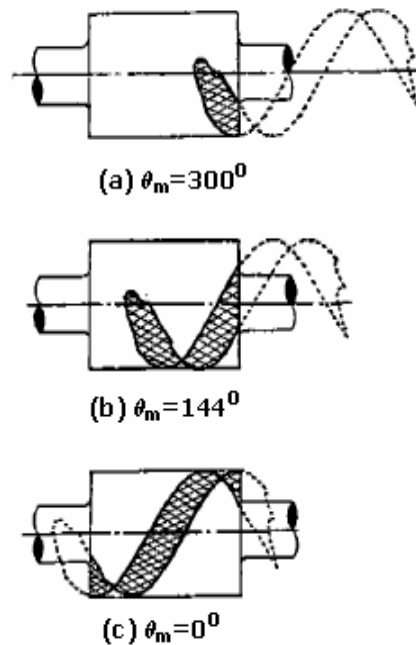


Figure 3.8: Change of sealing line length with male rotor rotation [65]

The leakage mass flow rate of mixture through various leakage paths into and out of the working chamber/cavities except through lobe tip-housing clearance is found by using the equation (3.8a). Due to the presence of oil, the exact mass ratio of oil to gas in the mixture is not known. However, the mass ratio in the mixture coming out from the leakage paths and through the discharge port can be calculated from experimental data. The following assumptions are made for the leakage of oil and gas mixture [69].

- (i) The oil-gas mixture is homogeneous in all leakage paths.
- (ii) The oil to gas mass ratio is same in all the leakage paths and equal to the mixture ratio in the discharge port.

From these assumptions, the mass ratio of oil to gas in the working chamber and through all leakage paths may be defined as:

$$\begin{aligned}\phi &= (\text{mass flow rate of oil through discharge port})/(\text{mass flow rate of gas through} \\ &\hspace{15em} \text{discharge port}) \\ &= (\text{leakage flow rate of oil})/(\text{leakage flow rate of gas}).\end{aligned}$$

In mathematical terms it can be expressed as,

$$\phi = \frac{\dot{m}_l}{\dot{m}_g} = \frac{\dot{m}_{li}}{\dot{m}_{gi}} \quad (3.9)$$

The specific heat ratio of oil-gas mixture influences the leakage rate. Exact determination of adiabatic index is rather difficult due to the presence of oil. Fujiwara and Osada [64] have defined the apparent ratio of specific heats and effective gas constant for oil-gas mixture. The modified specific heat ratio and gas constant for the mixture are defined as:

$$\beta = \frac{C_p + \phi C_l}{C_v + \phi C_l} \quad (3.10)$$

$$R_m = \frac{1}{1 + \phi} R \quad (3.11)$$

The ratio of specific heats of pure gas can be defined as:

$$k = \frac{C_p}{C_v} \quad (\text{of the gas species being compressed}) \quad (3.12)$$

The average leakage area in leakage equation is determined by multiplying sealing line length with an average gap (clearance) for each type of leakage. The average gap/clearance is determined from the actual clearance measurements of the compressor. The flow coefficients are empirically selected to account for the presence of oil in each type of leakage flow.

The gap between the lobe tip and the rotor casing is filled with higher density fluid, i.e. oil alone, due to the action of centrifugal force, and thus the leakage flow is

in a single phase. The rate of oil leakage through this clearance from both male and female rotor tip clearances can be calculated using the equation of incompressible viscous flow through a narrow gap between two horizontal plates where one plate is stationary and the other plate is moving. The moving plate is the lobe tip having length equal to lobe tip width. The mass of oil leakage along the lob tip sealing line (S) can be written as [117]:

$$\dot{m}_l = S\rho_l \left[\frac{v_t a}{2} - \frac{(P_2 - P_1)a^3}{12\mu_l w_t} \right] \quad (3.13)$$

where ρ_l is the density of oil, w_t is lobe tip width and a is the clearance perpendicular to flow direction.

Unlike reciprocating compressors, screw compressors are of rotary type and have a number of working chambers. The total number of working chambers depends on male and female lobe combination. Simultaneous suction, compression and discharge processes take place in all the grooves with leading or lagging phase angle of $360^\circ/n_m$. The phase angle between two adjacent working chambers depends on the number of lobes on male rotor. It is assumed that one pair of male and female cavities under study are at an angle θ_m° of male rotor rotation. The leakage gas and oil mass into these cavities are from the preceding working chamber cavities, which are at an angle of $(\theta_m+360/n_m)^\circ$. Similarly, the oil and gas masses leak to the succeeding cavities at $(\theta_m-360/n_m)^\circ$. The leakage mass flow rate of homogeneous mixture of oil and gas during compression and discharge process through various leakage paths are calculated by using equation 3.8(b). Equation (3.13) is used to calculate the leakage of only oil through rotor tip-housing clearance. The same equations are employed to calculate the leakages into and out of the working chamber or compressor cavities on which the numerical study is focussed. In leakage calculation, one pair of male and female cavities is considered, since all the cavities are similar in all aspects. The leakage rate of gas mass and oil mass can be calculated separately from the equation of the leakage rate of mixture for a known mass fraction ϕ .

Gas leakage into the cavities

The gas mass leakage into the working chamber are (i) leakage through leading blowhole (ii) leakage from male rotor end face at the discharge side and (iii) leakage from female rotor end face at the discharge side.

The values of flow coefficients used in the simulation vary according to the type of leakage, male rotor tip speed, and injected oil quantity. Using the nozzle equation (3.8a), the leakage rate of gas mass through the leading blowhole into the working chamber at any instant can be estimated by using the relation:

$$\dot{m}_{gbi} = \frac{C_{bl} A_{bl} P_1}{\sqrt{T_1}} \sqrt{\frac{\beta \left(\frac{2}{\beta-1} \right)^{\frac{\beta+1}{\beta-1}}}{R_m}} / (1 + \phi) \text{ for } 0 \leq r \leq \left(\frac{2}{\beta+1} \right)^{\frac{\beta}{\beta-1}} \quad (3.14)$$

where C_{bl} , A_{bl} are the discharge coefficient and leakage area respectively. If $(C_{dmi}$, A_{dmi}), $(C_{dfi}$, $A_{dfi})$ are the flow coefficients and leakage areas of male and female rotors at the discharge end side, the net gas mass leakage rate into the working chamber through all the leakage paths including blowhole can be computed by using the expression:

$$\dot{m}_{gi} = \frac{1}{(1 + \phi)} (C_{bl} A_{bl} + C_{dmi} A_{dmi} + C_{dfi} A_{dfi}) \frac{P_1}{\sqrt{T_1}} \sqrt{\frac{\beta \left(\frac{2}{\beta-1} \right)^{\frac{\beta+1}{\beta-1}}}{R_m}} \quad (3.15)$$

Gas leakage out of the cavities

The leakage rate of gas mass from the compression cavities to the adjacent chambers is through (i) trailing blowhole (ii) interlobe clearance (iii) discharge end clearance of male cavity and (iv) the discharge end clearance of female rotor cavity. It may be noted that the leakage through interlobe clearance goes directly to the suction cavities where as leakage through trailing blowhole goes to its succeeding cavities. Similarly, the leakage gas mass goes to its succeeding cavities due to the clearance between male and female rotors with the discharge end plate.

Using the same nozzle equation (3.8a), the net gas mass leakage going out of the working cavities from all the leakage paths of the compressor can be estimated by using the equation shown below:

$$\dot{m}_{go} = \frac{1}{(1 + \phi)} (C_{bt} A_{bt} + C_{dmt} A_{dmt} + C_{dti} A_{dti}) \frac{P_1}{\sqrt{T_1}} \sqrt{\frac{\beta \left(\frac{2}{(\beta - 1)} \right)^{\frac{\beta+1}{\beta-1}}}{R_m}} + \dot{m}_{gil} \quad (3.16a)$$

where

$$\dot{m}_{gil} = \frac{1}{(1 + \phi)} (C_{il} A_{il}) \frac{P_1}{\sqrt{T_1}} \sqrt{\frac{\beta \left(\frac{2}{(\beta - 1)} \right)^{\frac{\beta+1}{\beta-1}}}{R_m}} \quad (3.16b)$$

For interlobe leakage calculations, the downstream pressure P_2 is equal to suction pressure (P_s), and (C_{bt}, A_{bt}) , (C_{dmt}, A_{dmt}) , (C_{dti}, A_{dti}) , (C_{il}, A_{il}) are the flow coefficients and leakage areas of trailing blowhole, discharge end of male rotor, discharge end of female rotor, and at interlobe leakage respectively.

Oil leakage into the cavities

The oil mass leakage rate into the working chamber is through rotor tip housing clearance from both male and female rotors in addition to the oil leakage associated with the gas leakage given by equation (3.15). The total oil mass leakage rate into the working chamber can be calculated using the relation:

$$\dot{m}_{li} = \dot{m}_{lrmi} + \dot{m}_{lrff} + \phi \dot{m}_{gi} \quad (3.17)$$

where \dot{m}_{lrmi} , \dot{m}_{lrff} are the oil leakage rates through male and female rotor tip-housing clearances respectively and $\phi \dot{m}_{gi}$ is the leakage oil mass associated with the mixture leakage.

The oil leakage flow rate through rotor tip-housing clearance from leading working chamber of male rotor is estimated by equation (3.13) as:

$$\dot{m}_{lmi} = S_{ml} \rho_l \left[\frac{v_{tm} a}{2} - \frac{(P_2 - P_1) a^3}{12 \mu_l W_{tm}} \right] \quad (3.18)$$

where S_{ml} is the sealing line length of male rotor at rotor tip-housing clearance. Similarly, leakage from the leading female rotor groove is calculated by the relation:

$$\dot{m}_{lfi} = S_{fl} \rho_l \left[\frac{v_{tf} a}{2} - \frac{(P_2 - P_1) a^3}{12 \mu_l W_{tf}} \right] \quad (3.19)$$

where S_{fl} is the sealing line length of female rotor at rotor tip-housing clearance. The oil leakage associated with the gas leakage can be calculated using equation (3.15) by multiplying the value of \dot{m}_{gi} with the mass fraction ' ϕ '.

Oil leakage out of the cavities

Similar to the leakage of oil into the cavities, oil mass leakage out of the compression cavities is composed of two parts: (i) oil leakage alone along the sealing line length between the tips of the male and female rotors and the housing and (ii) oil leakage associated with gas leakage.

The total leak rate of oil mass from the working chamber to the adjacent grooves is given as:

$$\dot{m}_{lo} = \dot{m}_{lmo} + \dot{m}_{lfo} + \phi \dot{m}_{go} \quad (3.20)$$

where \dot{m}_{lmo} , \dot{m}_{lfo} are the oil leak rates through the clearance between the tips and the housing. The last term is the oil content in the leakage of mixture of gas and oil. The oil mass leak rate from the male rotor cavity through rotor tip-housing clearance to the succeeding working chamber can also be estimated by using equation (3.13) as:

$$\dot{m}_{lmo} = S_{mt} \rho_l \left[\frac{v_{tm} a}{2} - \frac{(P_2 - P_1) a^3}{12 \mu_l W_{tm}} \right] \quad (3.21)$$

where S_{mt} is the sealing line length of trailing male rotor.

Similarly, the leakage from the female working chamber to the succeeding groove is calculated by using the relation:

$$\dot{m}_{lrf0} = S_{ft} \rho_l \left[\frac{v_{tf} a}{2} - \frac{(P_2 - P_1) a^3}{12 \mu_l W_{tf}} \right] \quad (3.22)$$

where S_{ft} is the sealing line length of trailing female rotor.

3.3 Suction Process

Screw compressor performance is governed by the interactive effects of thermodynamics, heat transfer and machine geometry. This can be calculated reliably only by their simultaneous consideration.

The analysis of suction process of a compressor is essential to know the amount of fresh gas mass inducted into the suction cavities, the quantity of gas mass inducted being a function of the temperatures of inlet gas and cavity walls. The temperature T_1 at the end of suction process is higher than the temperature T_s of the freshly inducted gas because of the heat transfer with the oil present in the suction chamber.

The following assumptions have been made in analyzing the suction process. Since the pressure and temperature fluctuations are generally small, the analysis of the suction process is simplified with the following quantities being assumed to be constant.

- ❖ Inlet velocities of gas and oil
- ❖ Temperature of gas and oil
- ❖ Pressure drop across the inlet port
- ❖ Heat flow from gas to oil (or from oil to gas)

Using the above assumptions, the state of the gas and the oil at the end of suction process are calculated using mass and energy balance. It is possible to describe their temperatures explicitly in terms of the input parameters.

The sensible heating of fresh inducted gas mass is:

$$Q = C_p M_1 (T_1 - T_s) \quad (3.23)$$

where T_1 is temperature and M_1 the mass of the fresh gas inducted during suction process.

If the temperature rise of inducted gas is small comparison with the difference of temperatures between the injected lubricating oil and the inducted gas, the convective heat transfer between the leaked oil and inducted gas during suction process may be expressed as:

$$Q = hA(T_{oil} - T_s)t_s \quad (3.24)$$

where t_s is the suction duration in seconds.

Under ideal conditions, the heat lost by the oil must be equal to the heat gained by the gas. From equations (3.23) and (3.24), the mean temperature of inducted gas can be written as:

$$T_1 = \frac{hA(T_{oil} - T_s)t_s}{M_1 c_p} + T_s \quad (3.25)$$

Using the ideal gas equation of state, the total amount of gas mass, including leakage gas mass, occupying the suction volume at (P_s, T_s) can be written as:

$$M_{ts} = \frac{P_s V_{t1}}{RT_s} \quad (3.26)$$

where V_{t1} is the geometrical volume of one pair of male and female rotor cavities.

$$V_{t1} = (A_m + A_f)L$$

The actual gas mass contained in the volume at the end of suction process (P_s, T_1) is estimated to be:

$$M_{t1} = \frac{P_s V_{t1}}{RT_1} = M_{ts} \frac{T_s}{T_1} \quad (3.27)$$

The total gas mass at (P_s, T_1) is the sum of fresh charge inducted and the leaked gas mass. Thus:

$$M_{t1} = M_1 + M_{il} \quad (3.28a)$$

The leakage gas mass rate is given as:

$$\dot{m}_{gl} = \dot{m}_{gj} - \dot{m}_{go} \quad (3.28b)$$

The expressions for \dot{m}_{gj} , \dot{m}_{go} are given by the equations (3.15) and (3.16a) respectively. The total amount of gas mass leakage into the suction cavities over the suction duration t_s is

$$M_{il} = \dot{m}_{gl} \times t_s \quad (3.28c)$$

Using equation (3.27), the fresh charge at (P_s, T_1) can be expressed by the relation:

$$M_1 = M_{ts} \frac{T_s}{T_1} - M_{il} \quad (3.29)$$

It may be noted that M_1 is the mass of fresh charge at (P_s, T_1) . M_{ts} is the total mass of gas at (P_s, T_s) and M_{il} is leakage gas mass at (P_s, T_1) . Substituting the value of M_1 from equation (3.29) in equation (3.25), we get a quadratic equation in T_1 as:

$$-c_p M_{il} T_1^2 + T_1 [c_p M_{t1} T_s + c_p M_{il} T_s - hA(T_{oil} - T_s)t_s] - c_p M_{t1} T_s^2 = 0 \quad (3.30)$$

The solution of the quadratic equation (3.30) gives the temperature of gas mass at the end of suction process. The parameter M_{il} is to be determined from the simulation of compression chamber which has been described in section 3.2.

Heat Transfer between Gas and Oil

One of the important problems which require careful investigation is the role of the injected oil into the working chamber. Oil is injected into the compression cavities for sealing, cooling and lubrication purpose. The thermodynamics of suction and compression processes change substantially with oil injection.

To enhance cooling efficiency, oil must be atomized into a spray of fine droplets to enhance the area of the contact surface between the gas and the oil. The atomization is performed by using specially designed nozzles or by simple high-pressure injection. The distribution of droplet sizes is controlled by oil-gas mass flow and velocity ratio for a given oil injection system. In recent years, many authors have simulated the behaviour of oil injected compressors to predict the performance. In suction process, the gas is warmed up by the hot leaked oil film. Singh and Bowman [81] analyzed the movement of oil droplets in the working space and calculated the heat transfer between the gas and the oil. Stosic *et al.* [82-84] used an oil droplet model to study the influence of droplet size on heat transfer rate and determined the heat transfer coefficient using experimental data. Recently a simpler procedure has been adopted by Fujiwara and Osada [64] in which the heat transfer coefficient is formulated and calculated basing on the analysis of suction process. The same method has been adopted in this study to determine the heat transfer coefficient for different working gases. At the beginning of suction process, a fresh charge at suction condition is taken into the suction chamber. At the end of suction process, the temperature of this gas rises to a level which is between the suction and the leaked lubricating oil temperature at suction pressure.

The displacement volume of the working chamber is the theoretical volume of one pair of male and female rotor grooves. This volume is filled with the fresh inducted gas and the leaked gas from the previous compression process from a neighbouring flutes at pressure P_s and temperature T_1 occurring at the end of the suction process. Though there is a leakage of oil through the interlobe clearance, its volume is small compared to that of the leaked gas. However, the mass of leaked oil may be large compared to that of the leaked gas. A schematic model of the working chamber at the end of suction process is shown in Figure.3.9.

The heat exchange between oil and the leaked gas is negligible because both are leaked quantities and are therefore assumed to be in thermal equilibrium. The

pressure drop across the inlet port is assumed to be negligible. With these assumptions, the amount of heat transfer from oil to the inducted gas may be estimated using the expression:

$$Q = c_p M_1 (T_1 - T_s) \quad (3.31)$$

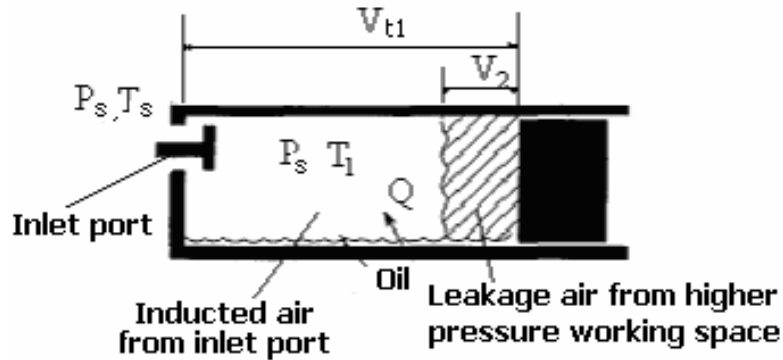


Figure 3.9: Model of the working chamber of an oil injected twin screw compressor at the end of suction process [64]

Assuming the working gas to be ideal, the state equation of gas at the end of suction condition can be written as:

$$P_s V_1' = M_1 R T_1 \quad (3.32)$$

where M_1 is the actual fresh mass entering the suction chamber at (P_s, T_1) for an available suction volume of V_1' . The equivalent volume V_1 necessary for the same mass at suction condition (P_s, T_s) is given by the relation:

$$P_s V_1 = M_1 R T_s \quad (3.33)$$

Since $T_s < T_1$, the actual volume of fresh charge decreases from V_1' to V_1 .

Since the heat capacity of the oil is very large compared to that of the gas, the temperature variation of oil during gas induction into the suction chamber (cooling effect) and the heating effect on the compression process are small compared to the temperature variation of the gas during suction and compression

processes. Therefore, the temperature of leaked oil is assumed to be constant at T_{oil} which is also the temperature of oil in the suction chamber.

The total suction volume (geometrical volume) of the gas at the end of suction process (P_s, T_1) is,

$$V_{t1} = V_1' + V_2 \quad (3.34)$$

The leaked gas does not take part in the heat transfer process since it is assumed to be at (P_s, T_1). Thus from equation (3.32) and (3.34)

$$P_s(V_{t1} - V_2) = M_1RT_1 \quad (3.35)$$

Substituting the values of T_s and T_1 from respective equations (3.33) and (3.35) in equation (3.31), we get:

$$Q = \frac{c_p}{R} P_s V_{t1} \left(1 - \frac{V_1 + V_2}{V_{t1}}\right) \quad (3.36)$$

When the temperature rise of the inducted gas is small compared with the temperature difference between T_{oil} and T_s , the convective heat transfer between gas and the oil during suction process can be described by the relation:

$$Q = Ah(T_{oil} - T_s)t_s \quad (3.37)$$

Eliminating Q between equations (3.36) and (3.37),

$$Ah(T_{oil} - T_s)t_s = \frac{c_p}{R} P_s V_{t1} \left(1 - \frac{V_1 + V_2}{V_{t1}}\right) \quad (3.38a)$$

The above equation can be expressed in terms of volumetric efficiency as:

$$Ah(T_{oil} - T_s)t_s = \frac{c_p}{R} P_s V_{t1} \left(1 - \eta_{ev} - \frac{V_2}{V_{t1}}\right) \quad (3.38b)$$

Since the heat capacity of the oil in the working chamber is much larger than that of the gas, the temperatures of the oil in the compression and discharge steps are not affected very much by the inlet gas temperature. Therefore T_{oil} , leaked gas volume V_{2r} , and the heat transfer coefficient are assumed to be independent of suction gas temperature. Thus, differentiating the equation (3.38b) with respect to T_s on both sides yields:

$$h = \frac{kP_s V_{t1}}{(k-1)A t_s} \frac{d\eta_{ev}}{dT_s} \quad (3.39)$$

Equation (3.39) relates the heat transfer coefficient to the slope of the volumetric efficiency vs gas inlet temperature curve. Applying experimental data to this equation, the heat transfer coefficient can be determined for any working gas. But there is no exact information available concerning the heat transfer area between inducted gas and the oil. Fujiwara and Osada [64] defined the representative heat transfer area as:

$$A = (V_{t1})^{\frac{2}{3}} \quad (3.40)$$

They have also presented the experimental relationship between Nusselt number and rotational Reynolds number. Figure 3.10 depicts the experimental relation between Nusselt number and rotational Reynolds number for three different oil-supplying conditions. The line is approximated by the equation:

$$Nu = 0.51(Re_w)^{0.74} \quad (3.41)$$

The Nusselt number and the rotational Reynolds number are defined as:

$$Nu = \frac{hD_m}{\lambda} \quad (3.42a)$$

and

$$Re_w = \frac{\omega D_m^2}{\nu} \quad (3.42b)$$

where D_m is the male rotor diameter, which is also the characteristic length in Nusselt number calculation.

The relations given by the equations (3.42a) and (3.42b) are based on generalised dimensionless parameters which are independent of time in the suction process. Hence, it has been argued that the same relation can be extended to estimate the heat transfer coefficient in compression and discharge processes for computer simulation.

Symbol	Q_{oil} (litre/min)	T_{oil} ($^{\circ}C$)
•	20	50
×	35	50
Δ	35	70

Q_{oil} is oil supplying rate

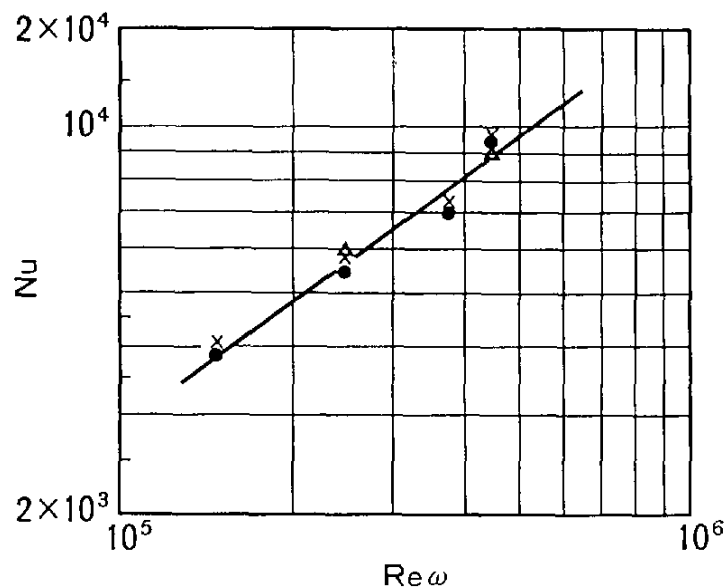


Figure 3.10: Experimental relations between Nusselt number and rotational Reynolds number [64]

3.4 *Compression and Discharge Process*

Analysis of the compression and discharge processes are required to find the variation of gas temperature (or pressure) for different angular positions of male rotor. For a constant angular speed of the rotor, the variation of temperature (or pressure) can be expressed as time rate quantities. Using ideal gas law, the variation

of one thermodynamic property can be related with that of the other properties. The analysis of compression process in a screw compressor is carried out on the principles of the First Law of Thermodynamics for a flow system. The control volume for the analysis of gas phase is shown in Figure 3.11. The control volume for this analysis is based on the following assumptions.

- Gas properties are uniform throughout the control volume at any instant of time.
- The working substance is a perfect gas with constant specific heats.
- Heat transfer to the casing and rotor walls is negligible.
- Gas and oil never change phase.
- Average clearances are used in determining leakage flows. It is assumed that such averaging gives a good representation of the actual leakage flows.
- Pressure is homogeneous throughout the working space at any instant.
- Oil is an incompressible fluid.
- Heat exchange between gas and oil is in proportion to the temperature difference between the gas and the oil in the cavities.
- The oil and gas are assumed to be separate fluids and their interaction takes place only through heat transfer.
- It is assumed that the heat of compression is transferred only to the injected oil.
- Gas and oil states are homogeneous throughout the working space at any instant.

Mass balance of gas over the control volume is rewritten as:

$$\frac{dM_g}{dt} = \dot{m}_{gi} - \dot{m}_{go} \quad (3.43)$$

The rate of change of energy of the control volume (with negligible kinetic and potential energies) in the flow process can be written as:

$$\frac{dE_v}{dt} = \frac{dQ}{dt} - \frac{dW}{dt} + \frac{dH_g}{dt} + \frac{dH_l}{dt} \quad (3.44a)$$

For a stationary control volume, the kinetic and potential energies are assumed to be negligible so that the above equation can be written in terms of internal energy of the system as:

$$\frac{dU_g}{dt} = \frac{dQ}{dt} - \frac{dW}{dt} + \frac{dH_g}{dt} + \frac{dH_l}{dt} \quad (3.44b)$$

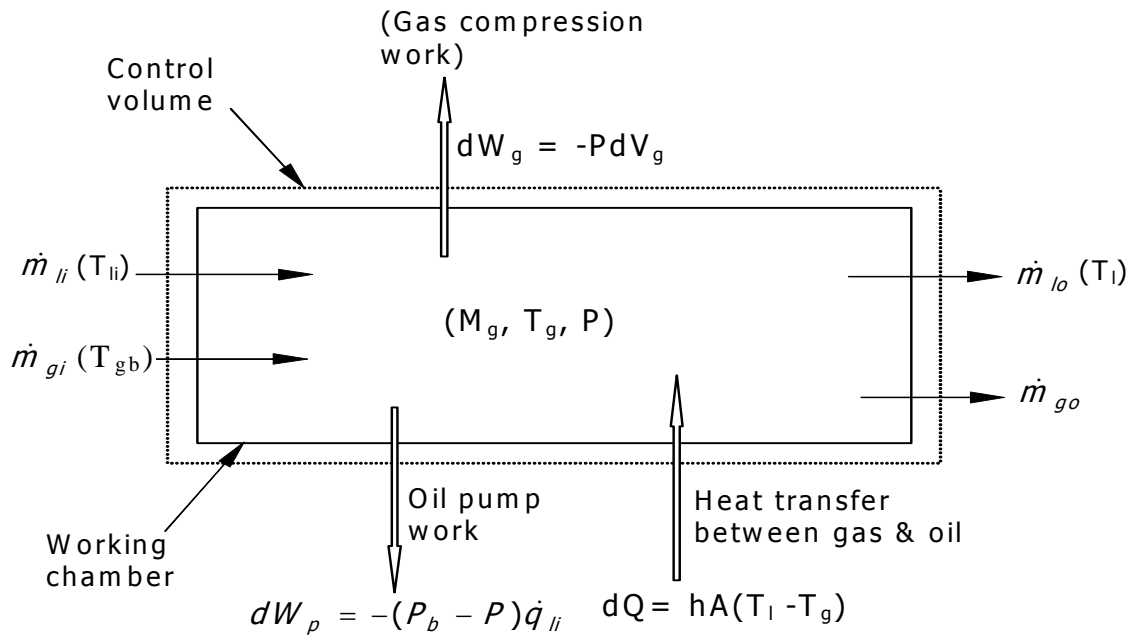


Figure 3.11: Schematic diagram for First Law analysis of control volume for gas phase

Over a time interval dt , the change in internal energy from the above equation can be written as:

$$dU_g = dQ - dW + dH_g + dH_l \quad (3.45)$$

The internal energy of gas in the control volume can also be written as:

$$U_g = C_v M_g T_g \quad (3.46)$$

The internal energy change in time dt from the above equation can be expressed as:

$$dU_g = C_v M_g dT_g + C_v T_g dM_g \quad (3.47)$$

The net enthalpy input in time dt (input enthalpy-output enthalpy) of gas due to leakage is given by the relation:

$$dH_g = C_p T_{gb} dM_{gi} - C_p T_g dM_{go} \quad (3.48)$$

Since oil temperature remains constant for a small time period dt , the net enthalpy input of leakage oil is due to the difference in their flow work and is expressed as:

$$dH_l = P_b \frac{\dot{m}_{li}}{\rho_l} dt - P \frac{\dot{m}_{lo}}{\rho_l} dt \quad (3.49)$$

The gas work done in time dt due to the change in volume of cavities is given by:

$$dW_g = PdV_g \quad (3.50)$$

The change in net gas volume in time dt is defined as:

$$dV_g = dV - \frac{\dot{m}_{li}}{\rho_l} dt + \frac{\dot{m}_{lo}}{\rho_l} dt \quad (3.51)$$

The oil pump work due to leakage is defined as:

$$dW_p = -(P_b - P) \frac{\dot{m}_{li}}{\rho_l} dt \quad (3.52)$$

The heat exchange between the gas and oil is given by the relation:

$$dQ = hA(T_l - T_g)dt \quad (3.53)$$

Substituting equations (3.47), (3.48), (3.49), (3.50), (3.51) (3.52), and (3.53) in equation (3.45) and rearranging, the rate of change of working gas temperature is obtained as:

$$\begin{aligned} \frac{dT_g}{dt} = & \left[-\frac{(k-1)T_g}{V_g} \left(\frac{dV}{dt} - \frac{P_b}{P} \frac{\dot{m}_{li}}{\rho_l} + \frac{\dot{m}_{lo}}{\rho_l} \right) + \frac{\dot{m}_{gi}}{M_g} (kT_{gb} - T_g) \right. \\ & \left. - \frac{\dot{m}_{go}}{M_g} (k-1)T_g - \frac{hA}{C_v M_g} (T_g - T_l) \right] \end{aligned} \quad (3.54)$$

The first term on the right-hand side of the above equation relates to the change in geometrical volume including the rate of leakage of oil volume. The second and third terms represent the effect of gas leakage into and out of the compression cavities respectively. The last term is derived from the heat transfer between gas and oil.

Since oil is an incompressible fluid, the rate of pressure change in the cavities is related to the rate of change of gas volume. The gas volume change is given by the formula:

$$\frac{dV_g}{dt} = \frac{dV}{dt} + \frac{\dot{m}_{lo}}{\rho_l} - \frac{\dot{m}_{li}}{\rho_l} \quad (3.55)$$

Assuming that the working fluid is an ideal gas, the equation of state is expressed as:

$$PV_g = M_g RT_g \quad (3.56)$$

The differential form of the above equation is:

$$\frac{dP}{dt} = \frac{1}{V_g} \left[-P \frac{dV_g}{dt} + RT_g \frac{dM_g}{dt} + RM_g \frac{dT_g}{dt} \right] \quad (3.57)$$

Substitution of equations (3.43), (3.54), and (3.55) in equation (3.57) results in the relation:

$$\begin{aligned} \frac{dP}{dt} = & \frac{1}{V_g} \left[-kP \left(\frac{dV}{dt} + \frac{\dot{m}_{lo}}{\rho_l} \right) + (kP_b - P_b + P) \frac{\dot{m}_{li}}{\rho_l} + k \frac{T_{gb} PV_g}{T_g M_g} \dot{m}_{gi} \right. \\ & \left. - k \frac{PV_g}{M_g} \dot{m}_{go} - \frac{PV_g hA}{C_v M_g T_g} (T_g - T_l) \right] \end{aligned} \quad (3.58)$$

The rate of change of oil temperature in the compressor cavities can be obtained from energy balance over the control volume for oil phase separately. The schematic diagram of control volume is shown in Figure 3.12. This analysis yields the temperature of oil over a differential time interval as a parameter for the calculation of temperature and pressure variations of gas in equations (3.54) and (3.58). Since only the temperature variation of oil is required, the control volume is assumed to be undergoing a constant pressure process.

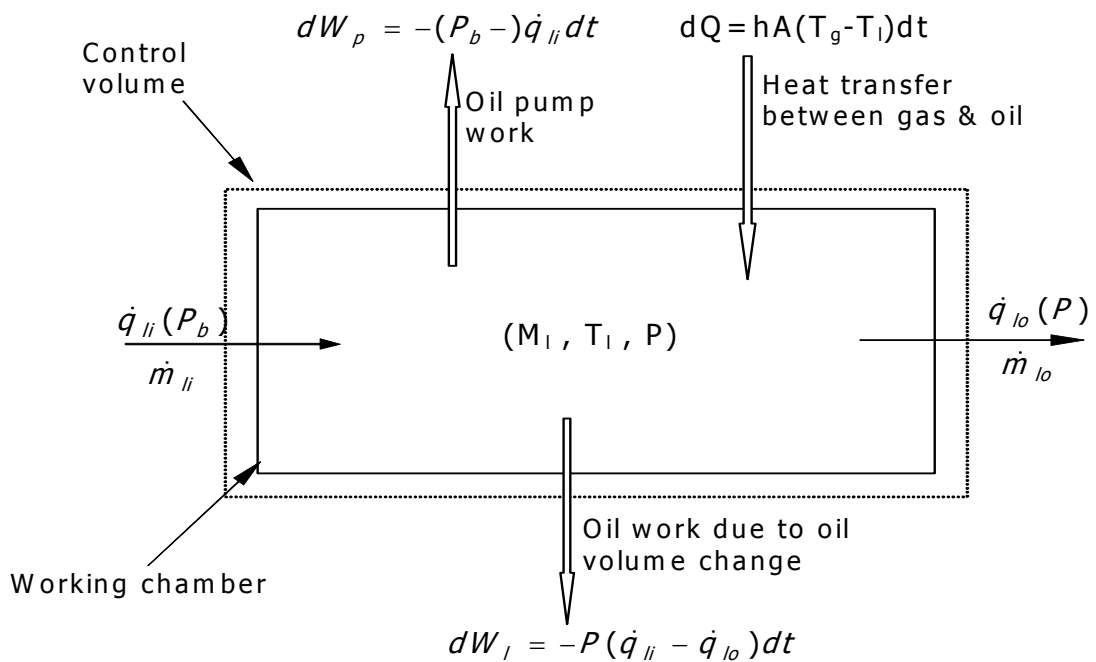


Figure 3.12: Schematic diagram for First Law analysis of control volume for oil phase

The mass balance equation for the oil is rewritten as:

$$\frac{dM_l}{dt} = \dot{m}_{li} - \dot{m}_{lo} \quad (3.59)$$

For a stationary control volume, the kinetic and potential energies of oil are assumed to be negligible. Hence, the rate of internal energy change of oil can be written as:

$$\frac{dU_I}{dt} = \frac{dH_I}{dt} + \frac{dQ_I}{dt} - \left(\frac{dW_I}{dt} + \frac{dW_p}{dt} \right) \quad (3.60)$$

Over a time interval dt , the above equation can be stated as:

$$dU_I = dH_I + dQ_I - (dW_I + dW_p) \quad (3.61)$$

The change in internal energy of oil can also be expressed in terms of the enthalpy change and the flow work as shown below.

$$dU_I = dH_I - \left(P_b \frac{\dot{m}_{li}}{\rho_I} - P \frac{\dot{m}_{lo}}{\rho_I} \right) dt \quad (3.62)$$

The enthalpy change of oil can be written in terms of change of mass and temperature as:

$$dH_I = C_I M_I dT_I + C_I T_I dM_I \quad (3.63)$$

The net enthalpy input of oil in time dt due to leakage is then written as:

$$dH_I = (\dot{m}_{li} C_I T_{lb} - \dot{m}_{lo} C_I T_I) dt \quad (3.64)$$

The heat gained by oil from the working gas during the compression process is:

$$dQ = hA(T_g - T_I) dt \quad (3.65)$$

The work done due to change in oil volume can be written as:

$$dW_I = P \left(\frac{\dot{m}_{li}}{\rho_I} - \frac{\dot{m}_{lo}}{\rho_I} \right) dt \quad (3.66)$$

The pump work spent on leakage of oil can be expressed as:

$$dW_p = (P_b - P) \frac{\dot{m}_{li}}{\rho_l} dt \quad (3.67)$$

Substituting equations (3.62), (3.63), (3.64), (3.65), (3.66), and (3.67) in equation (3.61) and rearranging, the rate of change of oil temperature is obtained as:

$$\frac{dT_l}{dt} = (T_{lb} - T_l) \frac{\dot{m}_{li}}{M_l} + \frac{hA}{M_l C_l} (T_g - T_l) \quad (3.68)$$

In summary, we have derived the following set of equations that describes the compression-discharge process.

$$\frac{dM_g}{dt} = \dot{m}_{gi} - \dot{m}_{go} \quad (E_1)$$

$$\frac{dM_l}{dt} = \dot{m}_{li} - \dot{m}_{lo} \quad (E_2)$$

$$\frac{dV_g}{dt} = \frac{dV}{dt} + \frac{\dot{m}_{lo}}{\rho_l} - \frac{\dot{m}_{li}}{\rho_l} \quad (E_3)$$

$$\begin{aligned} \frac{dP}{dt} = \frac{1}{V_g} [& -kP \left(\frac{dV}{dt} + \frac{\dot{m}_{lo}}{\rho_l} \right) + (kP_b - P_b + P) \frac{\dot{m}_{li}}{\rho_l} + k \frac{T_{gb} PV_g}{T_g M_g} \dot{m}_{gi} \\ & - k \frac{PV_g}{M_g} \dot{m}_{go} - \frac{PV_g hA}{C_v M_g T_g} (T_g - T_l)] \end{aligned} \quad (E_4)$$

$$\begin{aligned} \frac{dT_g}{dt} = [& -\frac{(k-1)T_g}{V_g} \left(\frac{dV}{dt} - \frac{P_b}{P} \frac{\dot{m}_{li}}{\rho_l} + \frac{\dot{m}_{lo}}{\rho_l} \right) + \frac{\dot{m}_{gi}}{M_g} (kT_{gb} - T_g) - \frac{\dot{m}_{go}}{M_g} (k-1)T_g \\ & - \frac{hA}{C_v M_g} (T_g - T_l)] \end{aligned} \quad (E_5)$$

$$\frac{dT_l}{dt} = (T_{lb} - T_l) \frac{\dot{m}_{li}}{M_l} + \frac{hA}{M_l C_l} (T_g - T_l) \quad (E_6)$$

In the above set of equations (E₁) to (E₆), time t is the independent variable and M_g, M_l, V_g, P, T_g, and T_l are the six dependent variables whose history of change is described the six equations over a cycle.

3.5 Performance Evaluation

Many efficiency definitions exist in literature that qualify the mass flow and power performance characteristics of a compressor. Different definitions are often used interchangeably throughout the compressor industry. The performance index of a compressor is characterised by its volume or mass handling capacity and specific power consumption. The losses such as friction and transmission loss are redundant and can be used for expression of overall performance. Thus the performance index of a compressor is assigned by two efficiencies: volumetric efficiency and power efficiency. The power efficiency may be called adiabatic, isothermal or polytrophic efficiency depending on the compression process. An excellent review by Ueno and Hunter [118] gives the volumetric and power efficiencies of reciprocating compressor.

The volumetric efficiency of a reciprocating compressor is based on expansion of entrapped gas left at the end of compression in the clearance volume. Unlike reciprocating compressor, the volumetric efficiency of screw compressor depends on the leakage gas volume through the clearances from the discharge end to suction cavities. A schematic diagram of reciprocating compressor analogous to oil injected twin-screw compressor given by Fujiwara *et al.* [65] is shown in Figure 3.13.

Volumetric efficiency

It is evident from Figure 3.13 that the actual amount of fresh charge taken during suction process decreases due to recirculation of leakage gas. The volumetric efficiency can be defined either in terms of volume flow rate or in terms of mass flow rate to yield the same value.

$$\begin{aligned} \eta_v &= (\text{Volume of gas delivered at suction condition for a pair of rotor cavities}) / \\ &\quad (\text{volume of meshed male and female rotor cavities}) \\ &= (\text{Mass delivered for a pair of rotor cavities}) / (\text{Theoretical mass of gas} \\ &\quad \text{contain for the same volume at suction condition}) \end{aligned}$$

The amount of mass present at the end of suction process is:

$$M_{t1} = \frac{P_s V_{t1}}{RT_1} = \frac{P_s V_1}{RT_s} \quad (3.69)$$

where V_{t1} is the volume of suction chamber, V_1 is the equivalent volume of gas at suction temperature, and T_1 is temperature of gas in the suction chamber.

The theoretical amount of gas mass is:

$$M_{ts} = \frac{P_s V_{t1}}{RT_s} \quad (3.70)$$

But the surface temperature of a pair of grooves will be different from the gas temperature under suction conditions. Hence, it is necessary to find the gas mass inducted at the average surface temperature of the suction chamber. The gas mass inducted at average surface temperature of suction cavities may be defined as

$$M_{t1} = M_{ts} \frac{T_s}{T_1} \quad (3.71)$$

Thus, M_{t1} is the amount of gas mass present in the suction chamber consisting of a pair of cavities including the leakage mass. The theoretical gas flow rate at temperature T_1 over a suction duration t_s is:

$$\dot{m}_t = \frac{M_{t1}}{t_s} \quad (3.72)$$

The net gas mass leakage rate from one pair of grooves is:

$$\dot{m}_{gl} = \dot{m}_{gj} - \dot{m}_{go} \quad (3.73)$$

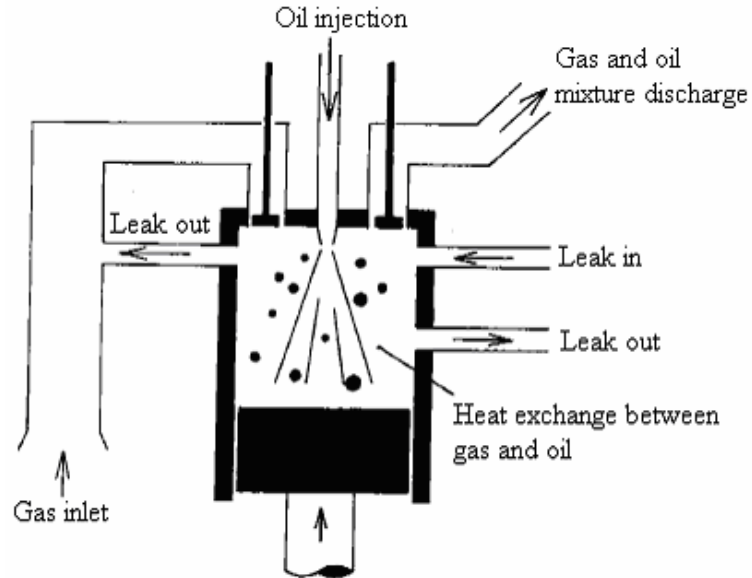


Figure 3.13: Schematic diagram of a reciprocating compressor analogous to an oil injected twin screw compressor [65]

The total leakage from all the cavities over a suction duration t_s is:

$$M_{il} = \dot{m}_{gl} \times t_s \quad (3.74)$$

Thus the rate of fresh gas mass flow is:

$$\dot{m}_{dt} = \dot{m}_t - \dot{m}_{gl} \quad (3.75)$$

The maximum rate of fresh gas mass flow is:

$$\dot{m}_{ts} = \frac{M_{ts}}{t_s} \quad (3.76)$$

Thus, the theoretical volumetric efficiency of screw compressor is derived to be:

$$\eta_{tv} = \frac{\dot{m}_{dt}}{\dot{m}_{ts}} = \frac{(M_{t1} - M_{il})}{M_{ts}} = \frac{M_{t1} - \dot{m}_{gl}t_s}{M_{ts}} \quad (3.77)$$

The theoretical volumetric efficiency is based on the theoretical mass flow rate. The experimental mass flow rate will always be less than the theoretical inducted mass flow rate due to imperfect nature of ports, wall friction and other losses. The experimental volumetric efficiency may be calculated based on the actual measurement of mass flow rate. The experimental volumetric efficiency is defined as:

$$\eta_{ev} = \frac{\dot{m}_e}{\dot{m}_{ts}} \quad (3.78)$$

In a screw compressor, injection of oil improves the volumetric efficiency. The improvement is due to the fact that oil acts as a sealant to decrease the leakage mass and that the injection of oil makes the compression process to approach isothermal situation. However, addition of excess oil decreases the volumetric efficiency due to the availability of less volume during the suction process to admit fresh charge of gas.

Adiabatic efficiency

If the compression is an adiabatic process, the adiabatic compression work is:

$$\dot{W}_{ad} = \dot{m}_{dt} c_p T_s \left[\left(\frac{P_d}{P_s} \right)^{\frac{k-1}{k}} - 1 \right] \quad (3.79)$$

where $k = C_p/C_v$ for the gas.

Similarly, for isothermal compression:

$$\dot{W}_{iso} = \dot{m}_{dt} R T_s \ln \left(\frac{P_d}{P_s} \right) \quad (3.80)$$

The theoretical mass flow rate \dot{m}_{dt} is usually different from the experimental mass flow rate \dot{m}_e . Thus based on experimental mass flow quantities, these works can be redefined as:

$$\dot{W}_{ad, re} = \dot{m}_e c_p T_s \left[\left(\frac{P_d}{P_s} \right)^{\frac{k-1}{k}} - 1 \right] \quad (3.81)$$

and

$$\dot{W}_{iso, re} = \dot{m}_e R T_s \ln \left(\frac{P_d}{P_s} \right) \quad (3.82)$$

The actual power input to the compressor for only gas compression is calculated from the area of the indicator diagram. The indicator diagram is the actual power for compression work, which is obtained from an experimentally measured p-v curve. This curve may be obtained through the difficult and expensive process of conducting compressor tests with pressure transducers located within the pair of cavities. Alternatively, the power can be estimated in terms of enthalpy gain of the flow and the heat transfer rate, assuming that we can measure the discharge and suction temperatures accurately. This estimate may be expressed as shown below.

$$\dot{W}_{act, e} = \dot{m}_e c_p (T_d - T_s) \begin{cases} +Q_{removed} & \text{(Heat leaving the system)} \\ -Q_{added} & \text{(Heat entering the system)} \end{cases} \quad (3.83)$$

The temperature difference ($T_d - T_s$) is the experimentally measured difference between the discharge and suction temperatures. It is common to ignore the heat transfer in the above equation because of the difficulty in its quantification and also because, in the event of rapid compression, the heat flux per cycle is generally small with respect to the change in gas enthalpy. This assumption may produce gross errors in the estimate of actual power.

The efficiency definitions based on the above descriptions are:

$$\text{Theoretical adiabatic efficiency, } \eta_{ad} = \frac{\dot{W}_{ad}}{\dot{W}_{act, e}} \quad (3.84)$$

$$\text{Experimental adiabatic efficiency, } \eta_{ad,e} = \frac{\dot{W}_{ad,e}}{\dot{W}_{act,e}} \quad (3.85)$$

$$\text{Theoretical isothermal efficiency, } \eta_{iso} = \frac{\dot{W}_{iso}}{\dot{W}_{act,e}} \quad (3.86)$$

$$\text{Experimental isothermal efficiency, } \eta_{iso,e} = \frac{\dot{W}_{iso,e}}{\dot{W}_{act,e}} \quad (3.87)$$

To overcome all these practical difficulties, the efficiency is defined in terms of system power, which can be measured reasonably accurately by an energy meter. The system power is the power required for an entire compression system and is the sum of the shaft power and several additional power requirements due to the presence of controllers and other peripheral systems. Based on the experimental shaft power, the overall efficiency can be defined as:

$$\text{Overall theoretical adiabatic efficiency, } \eta_{over,ad} = \frac{\dot{W}_{ad}}{\dot{W}_{sys,e}} \quad (3.88)$$

$$\text{Overall experimental adiabatic efficiency, } \eta_{over,ad,e} = \frac{\dot{W}_{ad,e}}{\dot{W}_{sys,e}} \quad (3.89)$$

$$\text{Overall theoretical isothermal efficiency, } \eta_{over,iso} = \frac{\dot{W}_{iso}}{\dot{W}_{sys,e}} \quad (3.90)$$

$$\text{Overall experimental isothermal efficiency, } \eta_{over,iso,e} = \frac{\dot{W}_{iso,e}}{\dot{W}_{sys,e}} \quad (3.91)$$

A more appropriate efficiency definition is specific overall efficiency, which is defined as follows.

$$\text{Specific overall adiabatic efficiency, } \bar{\eta}_{over,ad} = \frac{\left(\frac{\dot{W}_{ad}}{\dot{m}_{dt}} \right)}{\left(\frac{\dot{W}_{sys}}{\dot{m}_e} \right)} \quad (3.92)$$

$$\text{Specific overall isothermal efficiency, } \bar{\eta}_{over,iso} = \frac{\left(\frac{\dot{W}_{iso}}{\dot{m}_{dt}} \right)}{\left(\frac{\dot{W}_{sys}}{\dot{m}_e} \right)} \quad (3.93)$$

Equations (3.88) and (3.89) have been used to calculate the theoretical and experimental adiabatic efficiencies in the study, the results being presented in Chapter IV and V.

Chapter IV

NUMERICAL MODEL

Rotary twin-screw compressors are widely used in industry, particularly in refrigeration and cryogenic plants and for generating compressed air in industrial applications. Unlike other compressors, the compression mechanism in oil injected twin-screw compressor is complex. Hence it is difficult to estimate compressor performance analytically. Experimental investigations, on the other hand become too expensive because the manufacturing deviations from one compressor to another for the same capacity and for the same use are significant. Also, large number of specimen rotors have to be fabricated and tested to arrive at any reasonable conclusion. For example, interlobe clearance which has significant influence on volumetric efficiency can hardly be kept constant among different types of test rotors.

The operation of any compressor requires an input of mechanical work, which is eventually converted to heat, principally the heat of compression. The operation of compressor also results in mechanical, dynamic and frictional losses. Therefore, the efficiency of compressor is mainly dependent on the quality of rotor design. Apart from flow through leakage gaps, the quantity and type of lubricant used have significant effect.

The pressure and temperature of inducted gas and the temperature of injected oil have direct effect on temperature of the gas in suction cavities. Oil to gas mass ratio, pressure ratio, interlobe clearance, blowhole area, male wrap angle, and rotational speed of male rotor determine volumetric and adiabatic efficiencies. In this chapter, we have analysed the influence of these operating parameters on volumetric efficiency basing on the solution of governing equations derived in chapter III. As an example, data on particular compressors available in our laboratory have been taken as input parameters.

4.1 Evaluation of Heat transfer Coefficient

The value of the heat transfer coefficient between gas and oil is essential for simulation of the compression process. Fujiwara and Osada [64] determined the heat transfer coefficient using experimental performance data. The same methodology has been followed in this study. The heat transfer coefficient is determined from an experimental plot of the relative volumetric efficiency versus the suction temperature for four working fluids: air, nitrogen, argon and helium.

The expression for heat transfer coefficient as given by equation (3.39) in chapter III, is rewritten as:

$$h = \frac{kP_s V_{t1}}{(k-1)A t_s} \frac{d\eta_{ev}}{dT_s} \quad (4.1)$$

where k is ratio of specific heats, t_s is suction time, η_{ev} is experimental volumetric efficiency and T_s is suction temperature.

The heat transfer coefficient is related to gradient of volumetric efficiency which is assumed to be constant for constant heat transfer coefficient. At present, the estimation of volumetric efficiency is not essential to determine its gradient. This value can be easily obtained from the gradient of the relative volumetric efficiency. The relative efficiency is defined as the ratio of volumetric efficiency at a given temperature to the volumetric efficiency at a reference temperature.

$$\eta_{rel, ev} = \frac{\eta_{ev}}{\eta_{ev, std}} \quad (4.1a)$$

$$\begin{aligned} \eta_{rel, ev} &= \{ (V_{act} \text{ at a given temperature}) / (\text{Volume of the suction cavities}) \} / \{ (V_{act} \text{ at} \\ &\quad \text{reference temperature}) / (\text{Volume of the suction cavities}) \} \\ &= (\text{Volume flow rate at a given temperature}) / (\text{Volume flow rate at a reference} \\ &\quad \text{temperature}) \end{aligned}$$

Then

$$h = \frac{kP_s V_{t1}}{(k-1)A t_s} \eta_{ev, std} \frac{d\eta_{rel, ev}}{dT_s} \quad (4.1b)$$

$\eta_{ev, std}$ is an unknown but is expected have a value between 0.8 and 1. Considering the large uncertainty in the value of oil surface area, it is not worthwhile to determine h to very high accuracy. We may take a value of $\eta_{ev, std}$ to be unity for the purpose of calculating the value of heat transfer coefficient h . Then the working form of equation (4.1) becomes:

$$h = \frac{kP_s V_{t1}}{(k-1)A t_s} \frac{d\eta_{rel, ev}}{dT_s} \quad (4.1c)$$

The actual volume flow rate can be measured by rotameter at suction side for different suction temperatures. Using experimentally measured flow rate, relative volumetric efficiency as a function of inlet gas temperature for air, nitrogen argon, and helium are presented in Figures 4.1 to 4.4 respectively. It is observed that the relationships are linear in all four cases. The slopes of these lines give $\frac{d\eta_{rel, ev}}{dT_s}$ for the four working fluids. These values can be directly substituted in equation (4.1) to yield the heat transfer coefficient between gas and oil. The values of $\frac{d\eta_{rel, ev}}{dT_s}$ for air, nitrogen, argon, and helium are estimated to be $0.0026K^{-1}$, $0.0027K^{-1}$, $0.0026K^{-1}$ and $0.0025K^{-1}$ respectively. (Equations of the straight lines are given in their respective figures)

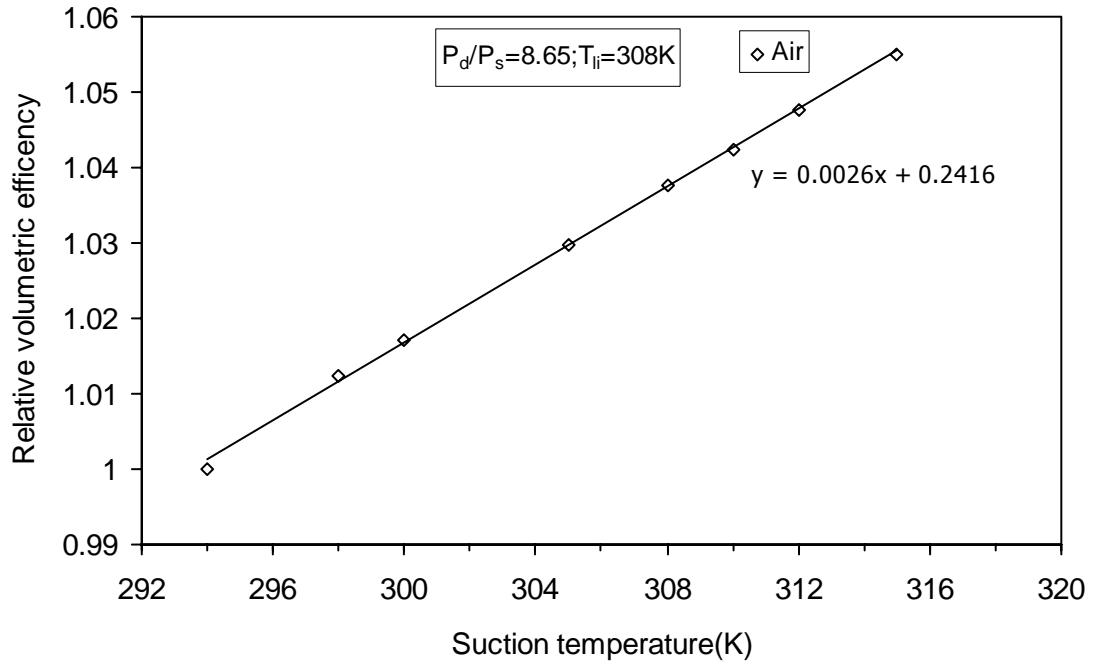


Figure 4.1: Experimental volumetric efficiency curve against suction temperature with air (efficiencies are relative to suction temperature of 294K).

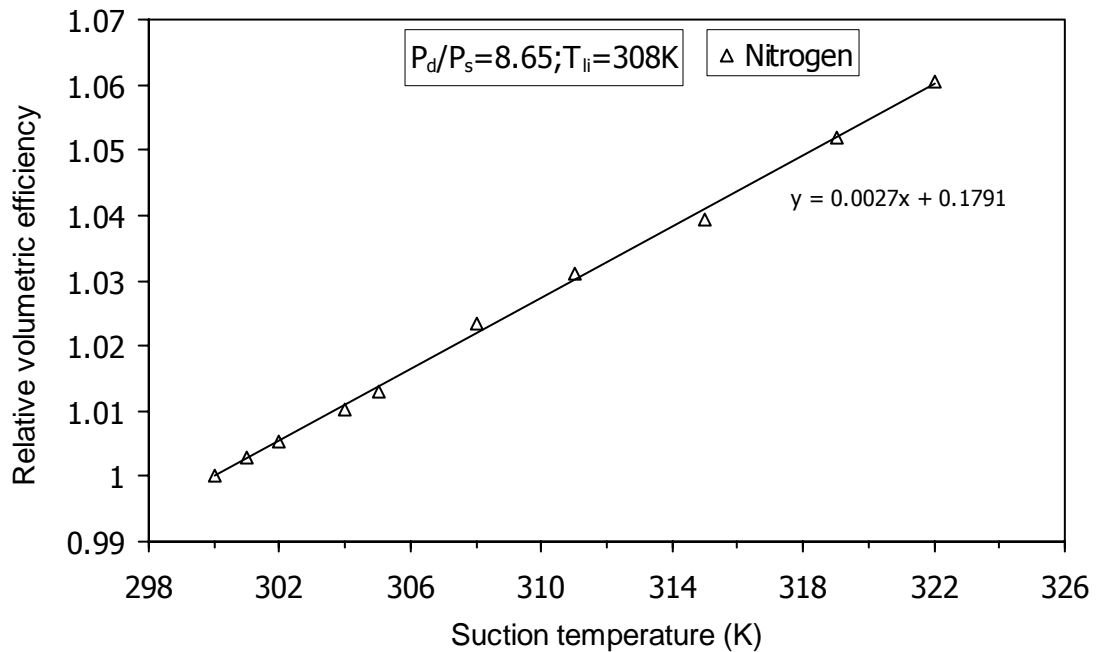


Figure 4.2: Experimental volumetric efficiency curve against suction temperature with nitrogen (efficiencies are relative to suction temperature of 300K).

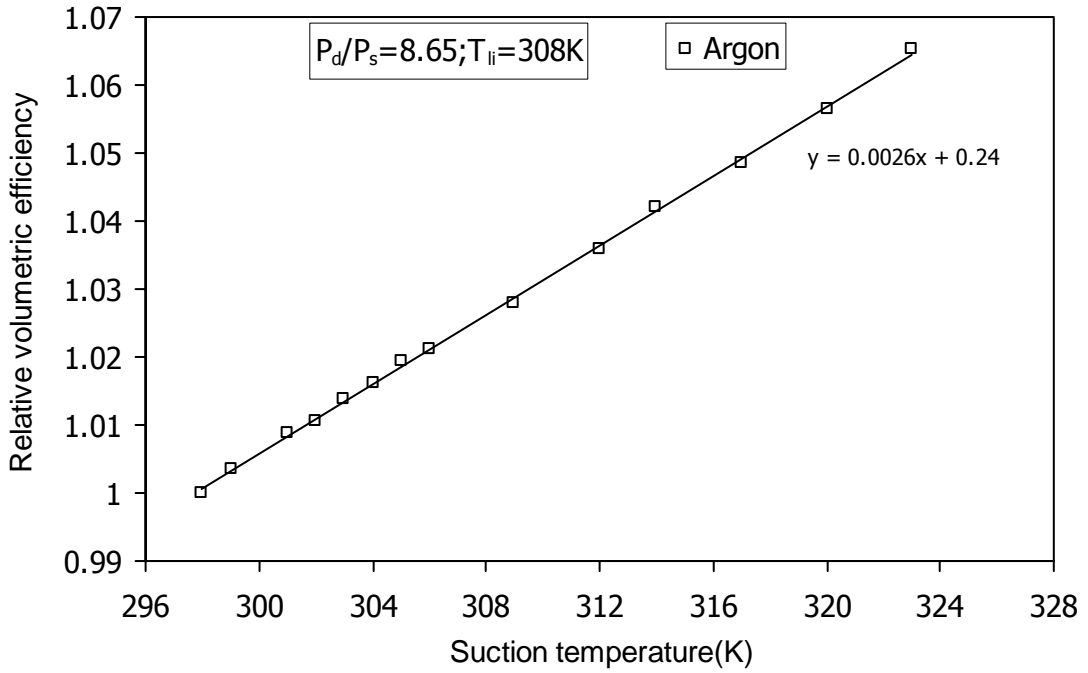


Figure 4.3: Experimental volumetric efficiency curve against suction temperature with argon (efficiencies are relative to suction temperature of 298K).

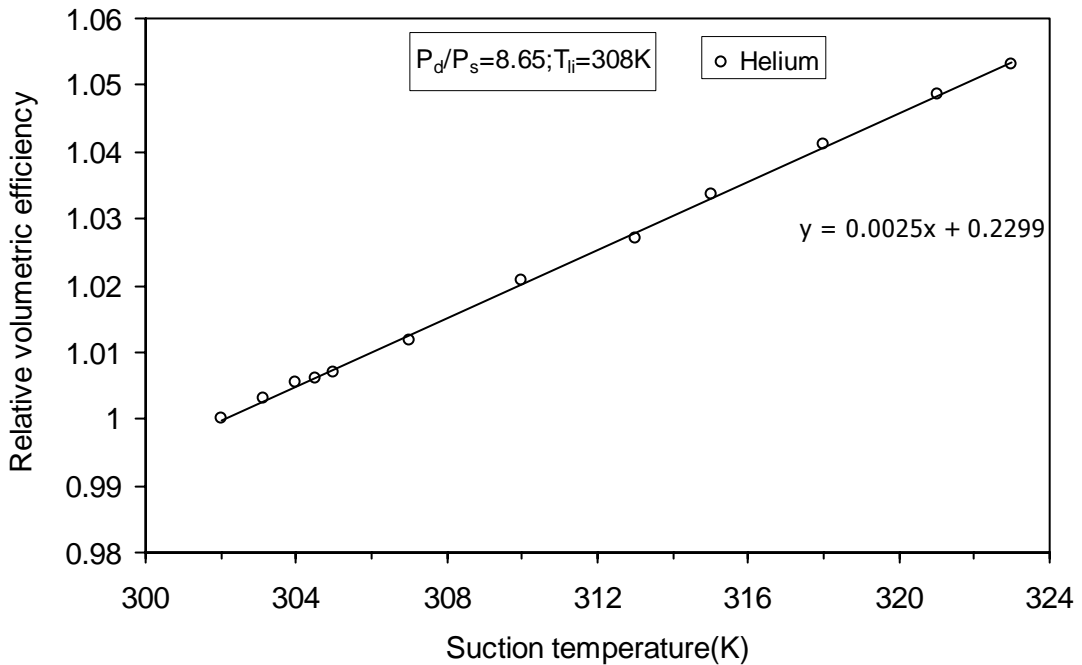


Figure 4.4: Experimental volumetric efficiency curve against suction temperature with helium (efficiencies are relative to suction temperature of 302K).

4.2. Summary of Governing Equations

The set of equations derived in chapter III are rewritten here before solving them. The leakage gas and oil flow rates and the state properties of gas during the compression and discharge process can be found with respect to time using these algebraic and differential equations. Temperature T_1 is the final temperature at the end of the suction step, but the initial temperature at the starting of the compression step.

The set of first order differential equations (3.43), (3.54), (3.55), (3.58), (3.59), and (3.68) and the algebraic equation (3.30) are reproduced here for ready reference. They have been renumbered for clarity of presentation.

$$-c_p M_{il} T_1^2 + T_1 [c_p M_{t1} T_s + c_p M_{il} T_s - hA(T_{oil} - T_s)t_s] - c_p M_{t1} T_s^2 = 0 \quad (4.2)$$

$$\frac{dV_g}{dt} = \frac{dV}{dt} + \frac{\dot{m}_{lo}}{\rho_l} - \frac{\dot{m}_{li}}{\rho_l} \quad (4.3)$$

$$\begin{aligned} \frac{dP}{dt} = \frac{1}{V_g} [& -kP \left(\frac{dV}{dt} + \frac{\dot{m}_{lo}}{\rho_l} \right) + (kP_b - P_b + P) \frac{\dot{m}_{li}}{\rho_l} + k \frac{T_{gb} P V_g}{T_g M_g} \dot{m}_{gi} \\ & - k \frac{P V_g}{M_g} \dot{m}_{go} - \frac{P V_g h A}{C_v M_g T_g} (T_g - T_l)] \end{aligned} \quad (4.4)$$

$$\begin{aligned} \frac{dT_g}{dt} = [& -\frac{(k-1)T_g}{V_g} \left(\frac{dV}{dt} - \frac{P_b}{P} \frac{\dot{m}_{li}}{\rho_l} + \frac{\dot{m}_{lo}}{\rho_l} \right) + \frac{\dot{m}_{gi}}{M_g} (kT_{gb} - T_g) - \frac{\dot{m}_{go}}{M_g} (k-1)T_g \\ & - \frac{hA}{C_v M_g} (T_g - T_l)] \end{aligned} \quad (4.5)$$

$$\frac{dT_l}{dt} = (T_{lb} - T_l) \frac{\dot{m}_{li}}{M_l} + \frac{hA}{M_l C_l} (T_g - T_l) \quad (4.6)$$

$$\frac{dM_g}{dt} = \dot{m}_{gi} - \dot{m}_{go} \quad (4.7)$$

$$\frac{dM_l}{dt} = \dot{m}_{li} - \dot{m}_{lo} \quad (4.8)$$

The set of six differential equations (4.3) to (4.8) describe the six variables V_g , P , T_g , T_l , M_g and M_l as function of time, during compression-discharge process, the algebraic equation (4.2) giving the initial temperature T_1 . The variable V and hence $\frac{dV}{dt}$, are known functions of time. The set of differential equations can be written in their respective functional form as:

$$\frac{dV_g}{dt} = f_1\left(\frac{dV}{dt}, \dot{m}_{li}, \dot{m}_{lo}, \rho_l\right) \quad (4.9)$$

$$\frac{dP}{dt} = f_2\left(T_g, V_g, P, M_g, T_l, \frac{dV}{dt}, P_b, T_{gb}, \dot{m}_{gi}, \dot{m}_{go}, \dot{m}_{li}, \dot{m}_{lo}, \rho_l\right) \quad (4.10)$$

$$\frac{dT_g}{dt} = f_3\left(T_g, V_g, P, M_g, T_l, \frac{dV}{dt}, P_b, T_{gb}, \dot{m}_{gi}, \dot{m}_{go}, \dot{m}_{li}, \dot{m}_{lo}, \rho_l\right) \quad (4.11)$$

$$\frac{dT_l}{dt} = f_4(T_g, T_l, T_{lb}, M_l, \dot{m}_{li}) \quad (4.12)$$

$$\frac{dM_g}{dt} = f_5(\dot{m}_{gi}, \dot{m}_{go}) \quad (4.13)$$

$$\frac{dM_l}{dt} = f_6(\dot{m}_{li}, \dot{m}_{lo}) \quad (4.14)$$

The variables P_b , T_{gb} , T_{lb} , the subscript b standing for locations beyond the working chamber, refer to the cavities that are ahead of and behind the cavities being analysed. The pressure and temperature of gas and oil in these cavities need to be known at time t for calculating of gas and oil leakage into and out of the working chamber. The values of the variables P_b , T_{gb} , T_{lb} in the lagging chamber at time t are equal to those of P , T_g , T_l at a time $t - \frac{1}{N_m n_m}$, while those in the leading chamber are equal to the value of P , T_g , T_l at a time $t + \frac{1}{N_m n_m}$. The leakage flow rates of gas and oil are calculated from equations (3.15), (3.16a), (3.17), and (3.20).

Equation (4.2) is utilized to determine T_1 , the fluid temperature at the end of the suction process, once the leakage flow rates of gas and oil are established. This

temperature is an input parameter for calculation of gas leakage. The density of oil (ρ_l) can be assumed to be constant and independent of oil temperature. Thus, in the above set of equations the variables V_g , P , T_g , T_l , M_g , and M_l are to be evaluated from six differential equations. Set of these equations poses the initial value problem which can be solved by a standard iterative algorithm until all the parameters are converged.

The theoretical volumetric and adiabatic efficiencies of twin-screw compressor are estimated after computing the leakage flow rates of gas and oil. Numerically it is convenient to find the volumetric efficiency in terms of mass flow rate rather than volume flow rate. Theoretical volumetric efficiency of twin-screw compressor is redefined at condition (P_s, T_1) as:

$$\eta_{rv} = \frac{\dot{m}_{dt}}{\dot{m}_t} = \frac{(M_{t1} - M_{il})}{M_t} = \frac{(M_{t1} - \dot{m}_{gl}t_s)}{M_{t1}} \quad (4.15)$$

Similarly, the experimental volumetric efficiency is redefined as:

$$\eta_{rev} = \frac{\dot{m}_e}{\dot{m}_t} \quad (4.16)$$

The theoretical adiabatic efficiency is defined as the ratio of theoretical work required to compress the gas adiabatically to the actual power input to the compressor system and is written as:

$$\eta_{ra} = \frac{\dot{W}_{ad}}{\dot{W}_{sys,e}} \quad (4.17)$$

The experimental adiabatic efficiency of the compressor is expressed as:

$$\eta_{rae} = \frac{\dot{W}_{ad,e}}{\dot{W}_{sys,e}} \quad (4.18)$$

4.3 *Input and output Parameters*

Simulation of compressor performance needs input data on the geometrical and process parameters. A list of parameters is given in tables 4.1 to 4.11 for 5.5 kW and 37 kW compressors.

Table 4.1: Rotor specifications of 5.5 kW prototype compressor

Name of constant	Value	Units
Number of lobes on the male rotor	5	none
Number of lobes on the female rotor	6	none
Male wrap angle	300	degree
Diameter of male rotor	72	mm
Diameter of female rotor	54	mm
Length of the rotor	90	mm
Cross sectional area of male rotor groove	210	mm ²
Cross sectional area of female rotor groove	170	mm ²
Lobe tip width of male rotor	0.5	mm
Lobe tip width of female rotor	1.8	mm
Rotational speed of male rotor	4350	rpm

Table 4.2: Clearances and Sealing line lengths obtained from experiment/actual measurements of 5.5 kW compressor

Constants	Value	Unit
Inter lobe clearance	0.027	mm
Rotor tip-housing clearance	0.03	mm
Clearance between rotor and discharge end face plate	0.03	mm
Leading blowhole area	2	mm ²
Trailing blowhole area	2	mm ²
Interlobe sealing line length	36	mm
Sealing line length of rotor tip housing of male rotor	180	mm
Sealing line length of rotor tip housing of female rotor	143	mm
Sealing line length at leading discharge end face of male rotor	18	mm
Sealing line length at leading discharge end face of female rotor	16	mm
Sealing line length at lagging discharge end face of male rotor	28	mm
Sealing line length at lagging discharge end face of female rotor	20	mm

Table 4.3 Flow coefficients in 5.5 kW compressor

Leakage path name	value	Units
Inter lobe clearance	0.65	none
Clearance between lobe tip and casing bore	0.7	none
Clearance between rotor and discharge end face plate	0.4	none
Leading blowhole	0.7	none
Trailing blowhole	0.6	none

Table 4.4: Input constants in 5.5 kW compressor

Name of constant	Value	Units
Heat transfer area between gas and oil (eq. 3.40)	0.00489	m ²
Density of oil (supplier's specifications)	843	kg/m ³
Specific heat of the oil (measured)	1.86	kJ/kg-K
Volume of a pair of male and female cavities	34.2×10 ⁻⁵	m ³

Table 4.5: Rotor specifications of 37 kW prototype compressor

Name of constant	Value	Units
Number of lobes on the male rotor	5	none
Number of lobes on the female rotor	6	none
Male wrap angle	300	degree
Diameter of male rotor	152	mm
Diameter of female rotor	118	mm
Length of the rotor	235	mm
Cross sectional area of male rotor groove	1075	mm ²
Cross sectional area of female rotor groove	1020	mm ²
Lobe tip width of male rotor	0.9	mm
Lobe tip width of female rotor	2.6	mm
Rotational speed of male rotor	2950	rpm

Table 4.6: Clearances and sealing line lengths obtained from experiment/actual measurements on 37 kW compressor

Constants	Value	Unit
Inter lobe clearance	0.035	mm
Rotor tip-housing clearance	0.03	mm
Clearance between rotor and discharge end face plate	0.029	mm
Leading blowhole area	3.3	mm ²
Trailing blowhole area	3.3	mm ²
Interlobe sealing line length	74	mm
Sealing line length of rotor tip housing of male rotor	460	mm
Sealing line length of rotor tip housing of female rotor	345	mm
Sealing line length at leading discharge end face of male rotor	34.5	mm
Sealing line length at leading discharge end face of female rotor	30	mm
Sealing line length at lagging discharge end face of male rotor	62.5	mm
Sealing line length at lagging discharge end face of female rotor	44	mm

Table 4.7: Flow coefficients in 37 kW compressor

Leakage path name	value	Units
Inter lobe clearance	0.62	none
Clearance between lobe tip and casing bore	0.67	none
Clearance between rotor and discharge end face plate	0.36	none
Leading blowhole	0.67	none
Trailing blowhole	0.58	none

Table 4.8: Input constants in 37 kW compressor

Name of constant	Value	Units
Heat transfer area between gas and oil (eq. 3.40)	0.02895	m ²
Density of oil (supplier's specifications)	843	kg/m ³
Specific heat of the oil (measured)	1.86	kJ/kg-K
Volume of a pair of male and female cavities	49.2×10 ⁻⁴	m ³

Table 4.9: Input variables to be calculated

Name of constant	Notation	Units
Modified gas constant for oil and gas mixture	R_m	J/kg-K
Specific heat ratio of oil and gas mixture	β	none
Specific heat ratio of gas	k	none
Heat transfer coefficient between gas and oil	h	W/m ² -K
Time required for suction process	t_s	sec
Time required for compression and discharge process	Γ	sec
Gas constant	R	J/kg K
Oil to gas mass ratio	ϕ	none
Male rotor tip speed	U_m	m/sec
Female rotor tip speed	U_f	m/sec

Table 4.10: Operating variables

Parameter	Notation	Units
Discharge pressure of working gas	P_d	N/m ²
Inlet pressure of working gas	P_s	N/m ²
Inlet temperature of the gas	T_s	K
Inlet temperature of the oil	T_{li}	K
RPS of the male rotor	N_m	rev/sec
Supplied Oil rate	m_{oil}	kg/sec
Density of gas	ρ_g	kg/m ³
Specific heat of gas at constant pressure	C_p	J/kg-K
Specific heat of gas at constant volume	C_v	J/kg-K

Table 4.11: Output Parameters

Parameter	Notation	Units
Pressure in the working space	P	N/m ²
Volume of the working space	V	m ³
Volume of gas in the working space	V _g	m ³
Temperature of gas in the working space	T _g	K
Temperature of oil in the working space	T _l	K
Mass of gas in the working space	M _g	kg
Mass of oil in the working space	M _l	kg
Leakage gas mass flow rate in to the cavity	m _{gi}	kg/sec
Leakage gas mass flow rate out of the cavity	m _{go}	kg/sec
Leakage oil mass flow rate in to the cavity	m _{li}	kg/sec
Leakage oil mass flow rate out of the cavity	m _{lo}	kg/sec

4.4 Solution of governing equations

The values of the variables P_b , T_{gb} , T_{lb} , m_{gi} , m_{go} , m_{li} , and m_{lo} are known at different time intervals from the results on the variables P , T_g , T_l over the full time duration for a known value of $\frac{dV}{dt}$ as discussed in the section 4.2. The flow coefficients can also be assumed to match with volumetric efficiency. Hence, the set of equations (4.9) to (4.14) can be reduced to another functional form consisting of six dependent variables V_g , P , T_g , T_l , M_g , and M_l . These equations represent the formulation of numerical solution by Runge-Kutta 4th order method as:

$$\frac{dV_g}{dt} = F_1(t, V_g, P, T_g, T_l, M_g, M_l) \quad (4.19)$$

$$\frac{dP}{dt} = F_2(t, V_g, P, T_g, T_l, M_g, M_l) \quad (4.20)$$

$$\frac{dT_g}{dt} = F_3(t, V_g, P, T_g, T_l, M_g, M_l) \quad (4.21)$$

$$\frac{dT_I}{dt} = F_4(t, V_g, P, T_g, T_I, M_g, M_I) \quad (4.22)$$

$$\frac{dM_g}{dt} = F_5(t, V_g, P, T_g, T_I, M_g, M_I) \quad (4.23)$$

$$\frac{dM_I}{dt} = F_6(t, V_g, P, T_g, T_I, M_g, M_I) \quad (4.24)$$

With their respective initial conditions at $t^0, V_g^0, P^0, T_g^0, T_I^0, M_g^0, M_I^0$ defined, 4th order Runge-Kutta method can be used to solve equations (4.19) to (4.24) for an incremental time step $h=\Delta t$ as outlined below. For convenience, the suffix i ($i=1$ to 6) is used to represent the k values of V_g , P , T_g , T_I , M_g and M_I respectively.

$$k_1(i) = hF_i(t^0, V_g^0, P^0, T_g^0, T_I^0, M_g^0, M_I^0) \quad (4.25)$$

$$k_2(i) = hF_i\left[t^0 + \frac{h}{2}, V_g^0 + \frac{k_1(1)}{2}, P^0 + \frac{k_1(2)}{2}, T_g^0 + \frac{k_1(3)}{2}, T_I^0 + \frac{k_1(4)}{2}, M_g^0 + \frac{k_1(5)}{2}, M_I^0 + \frac{k_1(6)}{2}\right] \quad (4.26)$$

$$k_3(i) = hF_i\left[t^0 + \frac{h}{2}, V_g^0 + \frac{k_2(1)}{2}, P^0 + \frac{k_2(2)}{2}, T_g^0 + \frac{k_2(3)}{2}, T_I^0 + \frac{k_2(4)}{4}, M_g^0 + \frac{k_2(5)}{2}, M_I^0 + \frac{k_2(6)}{2}\right] \quad (4.27)$$

$$k_4(i) = hF_i\left[t^0 + h, V_g^0 + k_3(1), P^0 + k_3(2), T_g^0 + k_3(3), T_I^0 + k_3(4), M_g^0 + k_3(5), M_I^0 + k_3(6)\right] \quad (4.28)$$

$$k(i) = \frac{1}{6}[k_1(i) + 2k_2(i) + 2k_3(i) + k_4(i)] \quad (4.29)$$

Hence, the values of six parameters after the first time step are,

$$V_g^1 = V_g^0 + k(1) \quad (4.30)$$

$$P^1 = P^0 + k(2) \quad (4.31)$$

$$T_g^1 = T_g^0 + k(3) \quad (4.32)$$

$$T_l^1 = T_l^0 + k(4) \quad (4.33)$$

$$M_g^1 = M_g^0 + k(5) \quad (4.34)$$

$$M_l^1 = M_l^0 + k(6) \quad (4.35)$$

To compute the variables $V_g^2, P^2, T_g^2, T_l^2, M_g^2, M_l^2$ at second time step, the variables $V_g^0, P^0, T_g^0, T_l^0, M_g^0, M_l^0$ are replaced by $V_g^1, P^1, T_g^1, T_l^1, M_g^1, M_l^1$.

The calculation of compression process is done by taking small male rotor rotation angle ' $\delta\theta$ ' in terms of time. It is assumed that the compression process starts when the suction process is completed and the tooth gap volume has reached its maximum. The compression-discharge time for 5.5 kW compressor at 4350 rpm is 0.01425 s for a wrap angle of 300° . For 10 number of time steps, the time for each step (Δt) is approximately 0.001425 s. At steady state, all the changes in the compressor working chamber/cavities are related to rotor turning and the state in a groove varies as function of rotor turning angle or time. Therefore, if the change in a state of one pair of grooves is calculated, the states in all other grooves can be known. All the governing equations summarized above are used for suction and discharge process simulation. Due to the overlapping of discharge processes over the discharge port area, the outlet pressure (discharge over certain angle of rotation of male rotor) is assumed to be constant. Thus for time step of 10 divisions, compression process is assumed to be 8 divisions and discharge process is 2 divisions with 60° overlap. Also

based on built-in volume ratio, the compression process is completed when the built in volume ratio reaches $5/6^{\text{th}}$ of the initial volume.

To calculate the leakage flow rate, the state of the grooves beyond the leakage path must be known a priori. But this information is not available at the beginning of the calculation. Therefore, to start with, the state in the grooves is computed assuming no leakage. Subsequently the leakage flow is calculated and the state is corrected following the Runge-Kutta procedure. This calculation is iterated until the system converges. Finally the volumetric and adiabatic efficiencies are calculated. An over view of the flow chart is given in Figure 4.5. A more elaborate step by step solution procedure is given below.

- Step 1:** Assuming no leakage initially. The initial values of $T_{gb} = T_g = T_1 = 300 \text{ K}$, $P_b = P = 1.0132 \text{ bar}$, $V_g = \text{suction gas volume}$ are assumed. Also appropriate values of flow coefficients are assumed to match with experimental volumetric efficiency.
- Step 2:** With the time steps of $\Delta t = 0.001425 \text{ s}$, equations (4.19) to (4.24) is solved by Runge-Kutta 4th order method. The functional relations for solution are given by equations (4.3) to (4.8). The equation (4.2) is solved for the suction temperature, T_1 .
- Step 3:** The step 2 is repeated for the up gradation of variables T_g , V_g , P , T_1 , M_g , M_l , and T_1 to achieve local convergence.
- Step 4:** If the change in all six variables in step 3 between two successive iterations is less than 10^{-6} , the local convergence criteria is assumed to be satisfied for that time division.
- Step 5:** For the subsequent time step Δt , the steps 2 to 4 are carried out till the end of compression process.
- Step 6:** If all the variables satisfy the convergence criteria between two successive iterations for the compression process, the programme is assumed to be independent of time divisions and it is globally converged. Otherwise, the time step is halved and the steps 2 to 6 are repeated.
- Step 7:** Since the values of relevant variables for the calculation of leakage are available at time $(t-\Delta t)$, t and $(t+\Delta t)$, these variables are again

recalculated in the presence of leakages. The leakage values are calculated from equations (3.15), (3.16a), (3.17), and (3.20).

- Step 8:** The steps 2 to 7 are repeated.
- Step 9:** The volumetric efficiency is calculated and compared with the experimental values.
- Step 10:** If the difference in volumetric efficiency is not acceptable, then a set of new flow coefficients are assumed.
- Step 11:** The steps 2 to 10 are repeated.
- Step 12:** The programme is terminated when the convergence criteria are satisfied in the steps 4, 6 and 10.

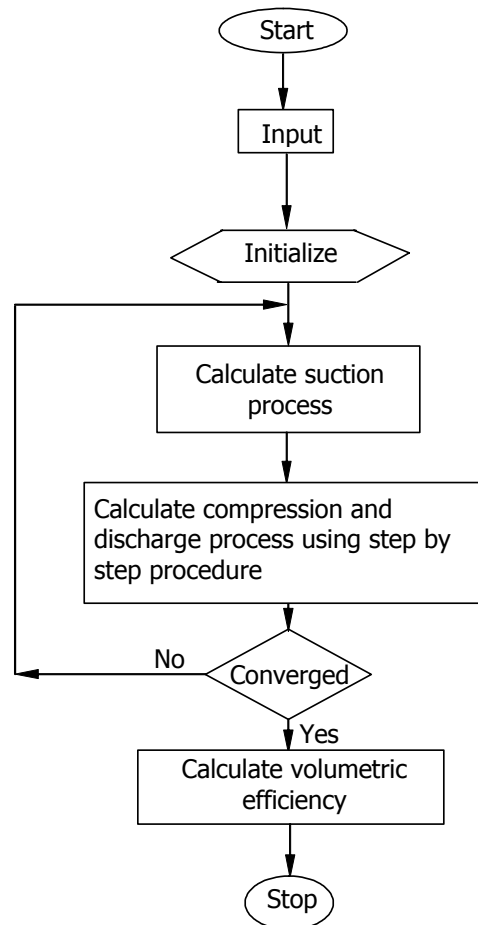


Figure 4.5: Flow diagram for numerical solution

4.5 *Results and Conclusions*

A numerical model of the oil injected twin-screw compressor has been developed covering both suction and compression-discharge processes to predict the performance of an oil injected twin screw compressor applied to compression of different working gases. Heat transfer coefficient between gas and oil used in numerical calculations is determined from experimental observations. The flow coefficients have been determined from experimentally obtained compressor efficiencies.

The objective of the present investigation is to evaluate the performance and study the possible effects of operational parameters on performance of commercially available air compressor with different working gases. All the selected gases are tested with two compressors of similar type but different capacities. Air is a mixture of nitrogen, oxygen, moisture and traces of other gases, with a molecular weight approximately 29. The thermophysical properties of nitrogen are nearer to that of air. In addition to air and nitrogen, we have used to two monatomic gases: argon and helium.

The influence of interlobe clearance on the p-v diagram profile with all four working gases is presented in Figures 4.6 to 4.9. These figures show that the area of the p-v diagram decreases with increase of interlobe clearance for all the working gases. This decrease is more severe for helium as shown in Figure 4.9. This is because of higher leakage rate from the compression chamber by interlobe leakage.

Figure 4.10 gives the temperature history of all four working gases during the compression and discharge process. The rise in temperature of all the gases during compression process appears higher than that observed in practice. It is because of the assumption that heat is transferred from gas to oil only. In reality, a significant portion of the heat generated will be transferred to the screw rotors and the casing in addition to the injected oil. The temperature profile for air and nitrogen are almost identical because of the near equality of their thermophysical properties. The rise in gas temperature in case of argon is highest due to the monatomic nature of the gas and high molecular weight. Temperature rise with helium is small because of low molecular weight and low density. The influence of oil to gas mass ratio on gas temperature rise for all the four working gases during compression process is

presented in Figures 4.11 to 4.14. It may be observed that the effect of oil to gas mass ratio beyond a certain limit has little effect on gas temperature.

The leakage of gas and oil through interlobe clearance goes directly to the suction chamber and reduces the charging efficiency. The variation of volumetric efficiency with interlobe clearance at a fixed injected oil temperature and at different rotational speeds of male rotor with different working gases is shown in Figures 4.15 to 4.18. The variation of volumetric efficiency of helium is relatively higher due to higher leakage rate. Variation of volumetric efficiency with interlobe clearance for different gases at fixed male rotor rotational speed, pressure ratio and injected oil temperature is presented in Figure 4.19. The influence of interlobe clearance on volumetric efficiency is relatively higher for helium than for the other three gases.

Figure 4.20 helps to visualize the influence of rotational speed of male rotor on volumetric efficiency with different working gases at fixed interlobe clearance, suction conditions and injected oil temperature. At lower rotational speed the volumetric efficiency of compressor with helium is less than that with the other gases. At higher rotational speed, the efficiency difference among working gases is low.

The influence of wrap angle on volumetric efficiency of a compressor is shown in Figure 4.21. It shows that the effect of male wrap angle on volumetric efficiency is small as seen in the figure. The effect of blowhole area on volumetric efficiency is shown in Figure 4.22. The variation of volumetric efficiency with increase in blowhole area with air, nitrogen and argon is relatively small at fixed rpm. But the effect is significant with helium as the working gas.

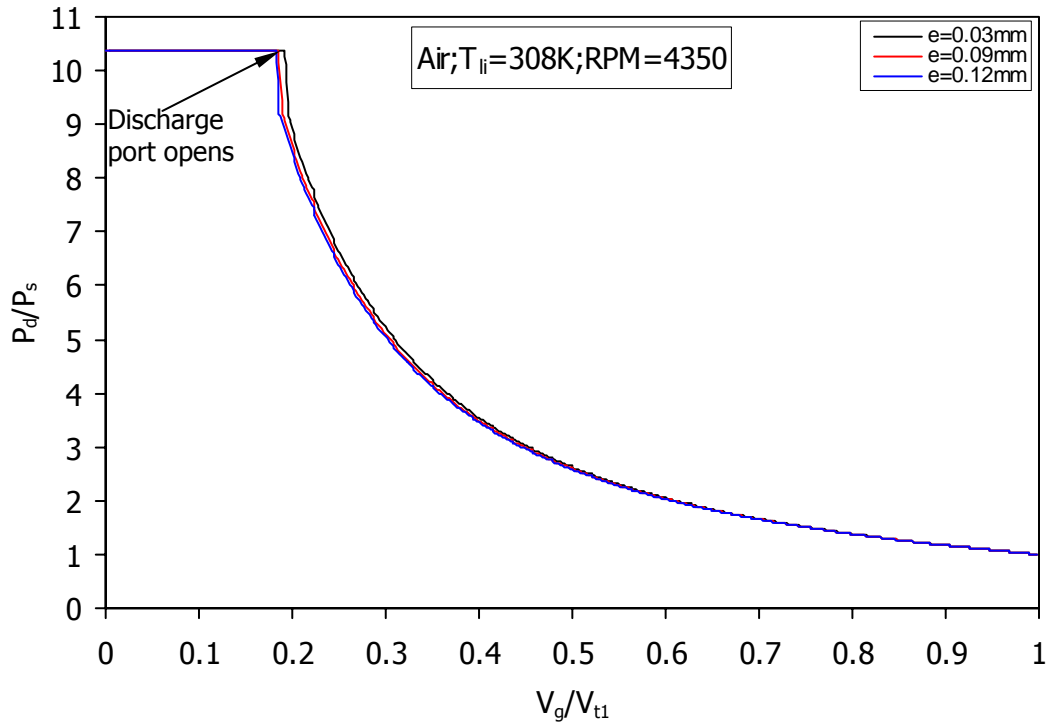


Figure 4.6: Effect of interlobe clearance (e) on p-v diagram with air at a fixed injected oil temperature and inlet condition.

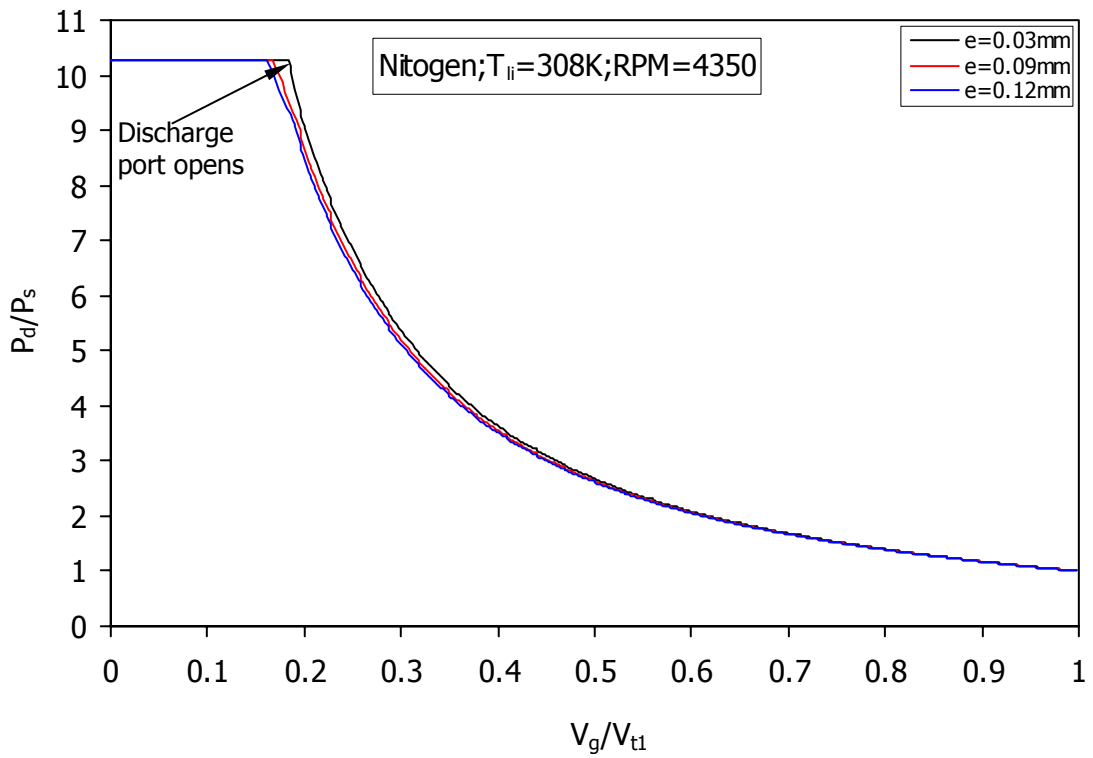


Figure 4.7: Effect of interlobe clearance (e) on p-v diagram with nitrogen at a fixed injected oil temperature and inlet condition.

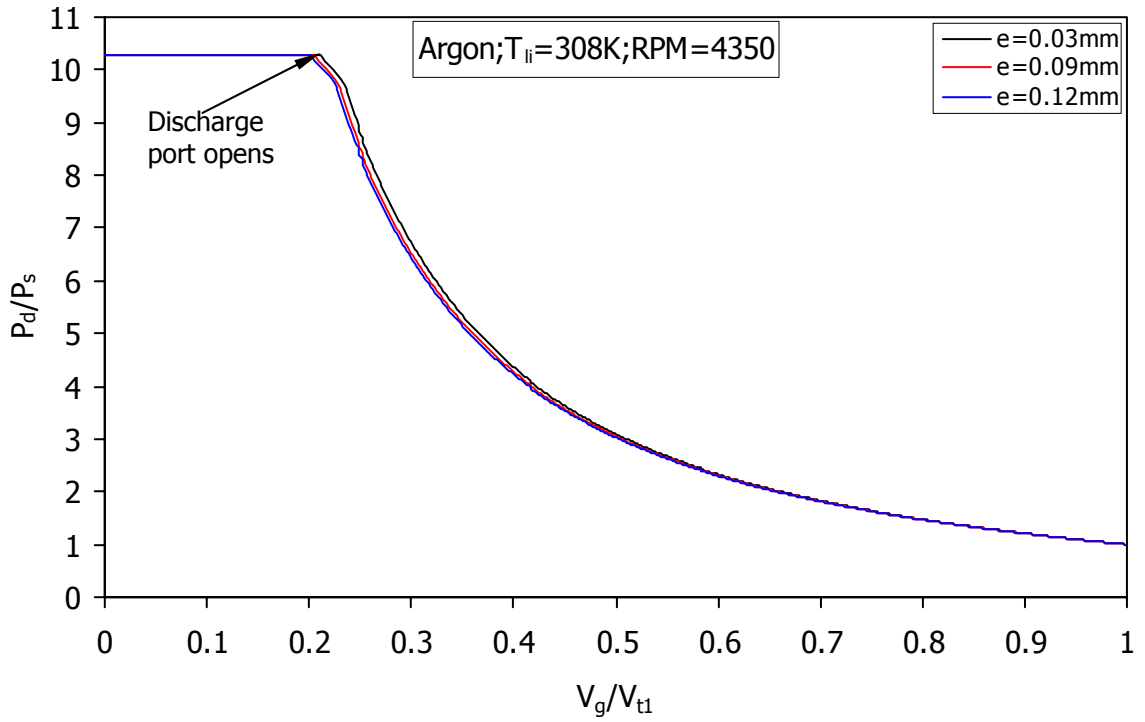


Figure 4.8: Effect of interlobe clearance (e) on p-v diagram with argon at a fixed injected oil temperature and inlet condition.

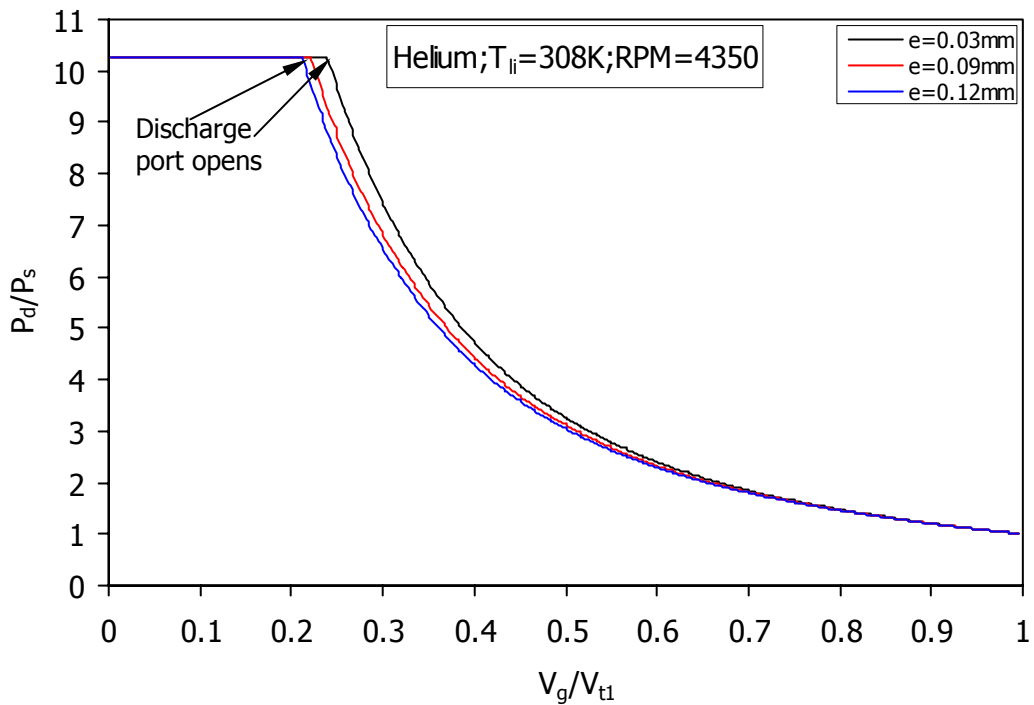


Figure 4.9: Effect of interlobe clearance (e) on p-v diagram with helium at a fixed injected oil temperature and inlet condition.

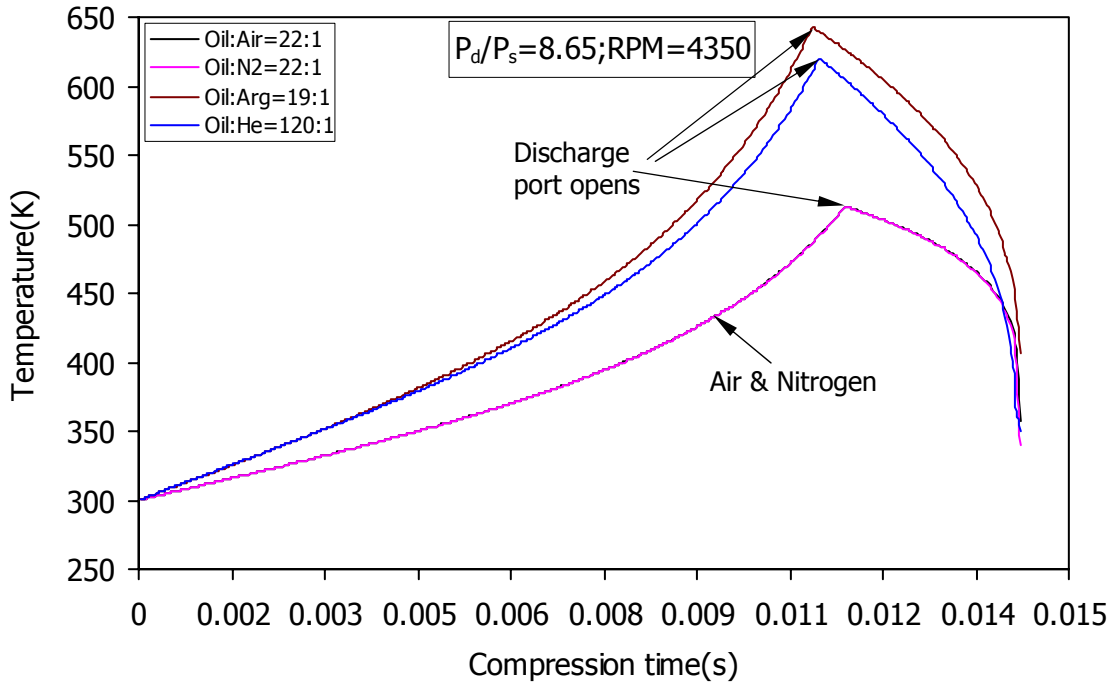


Figure 4.10: Comparison of working gas temperatures during compression-discharge process at their experimental oil-gas mass ratio.

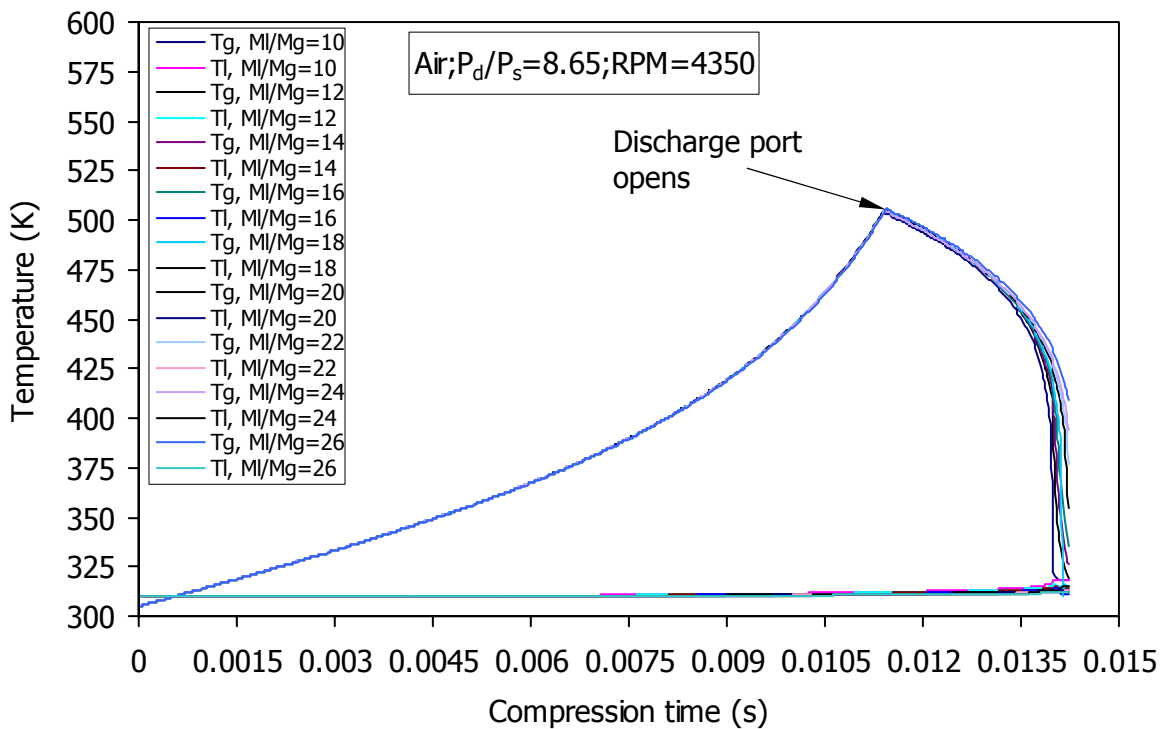


Figure 4.11: Variation of gas and oil temperature during compression-discharge process with air at different oil-gas mass ratio (M_i/M_g) and at a fixed pressure ratio and rotational speed.

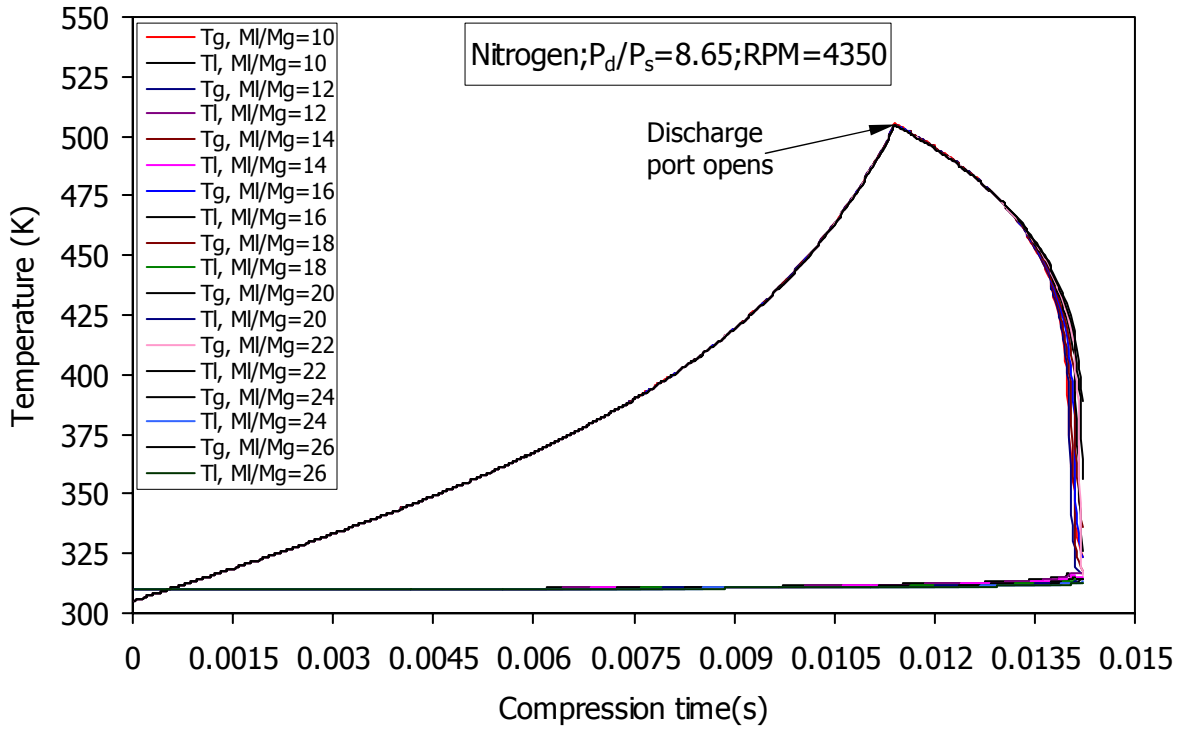


Figure 4.12: Variation of gas and oil temperature during compression-discharge process with nitrogen at different oil-gas mass ratio (M_l/M_g) and at a fixed pressure ratio and rotational speed.

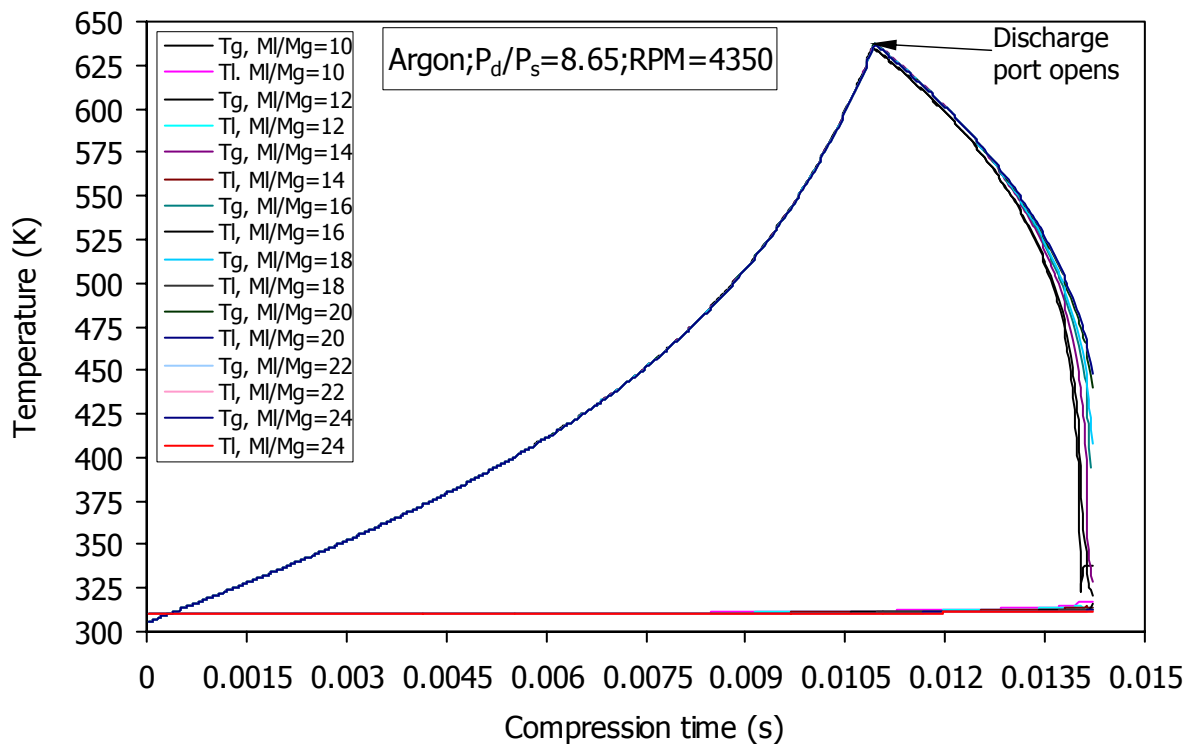


Figure 4.13: Variation of gas and oil temperature during compression-discharge process with argon at different oil-gas mass ratio (M_l/M_g) and at a fixed pressure ratio and rotational speed.

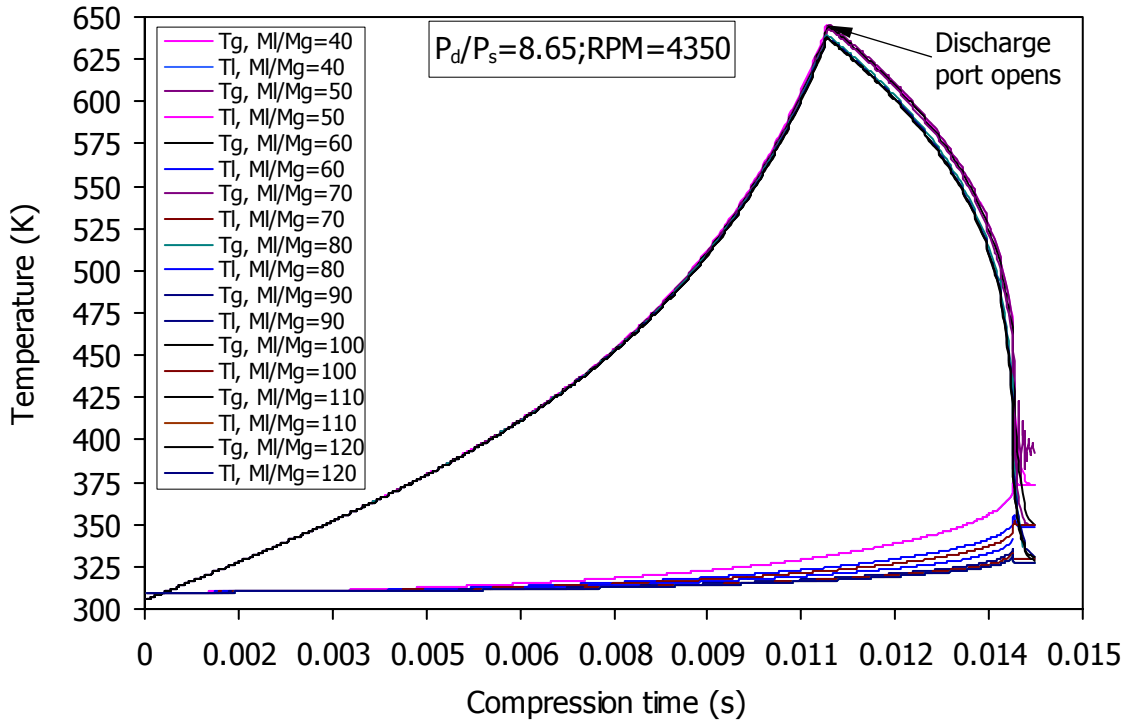


Figure 4.14: Variation of gas and oil temperature during compression-discharge process with helium at different oil-gas mass ratio (M_l/M_g) and at a fixed pressure ratio and rotational speed.

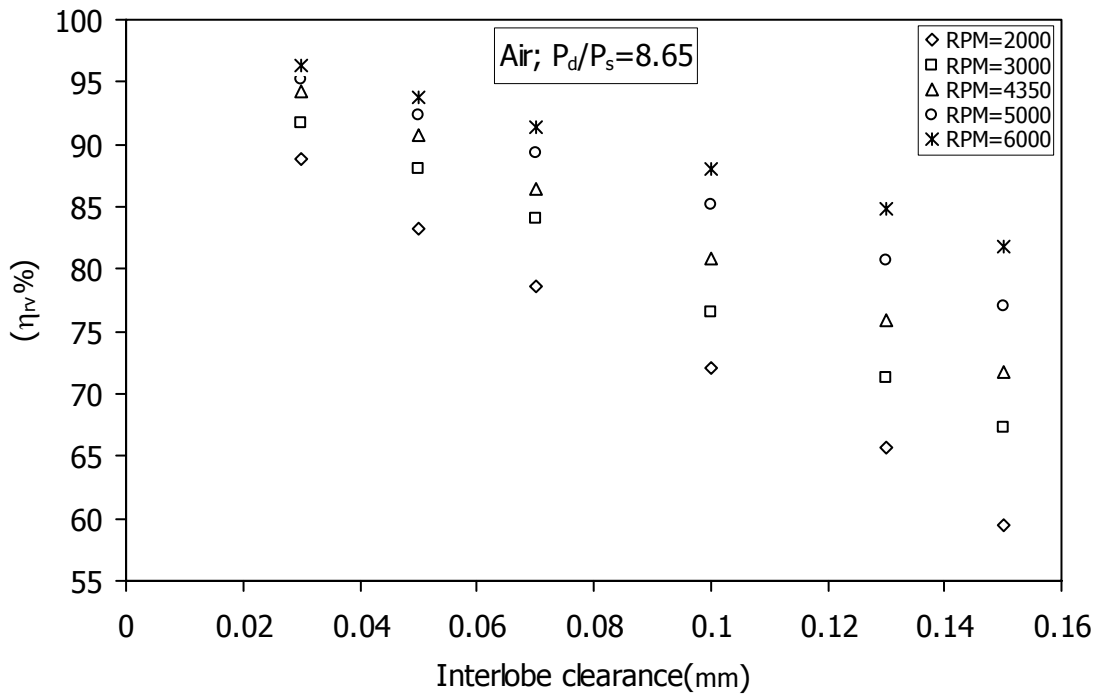


Figure 4.15: Influence of interlobe clearance and rotational speed on volumetric efficiency with air at constant injected oil temperature and suction condition.

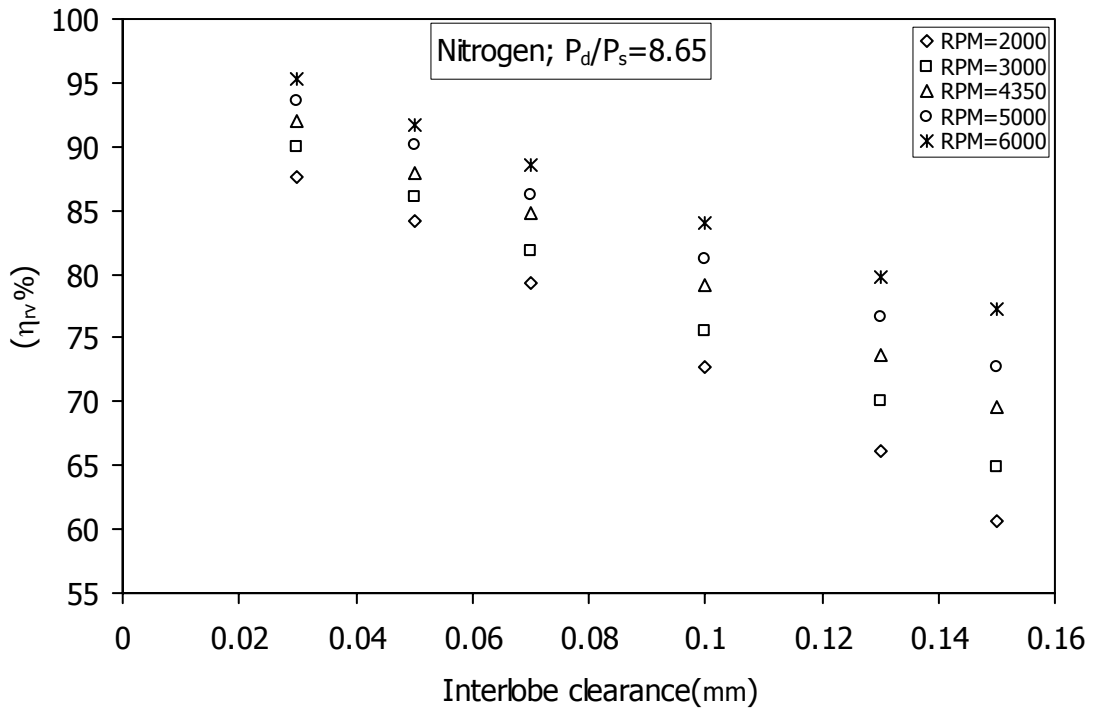


Figure 4.16: Influence of interlobe clearance and rotational speed on volumetric efficiency with nitrogen at fixed injected oil temperature and suction condition.

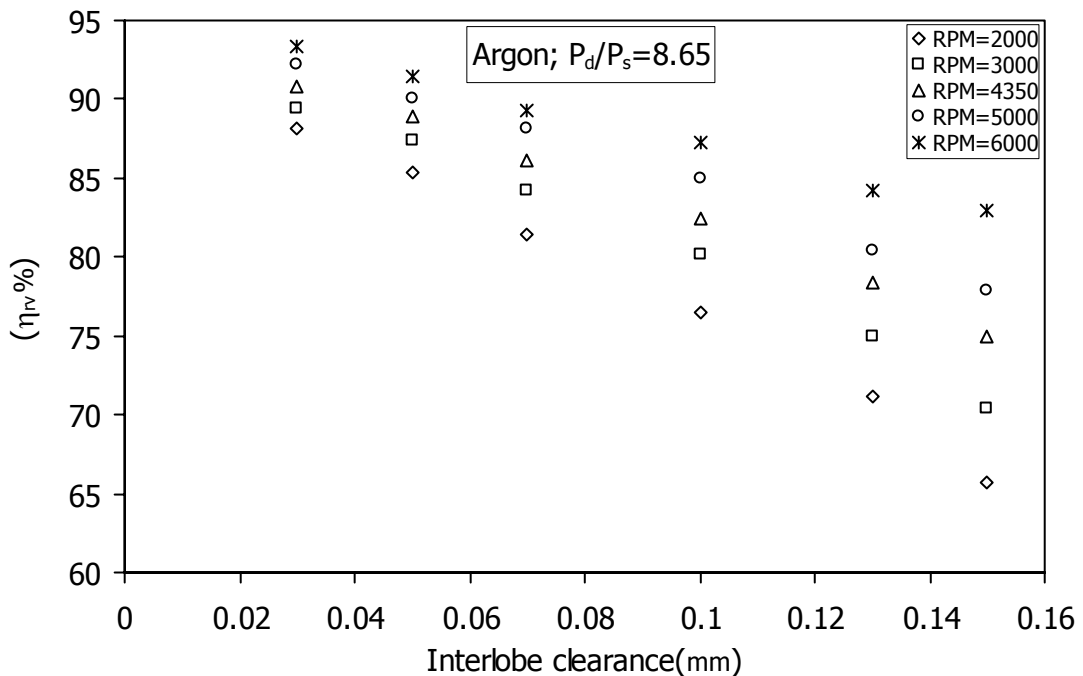


Figure 4.17: Influence of interlobe clearance and rotational speed on volumetric efficiency with argon at fixed injected oil temperature and suction condition.

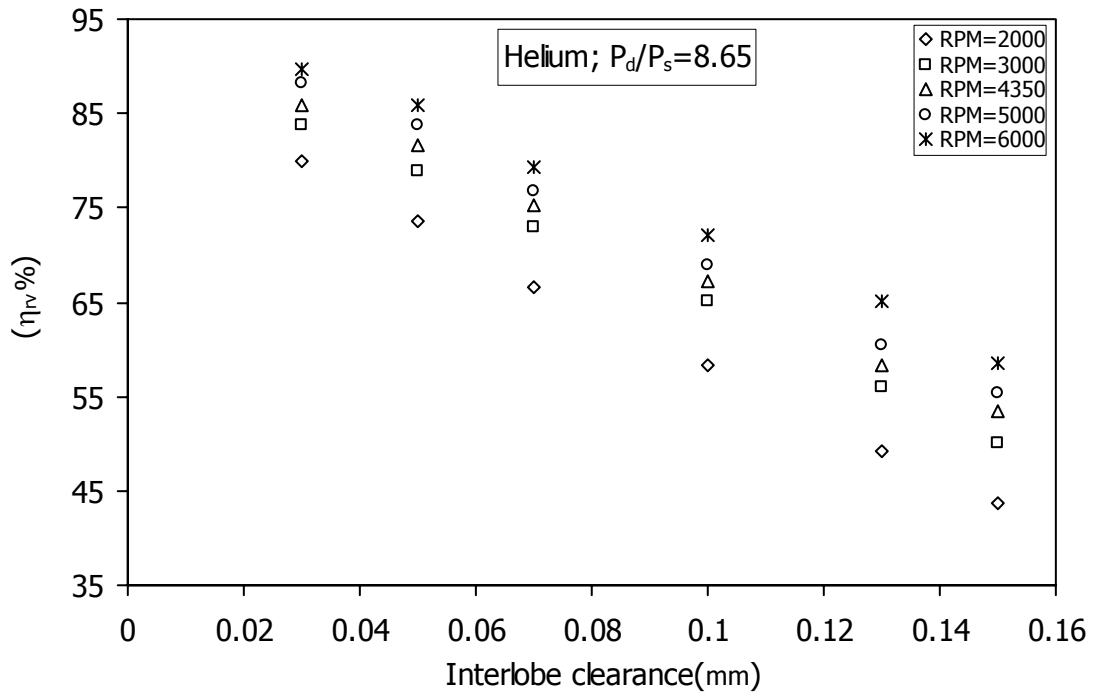


Figure 4.18: Influence of interlobe clearance and rotational speed on volumetric efficiency with helium at fixed injected oil temperature and suction condition.

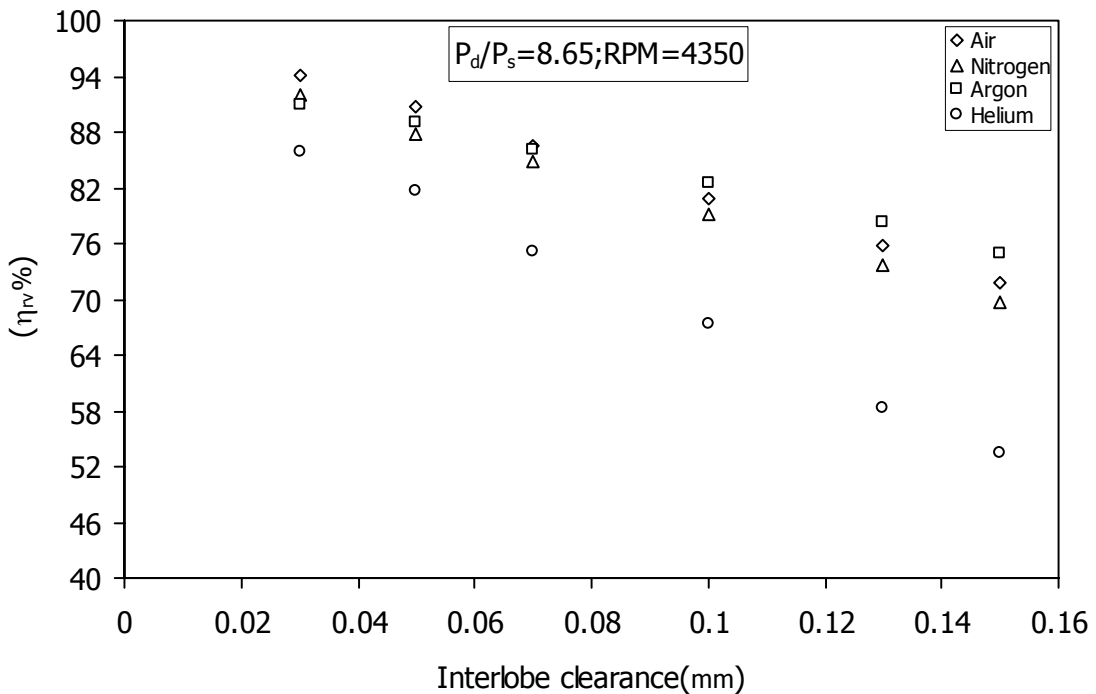


Figure 4.19: Variation of volumetric efficiency with interlobe clearance with different working gases at fixed rotational speed and injected oil temperature and at constant suction condition.

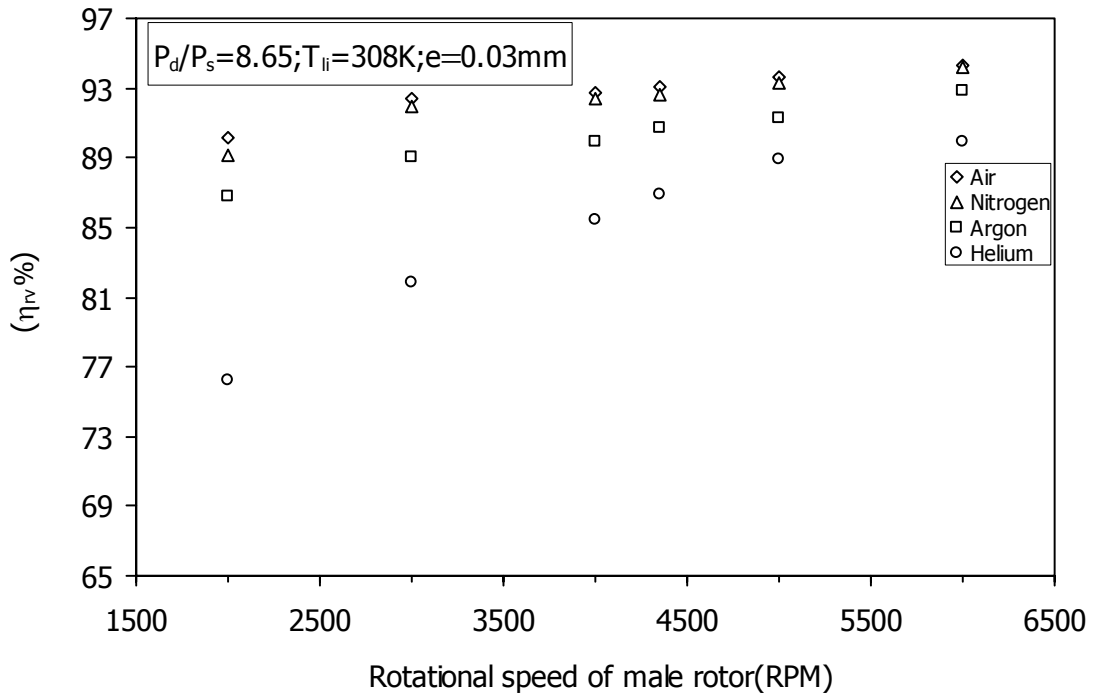


Figure 4.20: Variation of volumetric efficiency with different working gases at different rotational speeds at a fixed interlobe clearance and injected oil temperature and at a constant suction condition.

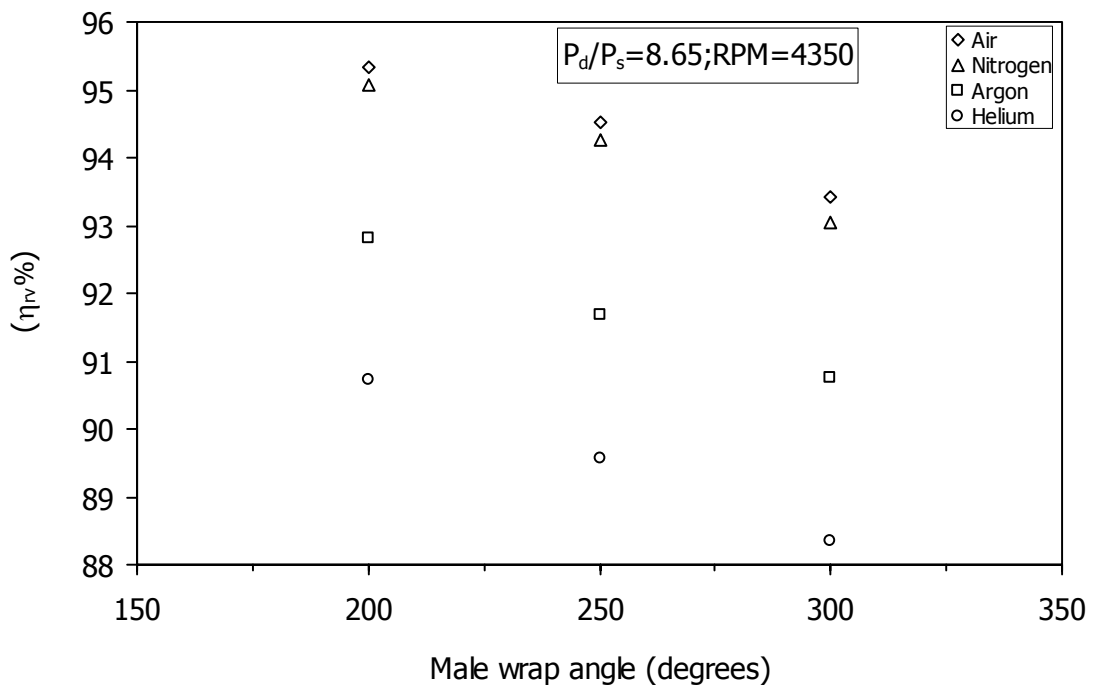


Figure 4.21: Influence of male wrap angle on volumetric efficiency with different working gases at fixed injected oil temperature and pressure ratio.

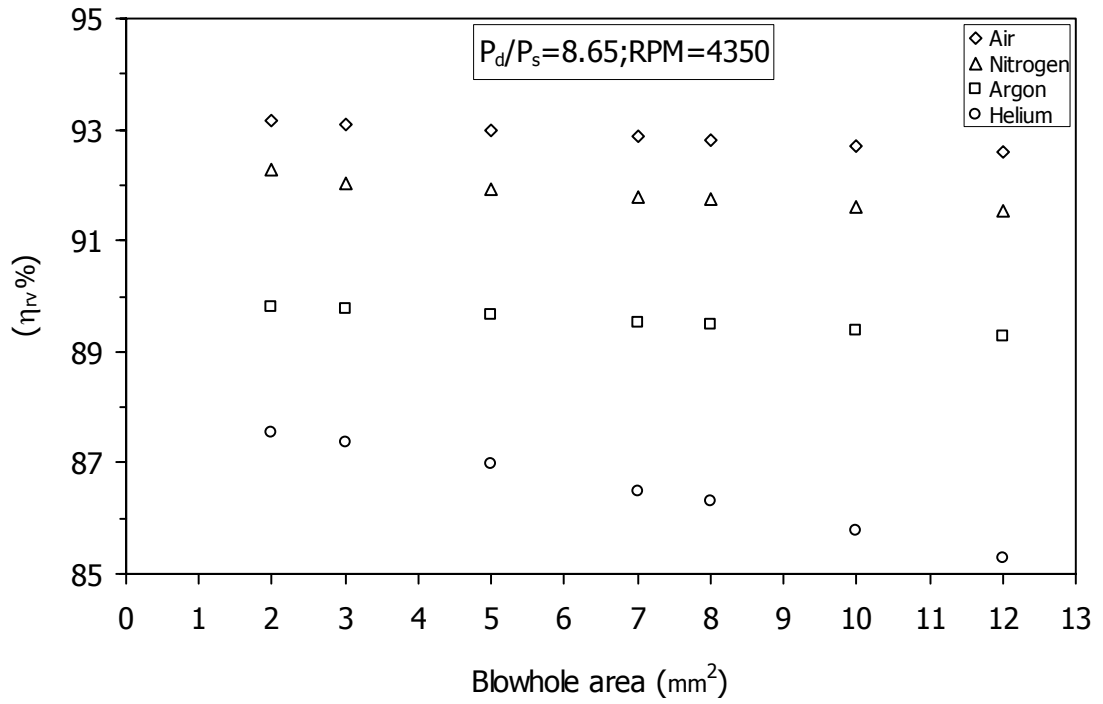


Figure 4.22: Effect of blowhole area on volumetric efficiency with different working gases at a fixed injected oil temperature and pressure ratio.

Chapter V

EXPERIMENTAL APPARATUS

Electrical power spent on compressors often accounts for the bulk of the energy requirement in a process industry. To minimize the power and maintenance cost, special care should be exercised when selecting such equipment. Commonly employed indicators of compressor performance are its volumetric and power efficiencies. Additionally, temperature rise to avoid condensation of moisture during air compression and temperature response of lubricants and coolants used are some of the major parameters to be considered. This chapter describes the features of the test system, instrumentation, calibration and measurement of volumetric and adiabatic efficiencies.

5.1 Compressor Test Rigs

The main motive of the present test is to study the performance of the lubricated twin-screw compressor under varying operating conditions, particularly its response to variation of the working gas. Two test benches have been installed in the laboratory which are identical in all aspects except for the compressor capacities. Two Kaeser (Germany) make air compressors of capacity 5.5 kW (Model SM 8) and 37 kW (Model BSD 72) are used for the experimental purpose. An upstream pressure regulating valve is provided at the discharge end of the compressor to regulate discharge pressure (5.5 bar to 11 bar) and a downstream pressure reducing valve is provided to regulate the suction pressure between 1.1 bar and 1.6 bar. The schematic diagram of the experimental test rig using a 5.5 kW compressor is shown in Figure 5.1. To maintain the purity of working gases, the entire circuit has been evacuated before charging the gases.

5.5 kW Compressor Test Set up:

The internal circuit of the model SM 8 compressor (41 m³/hr, 5.5 kW) with piping, instrumentation and control units has been shown in Figure 5.2. The pressure controllers regulate the pressure at inlet and discharge of the machine at different operating conditions. The nomenclature of all the built-in components of the compressor is listed in Table 5.1. Photographs of compressor test bench are given in Figures 5.3 and 5.4 and a photograph of the screw rotors is given in Figure 5.5.

Table 5.1: Components of the Kaeser (Model SM 8) compressor system

1. Air filter	8. Oil separator cartridge
2. Inlet valve	9. Oil temperature controller
2.1. Oil filter with plug	10. Oil filter
3. Drive motor	11. Oil cooler
4. Air end	12. Minimum pressure check valve
4.1. Strainer	13. Air cooler
4.2. Pressure switch-wrong direction of rotation	16. Dirt trap
5.2. PT100 sensor	17. Nozzle
6. Oil separation tank	18/19. Combined control/vent valve
6.1. Pressure gauge	18. Control valve
6.2. Hose coupling (oil end)	19. Vent valve
6.3. Hose coupling (air end)	20. Shut off valve-Vent line
6.6. Shut off valve-Oil drain	21. Silencer
6.9. Oil level sight glass (Min./Max. oil level)	59.1. Pressure measuring transducer-air main pressure
7. Pressure relief valve	



Figure 5.3: Experimental test setup with SM 8 compressor.

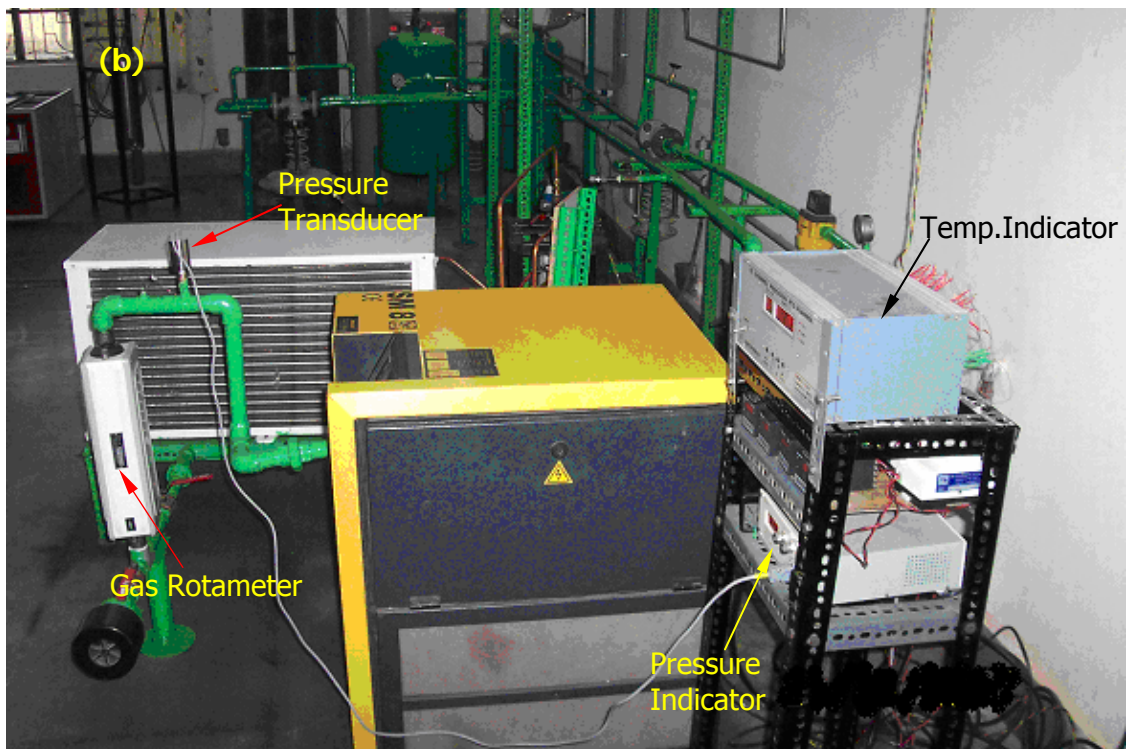


Figure 5.4: Close up view of compressor test rig using SM 8 compressor.

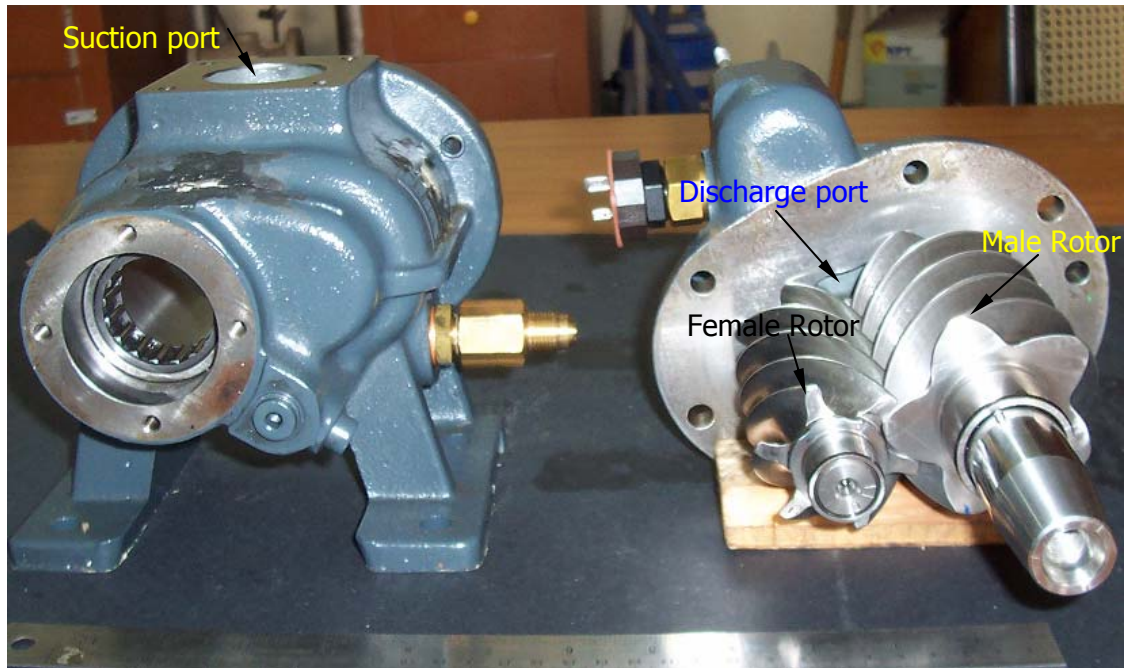


Figure 5.5: Photograph of screws & casing of SM 8 compressor air end.

37 kW Compressor Set up:

The larger set up is built around a Kaeser Model BSD 72 compressor of 37 kW capacity and free air delivery of 336 m³/hr. The 37 kW test bench is similar to that of the SM 8 compressor test setup except for the compressor capacity. The schematic diagram of 37 kW experimental test setup has been shown in Figure 5.6. The internal circuit of the compressor with internal piping, instrumentation and control units are shown in Figure 5.7. Controllers are used to regulate the compressor package for safe operation at different operating conditions. The nomenclature of all the built-in components within the compressor cabinet is listed in Table 5.2. Photographs of the experimental setup have been shown in Figures 5.8 to 5.11. Because of the larger size of the equipment, gas reservoirs, connecting pipes and the components of the set up are distributed over two rooms and the outdoors. Figure 5.12 shows the screws of the BSD 72 compressor. Figure 5.13 shows the rotors of the larger and smaller compressors to give a perspective of the relative sizes.

Table 5.2: Components of the Kaeser (Model BSD 72) compressor system

1. Air filter	10. Oil filter
1.1. Vacuum switch-Air filter	10.1. Differential pressure switch-oil filter
1.2. Dust collector	10.3 Oil flow reduction valve
2. Inlet valve	11. Oil cooler
2.1. Oil filter with plug	11.6. Shut off valve with hose coupling-oil drain
3. Drive motor	12. Minimum pressure check valve
3.1. Fan motor	13. Air cooler
4. Air end	13.1. Hose coupling
4.2. Pressure switch-wrong direction of rotation	16. Dirt trap
5.2. PT100 sensor	17. Nozzle
6. Oil separator tank	18/19. Combined control/vent valve
6.1. Pressure gauge	18. Control valve
6.2. Hose coupling (oil end)	19. Vent valve
6.3. Hose coupling (air end)	20. Shut off valve-Vent line
6.6. Shut off valve with hose coupling-oil drain	21. Silencer
6.13. Oil level indicator	53. Coupling
7. Pressure relief valve	59.1. Pressure measuring transducer-Air main pressure
8. Oil separator cartridge	59.2. Pressure measuring transducer-Internal pressure
9. Oil temperature controller	

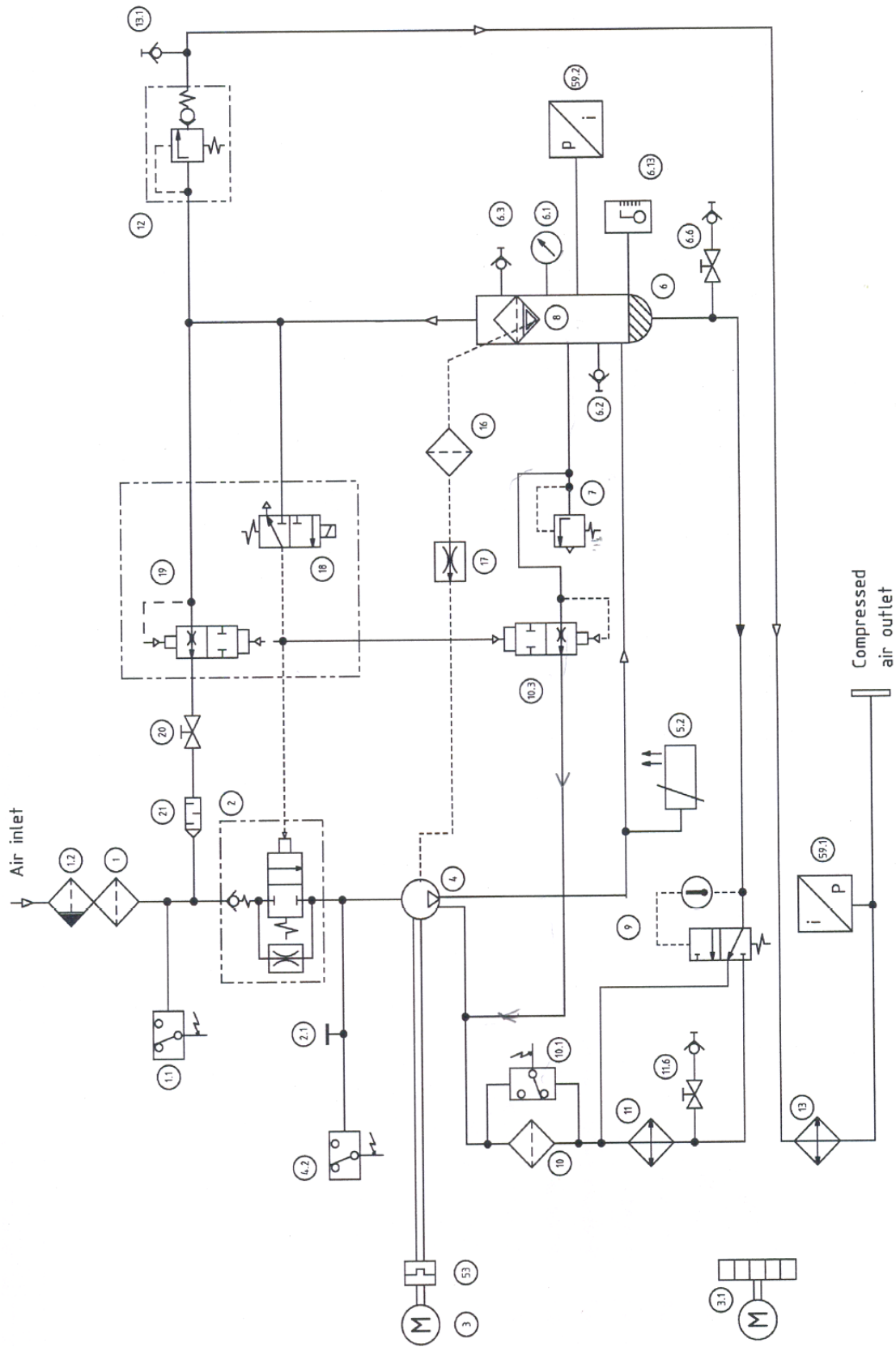


Figure 5.7: Piping and instrumentation diagram (inside compressor cabinet) of BSD 72 compressor system.



Figure 5.8: Photograph of 37 kW compressor test rig (partial).



Figure 5.9: Photograph of 37 kW compressor test rig (another view).

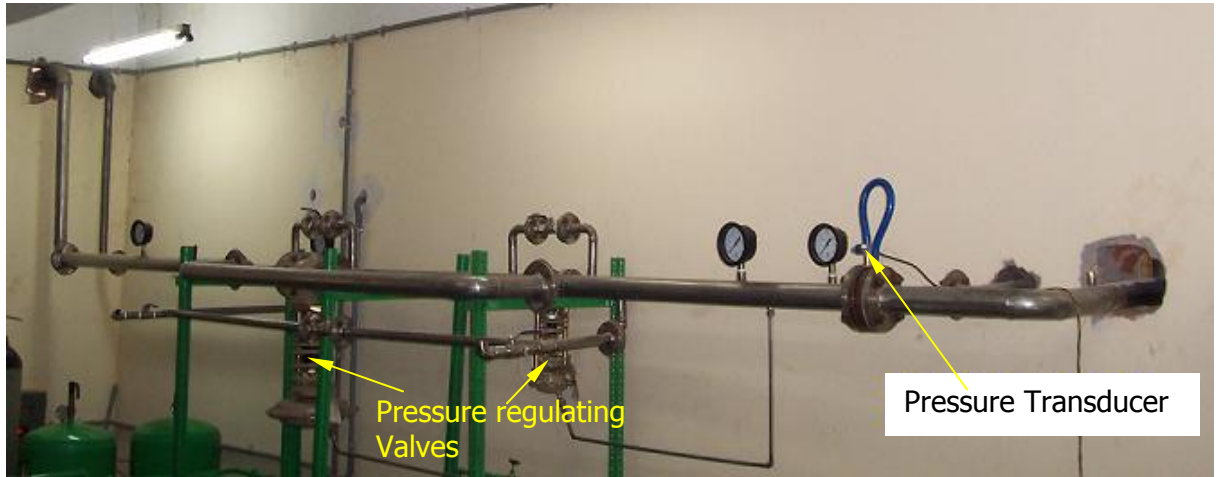


Figure 5.10: Photograph of piping and instrumentation of 37 kW compressor test rig (partial).



Figure 5.11: Photograph of 37 kW compressor receivers.

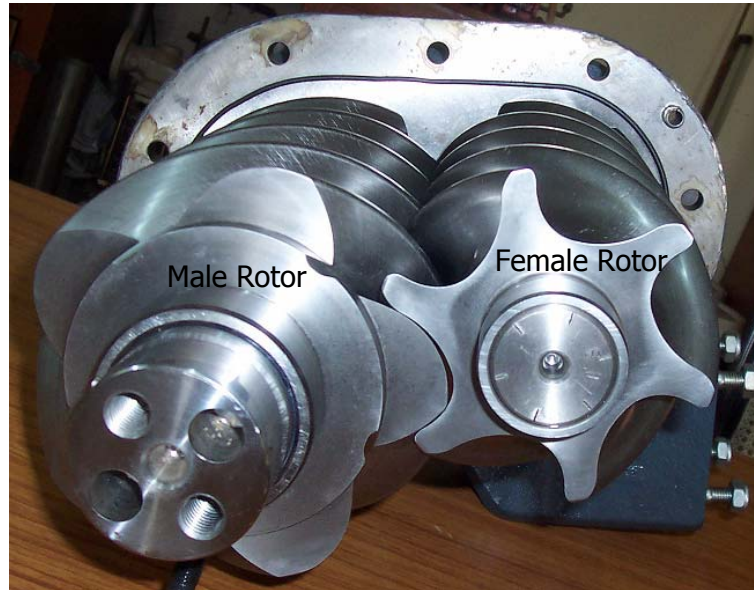


Figure 5.12: Screws of 37 kW compressor.

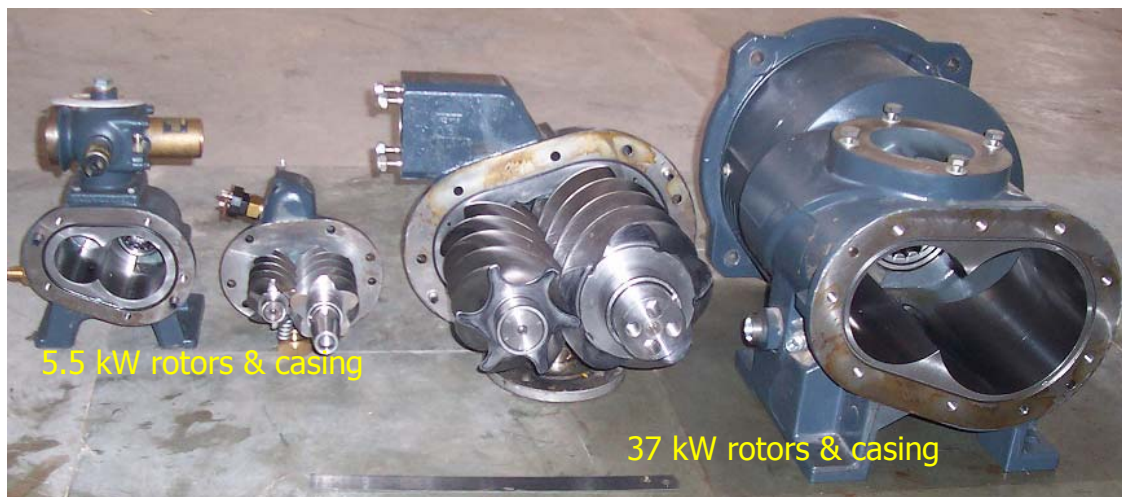


Figure 5.13: Photograph of 5.5 kW and 37 kW compressor rotors and their casings.

The oil flow system

Lubricating oil plays a special role in screw compressors. It removes the heat of compression of the gas, lubricates the contacting surfaces and seals the gaps between the rotors and the casing. In air compressors, it helps in maintaining the operating temperature above 80°C to ensure that even under discharge conditions,

the moisture does not condense. This situation is ensured in air compressors by deliberately undersizing the oil cooling heat exchanger and using a temperature regulator. In case of gas compression applications, where there is no moisture to condense, this special provision can be dispensed with. In stead, an additional heat exchanger is added to the existing heat exchanger to cool the lubricating oil to as low temperature as possible.

The oil flow system with secondary cooler has been shown in Figure 5.14. After passing through the inbuilt heat exchanger of the compressor, the lubricating oil flows to the externally connected heat exchanger before being injected into the compressor. Oil flow can be regulated with the help of externally connected oil flow control valves. The flow rate of oil is measured with a rotameter.

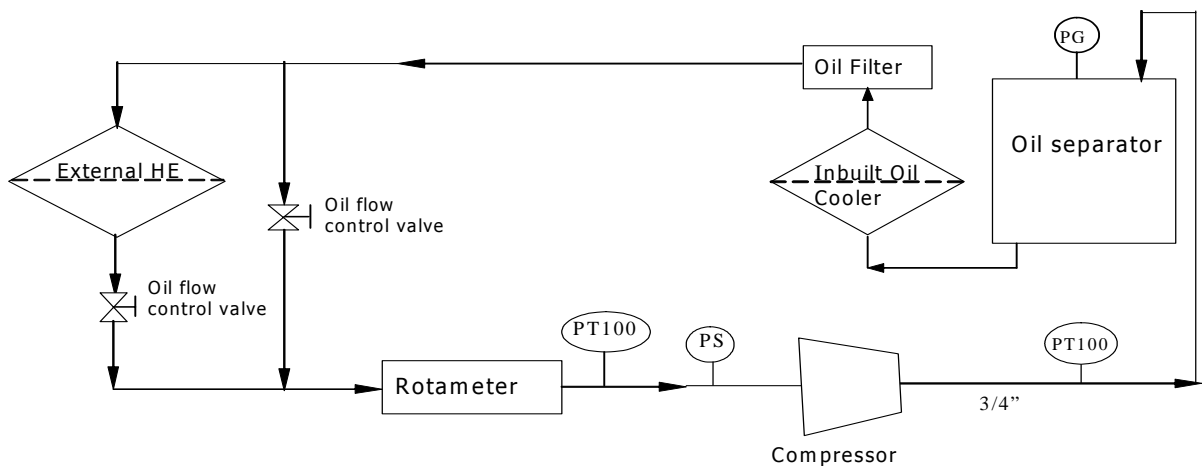


Figure 5.14: Schematic of the oil flow system for SM 8 and BSD 72 compressors.

5.2 Selection of equipment

The following are the specifications of various equipment, instruments and other accessories used in building the experimental test setup.

(i) Compressor 1

Make	: Kaeser (Germany)
Model	: SM 8
Profile of screw	: Sigma
Free air delivery	: 41 m ³ / hr (at designed discharge pressure)

Suction pressure	: Atmospheric
Maximum Pressure	: 11 bar
Motor	: 5.5 kW, 20 amp, 3Φ, 50Hz, 400V±10%, 3000 rpm (belt driven)
Oil capacity	: 5 L
Cooling	: Air

(ii) Compressor 2

Make	: Kaeser (Germany)
Model	: BSD 72
Profile of screw	: Sigma
Free air delivery	: 336 m ³ /hr (at designed discharge pressure)
Suction pressure	: Atmospheric
Maximum Pressure	: 12 bar
Motor	: 37 kW, 74 amps, 3 Φ, 50 Hz, 415V±10%, 3000 rpm (direct coupled)
Oil capacity	: 24 L
Cooling	: Air

(iii) Filters

Particulate filter

Make	: Kaeser (Germany)
Model	: FD-48
Separated Practical size	: > 1 μm
Efficiency	: 99.99999% (manufacturers' specification)
Oil content	: ≤ 1 mg/m ³
Pressure drop	: 0.07 bar

Activated carbon combination filter

Make	: Kaeser Compressors (Germany)
Model	: FFG-10
Separated Practical size	: > 0.01 μm
Oil content	: ≤ 0.001 mg/m ³

Oil vapour content : 0.003 mg/m³
Pressure drop : 0.21 bar

(iv) Self operated pressure control valves

Excess pressure regulating valve

Make : Samson Controls Pvt Ltd
Type : 41-73, upstream pressure control
Size : 3/4", 1"
Actuator size : 40 cm²
Set pressure range : 5.5 to 10 bar
Max. Allowable leakage at 16 bar : 0.1 LPM

Material

a) Body : A216 WCB
b) Seat : SS 316



Figure 5.15: Assembled view of self operated excess pressure regulating valve.

Pressure reducing valve

Make : Samson Controls Pvt Ltd
Type : 41-23, down stream pressure control
Size : 1", 2 1/2"

Actuator size : 640 cm²
 Set pressure range : 1.1 to 1.6 bar
 Max. Allowable Leakage at 11 bar : 0.4 LPM

Material

a) Body : A216 WCB
 b) Seat : SS316ST6



Figure 5.16: Assembled view of self operated pressure reducing valve.

(v) Lubricating oil

Name : Sigma fluid plus
 Make : Kaeser (Germany)
 Type : Synthetic poly-alpha-olefins
 Viscosity at 40⁰C : 70 mm² /s
 Viscosity at 100⁰C : 10.6 mm² /s
 Density at 15⁰C : 843 kg/m³
 Specific heat : 1.8683 kJ/kg
 Flash point : 260⁰C
 Pour point : -39⁰C

(vi) Testing gases

Three testing gases have been selected to test the compressors apart from air.

Nitrogen

The nitrogen gas produced in the Cryogenics Laboratory has been used for testing. The purity of the nitrogen gas produced is 98% (nitrogen generator manufacturer's specification)

Argon (supplier's specifications)

Argon minimum percentage per mole	: 99.985
Moister	: 23.0 ppm
Oxygen	: 50 ppm
Nitrogen	: 50 ppm
Hydrogen	: 50 ppm

Helium (supplier's specifications)

Grade	: 4.5
Minimum purity	: 99.995%
Oxygen	: 10 ppm (max.)
Nitrogen	: 20 ppm (max.)
Moister	: 4.0 ppm (max.)
Hydrocarbon/CH ₄	: 0.5 ppm (max.)

(vii) Pipes

Pipes, tubes and fittings have been procured from local market. Stainless steel pipes and valves are used for 37 kW compressor test rig and GI pipes and MS valves have been used for 5.5 kW compressor test setup.

5.3 Instrumentation

The instrumentation system comprises of instruments to measure gas and oil flow rate, electrical energy input, temperature, and pressure at relevant stations. A

rotameter has been used for gas flow rate measurement in the 5.5 kW compressor and orifice meter for 37 kW compressor. Excess pressure regulating and pressure reducing valves have been used to regulate the pressures. Pressure gauges and pressure transducers have been used on both the compressor test rigs at relevant stations for pressure measurement. Platinum resistance thermometers have been used for the measurement of surface temperature of compressors and of gas and oil streams. A tachometer has been used for the measurement of rotational speed of the compressors. Energy meter and stop watch for measurement of electrical input to the compressors. The specific instruments are as follows.

(a) Rotameter for gas flow measurement

Make : Alflow
 Range : 0 to 1250 LPM
 Accuracy : ± 12 L/min

(b) Rotameter for oil flow measurement

Make : Alflow
 Range : 0 to 50 LPM, 0 to 200 LPM
 Accuracy : ± 1 L/min

(c) Orifice meter

Make : Rosemount Inc.
 Type : Plate type, square edged, corner tapping,
 Line size : 2 1/2" inch
 Orifice bore size : 1.67 inch
 Discharge coefficient : 0.6082
 Flow rate
 Minimum accurate flow : 0.01 m³/sec
 Maximum : 0.12 m³/sec

(d) Pressure Sensors

Make : Honeywell
 Model : 24PC Series
 Type : Differential pressure sensors

Range : From 3 bar to 18 bar
Accuracy : ± 0.01 bar



Figure 5.17: Photograph of pressure transducer with mechanical fittings.

(e) Temperature Sensors

Make : Omega
Model : PT100
Type : Thin film
Accuracy : ± 0.3 C

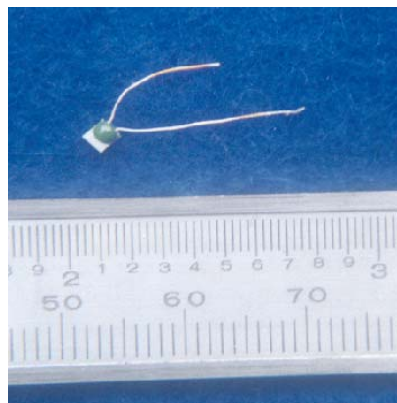


Figure 5.18: A thin film type platinum resistance temperature sensor (PT100).

5.4 Measurement of Volumetric and Adiabatic efficiencies

Volumetric Efficiency

Volumetric efficiency of a compressor is defined as the actual amount of gas volume delivered at some reference condition to the theoretical volume of gas delivered at the same condition. The experimental volumetric efficiency equation (4.16) at condition (P_s, T_1) is reproduced below for ready reference.

$$\eta_{rev} = \frac{\dot{m}_e}{\dot{m}_t} \quad (5.1)$$

where \dot{m}_e is the experimentally measured flow rate and \dot{m}_t is the ideal flow rate compatible with machine geometry and speed. The actual gas volume flow rate \dot{m}_e is measured with a rotameter, which has been calibrated for volume flow rate at reference condition (P_r, T_r) . The mass flow rate of compressor at condition (P_s, T_1) is obtained by using the formula [119]:

$$\dot{m}_e = \rho_s V_m \sqrt{\frac{P_s \times T_r}{P_r \times T_s}} \quad (5.2)$$

where, ρ_s is the density of gas at (P_s, T_1) and V_m is the volume flow rate of the gas. The gas density has been taken from standard thermodynamic tables [120]. The theoretical mass flow rate is calculated using the equation of state for perfect gas at condition (P_s, T_1) and is given by the equation:

$$\dot{m}_t = \frac{P_s V_{t1}}{RT_s} n_m N_m \quad (5.3)$$

where n_m , N_m are the number of lobes and rotational speed (rps) of male rotor respectively.

Adiabatic efficiency

The theoretical adiabatic efficiency is defined at condition (P_s, T_1) as:

$$\eta_{ra} = \frac{\dot{W}_{ad}}{\dot{W}_{sys,e}} \quad (5.4)$$

where $\dot{W}_{sys,e}$ is the power consumed by the compressor system. The adiabatic compression work \dot{W}_{ad} is estimated by using the standard relation [118]:

$$\dot{W}_{ad} = \dot{m}_{dt} c_p T_1 \left[\left(\frac{P_d}{P_s} \right)^{\frac{k-1}{k}} - 1 \right] \quad (5.5)$$

The power consumed by the compressor system is measured either with a three phase Wattmeter or with an energy meter plus a watch. We have used the later approach.

$$\dot{W}_{sys,e} = \frac{3600}{N_e} \frac{n_e}{t_e} \quad (5.6)$$

where N_e is the energy meter constant and t_e is the time taken for n_e revolutions of energy meter disc.

Chapter VI

EXPERIMENTAL RESULTS AND CONCLUSIONS

This chapter presents the results of experimental studies that have been discussed in chapter V. Procedure for actual measurements and data reduction have been presented. The operating parameters covered under the study are:

- Suction temperature
- Suction pressure
- Discharge pressure or pressure ratio
- Injected oil temperature
- Oil injection rate

6.1. Measurement of Volumetric Efficiency

The volumetric efficiency of the compressors under different operating parameters is presented in Figures 4.1 to 4.12. During experimentation, maximum care has been taken to maintain the purity of gas in the closed loop test rig. To ascertain the purity of gas in the test rig, the entire circuit was evacuated before charging different working gases. During experimentation, the maximum discharge pressure was maintained at 10 bar, the maximum designed discharge pressure of the compressor being 11 bar. It has been observed that the calculated volumetric efficiency (%) was more than the experimentally measured volumetric efficiency by approximately 2% in almost all cases. This is attributed to the assumption in the numerical model that the volume occupied by the oil in the compressor cavities is negligible. The other non idealities such as ideal gas assumption and values of coefficient of leakage may also be contributing to this difference. The difference is within the experimental uncertainties.

Figure 6.1 gives the influence of inducted gas temperature on volumetric efficiency with different working gases at a fixed pressure ratio and injected oil temperature in the SM 8 (5.5 kW) compressor. It is observed that the volumetric efficiency increases with inlet temperature. This effect is attributed to the fact that the actual inlet mass flow rate remains almost constant during the experiment, the large mass of the oil imposing a thermostatic effect. Hence, in the expression of volumetric efficiency, the numerator remains nearly constant while the denominator decreases with increase of inlet temperature, which leads to higher volumetric efficiency.

The variation of experimentally measured volumetric efficiency with suction gas temperature in the 5.5 kW and 37 kW compressors has been shown in Figure 6.2. It has been observed that the volumetric efficiency of 37 kW compressor is somewhat lower than that of the 5.5 kW compressor for all working gases. This may be due to manufacturing deviations of the 37 kW compressor. Figures 6.3 to 6.5 give the variation of volumetric efficiency with suction gas pressure at a fixed pressure ratio in the same compressors. The increase in volumetric efficiency with increase in suction pressure may be assigned to the increase in volume flow rate of gas without proportionate increase in oil flow rate.

The influence of injected oil temperature on different working gases at a fixed pressure ratio is shown in Figure 6.6. From the figure, it is observed that lower injected oil temperature results in better volumetric efficiency. The influence of injected oil quantity at a fixed pressure ratio and injected oil temperature is presented in Figures 6.7 and 6.8 for different working gases. It may be observed that the influence of oil injection rate on volumetric efficiency is not same for different working gases. The influence of injection quantity on volumetric efficiency is relatively stronger with helium than with the other three gases in both the compressors.

The variation of volumetric efficiency with pressure ratio is shown in Figures 6.9 to 6.12. This variation is due to the fact that increase in pressure ratio enhances the leakage and thus degrades the efficiency. It has also been seen from the figures that volumetric efficiency can be improved by lowering the injected oil temperature. Volumetric efficiency decreases with increase in pressure ratio and decreases with increases of oil inlet temperature. For the same pressure ratio and the same oil injection temperature, volumetric efficiency is the lowest for helium followed by

argon, nitrogen and air. This may be due to the fact that helium is a light gas and leaks more easily. On the other hand, monatomic gas generates higher temperature leading to decrease in oil viscosity and consequently higher leakage rate. This is the case with argon. The variation of volumetric efficiency with oil to gas mass ratio has been presented in Figures 6.13 and 6.14. It is observed that increase in volumetric efficiency with mass ratio is marginal for air, nitrogen and argon in the range of mass ratio between 15 and 18. Helium being a lighter gas, operating oil to gas mass ratio is nearly 7 times of that with air.

The gas delivery rates of both the compressors have been presented in Figures 6.15 to 6.17. Experiments have been conducted at two different injected oil temperatures on 5.5 kW compressor keeping the inlet gas pressure constant. It is observed that the gas volume delivery rate decreases with increase in pressure ratio and with increase of oil injection temperature. The causes are the increase of leakage rate at higher pressures and reduction of inducted volume at higher temperature. These figures also show the relative variation of volume flow rates of different working gases. The lowest gas delivery rate is with helium followed by argon, nitrogen and air.

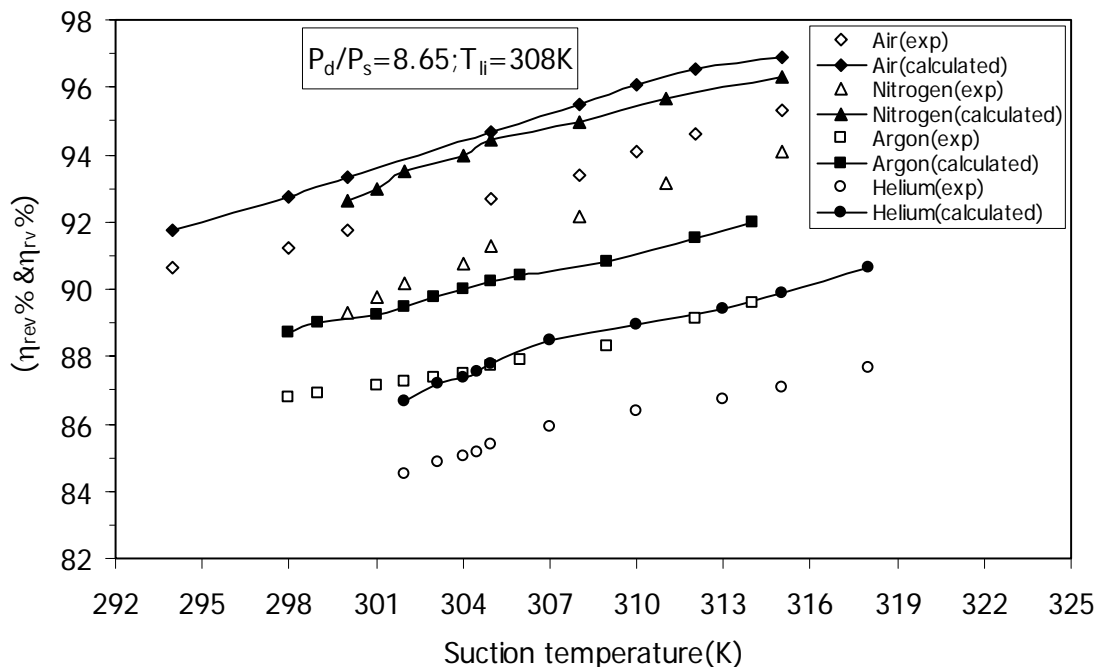


Figure 6.1: Influence of inlet gas temperature on volumetric efficiency with different working gases of 5.5 kW compressor at fixed injected oil temperature

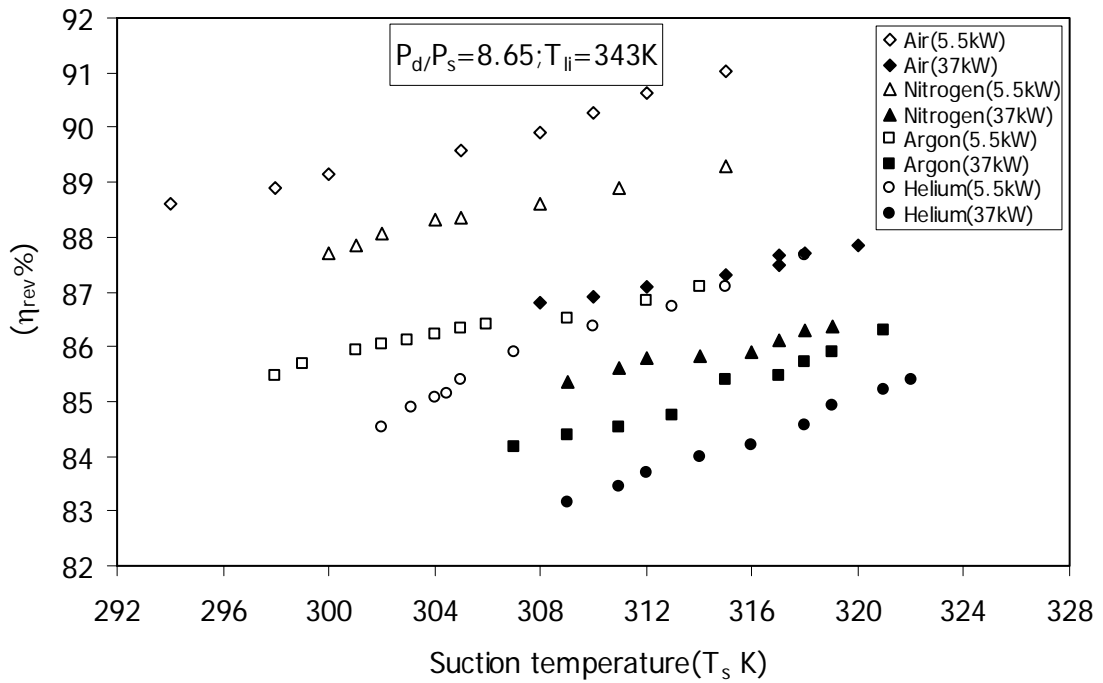


Figure 6.2: Variation of experimentally measured volumetric efficiency with inlet gas temperature with different working gases of 5.5 kW and 37 kW compressors at fixed suction pressure and injected oil temperature.

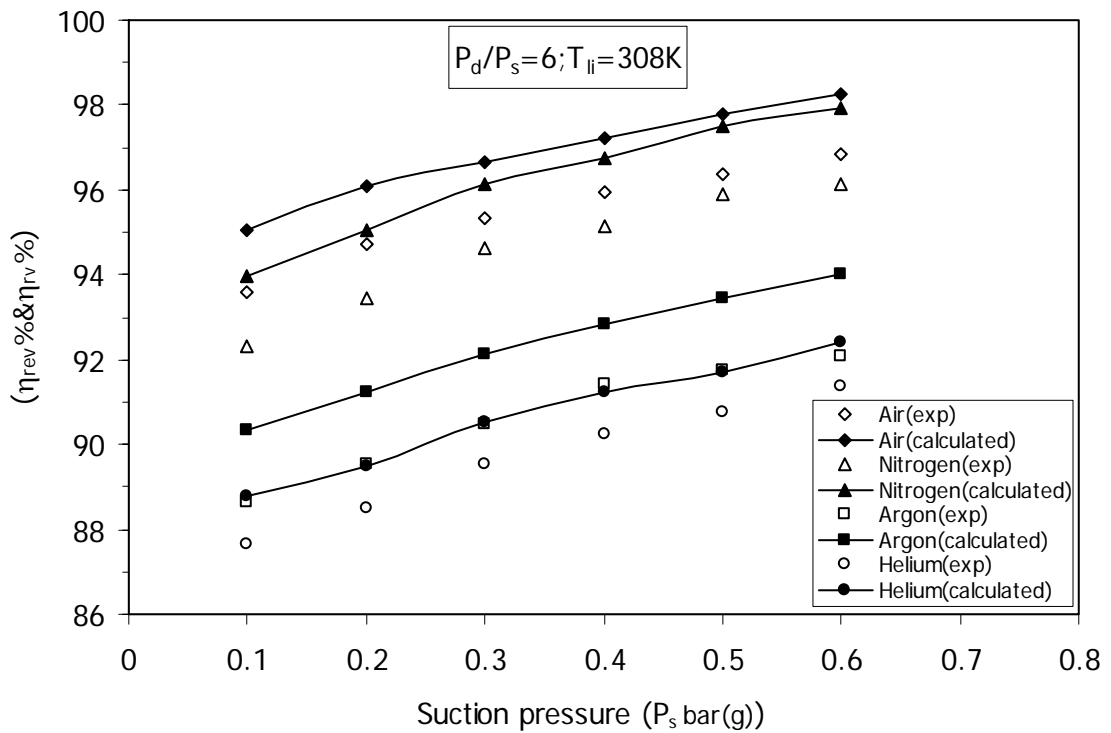


Figure 6.3: Effect of suction pressure on volumetric efficiency with different working gases of 5.5 kW compressor at fixed injected oil temperature.

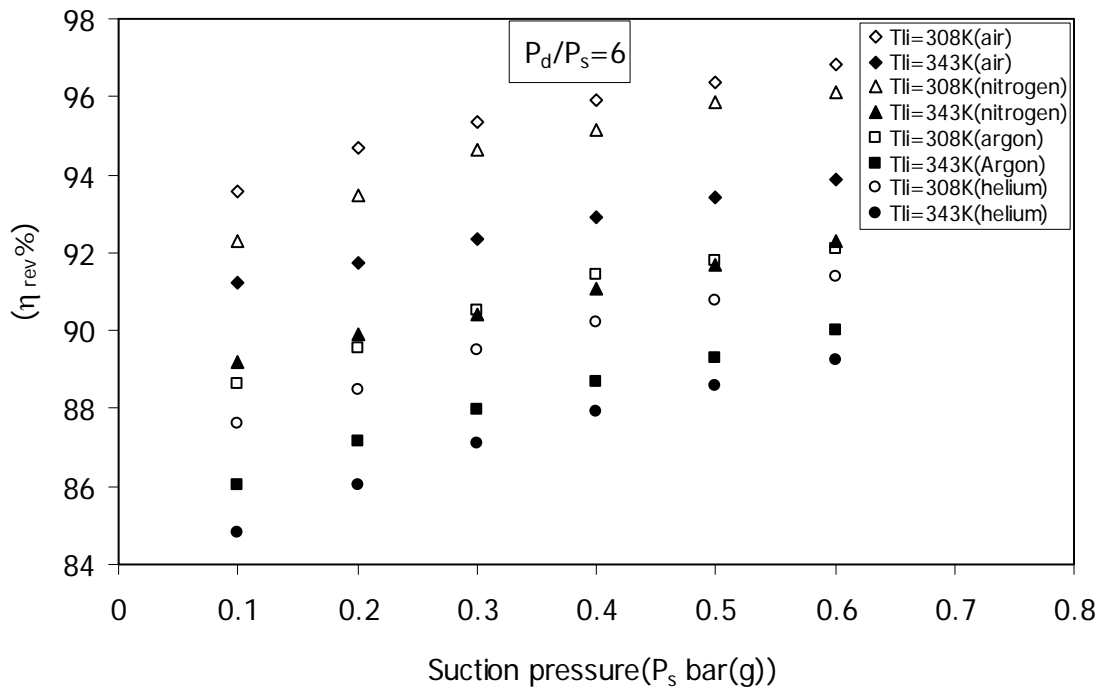


Figure 6.4: Effect of injected oil temperature on experimentally measured volumetric efficiency of 5.5 kW compressor.

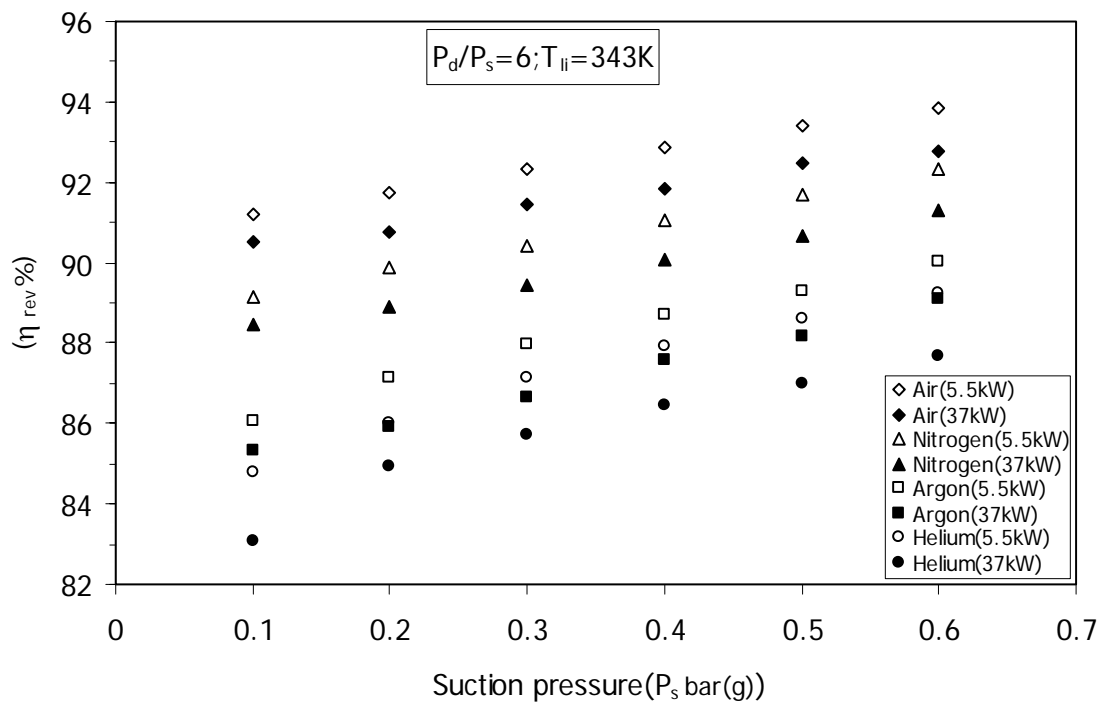


Figure 6.5: Comparison of experimentally measured volumetric efficiencies of 5.5 & 37 kW compressors at fixed injected oil temperature.

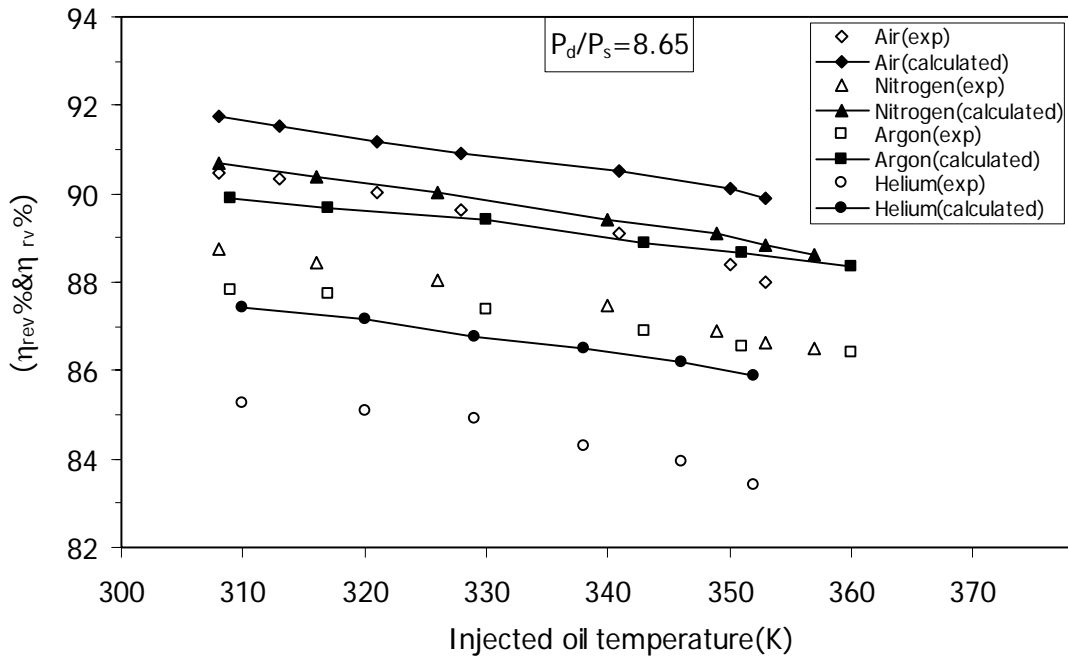


Figure 6.6: Influence of injected oil temperature on volumetric efficiency with different working gases of 5.5 kW compressor at constant suction pressure.

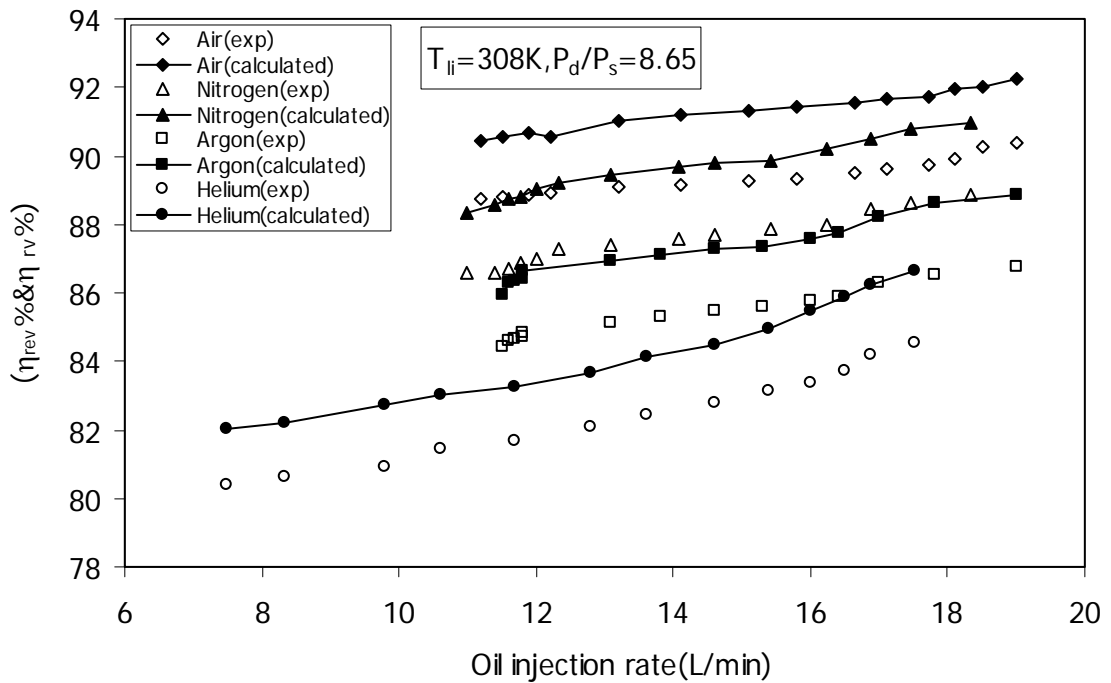


Figure 6.7: Influence of injected oil quantity on volumetric efficiency of 5.5 kW compressor at constant suction pressure.

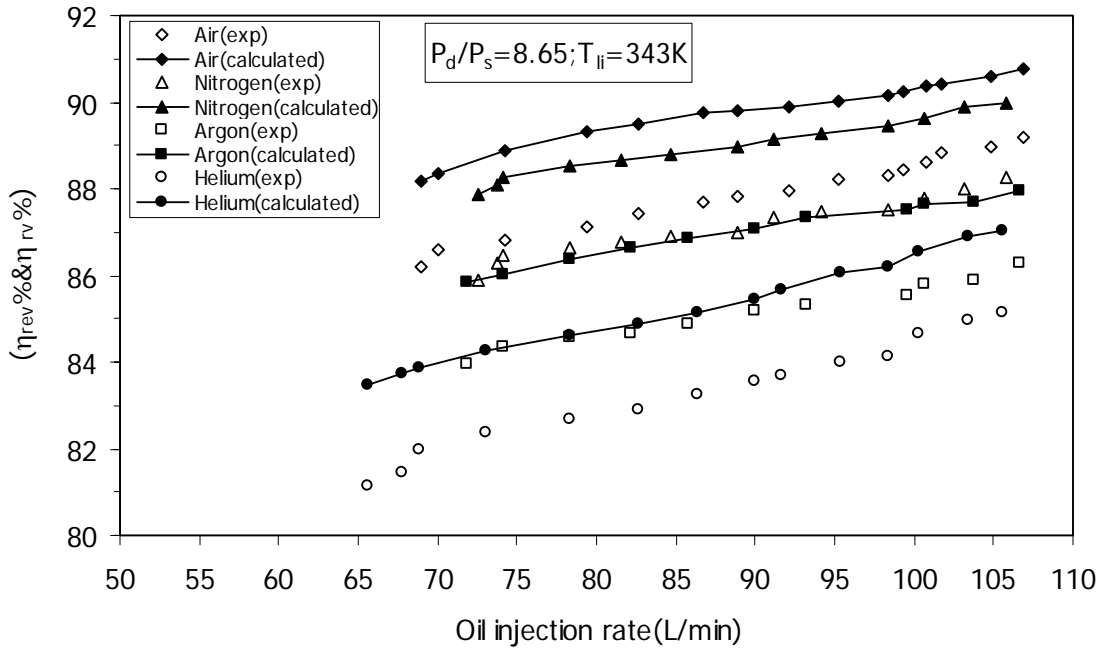


Figure 6.8: Influence of injected oil quantity on volumetric efficiency of 37 kW compressor at constant suction pressure.

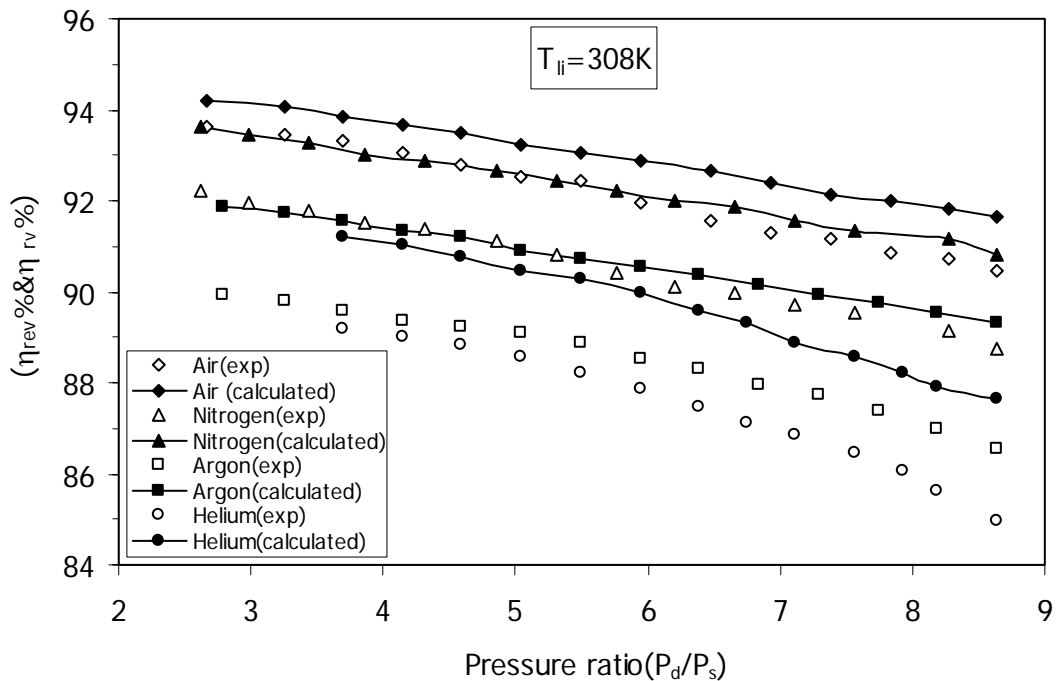


Figure 6.9: Variation of volumetric efficiency of 5.5 kW compressor with pressure ratio at fixed injected oil temperature and suction pressure .

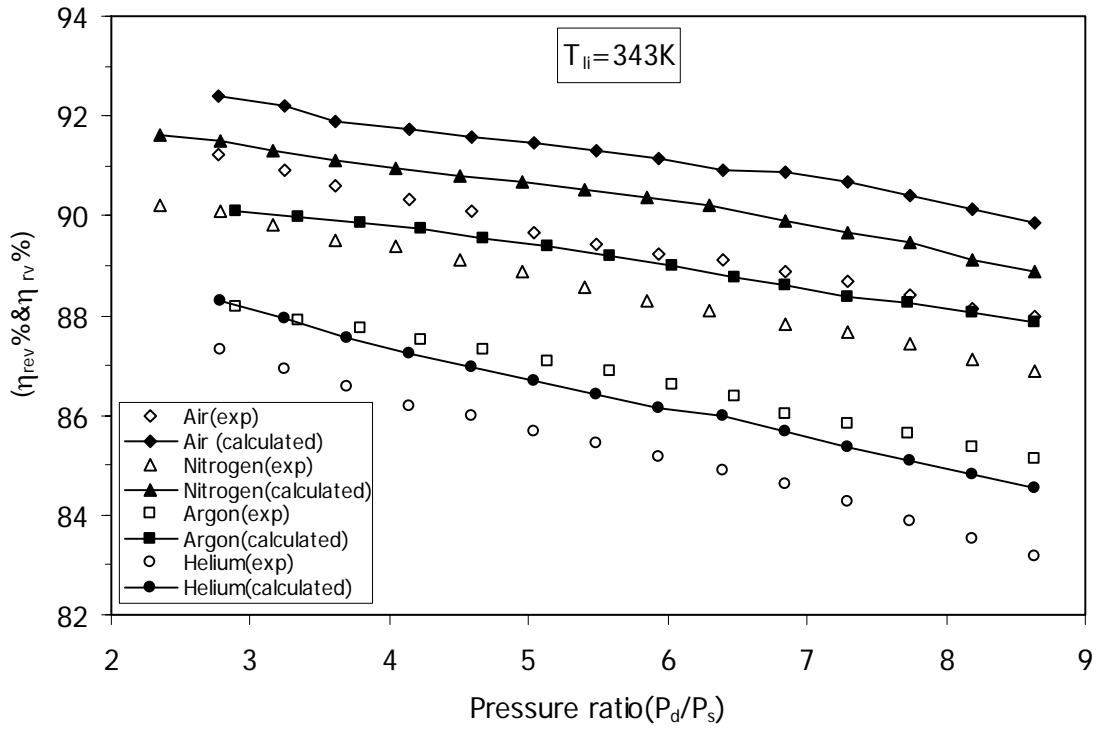


Figure 6.10: Variation of volumetric efficiency of 37 kW compressor with pressure ratio at fixed oil injected temperature and suction pressure .

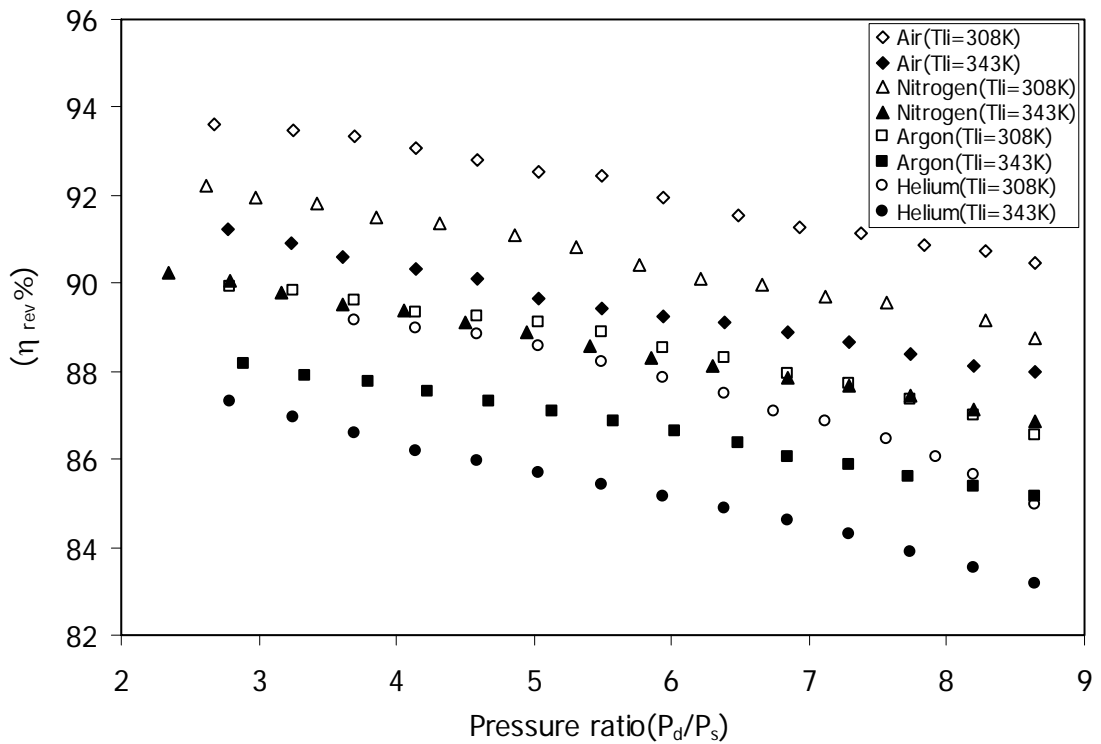


Figure 6.11: Variation of experimentally measured volumetric efficiency of 5.5 kW compressor at two different injected oil temperatures.

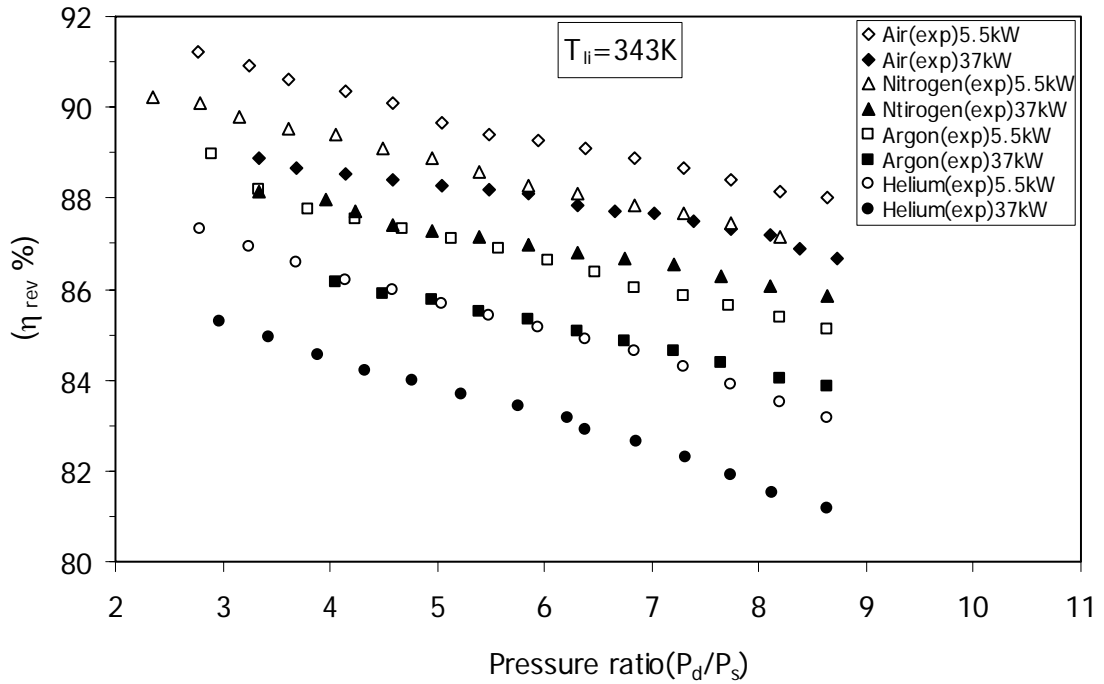


Figure 6.12: Variation of experimentally measured volumetric efficiency of 5.5 kW & 37 kW compressors with pressure ratio at fixed injected oil temperature and at constant suction pressure.

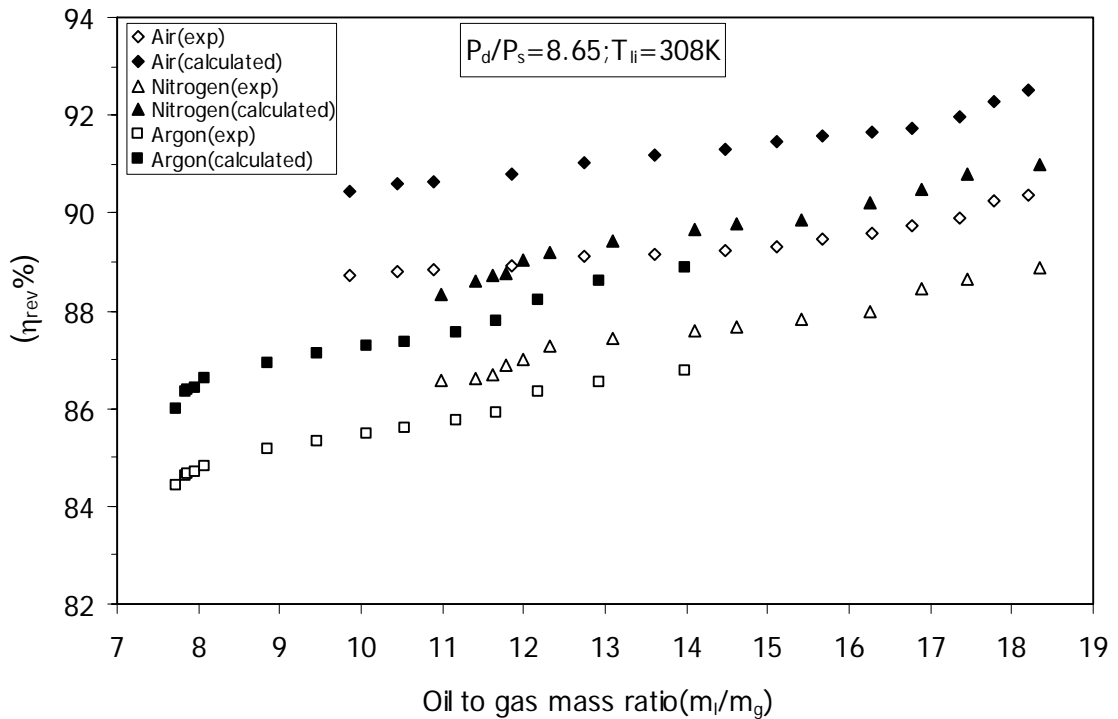


Figure 6.13: Influence of oil to gas mass ratio on volumetric efficiency of 5.5 kW compressor with different working gases at constant pressure ratio, fixed oil injection temperature and at constant suction pressure.

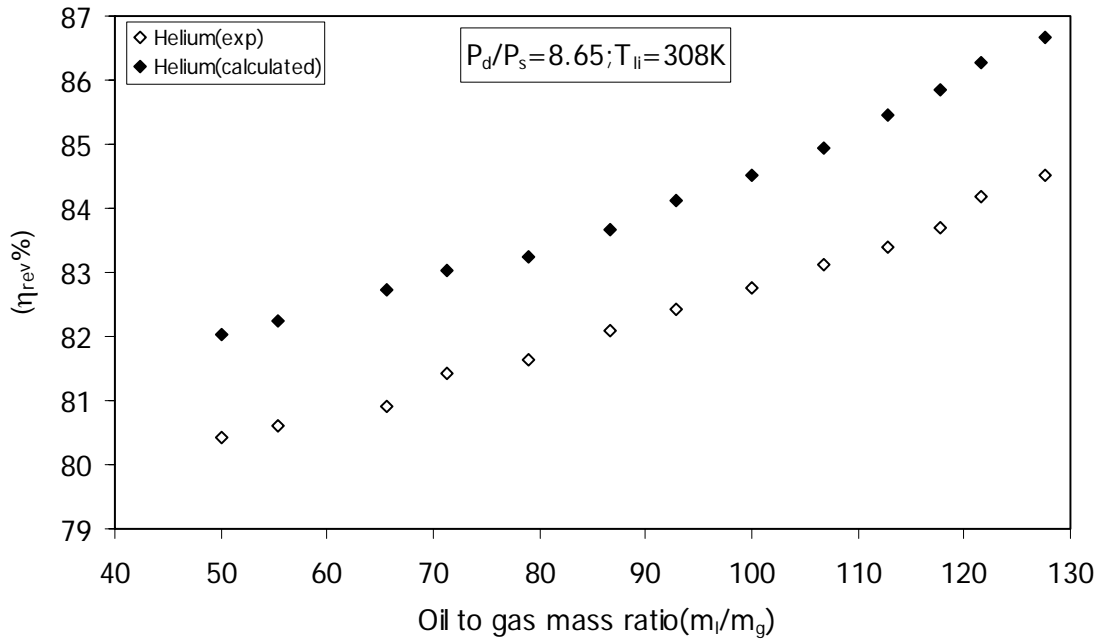


Figure 6.14: Influence of oil to gas mass ratio on volumetric efficiency of 5.5 kW compressor with helium as working gas at constant pressure ratio and at fixed injected oil temperature with constant suction pressure.

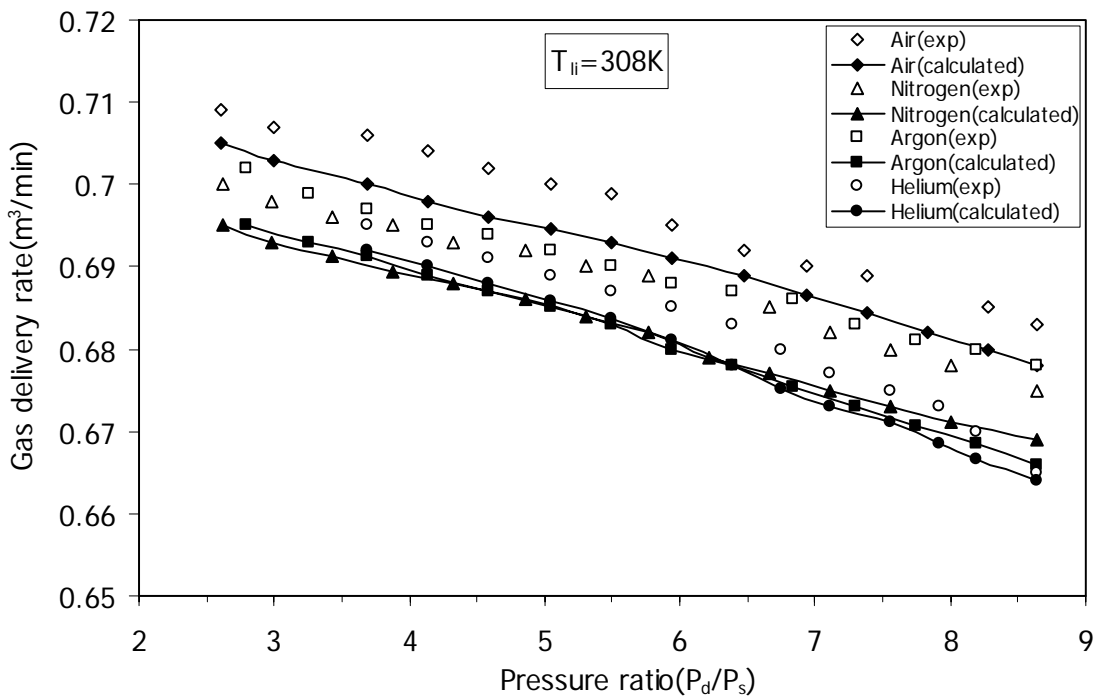


Figure 6.15: Variation of gas flow rate in 5.5 kW compressor with pressure ratio at fixed injected oil temperature and suction pressure.

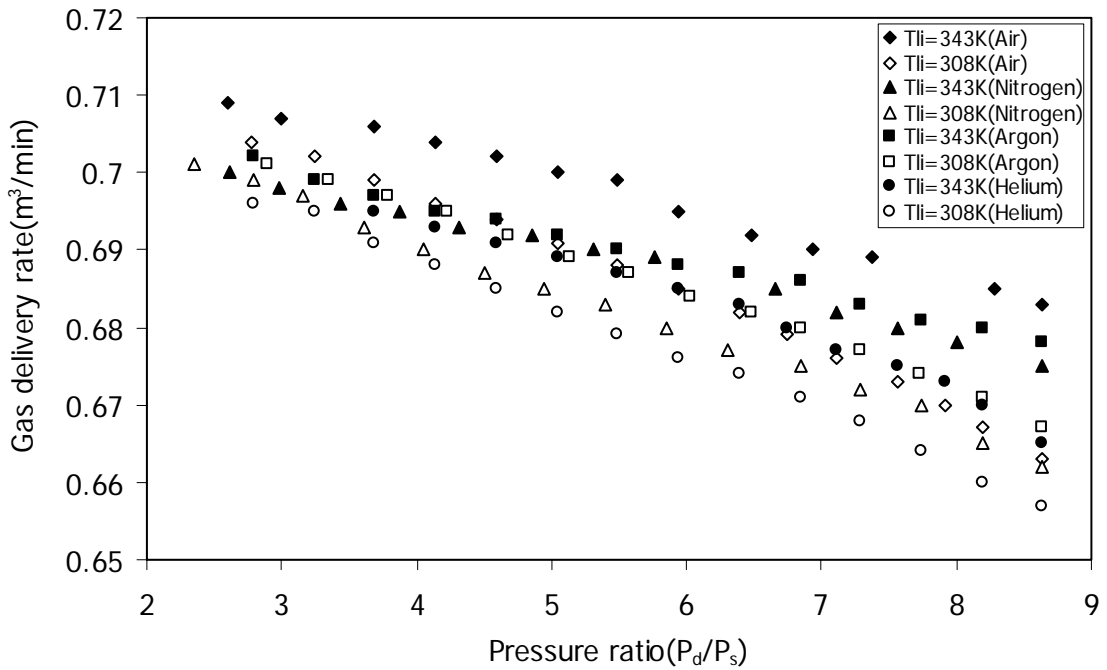


Figure 6.16: Variation of gas flow rate in 5.5 kW compressor with pressure ratio at two different injected oil temperatures and fixed suction pressure.

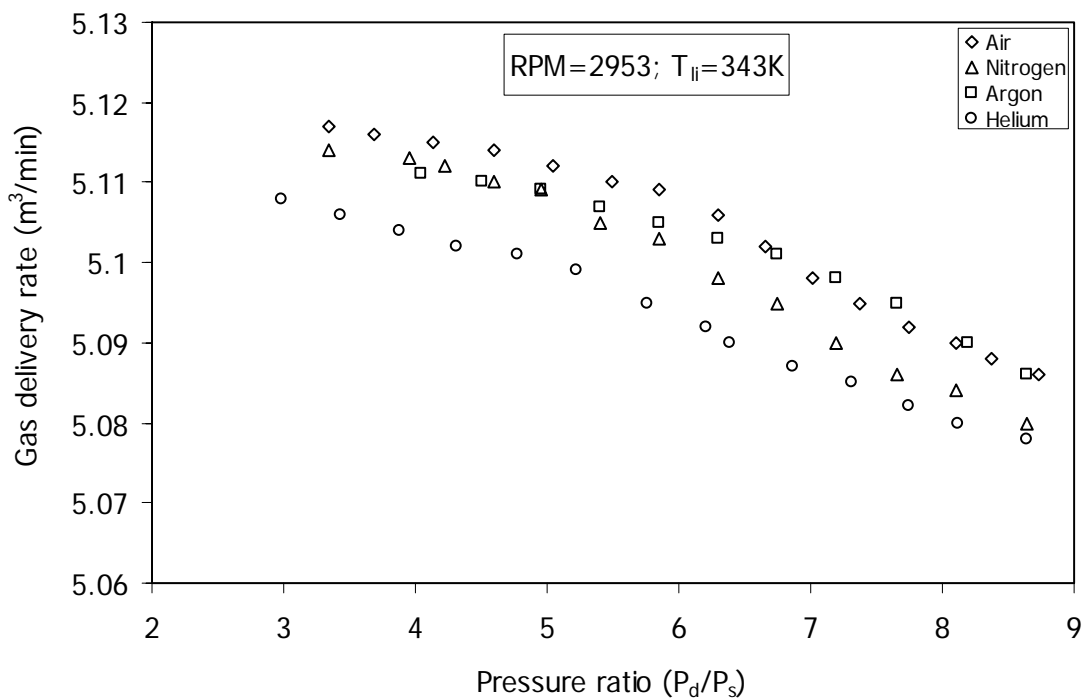


Figure 6.17: Variation of working gas flow rate in 37 kW compressor with pressure ratio at fixed injected oil temperature and suction pressure.

6.2. *Effect on Adiabatic Efficiency*

Results on measurement of adiabatic efficiency of 5.5 kW and 37 kW compressors are presented in Figures 6.18 to 6.31. Adiabatic efficiency is calculated at condition (P_s, T_1) instead of suction condition (P_s, T_s) , because it is easier to compare numerical results with the experimental values. Influence of inducted gas temperature on adiabatic efficiency with different working gases is shown in Figures 6.18 and 6.19. The nature of variation with inducted gas temperature is similar for all the working gases. The increase of adiabatic efficiency for a particular gas species is due to the increase in volumetric efficiency which decreases the actual amount of work consumed per unit mass of gas. Adiabatic efficiency is highest for argon and decreases for air, helium and nitrogen.

The variation of adiabatic efficiency with suction pressure is shown in Figures 6.20 to 6.22. In case of low oil injection temperature, helium shows lower adiabatic efficiency than nitrogen gas. However at higher injection temperature and at higher suction pressure, adiabatic efficiency with helium exceeds that with nitrogen. But helium has lower volume flow rate due to low volumetric efficiency and much lower mass flow rate due to its lower molecular weight compared to nitrogen.

The variation of adiabatic efficiency of both the compressors with suction temperature and suction pressure at a fixed injected oil temperature and pressure ratio is shown in Figures 6.19 and 6.22. The adiabatic efficiency is less for 37 kW compressor as compared to 5.5 kW compressor. This may be due to the low volumetric efficiency of the higher capacity compressor as explained in section 6.1.

Influence of injected oil temperature on adiabatic efficiency at a fixed pressure ratio with the 5.5 kW compressor is presented in Figure 6.23. It may be observed that the increase in efficiency with decrease in injected oil temperature is an obvious consequence of the increase in volumetric efficiency and it is similar for all the gases. The variation of adiabatic efficiency with injected oil temperature at constant pressure ratio has been studied on both the compressors and results are compared in Figure 6.24.

Variation of adiabatic efficiency with oil injection rate at fixed pressure ratio and fixed injection temperature is shown in Figures 6.25 and 6.26. The influence of oil injection rate on adiabatic efficiency, while compressing air, nitrogen or argon is rather weak beyond a certain injection rate. But it plays a significant role in

determining adiabatic efficiency while compressing a light gas like helium which can easily leak through narrow gaps if sufficient oil is not available to seal the gaps. Additionally, helium being a monatomic gas develops higher temperature on compression, which requires higher oil injection rate to maintain acceptable temperature.

The relation between adiabatic efficiency and pressure ratio for all the working gases at two different injected oil temperatures have been shown in Figures 6.27 to 6.29. It has been observed from the results that the nature of variation is similar for all the working gases. It may be observed from the figures that adiabatic efficiency curves show maximum values at different pressure ratios for different working gases. This is due to the fact that adiabatic efficiency increases with pressure ratio and volumetric efficiency decreases with pressure ratio. At higher pressure ratios, there is decrease in mass flow due to fall in volumetric efficiency, which in turn lowers the adiabatic efficiency. The variation of adiabatic efficiency with oil to gas mass ratio is shown in Figures 6.30 and 6.31. It may be observed that the operating oil to gas mass ratio is in the range of 15 to 18 for air, nitrogen and argon, whereas that for helium is nearly 7 times higher due to its low molecular weight.

The specific power consumption of the compressors against pressure ratio is shown in Figures 6.32 to 6.34. It may be observed that it is highest with helium followed by argon, nitrogen and air. Helium has the highest specific power consumption in mass terms due to higher work of compression for a lower volume flow rate, as well as its low density.

Apart from volumetric and adiabatic efficiencies, the oil and gas mixture temperature at compressor discharge for all the working gases at a fixed pressure ratio and oil injection temperature is presented in Figures 6.35 and 6.36 as a function of oil injection rate. It is seen from the figures that the oil and gas mixture temperature decreases for all the gases with oil injection rate. As expected, argon, a monatomic gas with high molecular weight shows the highest discharge temperature. At higher injected oil temperature, mixture temperatures are indistinguishable for the different working gases because the high oil to gas mass ratio dominates the prevailing temperature. The influence of working gas on the surface temperature of the air ends of the compressors has been presented in Figures 6.37 and 6.38. The nature of the curves is similar to that depicting the

dependence of discharge temperature of oil and gas mixture as shown in Figures 6.31 and 6.32. It is observed that the air end surface temperature is relatively higher when compressing helium and argon than when compressing diatomic gases like nitrogen and air.

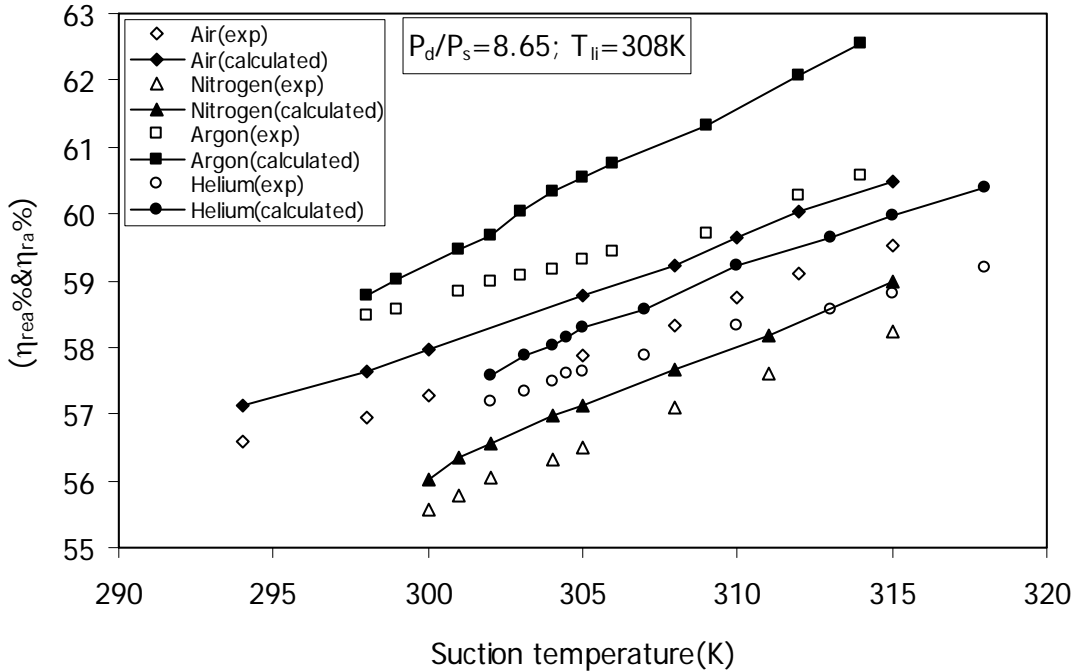


Figure 6.18: Influence of inducted gas temperature on adiabatic efficiency at constant suction pressure and injected oil rate in 5.5 kW compressor.

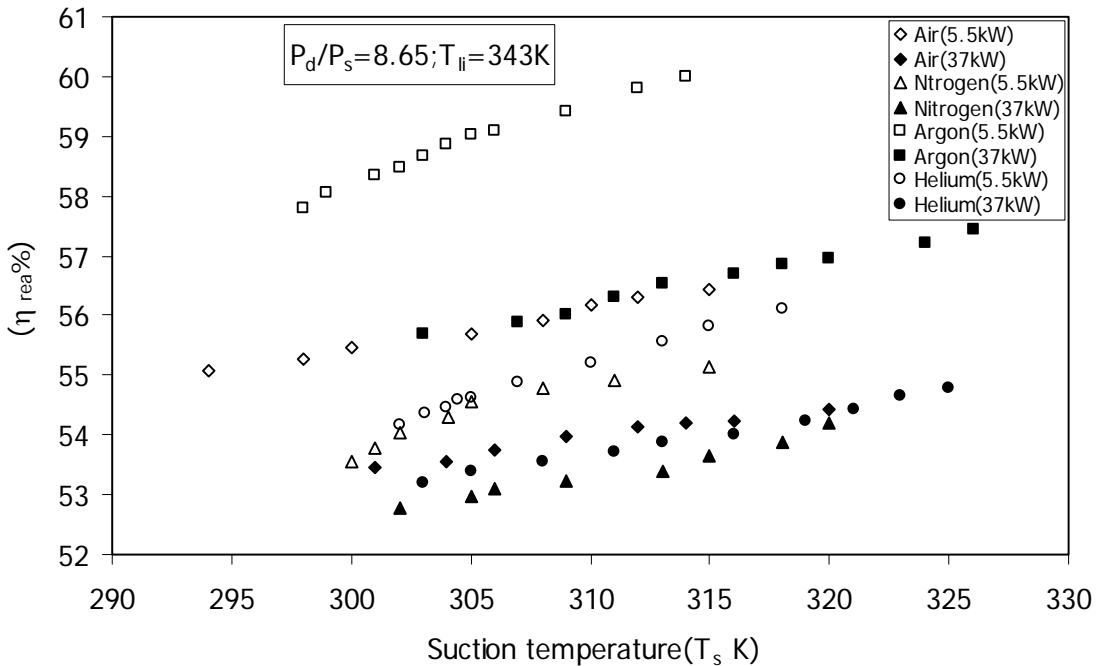


Figure 6.19: Comparison of adiabatic efficiency of 5.5 kW and 37 kW compressors at constant suction pressure and fixed injected oil temperature.

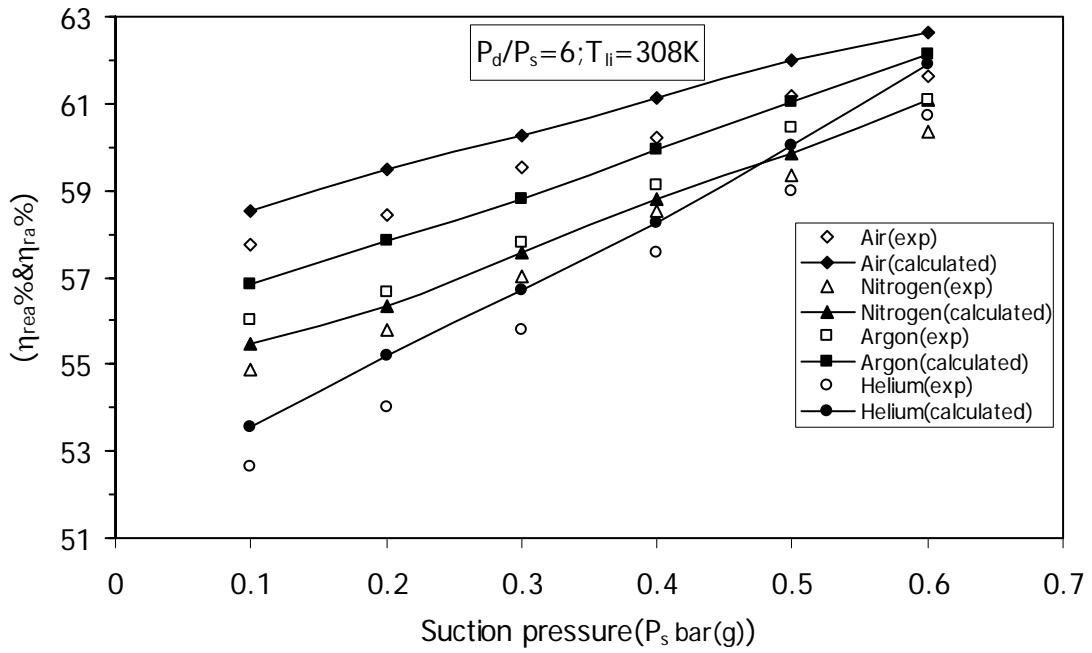


Figure 6.20: Influence of suction pressure of 5.5 kW compressor on different working gases at fixed injected oil temperature.

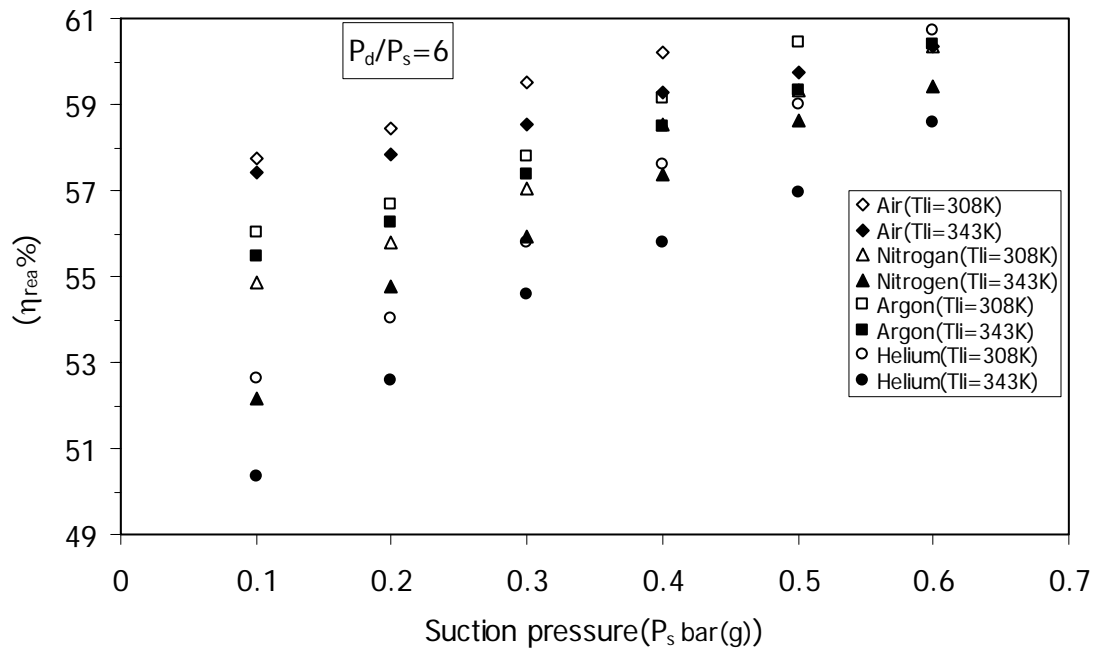


Figure 6.21: Influence of injected oil temperature on adiabatic efficiency of 5.5 kW compressor at different suction pressures with different working gases.

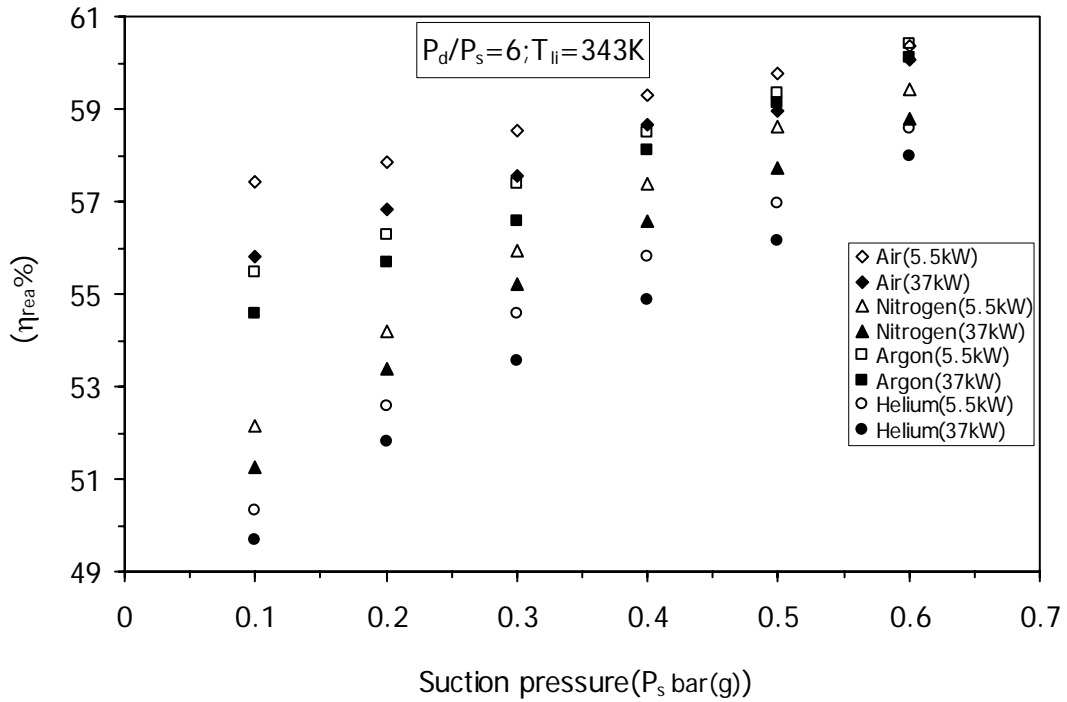


Figure 6.22: Variation of adiabatic efficiency with compressor capacity at fixed injected oil temperature and pressure ratio.

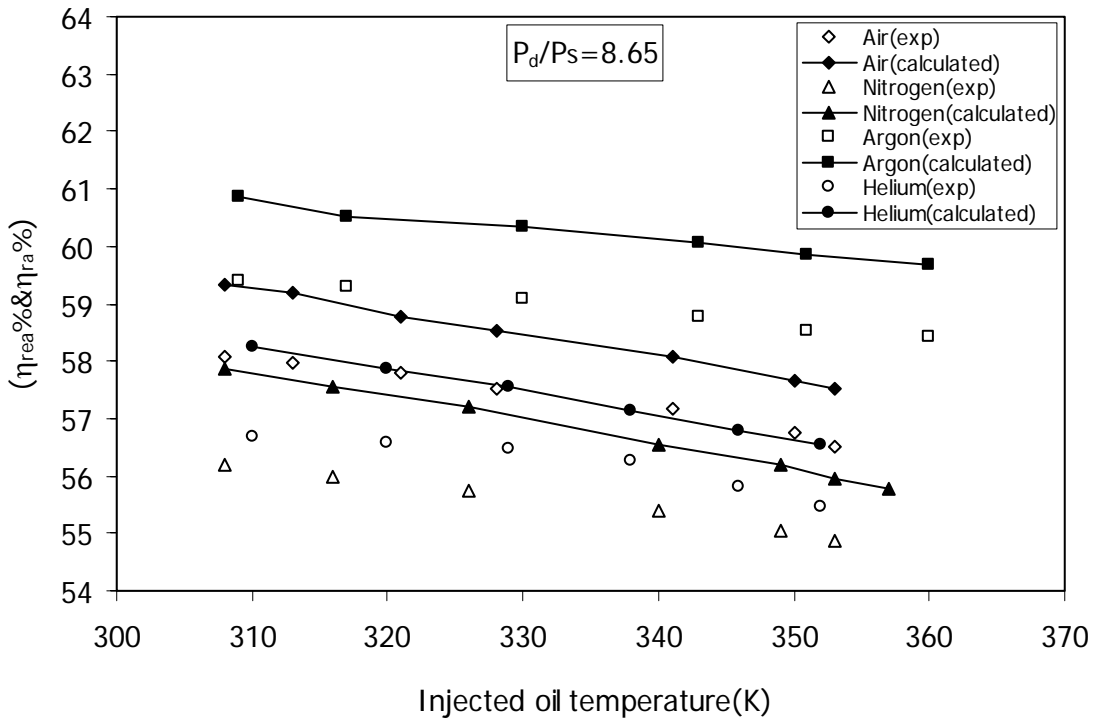


Figure 6.23: Influence of injected oil temperature on efficiency of 5.5 kW compressor with different working gases at fixed pressure ratio.

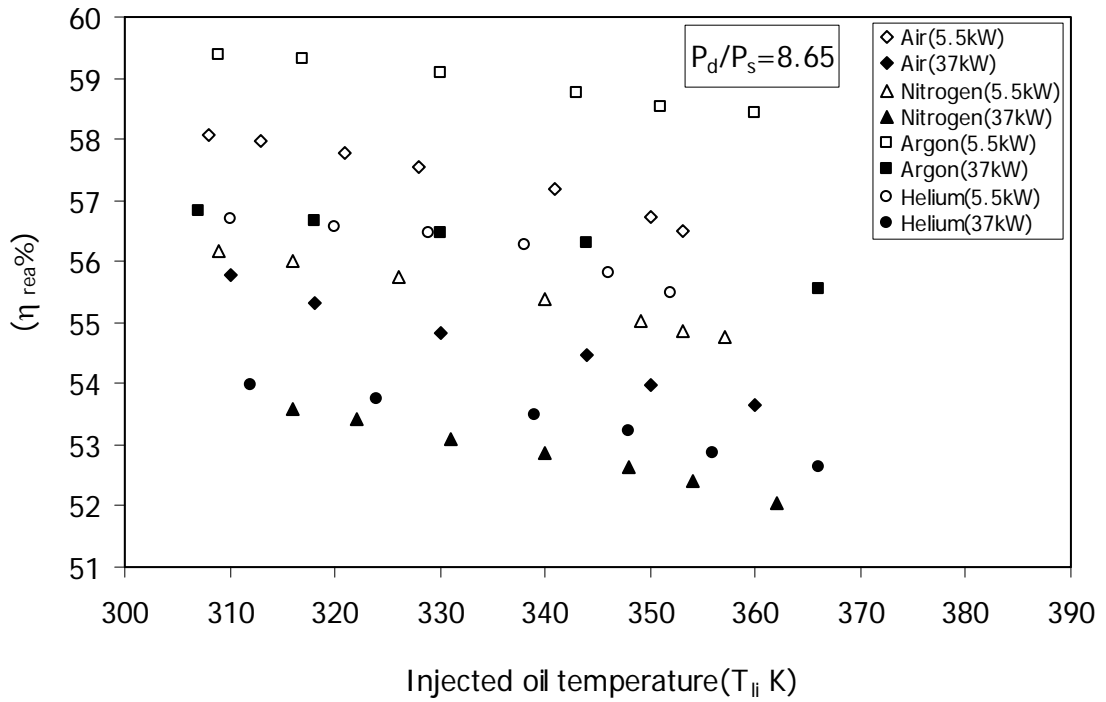


Figure 6.24: Variation of experimentally measured adiabatic efficiency with injected oil temperature at constant pressure ratio.

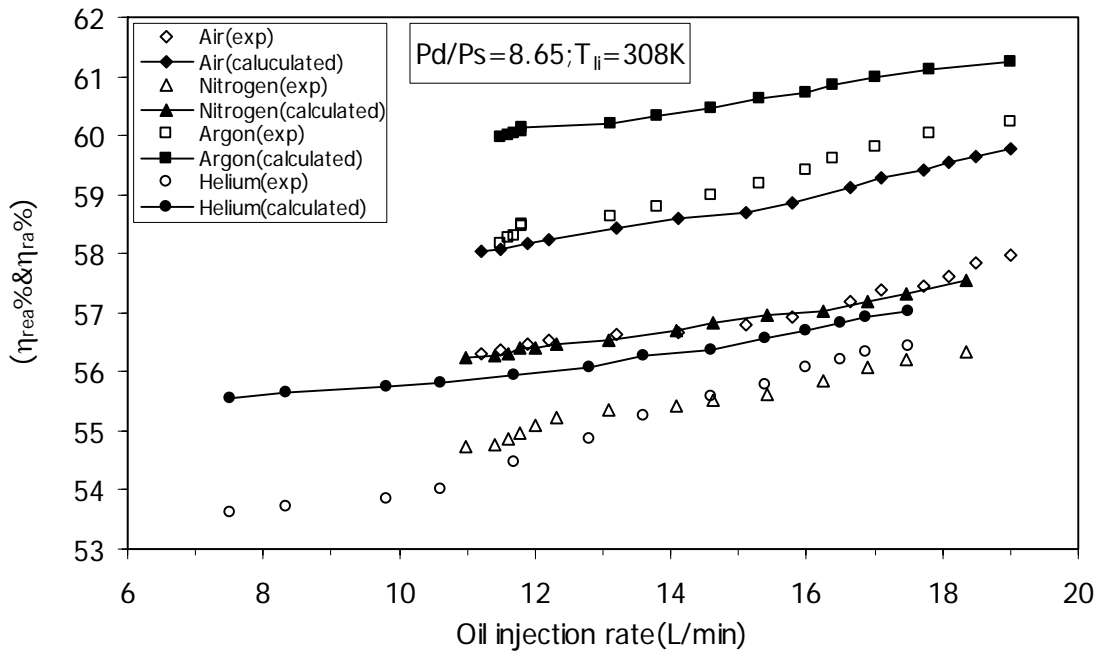


Figure 6.25: Influence of oil injection quantity on adiabatic efficiency at constant pressure ratio and fixed injected oil temperature in 5.5 kW compressor.

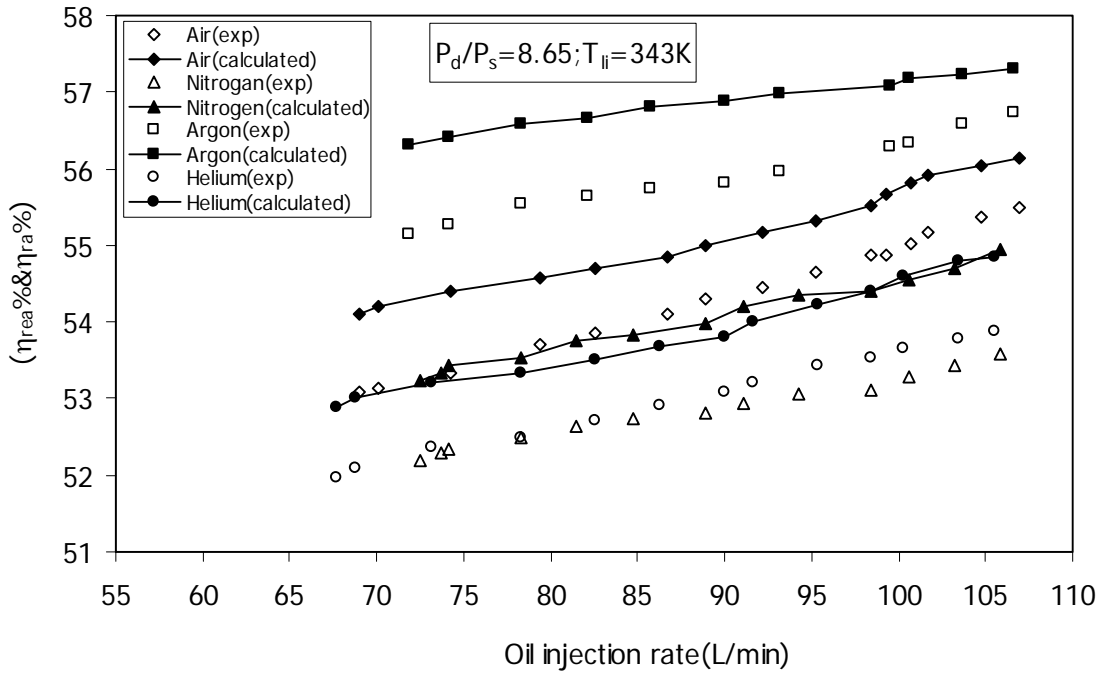


Figure 6.26: Influence of oil injection quantity on adiabatic efficiency of 37 kW compressor with different working gases at constant pressure ratio and fixed injected oil temperature.

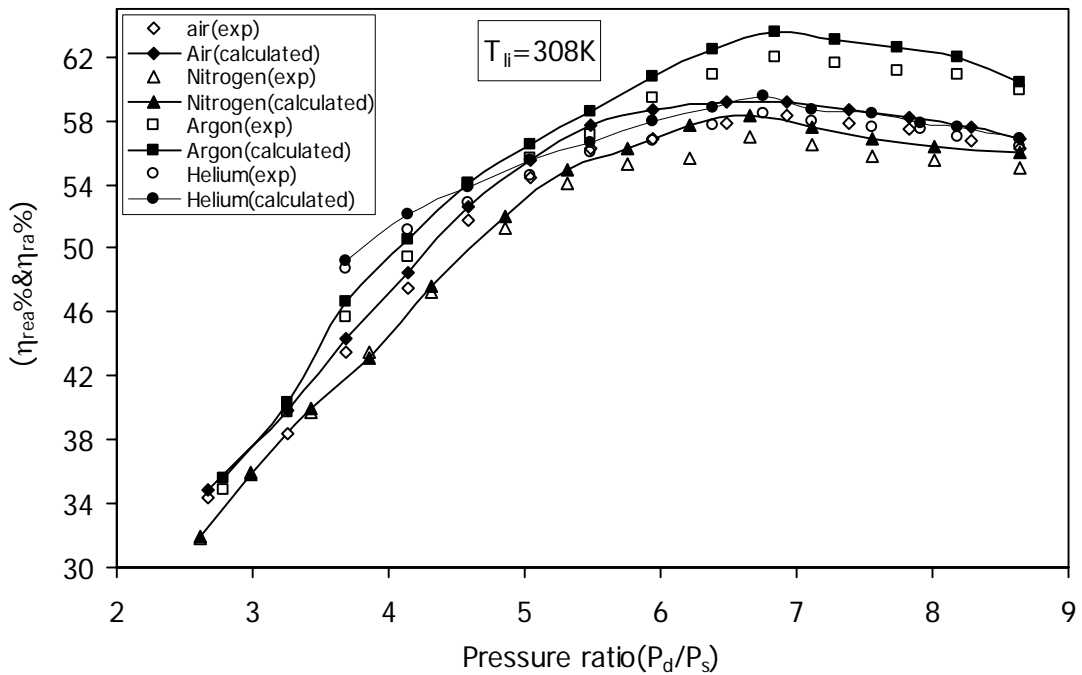


Figure 6.27: Variation of adiabatic efficiency of 5.5 kW compressor with pressure ratio at fixed injected oil temperature.

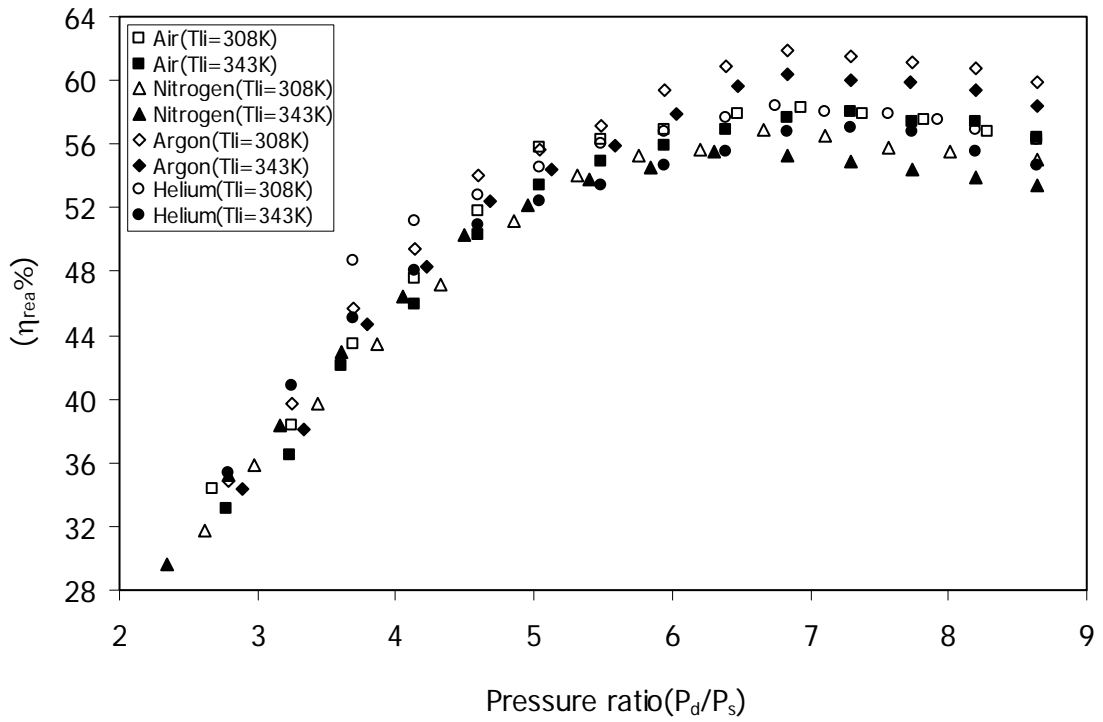


Figure 6.28: Comparison of experimentally measured adiabatic efficiencies of 5.5 kW compressor at different injected oil temperatures.

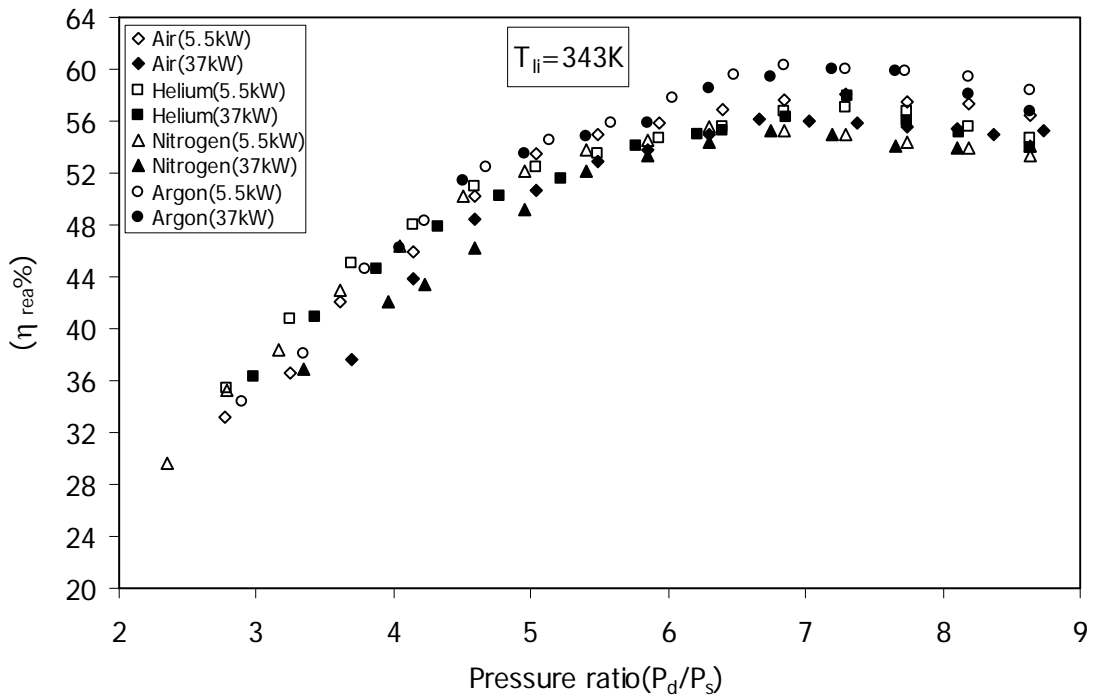


Figure 6.29: Variation of experimentally measured adiabatic efficiency with compressor capacity at fixed injected oil temperature.

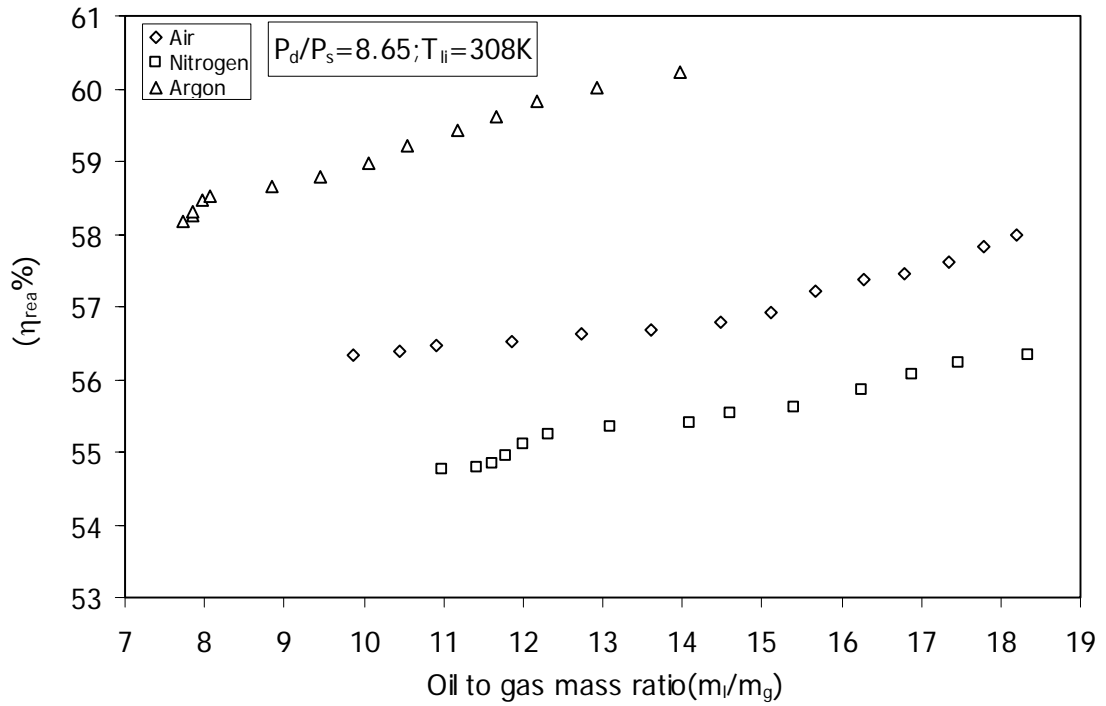


Figure 6.30: Variation of experimentally measured adiabatic efficiency with oil to gas mass ratio at fixed injected oil temperature and pressure ratio.

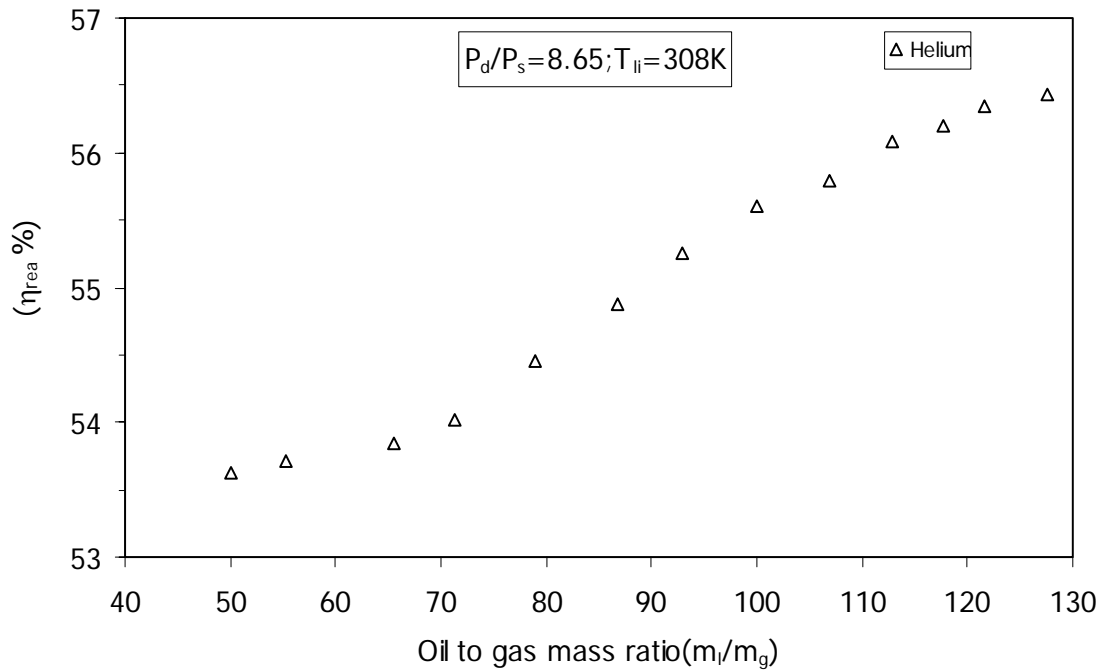


Figure 6.31: Variation of experimentally measured adiabatic efficiency with oil to gas mass ratio at fixed injected oil temperature and pressure ratio.

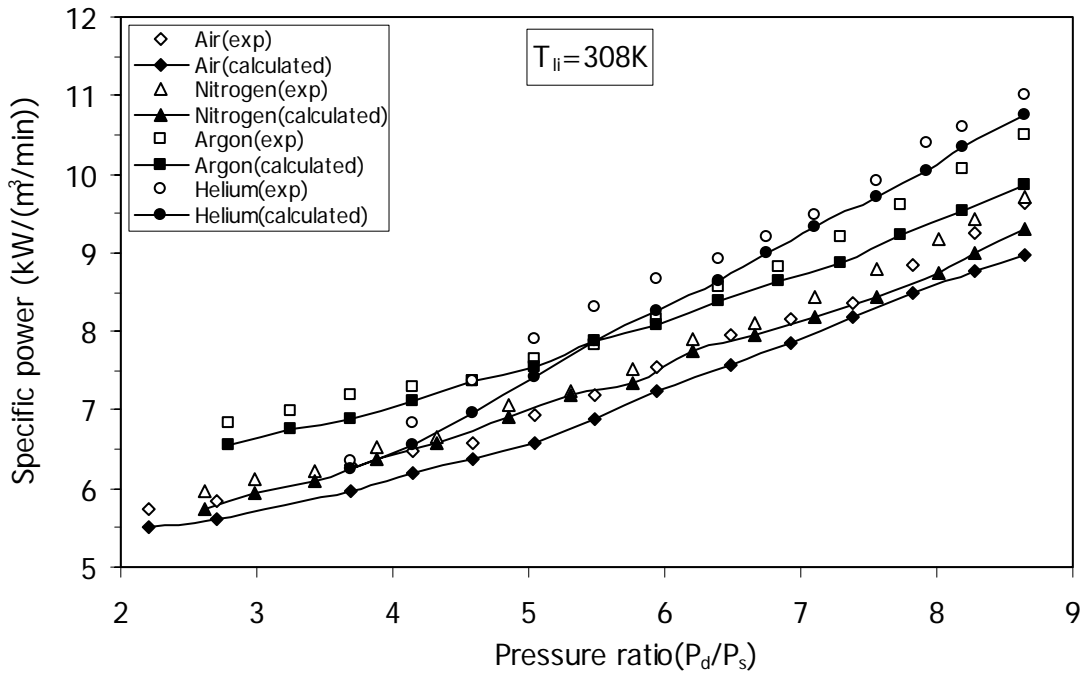


Figure 6.32: Variation of specific power in 5.5 kW compressor with pressure ratio with different working gases at fixed injected oil temperature and constant suction pressure.

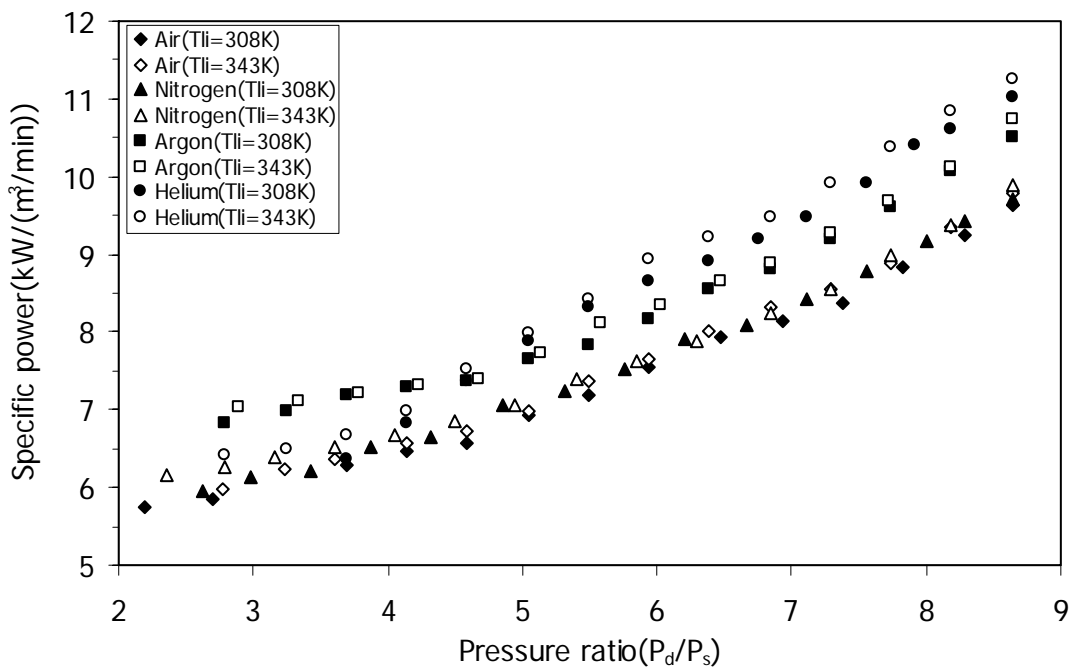


Figure 6.33: Comparison of specific power at two different injected oil Temperatures with different working gases at constant suction pressure in 5.5 kW compressor.

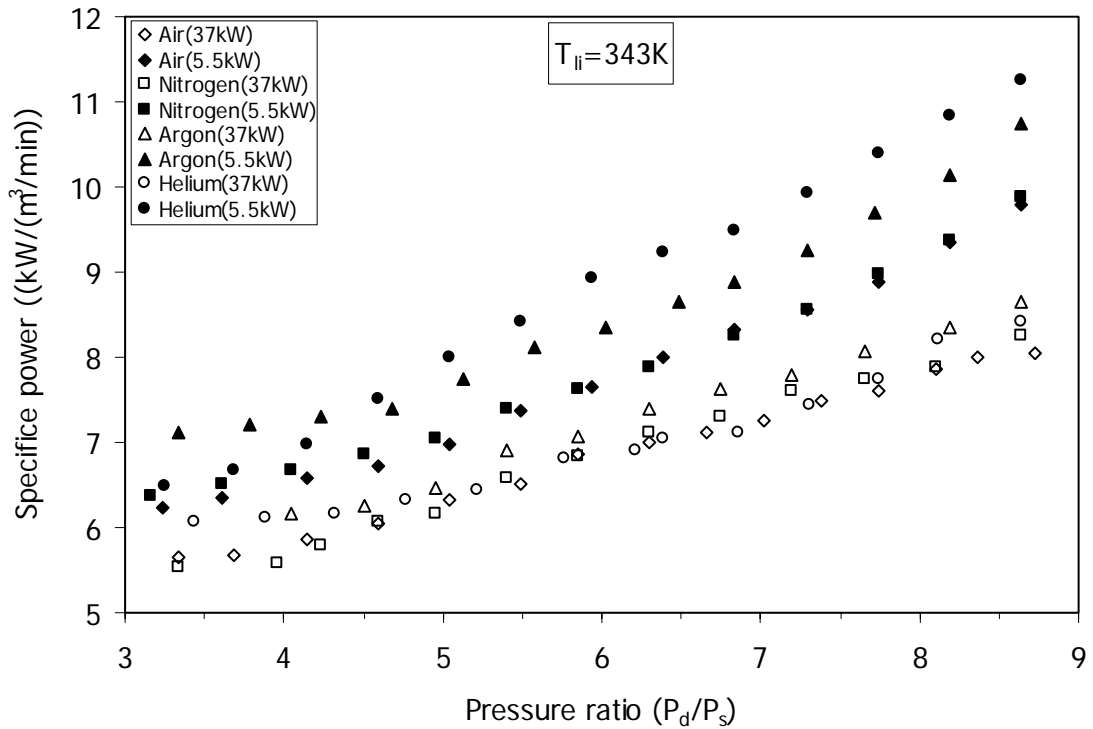


Figure 6.34: Variation of specific power with pressure ratio in two different compressors at fixed injected oil temperature and constant suction pressure.

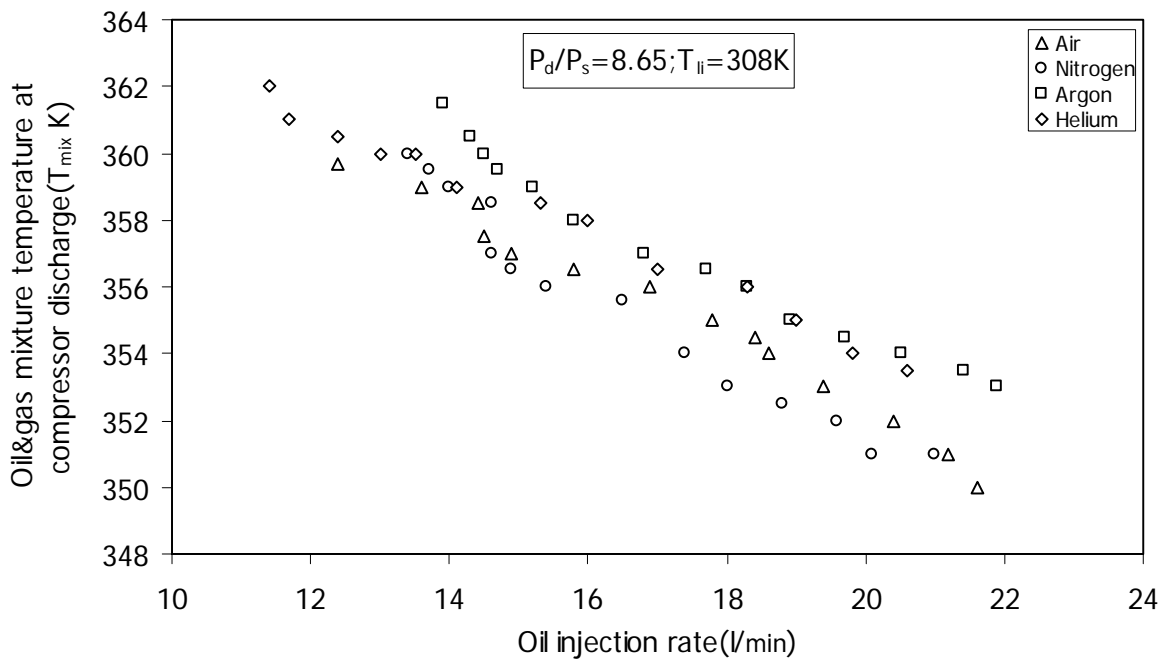


Figure 6.35: Variation of oil and gas mixture temperature at compressor discharge with oil injection rate at fixed injected oil temperature and constant suction pressure in 5.5 kW compressor.

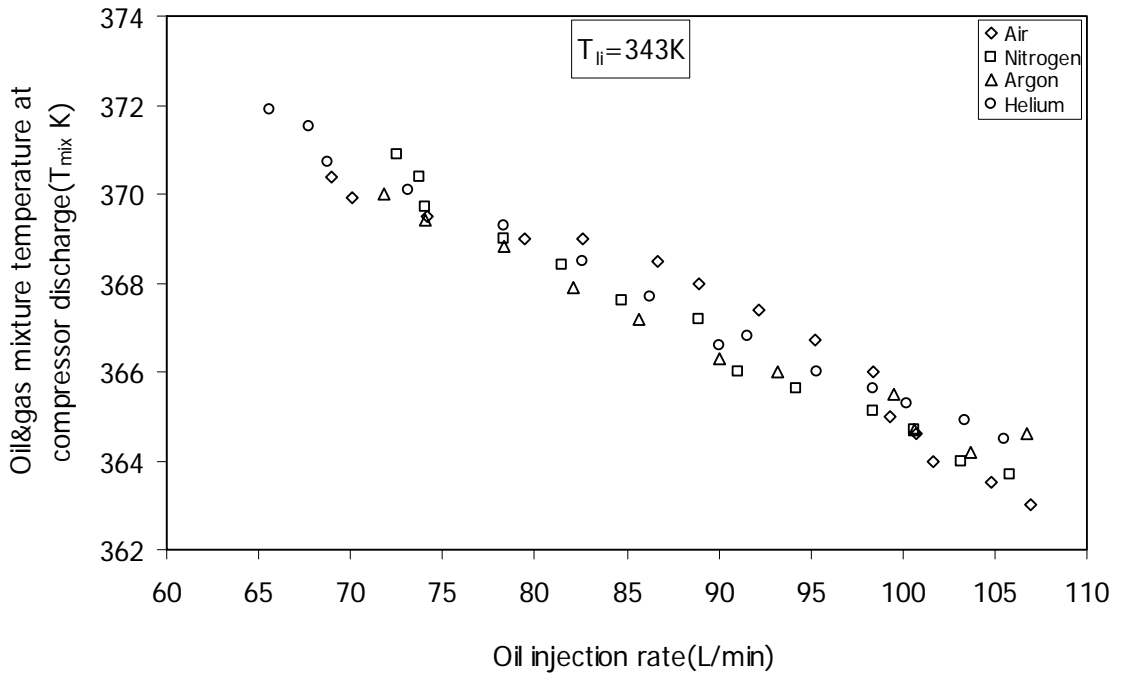


Figure 6.36: Variation of oil and gas mixture temperature at compressor discharge with oil injection rate at fixed injected oil temperature and constant suction pressure in 37 kW compressor.

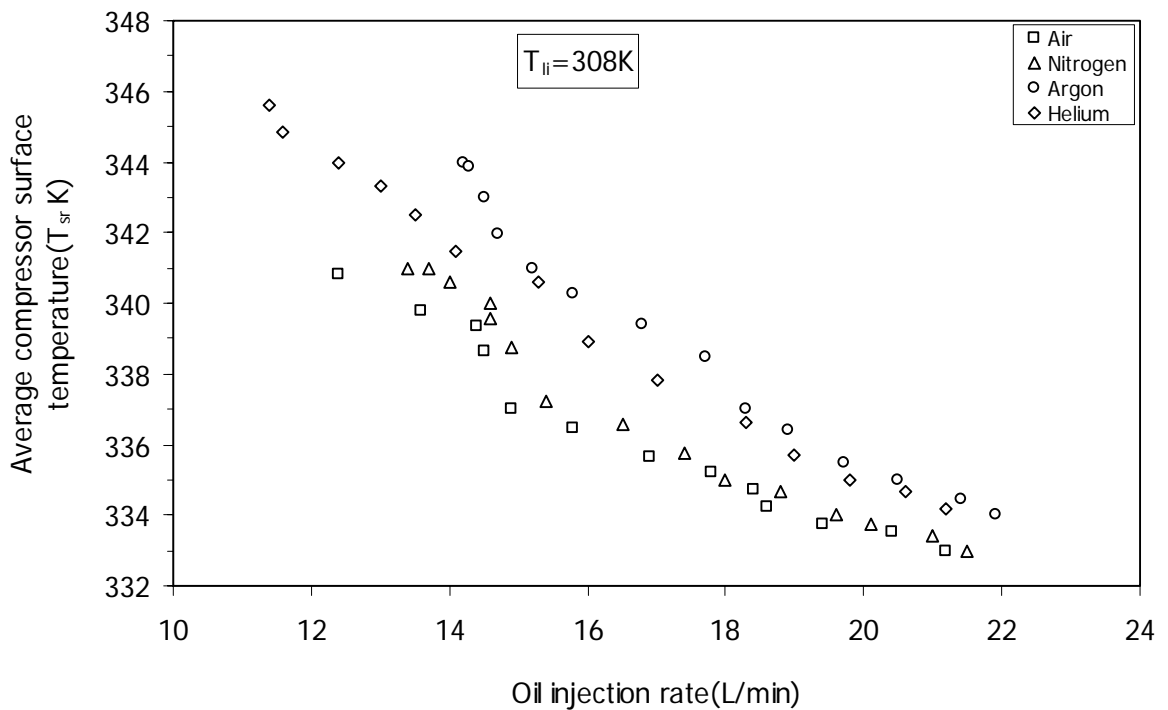


Figure 6.37: Variation of compressor surface temperature with oil injection rate at fixed injected oil temperature and constant suction pressure in 5.5 kW compressor.

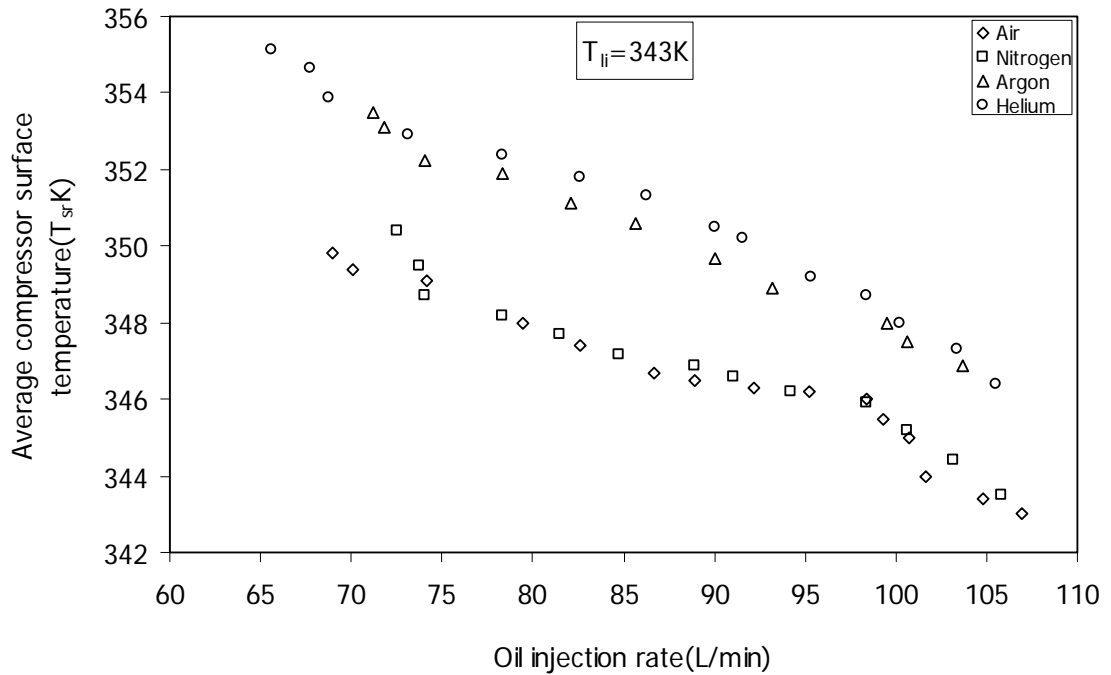


Figure 6.38: Influence of oil injection rate on compressor surface temperature at fixed injected oil temperature in 37 kW compressor.

6.3. Error Estimation in Experimental Results

The error in the measurement of volumetric and adiabatic efficiencies has been estimated from the measurement of individual variables for one set of data. The following major sources of bias and random errors are identified in our experimental system:

- (i) Installation effects of rotameter that consists of pulsating flow, pipe geometry and the location of rotameter, pressure and temperature taps.
- (ii) The fluid properties which are determined from pressure and temperature measurements
- (iii) Environmental considerations which may affect the performance of measuring instruments. (These include the ambient temperature, pressure and humidity.)
- (iv) The uncertainty in calibration of sensors and gauges is estimated to be of the order of ± 0.01 bar for pressure transducers, ± 0.015 bar for pressure gauges and $\pm 0.005^{\circ}\text{C}$ for temperature sensors (as per manufacturers' specifications).

- (v) An error in calibration of energy meter is found to be ± 5 W.s and the tachometer has ± 15 rpm (calibrated in the laboratory)
- (vi) The bias associated with the measurement of theoretical volume of one pair of male and female rotor grooves, which is found to be ± 0.5 cm³

All the individual variables which influence the result (volumetric and adiabatic efficiencies) have been measured N times and the associated precision error $S_{\bar{X}}$ along with other variables is shown in Table 6.1. Bias and random errors in the measurement of volumetric and adiabatic efficiencies have been calculated using the values listed in table 6.1. The table is specific for calculation of volumetric and adiabatic efficiency. This error estimation can be extended to yield an average error in the experimental procedure for the determination of volumetric and adiabatic efficiency.

Table 6.1: Average values and their error values for N samples

Parameter	Average value(\bar{X})	Bias error (B _r)	Precision error ($S_{\bar{X}}$)	Sample Size (N)
Suction pressure (P _s) bar	1.113	0.015	0.023	6
Suction Temperature(T _s) °C	308	0.005	0.3	6
Discharge pressure(P _d) bar	9.65	0.015	0.25	6
Speed of male rotor(N _m) rpm	4350	15	20	6
Volume flow rate of gas(V _m) L/min	675	25	12	6
Volume of a pair cavities(V _{t1}) cm ³	342	0.5	1	6
No.of revolutions of energy meter(n _e)	5			
Time for n _e rotations of energy meter disc (t _e) sec	38	0.05	0.2	6
Experimental mass flow rate(m _e) kg/s	0.0139	0.1	0.5	6
Theoretical mass flow rate(m _t) kg/s	0.0156	-	-	-
Experimental adiabatic power(W _{ade}) kW	3.642	-	-	-
Experimental system power(W _{sys}) kW	6.3	-	-	-

Bias in the measurement of volumetric efficiency

Gas flow rate has been measured with rotameter which has been calibrated for air. The gas density and gas characteristic constant has been taken from standard tables [120]. The volumetric efficiency equation is rewritten as:

$$\eta_{rev} = \frac{\dot{m}_e}{\dot{m}_t} \quad (6.5)$$

The bias in the measurement of volumetric efficiency can be estimated by using the relation:

$$\left(\frac{\Delta \eta_{rev}}{\eta_{rev}} \right)^2 = \left(\frac{\Delta \dot{m}_e}{\dot{m}_e} \right)^2 + \left(\frac{\Delta \dot{m}_t}{\dot{m}_t} \right)^2 \quad (6.6)$$

The rotameter employed for measurement of gas volume flow rate has been calibrated at reference conditions (T_r, P_r). The volume measured at the time of experimentation is different from the reference conditions due to dynamic nature of the environment. Hence, the mass flow rate of the compressor at suction conditions can be obtained by using the formula:

$$\dot{m}_e = \rho_s V_s = \rho_s V_m \sqrt{\frac{P_s \times T_r}{P_r \times T_s}} \quad (6.7)$$

The bias in the measurement of mass flow rate is estimated by using the relation:

$$\left(\frac{\Delta \dot{m}_e}{\dot{m}_e} \right)^2 = \left(\frac{\Delta V_m}{V_m} \right)^2 + \left(\frac{1}{2} \frac{\Delta P_s}{P_s} \right)^2 + \left(\frac{1}{2} \frac{\Delta T_s}{T_s} \right)^2 \quad (6.8)$$

The density of gas and the gas constant are taken at suction condition from standard tables/charts. Assuming that the uncertainties in the measurement of reference temperature and thermo-physical properties are negligible, the bias in the experimental mass flow rate is calculated as,

$$\left(\frac{\Delta \dot{m}_e}{\dot{m}_e}\right)^2 = \left(\frac{25}{675}\right)^2 + \left(\frac{1}{2} \times \frac{0.015}{1.11325}\right)^2 + \left(\frac{1}{2} \times \frac{0.005}{308}\right)^2 \quad (6.9a)$$

$$\left(\frac{\Delta \dot{m}_e}{\dot{m}_e}\right)^2 = 0.00137 + 0.0000454 + 0.000000000066 = 0.00142 \quad (6.9b)$$

The theoretical mass flow rate is calculated using the equation of state for perfect gas at same conditions and is given by the equation:

$$\dot{m}_t = \frac{P_s V_{t1}}{RT_s} n_m N_m \quad (6.10)$$

The bias associated with measurement of the theoretical mass flow rate is in the measurement of theoretical volume of one pair of male and female rotor grooves, speed measurement of the male rotor, and suction conditions. The bias in the determination of gas constant is assumed to be negligible. Hence, the bias in the measurement of theoretical mass flow rate is estimated by the relation:

$$\left(\frac{\Delta \dot{m}_t}{\dot{m}_t}\right)^2 = \left(\frac{\Delta V_{t1}}{V_{t1}}\right)^2 + \left(\frac{\Delta P_s}{P_s}\right)^2 + \left(\frac{\Delta T_s}{T_s}\right)^2 + \left(\frac{\Delta N_m}{N_m}\right)^2 \quad (6.11)$$

$$\left(\frac{\Delta \dot{m}_t}{\dot{m}_t}\right)^2 = \left(\frac{0.5}{34.2}\right)^2 + \left(\frac{0.015}{1.11325}\right)^2 + \left(\frac{0.005}{308}\right)^2 + \left(\frac{15}{4350}\right)^2 \quad (6.12a)$$

$$\begin{aligned} \left(\frac{\Delta \dot{m}_t}{\dot{m}_t}\right)^2 &= 0.0002137 + 0.0001816 + 0.000000000026 + 0.000012 \\ &= 0.0004073 \end{aligned} \quad (6.12b)$$

Substituting the values from equations (6.9b) and (6.12b) in equation (6.6), the bias in the measurement of volumetric efficiency is:

$$\left(\frac{\Delta\eta_{rev}}{\eta_{rev}}\right)^2 = 0.00142 + 0.0004073 = 0.001827 \quad (6.13a)$$

$$\left(\frac{\Delta\eta_{rev}}{\eta_{rev}}\right) \times 100 = \pm 4.27\% \quad (6.13b)$$

Precession error in the measurement of volumetric efficiency

The randomness in the determination of volumetric efficiency can be written as:

$$\left(\frac{\Delta\eta_{rev}}{\eta_{rev}}\right)^2 = \left(\frac{\Delta\dot{m}_e}{\dot{m}_e}\right)^2 + \left(\frac{\Delta\dot{m}_t}{\dot{m}_t}\right)^2 \quad (6.14)$$

The precision error in the measurement of experimental mass flow rate is estimated from the relation:

$$\left(\frac{\Delta\dot{m}_e}{\dot{m}_e}\right)^2 = \left(\frac{\Delta V_m}{V_m}\right)^2 + \left(\frac{1}{2} \frac{\Delta P_s}{P_s}\right)^2 + \left(\frac{1}{2} \frac{\Delta T_s}{T_s}\right)^2 \quad (6.15)$$

$$\left(\frac{\Delta\dot{m}_e}{\dot{m}_e}\right)^2 = \left(\frac{12}{675}\right)^2 + \left(\frac{1}{2} \times \frac{0.023}{1.11325}\right)^2 + \left(\frac{1}{2} \times \frac{0.3}{308}\right)^2 \quad (6.16a)$$

$$\left(\frac{\Delta\dot{m}_e}{\dot{m}_e}\right)^2 = 0.000316 + 0.000107 + 0.000000237 = 0.000423 \quad (6.16b)$$

The precision error in the measurement of theoretical mass flow rate is estimated by:

$$\left(\frac{\Delta\dot{m}_t}{\dot{m}_t}\right)^2 = \left(\frac{\Delta V_{t1}}{V_{t1}}\right)^2 + \left(\frac{\Delta P_s}{P_s}\right)^2 + \left(\frac{\Delta T_s}{T_s}\right)^2 + \left(\frac{\Delta N_m}{N_m}\right)^2 \quad (6.17)$$

$$\left(\frac{\Delta\dot{m}_t}{\dot{m}_t}\right)^2 = \left(\frac{2}{34.2}\right)^2 + \left(\frac{0.023}{1.11325}\right)^2 + \left(\frac{0.3}{308}\right)^2 + \left(\frac{20}{4350}\right)^2 \quad (6.18a)$$

$$\left(\frac{\Delta\dot{m}_t}{\dot{m}_t}\right)^2 = 0.00342 + 0.000427 + 0.00000095 + 0.000021 = 0.00386 \quad (6.18b)$$

Substituting the values of $\left(\frac{\Delta\dot{m}_e}{\dot{m}_e}\right)$ and $\left(\frac{\Delta\dot{m}_t}{\dot{m}_t}\right)$ from equations (6.16b) and (6.18b) in equation (6.14), the random error in volumetric efficiency measurement is given as:

$$\left(\frac{\Delta\eta_{rev}}{\eta_{rev}}\right)^2 = 0.000142 + 0.00386 = 0.00401 \quad (6.19a)$$

$$\left(\frac{\Delta\eta_{rev}}{\eta_{rev}}\right) \times 100 = \pm 6.33\% \quad (6.19b)$$

The number of degrees of freedom ν_r associated with combined precision P_r is found by using the Welch-Satterthwaite formula [121].

$$\nu_r = \frac{\left[\sum_{i=1}^J (\theta_i P_i)^2\right]^2}{\sum_{i=1}^J [(\theta_i P_i)^4 / \nu_i]} = \frac{P_r^4}{\sum_{i=1}^J [(\theta_i P_i)^4 / \nu_i]} \quad (6.20)$$

The numerator of the above equation can be defined as:

$$\begin{aligned} P_r^4 &= \left[\left(\frac{\Delta V_m}{V_m}\right)^2 + \left(\frac{\Delta V_{t1}}{V_{t1}}\right)^2 + \left(\frac{\Delta P_s}{P_s}\right)^2 + \left(\frac{\Delta T_s}{T_s}\right)^2 + \left(\frac{\Delta N_m}{N_m}\right)^2 \right]^2 \\ &= \left[\left(\frac{12}{675}\right)^2 + \left(\frac{2}{34.2}\right)^2 + \left(\frac{0.023}{1.1132}\right)^2 + \left(\frac{0.3}{308}\right)^2 + \left(\frac{20}{4350}\right)^2 \right]^2 \\ &= [3.16 \times 10^{-4} + 0.00342 + 4.27 \times 10^{-4} + 9.48 \times 10^{-7} + 2.114 \times 10^{-5}]^2 \\ &= [0.004184]^2 = 1.751 \times 10^{-5} \quad (6.20a) \end{aligned}$$

For all the individual variables, the experiment has been repeated six times to measure the precession error. For the sample size of 6 the degree of freedom $\nu_i = 5$, [since $\nu_i = (N-1) = 5$].

The denominator of equation (6.20) is rewritten as:

$$\sum_{i=1}^J (\theta_i P_i)^4 / \nu_i \quad (6.20b)$$

where $\nu_i = \nu_m = \nu_{t1} = \nu_s = \nu_{ts} = \nu_{nm} = 5$

Equation (6.20b) can be redefined in another form as:

$$\begin{aligned} &= \left[\left(\frac{\Delta V_m}{V_m} \right)^4 / \nu_m + \left(\frac{\Delta V_{t1}}{V_{t1}} \right)^4 / \nu_{t1} + \left(\frac{\Delta P_s}{P_s} \right)^4 / \nu_s + \left(\frac{\Delta T_s}{T_s} \right)^4 / \nu_{ts} + \left(\frac{\Delta N_m}{N_m} \right)^4 / \nu_{nm} \right] \\ &= \frac{1}{5} \left[\left(\frac{12}{675} \right)^4 + \left(\frac{2}{34.2} \right)^4 + \left(\frac{0.023}{1.1132} \right)^4 + \left(\frac{0.3}{308} \right)^4 + \left(\frac{20}{4350} \right)^4 \right] \\ &= 1/5 [9.989 \times 10^{-8} + 1.17 \times 10^{-5} + 1.82 \times 10^{-7} + 9.00 \times 10^{-13} + 4.47 \times 10^{-10}] \\ &= 1/5 [1.19 \times 10^{-5}] = 4.4 \times 10^{-6} \end{aligned}$$

Substituting the values from (6.20a) and (6.20b) in equation (6.20), the combined degree of freedom for the measurement of volumetric efficiency is calculated as:

$$\nu_r = \frac{P_r^4}{\sum_{i=1}^J [(\theta_i P_i)^4 / \nu_i]} = 1.751 \times 10^{-5} / 4.4 \times 10^{-6} = 3.98 \approx 4$$

From t- distribution table [121] for the degree of freedom 4, the t- value at 95% confidence level is 2.776. The combined uncertainty in the measurement of volumetric efficiency is estimated by using the equation [121] as:

$$U_{RSS} = \left[B_r^2 + (t \times P_r)^2 \right]^{\frac{1}{2}} \quad (6.21)$$

$$U_{RSS} = \left[(4.27)^2 + (2.776 \times 6.33)^2 \right]^{\frac{1}{2}} = 18.08\%$$

Therefore, the uncertainty in the measurement of volumetric efficiency is:

$$\left(\frac{\Delta \eta_{rev}}{\eta_{rev}} \right) = \pm 18.08\%$$

Bias in the measurement of adiabatic efficiency

The bias in the measurement of adiabatic efficiency has also been computed in the similar fashion as that of volumetric efficiency. The adiabatic efficiency is rewritten as:

$$\eta_{rea} = \frac{\dot{W}_{ad,e}}{\dot{W}_{sys,e}} \quad (6.22)$$

The bias in adiabatic efficiency determination can be written as:

$$\left(\frac{\Delta \eta_{rea}}{\eta_{rea}} \right)^2 = \left(\frac{\Delta \dot{W}_{ade}}{\dot{W}_{ade}} \right)^2 + \left(\frac{\Delta \dot{W}_{sys}}{\dot{W}_{sys}} \right)^2 \quad (6.23)$$

The experimental adiabatic efficiency is:

$$\dot{W}_{ad,e} = \dot{m}_e c_p T_s \left[\left(\frac{P_d}{P_s} \right)^{\frac{\gamma-1}{\gamma}} - 1 \right] \quad (6.24)$$

The bias in the measurement of experimental adiabatic power is obtained by the relation:

$$\left(\frac{\Delta \dot{W}_{ade}}{\dot{W}_{ade}}\right)^2 = \left(\frac{\Delta \dot{m}_e}{\dot{m}_e}\right)^2 + \left(\frac{\Delta T_s}{T_s}\right)^2 + \left(\frac{(\gamma-1)}{\gamma} \times \frac{\Delta P_d}{P_d}\right)^2 + \left(\frac{(\gamma-1)}{\gamma} \times \frac{\Delta P_s}{P_s}\right)^2 \quad (6.25a)$$

$$\begin{aligned} \left(\frac{\Delta \dot{W}_{ade}}{\dot{W}_{ade}}\right)^2 &= 0.00168+0.000000000264+0.00000242+0.00001482 \\ &= 0.001694 \end{aligned} \quad (6.25b)$$

The power consumed by the compressor system is rewritten as:

$$\dot{W}_{sys,e} = \frac{3600 n_e}{N_e t_e} \quad (6.26)$$

The bias associated with measurement of the system power is:

$$\left(\frac{\Delta \dot{W}_{sys}}{\dot{W}_{sys}}\right)^2 = \left(\frac{\Delta n_e}{n_e}\right)^2 + \left(\frac{\Delta t_e}{t_e}\right)^2 \quad (6.27a)$$

$$\left(\frac{\Delta \dot{W}_{sys}}{\dot{W}_{sys}}\right)^2 = \left(\frac{0.05}{5}\right)^2 + \left(\frac{0.1}{38}\right)^2 = 0.0001+0.0000069=0.000107 \quad (6.27b)$$

Substituting the values from equations (6.25b) and (6.27b) in equation (6.23), the bias in adiabatic efficiency measurement is given by:

$$\left(\frac{\Delta \eta_{rea}}{\eta_{rea}}\right)^2 = 0.001694+0.000107=0.0018 \quad (6.28)$$

$$\left(\frac{\Delta \eta_{rea}}{\eta_{rea}}\right) \times 100 = \pm 4.24\%$$

Precession error in the measurement of adiabatic efficiency

The randomness in the measurement of adiabatic efficiency can also be computed following the above procedure. The precision error in the measurement of adiabatic efficiency is:

$$\left(\frac{\Delta\eta_{rea}}{\eta_{rea}}\right)^2 = \left(\frac{\Delta\dot{W}_{ade}}{\dot{W}_{ade}}\right)^2 + \left(\frac{\Delta\dot{W}_{sys}}{\dot{W}_{sys}}\right)^2 \quad (6.29)$$

where

$$\left(\frac{\Delta\dot{W}_{ade}}{\dot{W}_{ade}}\right)^2 = \left(\frac{\Delta\dot{m}_e}{\dot{m}_e}\right)^2 + \left(\frac{\Delta T_s}{T_s}\right)^2 + \left(\frac{(\gamma-1)}{\gamma} \times \frac{\Delta P_d}{P_d}\right)^2 + \left(\frac{(\gamma-1)}{\gamma} \times \frac{\Delta P_s}{P_s}\right)^2 \quad (6.30a)$$

$$\left(\frac{\Delta\dot{W}_{ade}}{\dot{W}_{ade}}\right)^2 = 0.000142 + 9.48 \times 10^{-7} + 0.0000548 + 0.0000348 = 0.000232 \quad (6.30b)$$

The precision error associated with measurement of the system power is:

$$\left(\frac{\Delta\dot{W}_{sys}}{\dot{W}_{sys}}\right)^2 = \left(\frac{\Delta n_e}{n_e}\right)^2 + \left(\frac{\Delta t_e}{t_e}\right)^2 \quad (6.31a)$$

$$\left(\frac{\Delta\dot{W}_{sys}}{\dot{W}_{sys}}\right)^2 = \left(\frac{0.2}{5}\right)^2 + \left(\frac{0.5}{38}\right)^2 = 0.0016 + 0.00017 = 0.00177 \quad (6.31b)$$

Substituting the values of $\left(\frac{\Delta\dot{W}_{ade}}{\dot{W}_{ade}}\right)$ and $\left(\frac{\Delta\dot{W}_{sys}}{\dot{W}_{sys}}\right)$ from equations (6.30b) and (6.31b) in equation (6.29), the precision error in measuring adiabatic efficiency is:

$$\left(\frac{\Delta\eta_{rea}}{\eta_{rea}}\right)^2 = 0.000232 + 0.00177 = 0.002002 \quad (6.32a)$$

$$\left(\frac{\Delta\eta_{rea}}{\eta_{rea}}\right) \times 100 = 4.5\% \quad (6.32b)$$

The number of degrees of freedom ν_r associated with combined precision P_r is also found by using equation (6.20) and is rewritten as:

$$\nu_r = \frac{\left[\sum_{i=1}^J (\theta_i P_i)^2\right]^2}{\sum_{i=1}^J [(\theta_i P_i)^4 / \nu_i]} = \frac{P_r^4}{\sum_{i=1}^J [(\theta_i P_i)^4 / \nu_i]}$$

where the numerator of the equation is defined as:

$$P_r^4 = \left[\left(\frac{\Delta\dot{m}_e}{\dot{m}_e}\right)^2 + \left(\frac{\Delta P_d}{P_d}\right)^2 + \left(\frac{\Delta P_s}{P_s}\right)^2 + \left(\frac{\Delta T_s}{T_s}\right)^2 + \left(\frac{\Delta n_e}{n_e}\right)^2 + \left(\frac{\Delta t_e}{t_e}\right)^2 \right]^2$$

$$= [0.000142 + 0.000671 + 0.000427 + 9.48 \times 10^{-7} + 0.0016 + 0.00017]^2$$

$$= [3.01 \times 10^{-3}]^2 = 9.06 \times 10^{-6}$$

and the denominator is rewritten as:

$$\sum_{i=1}^J (\theta_i P_i)^4 / \nu_i$$

where $\nu_i = \nu_m = \nu_{pd} = \nu_{ps} = \nu_{ts} = \nu_n = \nu_{te} = 5$

The denominator of the combined degree of freedom expression is defined as:

$$= \left[\left(\frac{\Delta\dot{m}_e}{\dot{m}_e}\right)^4 / \nu_m + \left(\frac{\Delta P_d}{P_d}\right)^4 / \nu_{pd} + \left(\frac{\Delta P_s}{P_s}\right)^4 / \nu_{ps} + \left(\frac{\Delta T_s}{T_s}\right)^4 / \nu_{ts} + \left(\frac{\Delta n_e}{n_e}\right)^4 / \nu_n + \left(\frac{\Delta t_e}{t_e}\right)^4 / \nu_{te} \right]$$

$$= 1/5 [2.01 \times 10^{-8} + 4.5 \times 10^{-7} + 1.82 \times 10^{-7} + 8.98 \times 10^{-13} + 2.56 \times 10^{-6} + 2.89 \times 10^{-8}]$$

$$= 1/5 [3.241 \times 10^{-6}] = 6.48 \times 10^{-7}$$

Substituting the numerator and denominator values in equation (6.20), the combined degree of freedom for the measurement of adiabatic efficiency is found to be:

$$\nu_r = \frac{P_r^4}{\sum_{i=1}^J [(\theta_i P_i)^4 / \nu_i]} = 9.06 \times 10^{-6} / 6.48 \times 10^{-7} = 13.98 \approx 14$$

From t-distribution table [121] using degrees of freedom value 14, the t-value at 95% confidence level is 2.145. The combined uncertainty in the measurement of adiabatic efficiency using equation (6.21) is:

$$U_{RSS} = \left[B_r^2 + (t \times P_r)^2 \right]^{\frac{1}{2}}$$

$$U_{RSS} = \left[(4.24)^2 + (2.145 \times 4.5)^2 \right]^{\frac{1}{2}}$$

$$= 10.54\%$$

Hence, the uncertainty in the measurement of adiabatic efficiency is:

$$\left(\frac{\Delta \eta_{rev}}{\eta_{rev}} \right) = \pm 10.54\%$$

6.4. Conclusions

Inlet temperature of gas and oil, oil injection rate, oil to gas mass ratio, suction pressure and pressure ratio have been taken as operating parameters to present the variation of volumetric and adiabatic efficiencies on 5.5 kW and 37 kW air compressors. Apart from air as a working gas, the effect of using other working gases such as nitrogen, argon and helium are studied both experimentally and numerically. In the previous section, the results and the possible explanations have been widely discussed. The conclusions of the discussions have been briefly summarized in this section.

- The numerical calculation of volumetric and adiabatic efficiencies (%) by computer simulation differs from their experimental values by a margin of 2%.

One of the major sources of this discrepancy is the volume of oil which has not been considered in the computer simulation. The other sources are the assumptions of ideal conditions which deviate from the actual ones.

- Volumetric efficiency increases with increase in inlet gas temperature. This is due to the fact that inducted mass almost remains constant with inlet oil temperature and the theoretical inducted gas mass decreases with temperature.
- Due to the increase in volumetric efficiency, the adiabatic efficiency also increases with inlet temperature.
- Volumetric efficiency also increases with increase in suction pressure due to the increase in the actual inducted volume of gas, the theoretical inducted volume remaining constant.
- The increase in adiabatic efficiency with suction pressure is due to the increase in volumetric efficiency.
- The volumetric and adiabatic efficiencies increase with lowering of injected oil temperature. The volumetric and adiabatic efficiencies are increasing over a certain range of oil injection rate. This result shows that lowering of oil inlet temperature is more effective than injecting a higher quantity of oil. This may be due to the fact that more resident oil obstructs the volume flow of working gas.
- Volumetric efficiency decreases with pressure ratio because higher pressure ratio enhances gas leakage which decreases volumetric efficiency.
- Adiabatic efficiency undergoes a maximum with pressure ratio. This is because adiabatic efficiency initially increases with increase in pressure ratio due to proportionately reduced role of inefficiencies, but after certain pressure ratio adiabatic efficiency declines due to higher leakage.
- The gas delivery rate decreases with increase of pressure ratio due to leakage.
- The above conclusions have been observed with gases such as air, nitrogen, argon and helium. Molecular configuration (monatomic vs diatomic) and molecular weight also have a strong role in the behaviour of the efficiency terms.
- Specific power increases with pressure ratio. Due to low volumetric efficiency caused by leakage, helium has the highest value of specific power followed by argon. The characteristics of air and nitrogen are indistinguishable and intermediate between those two values.
- The variation of oil and gas mixture temperature with oil injection rate is within the range of 3°C for different gases.

- The plots of average surface temperature with oil injection rate shows that helium has the highest compressor surface temperature followed by argon due to their monatomic nature. The surface temperature in case of air and nitrogen are indistinguishable and are lower than those for helium and argon.
- The variation of volumetric efficiency with suction temperature, suction pressure, injected oil temperature, oil injection rate and pressure ratio has been studied. Helium shows the lowest efficiency followed by argon, nitrogen and air in ascending order. This is because helium being both light and monatomic in nature has highest rate and attains highest temperature on discharge. This is followed by argon which is a monatomic gas although it has a high molecular weight. The higher values of volumetric efficiency with nitrogen and air are due to their higher molecular weight.
- Variation of adiabatic efficiency with suction temperature, suction pressure, injected oil temperature, oil injection rate and pressure ratio has been carried out. In comparison, argon shows the highest efficiency followed that of air, helium and nitrogen in the descending order. It is because argon is a monatomic gas and has high molecular weight.
- It is recommended that increase in oil mass flow rate should be restricted to that necessary for sealing of working gas and any further improvement in efficiency should be done by decreasing oil injection temperature.
- Although the present experiment lacks the facility to increase the rotational speed, it is presumed that increasing the speed will improve the volumetric efficiency.
- In compressing atmospheric air, the discharge temperature should be at least 10 to 20°C above the dew point temperature to avoid condensation of moisture. But that is not a requirement for compressing other gases.
- An analysis of uncertainty in experimental measurement shows that the associated uncertainty in the measurement of volumetric efficiency is around 18%, whereas the uncertainty in that of adiabatic efficiency is around 11%.

Chapter VII

REMARKS AND SCOPE FOR FUTURE WORK

Oil injected twin screw compressors have found extensive application in industry, particularly in refrigeration, cryogenics and chemical processes. Still, the technology of screw compressor has remained largely proprietary. The work reported in this thesis is an attempt to understand the working of oil injected twin-screw compressor through experimentation and numerical analysis. One of the objectives of the research is to study the behaviour of commercially available low cost air compressors employed for compressing other gases. Three different gases nitrogen, argon, and helium have been used in the experimental study. In order to understand size effect if any, the experiments have been carried out on two compressors with capacities of 5.5 kW and 37 kW.

7.1. Concluding Remarks

Detailed conclusions based on the numerical and experimental results have been presented at the end of chapter VI. This section provides a brief summary of the work and a few concluding remarks. The following may be seen as the significant contributions of the project.

- The thesis presents an exhaustive review of literature on the subject of screw compressors, their design and performance. It can serve as a ready reference for other researchers in this field.
- The governing equations based on the control volume analysis have been derived for numerical simulation.
- A complete numerical model has been developed for the oil injected twin-screw compressor covering both the suction and the compression-discharge steps.
- The influence of interlobe clearance on the p-v diagram is analyzed.

- The area of p-v diagram decreases with increase of interlobe clearance for all working gases. It has been observed that the decrease is more severe for helium because of higher interlobe leakage. It is concluded that for helium applications, the interlobe clearance should be smaller to reduce interlobe leakage and to maintain proper volumetric and adiabatic efficiencies.
- The temperature history of the working gas and the injected oil during compression-discharge process has been studied and presented for all four working gases.
- The influence of important design parameters such as interlobe clearance, rotational speed of male rotor, male wrap angle, blowhole area etc. on volumetric and adiabatic efficiencies has been examined and quantitative results have been presented for all four working gases.
- Two experimental test set ups have been constructed in the Cryogenics Laboratory of NIT Rourkela to study the behaviour of small and medium size twin-screw air compressors. Experiments with two compressors of widely differing capacities helps in studying size effects in addition to other studies.
- Both the compressors have been tested with air, nitrogen, argon, and helium under different oil to gas mass ratio, oil injection quantity, injection temperature and other operating parameters.
- Heat transfer coefficient between working gas and oil has been determined from experimental observations for use in the numerical simulation.
- Flow coefficients necessary for numerical simulation have been determined for all the gases by matching with experimentally obtained efficiencies.
- It is generally observed that experimental volumetric efficiency is generally about 2% less than the numerical values for all the four working gases. This value is well within the experimental uncertainties.
- From experimental results, it has been observed that lowering the injected oil temperature is more effective than increasing injected oil quantity for improving volumetric efficiency.
- An uncertainty analysis has been carried out to compute the uncertainty in experimental results. The uncertainty in the measurement of volumetric and adiabatic efficiencies is found to be 18% and 11% respectively.

7.2. Scope for future work

This thesis constitutes a portion of a continuous process towards understanding the working mechanism of an oil injected twin-screw compressor particularly in Indian context. A small beginning has been made. It is hoped that in the near future, a much stronger programme will be built on the topic in the Cryogenics Laboratory. The following are some of the future plans that are to be taken up in the coming years.

- ✓ Determination of fluid flow and heat transfer characteristics of oil injected twin screw compressor using a commercially available CFD package and its experimental validation.
- ✓ Influence of injected oil properties, injection position and droplet size of injected oil on compressor performance.
- ✓ Incorporation of capacity control mechanism under different operating conditions.
- ✓ Development of a comprehensive design methodology of screw rotors for achieving optimum efficiency.

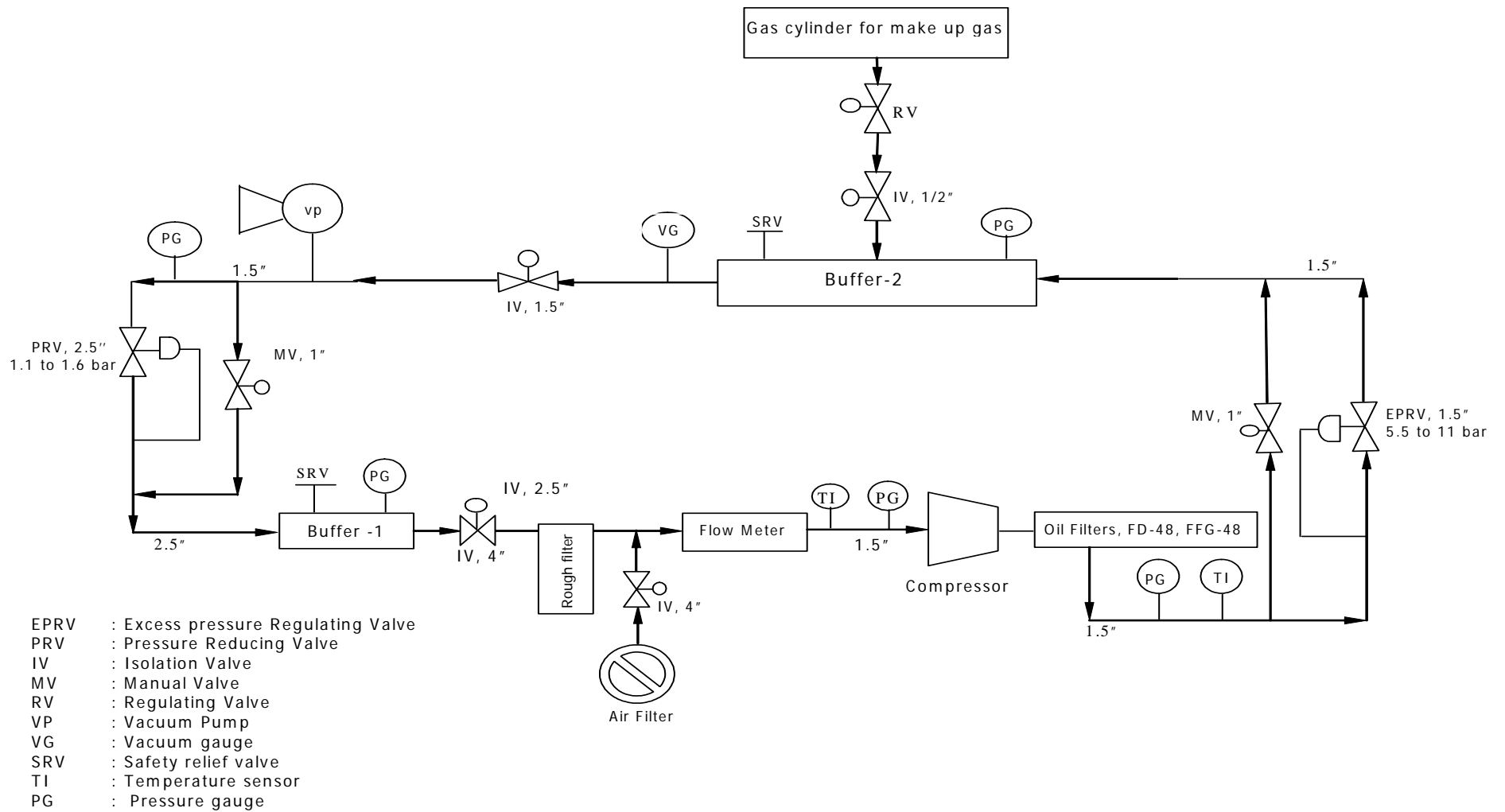


Figure 5.6: Schematic of the experimental test setup of Model BSD 72 compressor

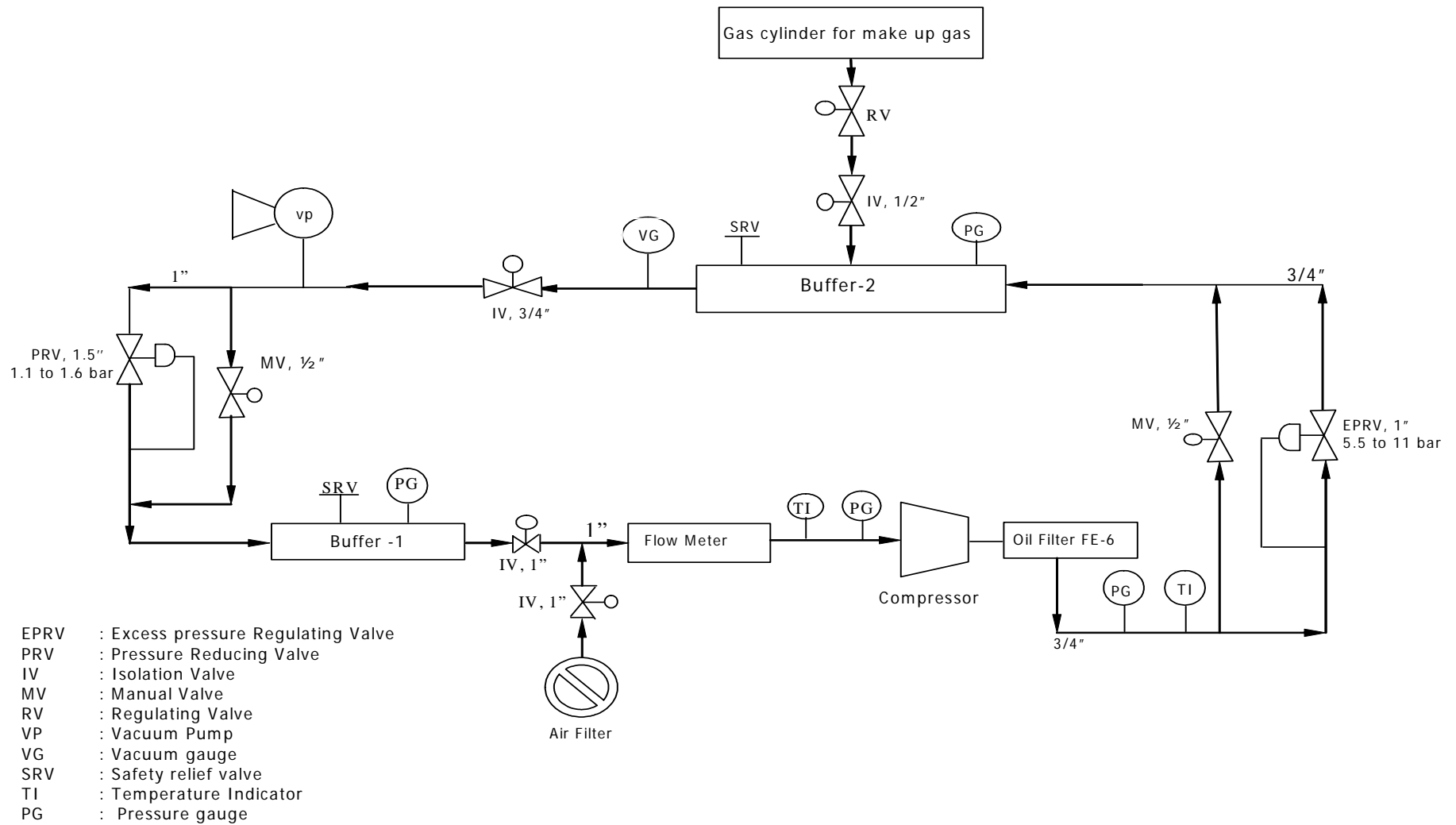


Figure 5.1: Schematic of the experimental test setup of Model, SM 8 compressor

References

- [1] **Arbon, I. M.** The Design and Application of Rotary Twin-Shaft Compressors in the Oil and the Gas Process Industry, Mechanical Engineering Publication Limited, London (1994)
- [2] **Brown, R. N.** Compressor: Selection and Sizing, Gulf Publishing Company Book Division, (1986)
- [3] **Taft, G.L.** Selection and Application of the Industrial Screw Compressors, Proceedings of the Purdue Compressor Technology Conference, Purdue, USA (1972), 306-310
- [4] www.arielcorp.com
- [5] **Stosic, N., Smith, I.K., Kovacevic, A.** Optimization of Screw Compressor Design, International Compressor Conference, Purdue, USA (2002), C21-23, 1177-1195. 71
- [6] **Paul, C.H.** Compressors Hand Book, McGraw Hill, (2001)
- [7] **Stocker, W. F.** Industrial Refrigeration Hand Book, McGraw Hill, (1998)
- [8] **Pillis, J.W.** Basics of Operation, Application and Troubleshooting of Screw Compressors, January 1998, (www.petroassist.com)
- [9] **Singh, P.J., Bowman, J.L.** Effect of Design Parameters on Oil Flooded Screw Compressor Performance, Proceedings of the International Compressor Engineering Conference, Purdue, USA (1986), Vol.I, 71-88
- [10] **Stosic, N.** Screw Compressors: Future Developments, Published on Internet; (1999) (www.city.ac.uk/~sj376).
- [11] **Stosic, N., Smith, I.K., Kovacevic, A.** Opportunities for Innovation with Screw Compressors, (www.city-compressors.co.uk)
- [12] **Stosic, N., Smith, I., Kovacevic, A.** Screw Compressors: Mathematical Modelling and Performance Calculation, Springer (2005)
- [13] **Kaiser, H., Kruse, H.** An Investigation on Reciprocating and Rotary Refrigeration Compressors, Proceedings of the International Compressor Engineering Conference, Purdue, USA (1984), 568-575
- [14] **Villadsen, V., Flemming, B. V.** A Balanced View of Reciprocating and Screw Compressor Efficiencies, Proceedings of the Purdue Compressor Technology Conference, Purdue, USA (1980), 26-32

- [15] **Sjoholm, L.** Different Operational Modes for Refrigeration Twin Screw Compressors, Proceedings of the Compressor Engineering Conference, Purdue, USA (1986), Vol.I, 89-104
- [16] **Bennewitz, C.** Software Support for Screw Rotor Design, Manufacture and Quality Control, International Compressor Engineering Conference Purdue, USA (1992), Vol.I, 431-438
- [17] **Tang, Y., Fleming, J.S.** Obtaining the Optimum Geometrical Parameters of Refrigeration Helical Screw Compressor, Proceedings of the International Compressor Engineering Conference, Purdue, USA (1992), Vol.I, 221-227
- [18] **Sjoholm, L.** Important Parameters for Small Twin Screw Refrigeration Compressors, Proceedings of the International Compressor Engineering Conference, Purdue, USA (1986), Vol.I, 1129-1144
- [19] **Singh, P.J., Schwartz, J.R.** Exact Analytical Representation of Screw Compressor Rotor Geometry, International Compressor Engineering Conference Purdue, USA (1990), Vol.I, 925-937
- [20] **Zhang, L., Hamilton, J.F.** Main Geometric Characteristics of Twin Screw Compressors, International Compressor Engineering Conference Purdue, USA (1992), Vol.I, 449-456
- [21] **You, C.X., Tang, Y., Fleming, J.S.** Optimum Rotor Geometrical Parameters in Refrigeration Helical Twin Screw Compressor, International Compressor Engineering Conference, Purdue, USA (1996), Vol.I, 1-6
- [22] **Zaytsev, D., Ferreira, I.C.A.** Profile Generation Method for Twin Screw Compressor Rotors Based on the Meshing Line, International Journal of Refrigeration, Volume 28, 5 744–755, Aug (2005)
- [23] **Stosic, N., Hanjalic, K.** General Method for Screw Compressor Profile Generation, International Compressor Engineering Conference, Purdue, USA (1996), Vol.I, 57-162
- [24] **Stosic, N., Hanjalic, K.** Development and Optimization of Screw Machines With a Simulation Model-Part I, Profile Generation, Journal of Fluid Engineering, (1997), 119, 659-662
- [25] **Stosic, N., Hanjalic, K.** Development and Optimization of Screw Engine Rotor Pairs on the Basis of Computer Modelling, Purdue Engineering Conference, Purdue, USA (1994), Vol.I, 55-60
- [26] **Stosic, N., Smith, I K., Kovacevic, A.** Rotor Interference as a Criterion for Screw Compressor Design, J. Engg. Design, Vol.14, 2 June (2003), 209–220
- [27] **Singh, P.J., Onuschak, A.D.** A Comprehensive, Computerized Method for Twin Screw Rotor Profile Generation and Analysis, Proceedings of the Purdue Compressor Technology Conference, Purdue, USA (1984), 519-527

- [28] **Stosic, N., Smith, I.K., Kovacevic A., Aldis, C.A.** The Design of a Twin Screw Compressor Based on a New Rotor Profile, *Journal of Engineering Design*, (1997), Vol. 8, 4 389-399
- [29] **Mccreath, P., Stosic, N., Smith, I.K., Kovacevic, A.** The Design of Efficient Screw Compressors for Delivery of Dry Air, *International Conference, Compressors and their Systems*, London, (2001)
- [30] **Xing, Z., Peng, X., Shu, P.** Development and Application of a Software Package for the Design of Twin-Screw Compressors, *International Compressor Engineering Conference*, Purdue, USA (2000), 1011-1018
- [31] **Mould, R., Richmond, G., Thrall, D.** Computer Aided Manufacture of Original Equipment Manufacturer Screw Compressor Rotors Design, *Proceedings of the Purdue Compressor Technology Conference*, USA (1982), 174-177
- [32] **Zhou, Z.** Computer Aided Design of a Twin Rotor Screw Refrigerant Compressor, *International Compressor Engineering Conference*, Purdue, USA (1992), Vol.I, 457-466
- [33] **Xing, Z., Deng, D., Shu, P.** A Computer Aided Design System for Twin-Screw Compressors, *Proceedings of the International Compressor Engineering Conference*, Purdue, USA (1992), Vol.I, 239-248
- [34] **Faydor, L., Litvin, Feng, P.H.** Computerized Design, Generation and Simulation of Meshing of Rotors of Screw Compressor, *Mechanism and Machine Theory*, (1997), Vol.32, 2 137-160
- [35] **Xiao, D. Z., Li, K. B., Wang, Z.Q., Liu, D.M.** Computer Aided Design Software Package for Conjugate Helical Surfaces, *Journal of Materials Processing Technology* Vol. 61, Issue 1-2, August (1996), 72-77
- [36] **Xiao, D. Z., Liu, D. T.** Computer Aided Curvature Analysis along the Contact Line of Conjugate Helical Surfaces, *Journal of Materials Processing Technology*, 61, (1996), 67-71
- [37] **Fleming, J.S., Tang, Y., And Anderson, H.** Optimization Techniques Applied to the Design of a Refrigeration Twin Screw Compressor, *International Compressor Engineering Conference*, Purdue, USA (1994), Vol.I, 641-646
- [38] **You, C.X., Tang, Y., and Fleming, J.S.** Optimum Lobe Tip Designs in Oil Injected Helical Twin Screw Compressors, *International Compressor Engineering Conference*, Purdue, USA, (1996), Vol.I, 7-11
- [39] **Xing, Z., Wu, H., Shu, P.** The Design of a New Generation of Twin-Screw Refrigeration Compressors, *16th International Compressor Engineering Conference* Purdue, USA, (2002), C21-5

- [40] **Venumadhav, K., Stosic, N., Smith, I.K., Kovacevic, A.** The Design of a family of Screw Compressors for Oil Flooded Operation, (www.city.ac.uk/~sj376)
- [41] **Stosic, N., Smith, I.K., Kovacevic, A.** Optimization of Screw Compressors, Applied Thermal Engineering, 23 (2003) 1177-1195
- [42] **Stosic, N.** On Gearing of Helical Screw Compressor Rotors, I Mech E, Journal of Mechanical Engineering Science, (1998), Vol.212, 588-594
- [43] **Stosic, N., Smith, I.K., Kovacevic, A.** Retrofit 'N' Rotors for Efficient Oil Flooded Screw Compressors, International Compressor Conference, Purdue, USA (2000), 917-924
- [44] **Hattori, H., Kawashima, N.** Dynamic Analysis of Rotor Journal Bearing System for Twin Rotary Screw Compressors, International Compressor Engineering Conference Purdue, USA (1990), Vol.I, 750-760
- [45] **Zhou, Z., Wang, D., Zhu, T., and Mao, J.** Analysis of the Applied Forces in Twin Screw Refrigerant Compressors, International Compressor Engineering Conference, Purdue, USA (1990), Vol.I, 8-17
- [46] **Fujiwara, A., and Sakurai, N.** Experimental Analysis of Screw Compressor Noise and Vibration, Proceedings of The 1986 International Compressor Engineering Conference, Purdue, USA (1986), Vol.I, 566-582
- [47] **Adams, G.P., Soedel, W.** Dynamic Simulation of Rotor Contact Forces in Twin Screw Compressors, International Compressor Engineering Conference, Purdue, USA, (1994), Vol.I, 73-78.
- [48] **You, C.X., Tang, Y., Fleming, J.S.** A Generalized Computer Program for Calculating the Bearing Loads in Helical Twin-Screw Compressors, International Compressor Engineering Conference, Purdue, USA (1994), Vol.I, 653-658
- [49] **Adams, G.P., and Qin, Z.H.** Compression Load Transmission in Screw Compressors, Journal of Sound and Vibration, (1997), 207 **5**, 671-691
- [50] **Adams, G.P., Soedel, W.** A Method for Computing the Compression Loads in Twin-Screw Compressor, International Compressor Engineering Conference Purdue, U.S.A (1994), Vol.I, 67-72
- [51] **Adams, G., Soedel, W.** Remarks on Oscillating Baring Loads in Twin Screw Compressors, International Compressor Engineering Conference Purdue, USA (1992), Vol.I, 439-448
- [52] **Stosic, N., Kovacevic, A., Smith, I.K.** Modelling of Screw Compressor Capacity Control, International Compressor Engineering Conference, Purdue, U.S.A (1998), Vol.I, 607-612

- [53] **Alyokhin, N.B., Malakhov, V.P.** Compressor Capacity Control, International Compressor Engineering Conference, Purdue, USA (1996), Vol.I, 19-24
- [54] **Sjoholm, L.** Variable Volume Ratio and Capacity Control in Twin-Screw Compressors, Proceedings of the International Compressor Engineering Conference, Purdue, USA (1986), Vol.I, 494-508
- [55] **Sauls, J.** Design of Unloader System for Moderate Capacity Refrigeration Screw Compressors, International Compressor Engineering Conference, Purdue, USA (1998), Vol.I, 583-588
- [56] **Mark, A. Firnhaber., Donald., Szarkowicz, S.** Modelling and Simulation of Rotary Screw Compressors, Proceedings of the Purdue Compressor Technology Conference, Purdue, USA (1980), 305-310
- [57] **Barblik, J., And Praha, C.K.D.** Analytical Model of an Oil Free Screw Compressor, Proceedings of the Purdue Compressor Technology Conference, Purdue, USA (1982), 356-364
- [58] **Alday, J.H., Hood, J.A.** A Program for Mathematical Modelling and Analysis of Rotary Screw Compressor Performance, Proceedings of the International Compressor Engineering Conference, Purdue, USA Vol.I, (1992), 249-258
- [59] **Sangfors, B.** Analytical Modelling of Helical Screw Machine for Analysis and Performance Prediction, Proceedings of the Purdue Compressor Technology Conference, Purdue, USA (1982), 135-139
- [60] **Zenan, Z., Jiashen, Z., Zhaolin, W. D. G.** The Application of Micro Computer in Optimum Design and Performance Forecast of Screw Compressor, Proceedings of the International Compressor Engineering Conference, Purdue, USA (1988), 244-249
- [61] **Pandeya, P., Soedel, W., Ray, W.** A Generalized Approach towards Compressor Performance Analysis, Proceedings of the Purdue Compressor Technology Conference, Purdue, USA (1978), 135-143
- [62] **Lundberg, A.A.** Comparison of SRM and Globoid Type Screw Compressors at Part Load, Proceedings of the Purdue Compressor Technology Conference, Purdue, USA (1978), 359-362
- [63] **Lundberg, A. A.** Comparison of SRM and Globoid type Screw Compressors at full Load, Proceedings of the Purdue Compressor Technology Conference, USA (1978), 353-358
- [64] **Fujiwara, M., Osada, Y.** Performance Analysis of Oil Injected Screw Compressor and its Application, International Journal of Refrigeration, (1995), Vol.18, 4 220-227

- [65] **Fujiwara, M., Kasuya, K., Matsunaga, T., Makoto, W.** Computer Modelling for Performance Analysis of Rotary Screw Compressor, Proceedings of the Purdue Compressor Technology Conference, Purdue, USA (1984), 536-543
- [66] **Fujiwara, M., Mori, H., And Suwama, T.** Prediction of the Oil free Screw Compressor Performance using Digital Computers, Proceedings of the Purdue Compressor Technology Conference, Purdue, USA (1974), 186-189
- [67] **Singh, P.J., and Patel, G.C.** A Generalized Performance Computer Program for Oil Flooded Twin-Screw Compressors, Proceedings of the Purdue Compressor Technology Conference, Purdue, USA (1984), 544-553
- [68] **Xiao, D., Xiong, Z., and Yu, Y.Z.** The Computer Simulation of Oil Flooded Refrigeration Twin-Screw Compressors, Proceedings of the Purdue Compressor Technology Conference, Purdue, USA (1986), Vol.I, 349-361
- [69] **Sangfors, B.** Computer Simulation of Oil Injected Twin-Screw Compressor, Proceedings of the Purdue Compressor Technology Conference, Purdue, USA (1984), 528-535
- [70] **Peng, N., Xing, Z., Deng, D., Shu, P.** New Rotor Profile and its Performance Prediction of Screw Compressor, International Compressor Engineering Conference, Purdue, USA Vol.I, (1990), 18-23
- [71] **Kishi, T., Nishio., T., Matsui, A., Ino, N.** The Improvement of Screw Compressor Performance Using a Newly Developed Rotor Profile, Advances in Cryogenic Engineering, (1993), Vol.39A, 879-885
- [72] **Kivotada, M.** Analysis of Screw Compressor Performance based on Indicator Diagrams, Proceedings of the International Compressor Engineering Conference, Purdue, USA (1992), Vol.I, 259-268
- [73] **Zhang, Z., Tan, Y., Shi, G. And Qian, Z.** Experimental Study of the Oil Injection Screw Air Compressor, Compressor Conference, Purdue, USA (2002), C19-4
- [74] **Sauls, J.** Development of a Comprehensive Thermodynamic Modelling System for Refrigerant Screw Compressors, International Compressor Engineering Conference, Purdue, USA (1996), Vol.I, 151-156
- [75] **Ignatiev, K.M., Tang, Y., Fleming, J.S.** Thermal Interaction in a Refrigeration Twin Screw Compressor during Compression Process, International Compressor Engineering Conference, Purdue, USA (1994), Vol.I, 629-634
- [76] **Huagen, W., Ziwen, X., Pengcheng, S.** Theoretical and Experimental Study on Indicator Diagram of Twin Screw Refrigeration Compressor, International Journal of Refrigeration, Vol.27, 4 (2004), 331-338

- [77] **Haugland, K.** Pressure Indication of Twin-Screw Compressor, International Compressor Engineering Conference, Purdue, USA (1990), Vol.I, 450-456
- [78] **Hanjalic, K., Stosic, N.** Development and Optimization of Screw Machines With a Simulation Model-Part II, Thermodynamic Performance Simulation and Design Optimization, ASME, Transactions, Journal of Fluids Engineering, **119**, (1997), 664-670
- [79] **Stosic, N., Smith, I.K., and Kovacevic, A.** Numerical Simulation of Fluid Flow and Solid Structure in Screw Compressors, ASME, International Mechanical Engineering Congress, New Orleans, USA (2002), 17-22
- [80] **Stosic, N., Smith, I.K., Zagorac, S.** C.F.D. Studies of Flow in Screw and Scroll Compressor, International Compressor Engineering Conference, Purdue, USA (1996), Vol.I, 181-186
- [81] **Singh, P. J., Bowman, J.L.** Heat Transfer in Oil Flooded Screw Compressors, Proceedings of the Compressor Engineering Conference, Purdue, USA (1986), Vol.I, 135-152
- [82] **Stosic, N., Kovacevic, A., Hanjalic, K., And Milutinovic, L.** Mathematical Modelling of the Oil Influence upon the Working Cycle of Screw Compressors, Proceedings of the Purdue Compressor Technology Conference, Purdue, USA (1988), 354-361
- [83] **Stosic, N., Milutinovic, L., Hanjalic, K., And, Kovacevic, A.** Investigation of the Influence of the Oil Injection upon the Screw Compressor Working Process, International Journal of Refrigeration, 15, No. 4, (1992), 205-219
- [84] **Stosic, N., Milutinovic, L., Hanjalic, K., and, Kovacevic, A.** Experimental Investigation of the Influence of Oil Injection upon the Screw Compressor Working Process, Proceedings of the Purdue Compressor Technology Conference, Purdue, USA (1990), 34-43.
- [85] **Peng, X., Xing, Z., Zang, X., Cui, T., and Shu, P.** Experimental Study of Oil Injection and its effect on Performance of Twin Screw Compressors, International Compressor Engineering Conference, Purdue, USA (2000), 1003-1010
- [86] **Hammerl, K., Tinder, L., Frank, M. K.** Modification in the Design of the Oil Injection System for Screw Compressors, International Compressor Engineering Conference, Purdue, USA (2000), 987-994
- [87] **Sangfors, B.** Computer Simulation of Effects from Injection of Different Liquids in Screw Compressors, International Compressor Engineering Conference, Purdue, USA (1998), Vol.I, 595-600
- [88] **Sjoholm, L.I., Short, G.D.** Twin Screw Compressor Performance and Complex Ester Lubricants with HCFC-22, International Compressor Engineering Conference, Purdue, USA (1990), Vol.I, 724-732

- [89] **Sjoholm, L.I., Short, G.D.** Twin-Screw Compressor Performance and Suitable Lubricants with HFC-134a, International Compressor Engineering Conference, Purdue, USA (1990), Vol.I, 733-740
- [90] **Tang, Y., and Fleming, J.S.** Simulation of the Working Process of an Oil Flooded Helical Screw Compressor with Liquid Refrigerant Injection, Proceedings of the International Compressor Engineering Conference, Purdue, USA (1992), Vol.I, 213-220
- [91] **Kangping, C., Zhenwu, T., and Hengyi, C.** The Development and Application of Water-Injected Twin Screw Compressor, Proceedings of the International Compressor Engineering Conference, Purdue, USA (1992), Vol.I, 269-277
- [92] **Westphal, C.R., and Bell, H.S.** Design and Development of a Water Flooded Screw Compressor Packaged Air Supply System, Proceedings of the Purdue Compressor Technology Conference, USA (1978), 341-352
- [93] **Ducruet, C., Hivet, B., Boone, J., Torreilles, M.** Test on a Twin-Screw Compressor: Comparison between Two Cooling Modes; Proceedings of the International Compressor Engineering Conference, Purdue, USA Vol.I, (1996), 175-180
- [94] **Tree, D.R., and Fresco, A.** Efficiency Study of Oil Cooling of a Screw Compressor, Proceedings of the UNSC/IIR Purdue Refrigeration Conference, Purdue, USA (1990), Vol.I, 110-119
- [95] **Depaepe, M., Bogaert, W., Mertens, D.** Cooling of Oil-Infected Compressors by Oil Atomization, Applied Thermal Engineering, Vol.25, Issues 17-18, December (2005), 2653-3202
- [96] **Stosic, N., Smith, I.K., and Kovacevic, A.** CFD Analysis of Screw Compressor Suction Flow, International Compressor Conference, Purdue, USA (2000), Vol.I, 909-916
- [97] **Sjoholm, L.I., Muralidhar, A.** Measurement of the Discharge Port for a Screw Compressor, Fifteenth International Compressor Engineering Conference, Purdue, USA (2000), 995-1002
- [98] **Koai, K.L., Soedel, W.** Gas Pulsations in Twin Screw Compressors, Part-I, Determination of Port Flow and Interpretation of Periodic Volume Source, International Compressor Engineering Conference, Purdue, USA (1990), Vol.I, 369-377
- [99] **Koai, K.L., Soedel, W.** Gas Pulsations in Twin Screw Compressors, Part-II, Dynamics of Discharge System and its Interaction with Port flow, International Compressor Engineering Conference Purdue, USA (1990), Vol.I, 378-387
- [100] **Koelet, P.** Industrial Refrigeration, Principles, Design and Applications, Mc Graw Hill, (1992).

- [101] **Xiong, Z.** The Dynamic Measurement and Mating Design of a Screw Compressor Rotor Pair, Proceedings of the International Compressor Engineering Conference, Purdue, USA (1984), 554-558
- [102] **Prins, J., and Ferreira, I. C.A.** Quasi one Dimensional Steady State Models for Gas Leakage, Part-I: Comparison and Validation, International Compressor Engineering Conference, Purdue, USA (1998), Vol.I, 571-576
- [103] **Prins J., and Ferreira, I.C.A.** Quasi One Dimensional Steady State Models for Gas Leakage, Part-II: Improvement of the Viscous Modelling, International Compressor Engineering Conference, Purdue, USA (1998), Vol.I, 577-582
- [104] **Hangiqi, L., Guangxi, J.** Research on Discharge Port of Oil Flooded Rotary Compressors, International Compressor Engineering Conference, Purdue, USA (1990), Vol.I, 292-299
- [105] **Singh, P.J., Bowman, J.L.** Calculation of Blowhole Area for Screw Compressors, International Compressor Engineering Conference, Purdue, USA (1990), Vol.I, 938-948
- [106] **Xiong, Z., And Xiao,D.** Study on Actual Profile Surface and Engaging Clearance of Screw Compressor Rotors, Proceedings of the International Compressor Engineering Conference, Purdue, USA (1986), Vol.I, 305-311,
- [107] **Vimmer, J.** Mathematical Modelling of Compressible Inviscid Fluid Flow Through a Sealing Gap in the Screw Compressor, Journal of Mathematics and Computers in Simulation, **61**, (2003), 187-197
- [108] **Zaytsev, D., and Ferreira, I.C.A.** Aspects of Two Phase Flow Screw Compressor Modelling, Part I: Leakage Flow and Rotor Tip Friction, International Compressor Engineering Conference, Purdue, USA (2000), 893-900
- [109] **Fleming, J.S., Tang, Y.** Analysis of Leakage in a Twin Screw Compressor and its Application to Performance Improvement, Proceedings of The Institution of Mechanical Engineers, Part E: Journal of Process Mechanical Engineering, Vol.209, **E2**, (1995), 125-136
- [110] **Abu-Hijleeh, B., Tu, J., Subic, A., Li, H., Ilie, K.** CFD Comparison of Clearance Flow in a Rotor-Casing Assembly using Asymmetric Vs Symmetric Lobe Rotors, American Society of Mechanical Engineers, Fluids Engineering Division (FED), Vol.259, (2003), 327-330
- [111] **Prins, J., Carlos, A., Ferreira, I.** Leakage Experiments on a Running Twin-Screw Compressor, International Compressor Engineering Conference, Purdue, USA (2002), C19-3

- [112] **Lee, K.S., Kim, W. S., Kim, K.Y., Kim, C.H.** A Study of the Leakage Performance for the Plain Seal with Injection, Proceedings of The International Compressor Engineering Conference, Purdue, USA (1992), Vol.I, 229-238
- [113] www.howdencompressors.co.uk
- [114] **Shaw, D.N.** Screw Compressors, Control of 'Vi' and Capacity, the Conflict, Proceedings of the International Compressor Engineering Conference, Purdue, USA (1988), Vol.I, 236-243
- [115] **Pietsch, A., and Nowotny, S.** Thermodynamic Calculation of a Dual Screw Compressor based on Experimentally Measured Values Taking Supercharge into Account, International Compressor Engineering Conference, Purdue, USA (1990), Vol.I, 44-50
- [116] **Yahya, S.M.** Fundamentals of Compressible Flow, New Age International Pvt. Ltd. (1996)
- [117] **Fox, R. W., McDonald, A. T.** Introduction to Fluid Mechanics, 2nd Edition, John Wiley & Sons (1973)
- [118] **Ueno, K., Hunter, K.S.** Compressor Efficiency Definitions, (2003) (www.vairex.com)
- [119] www.me.ua.edu
- [120] **ALLPROPS:** Thermodynamic Property Packages ([Http://www.Engr.Uidaho.Edu/Cats/Software](http://www.Engr.Uidaho.Edu/Cats/Software))
- [121] **Coleman, H.W., Steele, W.G.** Experimentation and Uncertainty Analysis for Engineers, John Wiley & Sons, (1989)
- [122] **Kegel, T.** Uncertainty Issues Associated with a Volumetric Primary Flow Standard for Compressible Flow Measurement (www.ceesi.com)
- [123] **Taylor, R.P., Hodge, B.K., James, C.A.** Estimating Uncertainty in Thermal Systems Analysis and Design, Applied Thermal Engineering, (1999) **19**, 51-73
- [124] **Moffat, R.J.** Describing the Uncertainties in Experimental Results Experimental Thermal and Fluid Science (1998) **1** (1) 3-17
- [125] **Brown, K.K., Coleman, H.W., Steele, W.G.** A Methodology for Determining Experimental Uncertainties in Regressions, Proceedings of the ASME Fluids Engineering Division, ASME (1996) FED- Vol. **242**, 263-273
- [126] **Youngs, W.** Screw Compressors: A Comparison of Applications and Features to Conventional Types of Machines, (www.gasprocessors.com)
- [127] **Arkharov, A., Marfenina, I., Trans, M.Ye., Kuznetsov, B.V.** Theory and Design of Cryogenic Systems, Mir Publishers, Moscow (1981)

- [128] **Martinez, A., And Pallaver, C.B.** Test of an Improved Oil Injected Helium Screw Compressor at Fermi Lab, *Advances in Cryogenic Engineering*, (1993), Vol. 39A, 887-892
- [129] **Martinez, A., and Pallaver, C.B.** Operation and Maintenance of Fermi Laboratory's 300kw Helium Screw Compressors, *Cryogenic Engineering Conference and International Cryogenic Material Conference*, Columbus, Ohio, (1995)
- [130] **Shaw, D.N.** Twin Screws of the Future for Air Conditioning and Refrigeration, *International Compressor Engineering Conference*, Purdue, USA, (1990), Vol.I, 1-7
- [131] **Mosemann, D., Krienke, S., and Nowotny, S.** Improvements of Refrigerating Screw Compressors of Large Capacity, *Proceedings of the International Compressor Engineering Conference*, Purdue, USA (1988), 250-255
- [132] **Mori, H., Kasuya, K., Suzuki, A., Takahashi, Y., Aoki, M.** Single Stage Oil Free Screw Compressor with a Compression Ratio of "Eight", *Proceedings of the International Compressor Engineering Conference*, Purdue, USA (1986), Vol.I, 105-118
- [133] **Moshe, Y., Dreksler, P.E.** The Two-Stage Compound Screw Low Molecular Weight Gas Compressor, *Proceedings of the International Compressor Engineering Conference*, Purdue, USA (1992), Vol.I, 31-40
- [134] www.gcbtechnicold.com
- [135] **Xiong, Z.** Use The Method of Magnetic Score to Measure the Dynamic Parameters of the Screw Compressors, *Proceedings of the International Compressor Engineering Conference*, Purdue, USA (1986), Vol.I, 321-333
- [136] **Wu, H., Peng, X., Xing, Z., Shu, P.** Experimental Study on P-V Indicator Diagrams of Twin Screw Refrigeration Compressor with Economizer, *Applied Thermal Engineering*, Vol. 24, **10** July (2004), 1491-1500
- [137] **Edstorm, S.E.** Modern way to Good Screw Rotors, *International Compressor Engineering Conference*, Purdue, USA (1992), Vol.I, 421-430
- [138] **Wardle, F.P., Jacobson, B., Dolfmsa, H., Hoglund, E., and Jonsson, U.** The Effects of Refrigerants on the Lubrication-Rolling Element Bearings used in Screw Compressors, *Proceedings of the International Compressor Engineering Conference*, Purdue, USA (1992), Vol.I, 523-534
- [139] **Jacobson, B.** Lubrication of Screw Compressor Bearings in the Presence of Refrigerants, *International Compressor Engineering Conference* Purdue, USA (1994), Vol.I, 115-120

- [140] **Stosic, N., Smith, I.K., Kovacevic, A.** A Twin Screw Combined Compressor and Expander for CO₂ Refrigeration System, International Compressor Engineering Conference Purdue, USA (2002), Vol.I, C 21-2
- [141] **Kovacevic, A., Stosic, N., And Smith, I.K.** CFD Analysis of Screw Compressor Performance (www.city.ac.uk/~sj376)
- [142] **Kovacevic, A., Stosic, N., and Smith, I.K.** The Influence of Rotor Deflection upon Screw Compressor Performance (www.city.ac.uk/~sj376)
- [143] **Fleming, J.S., Tang, Y., Cook, G.** The Twin Helical Screw Compressor Part 2: A Mathematical Model of the Working Process, Proceedings of the Institution of Mechanical Engineers, Part C: Journal of Mechanical Engineering Science, Vol. 212, **5** (1998), 369 - 380
- [144] **Bowater, F.J.** Large Screw Compressors in Refrigeration Industry, (www.fjb.co.uk)
- [145] **Laplante, J.R.** Rotary Compression Process; Prepared for the Gas Machinery Research Council Conference, (2003), (www.gmrc.org)